NAMBE 2003 Schedule of Events

Sunday, September 28, 2003
2:00-5:00: Exhibitor setup
5:00-7:00: Check-in, registration, and welcoming reception
7:30-9:30: Riber Users Meeting (Invitation Only)

Monday, September 29, 2003
7:00-5:00: Check-in and registration
7:00-8:00: Breakfast
8:00-5:00: Vendor exhibits
8:00-8:10: Welcoming remarks
8:10-10:10: **Quantum Structures I**
10:10-10:30: Coffee break
10:30-12:10: **Gallium Nitride-Based Growth and Devices**
12:10-1:30: Lunch
1:30-3:30: **Quantum Structures II**
3:30-5:00: **Poster Session I** and Refreshment break
7:00-9:00: Veeco/Applied EPI Users Meeting

Tuesday, September 30, 2003
7:00-5:00: Check-in and registration
7:00-8:00: Breakfast
8:00-5:00: Vendor exhibits
8:00-10:00: **Special Topics in MBE Growth and Characterization**
10:00-10:20: Coffee break
10:20-12:00: **Highly-Strained Materials: Growth and Characterization**
12:00-1:30: Lunch
12:00-1:30: NAMBE Advisory Board Lunch
1:30-3:30: **Materials for Spintronics and Quantum Information**
3:30-5:00: **Poster Session II** and Refreshment break
6:00-9:00: Banquet

Wednesday, October 1, 2003
7:00-5:00: Check-in and registration
7:00-8:00: Breakfast
8:00-3:00: Vendor exhibits
8:00-9:40: **Dilute Nitrides**
9:40-10:10: Coffee break
10:10-11:50: **Devices and Device Structures I**
11:50-1:30: Lunch
1:30-3:10: **Devices and Device Structures II**
End of Main Conference
3:00-5:00: Exhibitor move out

Thursday, October 2, 2003
7:00-3:30: Check-in and registration
7:00-8:00 Breakfast
8:00-10:00: Workshops
10:00-1030: Coffee break
10:30-12:00: Workshops
12:00-1:30: Lunch
1:30-3:30: Workshops
End of workshops and conference
Workshops:

1) Production of Next-Generation MBE Materials
2) Long Wavelength Optoelectronics
3) MBE for Quantum Information

NAMBE 2003

Table of Contents

NAMBE 2003 Conference Sessions**……1**

Monday AM I: **Quantum Structures I……...11**

Monday AM II: **Gallium Nitride Based Growth and Devices……..25**

Monday PM I: **Quantum Structures II……..37**

Poster Session 1**……51**

Tuesday AM I: **Special Topics in MBE Growth and Characterization . ……75**

Tuesday AM II: **Highly-Strained Materials: Growth and Characterization……...89**

Tuesday PM I: **Materials for Spintronics and Quantum Information……101**

Poster Session 2**……..113**

Wednesday AM I: **Dilute Nitrides……139**

Wednesday AM II: **Devices and Device Structures I……..151**

Wednesday PM I: **Devices and Device Structures II……....163**

Thursday Workshop 1: **Production of Next-Generation MBE Materials……174**

Thursday Workshop 2: **Long Wavelength Optoelectronics……..175**

Thursday Workshop 3: **MBE for Quantum Information……..176**

NAMBE 2003 Exhibitor Information **……182**

NAMBE 2003

Conference Chairman
Richard Mirin
NIST
325 Broadway
Boulder, CO 80305
(303) 497-7955
(303) 497-3387 (FAX)
mirin@boulder.nist.gov

Program Chairman
Archie Holmes
The University of Texas at Austin
Electrical and Computer Engineering
1 University Station C0803
Austin, TX 78712-0240
(512) 471-6903
(512) 471-8575 (FAX)
holmes@ece.utexas.edu

Conference Program Manager
Wendy McBride
NIST
325 Broadway
Boulder, CO 80305
(303) 497-3693
(303) 497- (FAX)
wmcbride@boulder.nist.gov

Proceedings Editor
William Goodhue
University of Massachusettes, Lowell
Department of Physics and Applied Physics
Lowell, MA 01854
(978) 934-3785
(978) 934-4994 (FAX)
William_Goodhue@uml.edu

NAMBE 2003 Program Committee
Archie Holmes, Univ. of Texas, Austin
William Goodhue, Univ. Of Mass. Lowell
Rod Beresford, Brown University
Thomas Block,Northrup Grumann
Brian Bennett, Naval Research Lab
Norman Cheng, Univ. of Illinois
James Gupta, NRC-Canada
Shane Johnson, Arizona State
Ron Kaspi, Air Force Research Lab
Dan Mars, Agilent
Joanna Mirecki-Millunchick, Univ. of Michigan
Hong Ng, Lucent Technologies
Gary Wicks, University of Rochester

NAMBE Advisory Board
Charles Tu, UCSD (Chairman)
Pallab Bhattacharya, Univ. of Michigan
Rod Beresford, Brown University
Norman Cheng, Univ. of Illinois
William Goodhue, Univ. of Mass., Lowell
James Harris, Stanford University
William Hoke, Raytheon
Richard Mirin, NIST
Ted Moustakas, Boston University
Maria Tamargo, City Univ. of New York
Anthony Springthorpe, NRC-Canada
George Turner, Lincoln Labs
Kang Wang, UCLA
Zbig Wasilewski, NRC-Canada
Gary Wicks, University of Rochester
Yong-Hang Zhang, Arizona State Univ.

NAMBE 2003

The NAMBE 2003 Conference would like to thank the following exhibitors for their sponsorship:

Riber	Portfolio
Wafer Technology	Portfolio
Veeco Instruments	Banquet
United Mineral and Chemical	Tuesday Coffee Break

List of NAMBE 2003 Exhibitors

Addon
AXT
Bede Scientific
DCA Instruments
GE Advanced Ceramics
Geo Gallium
InPACT
k-Space Associates
MBE-Komponenten GmbH
SINTEC Keramik USA
SPECS Scientific Instruments
Sumitomo Electric SemiConductor Materials Inc.
SVT Associates
United Mineral & Chemical
Vacuum Barrier Corp.
VBS International
Riber
Veeco Instruments
Wafer Technology

NAMBE 2003 Program

Monday, September 29, 2003

8:10-10:10: Quantum Structures I

Chair: Norman Cheng (University of Illinois)

MA-1: Enhancement of one dimensionality by stacking effect of self-organized In0.53Ga0.47As quantum wires grown on (221)B-oriented InP substrates by MBE
S. Shimomura, K. Hyodo, A.Shigenobu,Y. Ohno, T. Kitada, and S. Hiyamizu
Osaka University, Japan

MA-2: Temperature Stabilized 1.55 μm Photoluminescence in InAs Quantum-Dots grown on InP
Z. H. Zhang and K. Y. Cheng
University of Illinois at Urbana-Champaign

MA-3: Improvement on the InAs quantum dot size distribution by employing high temperature GaAs(100) substrate treatments
N. Saucedo-Zeni, A. Yu. Gorbatchev, A. Lastras-Martinez, and V.H. Méndez-Garcia
Universidad Autonoma de San Luis Potosi, Mexico

MA-4: Extending the Emission of InAs/GaAs Self-Assembled Quantum Dots Beyond 1.3 μm Using Capping Effects
B. J. Riel, P. J. Poole, Z. R. Wasilewski, and S. Raymond
National Research Council-Canada

MA-5: Study of Structural and Optical Properties of Quantum Dots-in-a-Well Heterostructures
P. Rotella, G. von Winckel, S. Raghavan, A. Stintz, and S. Krishna
University of New Mexico

MA-6: Heterostructures for Achieving Very Large Responsivity in InAs/GaAs Quantum Dot Infrared Photodetectors
S. Chakrabarti[a)], A.D. Stiff-Roberts[a)], P. Bhattacharya[a)], and S. Kennerly[b)]
[a)]University of Michigan; [b)]Army Research Laboratory

10:30-12:10: Gallium Nitride-Based Growth and Devices

Chair: Shane Johnson (Arizona State University)

MB-1: Periodically Poled GaN Grown by Molecular Beam Epitaxy
Hock M. Ng, Nils G. Weimann, Manish Bhardwaj, and Aref Chowdhury
Bell Laboratories, Lucent Technologies

MB-2: The Effect of Ga-rich Growth Conditions on the Optical Properties of GaN Films Grown by Plasma-assisted Molecular Beam Epitaxy
A.V. Sampath, G. A. Garrett, C. J. Collins, P. Boyd, J. Y. Choe, P. G. Newman, H. Shen, M. Wraback, and R.J. Molnar*
U.S. Army Research Laboratory; *MIT Lincoln Laboratory

MB-3: Efficient p-type doping of GaN films by MBE
A. Bhattacharyya, W. Li, C. Thomidis, T. D. Moustakas, and David J. Smith*
Boston University; * Arizona State University

MB-4: Lateral photocurrent spectroscopy investigation of excitonic absorption in AlGaN/GaN multiple quantum wells grown by molecular beam epitaxy
I. Friel, C. Thomidis, Y. Fedyunin, and T. D. Moustakas
Boston University

MB-5: Polarization-doped 3D electron slabs in graded III-V Nitride heterostructures: MBE growth, physics, and demonstration of the PolFET
D. Jena, S. Heikman, D. Buttari, A. Jimenez, S. Rajan, H. Xing, J. S. Speck, and U. K. Mishra
University of California, Santa Barbara

NAMBE 2003 Program

1:30-3:30: Quantum Structures II

Chair: Archie Holmes (University of Texas at Austin)

MC-1: Photoluminescence properties of CdSe quantum dots grown on ZnSe and $Zn_{0.97}Be_{0.03}Se$ by Molecular Beam Epitaxy
Xuecong Zhou[1], Martin Muñoz[1], Shiping Guo[1], Maria C. Tamargo[1], Yi Gu[2], Igor L. Kuskovsky[2], and G. F. Neumark[2]
[1]The City College of New York; [2]Columbia University

MC-2: Free carrier compensation of semi-metallic ErAs particles embedded in an InGaAs matrix
Daniel C. Driscoll[a], Micah P. Hanson[a], Mihail Suhkotin[b], Elliott Brown[b], and Arthur C. Gossard[a]
[a]University of California, Santa Barbara; [b]University of California, Los Angeles

MC-3: Growth and electrical properties of GaSb/ErSb composites
M. H. Hanson, D.C. Driscoll, J. Zimmerman, and A.C. Gossard
University of California, Santa Barbara

MC-4: The Selective Growth of InP Nanowires by Chemical Beam Epitaxy
P.J. Poole, J. Lefebvre, and J. Fraser
National Research Council-Canada

MC-5: Photoconductive characteristics in a trench-type InGaAs quantum wire
K.-Y.Jang[1,2,3], T.Sugaya[1,2], A.Shinoda[2,4], C.-K. Hahn[1,2], M. Ogura[1,2], and K. Komori[1,2]
[1]National Institute of Advanced Industrial Science and Technology(AIST); [2]CREST, Japan Science and Technology Corporation (JST); [3]Japan Science for the Promotion of Science (JSPS)-Domestic Research Fellow; [4]Shibaura Institute of Technology, Japan

MC-6: Si-based Quantum Dot LED grown by MBE
M. Jo[1], N. Yasuhara[1], K. Kawamoto[1], and S. Fukatsu[1, 2]
[1]The University of Tokyo, Japan; [2]PRESTO, Japan Science and Technology Corporation (JST), Japan

NAMBE 2003 Program

Poster Session 1: Monday, September 29, 2003, 3:30-500

P1-1: Magneto-Photoconductive Characterization of Quantum States of Barrier Shallow Donors in MBE Grown GaAs/AlGaAs Heterostructures
A. Naweed, W. D. Goodhue, W. J. Gorveatt, R. Giles, J. Waldman and V. Menon#
University of Massachusetts Lowell; # Princeton University

P1-2: Probing the Electronic Structures of III-V-Nitride Semiconductors by X-ray Photoelectron Spectroscopy
T.S. Lay[1], W.T. Kuo[1], L.P. Chen[1], Y.H. Lai[2], W.H. Hung[2],J.S. Wang[3], J.Y. Chi[3], D.K. Shih[4], H.H. Lin[4], C.M. Chuang[5], K.H. Chen[5]
[1]National Sun Yat-Sen University; [2]National Synchrotron Radiation Research Center,Taiwan; [3]Industrial Technology Research Institute,Taiwan; [4]National Taiwan University; [5]Institute of Atomic and Molecular Sciences, Academia Sinica

P1-3: Mg segregation in Mg-GaN MBE growth: A Simulation Investigation
Irena Stanley and Rama Venkat
University of Nevada, Las Vegas

P1-4: Epitaxial Growth on Gas Cluster Ion Beam Processed GaSb Substrates Using Molecular Beam Epitaxy
K. Krishnaswami[a], W.D. Goodhue[a], L.P. Allen[b], C. Santeufemio[b], X. Liu[c], M.C. Ospina[c], B. Zhu[a],J. Whitten[c], C. Sung[c], H. Dauplaise[d], D. Bliss[d], G. Dallas[e], D. Bakken[e], and K.S. Jones[f]
[a] Photonics Center, University of Massachusetts, Lowell; [b] Epion Corporation; [c] Center for Advanced Material, University of Massachusetts;[d] Air Force Research Laboratory/SNHC;[e] Galaxy Compound Semiconductors; [f] Department of Materials Science, University

P1-5: Optical and electrical characteristics of C60/GaAs
Masaaki Ogawa, Kazuki Nomoto, Yousuke Kida and Yoshiji Horikoshi
Waseda University, Japan

P1-6: Strong Lateral Confinement in Self-Organized InGaAs/InAlAs quantum wires grown on a (221)A oriented InGaAs ternary alloy substrate by MBE
K. Miyagawa, D. Suma, T. Kitada, S. Shimomura and S. Hiyamizu
Osaka University, Japan

P1-7: Stability of Pseudomorphic InGaAs Layers during annealing
A. Riposan, G.K.M. Martin, and J. Mirecki Millunchick
University of Michigan

P1-8: Contact-less Electroreflectance of CdSe/ZnSe Quantum Dots grown by MBE
Martín Muñoz, Shiping Guo, Xuecong Zhou, Maria C. Tamargo, Y.S Huang#, C. Trallero-Giner*, and A. H. Rodríguez*
City College of the City University of New York; # National Taiwan University of Science and Technology; * Universidad de La Habana San Lazaro y L, Cuba

P1-9: MBE growth of ZnO using initial Zn layer and MgO buffer layer on Si (111) substrates
Miki Fujita, Noriaki Kawamoto, Masanori Sasajima and Yoshiji Horikoshi
Waseda University, Japan

P1-10: Compositional Analysis of Graded AlxGa(-x)As Layers by X-ray Energy Dispersive Spectrometry
K. Mahalingam, R. Wheeler, K. G. Eyink, and S. T. Fenstermaker
Air Force Research Laboratory

P1-11: Low Temperature Si Growth on Si (001): Impurity Incorporation and Limiting Thickness for Epitaxy
J.-M. Baribeau, X. Wu, D.J. Lockwood, L. Tay, and G. I. Sproule
National Research Council-Canada

NAMBE 2003 Program

Tuesday, September 30, 2003

8:00-10:00: Special Topics in MBE Growth and Characterization

Chair: Hock Ng (Lucent)

TA-1: Studies of Oxide Desorption from GaAs Substrates via Ga_2O_3 to Ga_2O Conversion by Exposure to Ga Flux
Z. R. Wasilewski, J.-M. Baribeau, M. Beaulieu, X. Wu, G. I. Sproule, and J. W. Fraser
National Research Council-Canada

TA-2: Mn and Be co-doped GaAs for high hole concentration by LT-MEE
Koji Onomitsu, Hideo Fukui, Takashi Maeda, and Yoshiji Horikoshi
Waseda University, Japan

TA-3: Sb-Mediated Growth of Si and Be Doped AlGaAs by Molecular Beam Epitaxy
S. R. Johnson*, Yu. G. Sadofyev, K. Franzreb, Y. Cao, D. Ding, N. Samal, S. A. Chaparro, J. Wang, J. Xu, S. Q. Yu, and Y.-H. Zhang
Arizona State University

TA-4: Composition Verification of AlGaAs Epitaxial Layers using Inductively Coupled Plasma Optical-Emission Spectroscopy
K. A. Bertness, T. E. Harvey, A. J. Paul, L. H. Robins, G. C. Turk, T. A. Butler, and M. L. Salit
National Institute of Standards and Technology

TA-5: Single-phase growth studies of GaP on Si by solid-source MBE
X.Yu, P.S. Kuo, K Ma, M. M. Fejer, and J. S. Harris Jr.
Stanford University

TA-6: Intermixing and As Incorporation in GaAs/GaSb Multilayers
C. Dorin, C. Wauchope, and J. Mirecki Millunchick
University of Michigan

10:20-12:00: Highly-Strained Materials: Growth and Characterization

Chair: Rod Beresford (Brown University)

TB-1: Dislocation Structure and Surface Roughness of InAslAs graded buffer layers grown on InP for 6.05 and 6.0 angstrom applications
A.M. Noori*, R.S. Sandhu*,§, S.L. Hayashi*,§, E.D. Meserole*, A. Cavus§, C. Monier§, R.Hsing§, D. Sawdai§, M. Wojtowicz§, T. R. Block§, A. Gutierrez-Aitken§, and M.S.Goorsky*
*University of California,Los Angeles; §Northrop Grumman Space Technology

TB-2: Real-time strain evolution during growth of InAlAs/GaAs metamorphic buffer layers
C. Lynch, R. Beresford, and E. Chason
Brown University

TB-3: Effect of Buffer Layer on InSb Quantum Wells Grown on GaAs (001) Substrates
T.D. Mishima, J.C. Keay, N. Goel, M.A. Ball, S.J. Chung, M.B. Johnson, and M.B. Santos
University of Oklahoma

TB-4: Defect-Controlled Selective Epitaxial Growth of GaAs on Si substrate with Strained Short Period Superlattices
Takuto Tsuji, Hiroo Yonezu#, and Naoki Ohshima*
Takuma National College of Technology; #Toyohashi University of Technology; *Yamaguchi University

TB-5: Material Properties and Performance of Metamorphic Optoelectronic Integrated Circuits Grown by Molecular Beam Epitaxy on GaAs Substrates
W. Hoke, R. Leoni, C. Whelan, T. Kennedy, A. Torabi, P. Marsh, Y. Zhang, C. Xu*, and K.C. Hsieh*
Raytheon RF Components; *University of Illinois

1:30-3:10: Materials for Spintronics and Quantum Information

Chair: Gary Wicks (University of Rochester)

TC-1: MBE growth of high Curie temperature GaMnAs films
R P Campion, K W Edmonds, L Zhao, K Wang, B L Gallagher, and C T Foxon
University of Nottingham, United Kingdom

TC-2: Influence of Defects on Structural and Magnetic Properties of GaMnAs
J. Sadowski[1, 2, 3], J. Kanski[4], P. Svedlindh[5], V. Stanciu[5], J. Z. Domagala[3], J. Bak -Misiuk[3], A. Mikkelsen[2], C. Glover[6], and E. Hankiewicz[7]
[1]Copenhagen University, Denmark; [2] Lund University, Sweden; [3]Polish Academy of Sciences, Poland; [4]Chalmers University of Technology, Sweden; [5]Uppsala University, Sweden; [6]Australian National University, Australia; [7]Iowa State University, USA

TC-3: Reduced interface reaction during the epitaxial Fe growth on InAs for high efficiency spin injection
Kanji Yoh[1], Hiroshi Ohno[1], Kazuhisa Sueoka[1], and Manfred E. Ramsteiner[2]
[1]Hokkaido University, Japan; [2]Paul Drude Institute of Solid State Electronics, Germany

TC-4: Epitaxial Growth of a Spin-Polarized Ferromagnetic Oxide on Silicon: EuO/Si (001)
D.G. Schlom[1], V. Vaithyanathan[1], J. Lettieri[1], S.B. Ogale[2], S.K. Eah[3], J. Levy[3], J. Stephens[4], V. Sih[4], and D.D. Awschalom[4]
[1]Penn State University; [2]University of Maryland; [3]University of Pittsburgh; [4]University of California, Santa Barbara

TC-5: Epitaxial growth of two-dimensional Al(111) films on Si(111) – applications in quantum computing
D. A. Hite, R. W. Simmonds, K. M. Lang, R. McDermott, J. M. Martinis, and D. P. Pappas
National Institute of Standards and Technology

NAMBE 2003 Program

Poster Session 2: Tuesday, September 30, 2003, 3:30-500

P2-1: Integrated In-Situ Monitoring of MBE Processes
R. Hartmann, P. Chow, and T. Barnacle
SVT Associates

P2-2: Growth of Be-doped GaInP/GaAs HBTS by all Solid-source Multiwafer Production MBE
A. Wilk, M. Zaknoune, S. Godey, P. Gérard, S. Dhellemmes, C. Chaix, and F. Mollot
RIBER and IEMN

P2-3: High Material Quality of 830nm Laser device Grown by SSMBE for Printing Applications
I. C. Hernandez, G. K. Kuang, and M. McElhinney
Lasertel, Inc.

P2-4: Investigation of radiative and non-radiative centers in Al-doped ZnSe grown by molecular beam epitaxy
D. C. Oh[a], J. S. Song[b], J. H. Chang[c], T. Takai[a], F. Lu[d], T. Hanada[a], M. W. Cho[a], and T. Yao[a]
[a]Tohoku University, Japan; [b]Korea Maritime University; [c]NeosemiTech Corp., Korea; [d]Fudan University, China

P2-5: Flux Profile Modeling : Monte Carlo Simulation and Numerical Computation
Bharat Reddy Pemmireddy[1], Ramprasad Vijayagopal[1], Rama Venkat[1], Hwa Cheng[2], and Rich Bresnahan[2]
[1]University of Nevada, Las Vegas; [2]Applied Epi-Veeco

P2-6: Solid-Source Molecular Beam Epitaxy (SSMBE) growth of GaInNAs on InP substrate
Junxian Fu, Seth Bank, Mark Wistey, James S. Harris, Jr
. Stanford University

P2-7: Optimisation of SiGe/Si hetero-interface in GSMBE aided by RHEED intensity oscillations
X.B. Li and J. Zhang
Imperial College London, United Kingdom

P2-8: Molecular beam epitaxial growth of antimony compounds on indium-free GaSb substrates
J.B. Héroux, C. Pei and W. I. Wang
Columbia University

P2-9: Real-time Ion Count from Nitrogen Plasma Source
Mark A. Wistey, Seth R. Bank, Homan B. Yuen, Lynford L. Goddard, and James S. Harris
Stanford University

P2-10: Regrowth of Extrinsic Contacts for High-Speed InP-based HBT Devices
V. Gambin, D. Mensa, M. Lange, A. Cavus, D. Sawdai, T. Block, A. Gutierrez-Aitken, and A.Oki
Northrop Grumman Space Technology

P2-11: Optical Properties of Very Low Temperatures Grown Compound Semiconductor by MBE
K. L. Chang, J. H. Epple, K. Y. Cheng, and K. C. Hsieh
University of Illinois at Urbana-Champaign

NAMBE 2003 Program

Wednesday, October 1, 2003

8:00-9:40: Dilute Nitrides

Chair: James Gupta (NRC)

WA-1: Influence of the N_2 background pressure on the incorporation of Arsenic during MBE growth of GaAs
T. Dieing and B.F. Usher
La Trobe University, Australia

WA-2: The effect of hydrogen on the formation of gallium vacancies in GaInNAs
A.J. Ptak, Sarah Kurtz, R.C. Reedy, W.K. Metzger, M.H. Weber*, and K.G. Lynn*
National Renewable Energy Laboratory; *Washington State University

WA-3: Similarities between GaInNP and GaInNAs grown on GaAs (001) substrates
Y. G. Hong, A. Nishikawa, and C. W. Tu
University of California, San Diego

WA-4: Temperature dependence of optical properties of GaInNAs quantum dots grown on GaAs (001)
A. Nishikawa, Y. G. Hong, and C. W. Tu
University of California, San Diego

WA-5: 1.3 micron single lateral mode lasers based on InAs QDs and InGaAsN quantum wells
A.R.Kovsh[1,2], D.A.Livshits[1,2], N.A.Maleev[1,2], A.E.Zhukov[1], V.M.Ustinov[1],J.S.Wang[2], R.S.Hsiao[2], G.Lin[2], J.Y.Chi[2], and N.N.Ledentsov[3]
[1]Ioffe Physico-Technical Institute, Russia; [2]Industrial Technology Research Institute,Taiwan; [3]Technical University of Berlin, Germany

10:10-11:50: Devices and Device Structures I

Chair: Brian Bennett (NRL)

WB-1: High-Power Room-Temperature Continuous Operation of Molecular Beam Epitaxy grown Type-I In(Al)GaAsSb/GaSb diode lasers at 2.7 and 2.8 microns
J.G. Kim#, L. Shterengas*, R. Martinelli# G. Belenky*
#Sarnoff Corporation; *State University of New York at Stony Brook

WB-2: Correlation of Growth Conditions with Photoluminescence and Lasing Properties of Mid-IR Antimonide Type-II "W" Structures
C. L. Canedy, W. W. Bewley, C. S. Kim, M. Kim, I. Vurgaftman, and J. R. Meyer
Naval Research Laboratory

WB-3: MBE Growth of High Power 980 nm Pump Lasers Using In-situ and Ex-situ Monitoring for Production Control
W. Liu, A. Kussmaul, S. Deng, G. Yang, and S.C. Palmateer
Corning Lasertron

WB-4: MBE Growth of Quantum Cascade Lasers on GaAs (111)B Substrates for Second Harmonique Generation
X. Marcadet, V. Ortiz, J.-Y. Bengloan, M. Calligaro, Isabelle Maurin*, and Carlo Sirtori*
Thales Research & Technology, France; *Université Denis Diderot, France

WB-5: Polarization-Controlled lasing of a self-organized InGaAs quantum wire VCSEL grown on (775)B-oriented GaAs substrates by MBE
Y. Ohno[a], Y. Takasuka[b, c], M. Ogurac, K. Komori[c], S. Shimomura[a] and S. Hiyamizu[a]
[a]Osaka University, Japan; [b]Shibaura Institute of Technology, Japan; [c]National Institute of Advanced Industrial Science and Technology, Japan

1:30-3:10: Devices and Device Structures II

Chair: Dan Mars (Agilent)

WC-1: Comparison of As- and P-Based Metamorphic Buffers for High Performance InP HBT and HEMT Applications
D. Lubyshev, J. M. Fastenau, X.-M. Fang, Y. Wu, C. Doss, and W. K. Liu
IQE, Inc.

WC-2: Regrowth of InAlAs/InGaAs/InP DHBT Active Layers
V. Gambin, D. Mensa, M. Lange, A. Cavus, D. Sawdai, T. Block, A. Gutierrez-Aitken, and A.Oki
Northrop Grumman Space Technology

WC-3: Metamorphic 6.00 Å HBTs on InP by MBE
M. Lange, C. Monier, R. Sandhu, A. Cavus, T. Block, V. Gambin, D. Sawdai, and A. Gutierrez-Aitken
Northrop Grumman Space Technology

WC-4: Comparison AlInAs and InAsP Tunnel Barriers for Implementation in InAs-Based Bipolar Transistors
K. L. Averett[1] X. Wu[2], M. W. Koch[2], and G. W. Wicks[2]
[1]Air Force Research Laboratory; [2]University of Rochester

WC-5: MBE Growth of AlGaPSb/InP DBRs on InP
J. F. Klem[1], D. K. Serkland[1], J. Kim[2], and T.- Y. Wang[2]
[1]Sandia National Laboratories; [2]Honeywell International

End of Main Conference

NAMBE 2003 Program

Thursday, October 2, 2003

Workshops are scheduled from 8:00-3:00, including a morning coffee break and lunch.

1. **Production of Next-Generation MBE Materials**
   Chairman: Tom Block, Northrop Grumman Space Technology (thomas.block@ngc.com)
   This workshop will explore moving next-generation MBE materials into production. The format of the workshop will be presentations by experts in the different materials, followed by group discussions. Each speaker will address the following topics in their presentation:
   - Advantages of new materials over existing production technologies
   - Applications and opportunities for new materials
   - Significant growth-mechanics related challenges remaining
   - Equipment improvements desirable for production

   The final portion of the workshop will follow up previous workshops on in-situ measurement and safety.

   List of Invited Speakers:

   Ben Heying, Northrop Grumman Space Technology
   "GaN for electronics"
   Henning Riechert, Infineon Technologies
   "Dilute nitrides"
   Brian Bennett, Naval Research Labs
   "Sb materials for electronics,"
   Aaron Ptak, National Renewable Energy Lab
   "Novel III-Vs for solar cells,"
   Amy Liu, IQE
   "Novel III-V production technology"
   Paul Pinsukanjana, Intelligent Epitaxy Technology
   "In-situ monitoring and control in MBE,"
   Kris Bertness, National Institute of Standards and Technology
   "Absolute composition calibration standards,"
   Thomas Block, Northrop Grumman Space Technology
   "Phosphorous maintenance safety,"

2. **Long Wavelength Optoelectronics**
   Chairman: Yong-Hang Zhang, Arizona State University (yhzhang@asu.edu)

   The Long Wavelength Optoelectronics Workshop offers a great forum for the MBE growth of optoelectronic materials and devices. More emphasis will be placed on the growth and materials related issues, new approaches for their improvement, and device concepts. It will be organized in two serial sessions, i) Near IR Session, which will cover the wavelengths up to 2 micron; ii) MWIR and Beyond, which covers from 2 micron up to THz radiation. The workshop will be casual and stimulating. We strongly encourage every attendee, from university graduate students to senior researchers, to actively participate.

List of Invited Speakers

Near IR Session

James Harris, Stanford University.
"GaInNAsSb, A New Material in the Quest for Communication Lasers"
James Gupta, NRC, Canada
"MBE Growth of Dilute Nitrides for Long Wavelength Optoelectronics"
Shane Johnson, S. Chaparro, P. Dowd, *et. al.*, Arizona State University and Lytek Corporation
"Long Wavelength GaAsSb/GaAs VCSEL on GaAs Substrate"
A.R.Kovsh, A.F.Ioffe Physico-Technical Institute and Industrial Technology Research Institute, Hsinchu, Taiwan, ROC.
"Recent Achievements in MBE Technology of Long-Wavelength (1.3 -1.5 um) Quantum Dot Lasers Based on GaAs"

MWIR and Beyond

John Reno, Sandia National Laboratory
"MBE growth of THz Quantum Cascade Lasers on GaAs,"
Cory J. Hill, Baohua Yang, and Rui Q. Yang, Jet Propulsion Laboratory, California Institute of Technology
"Growth of Antimonide-Based Interband Cascade Lasers on Gallium Arsenide Substrates,"
Z. Shi, F. Zhao, A. Majumda, H. Z. Xu, X. Lu, L. Jayasinghe, S. Khosravani, V. Kelkar, R. Singh, D. Ray, University of Oklahoma
"MBE growth of Mid-infrared IV-VI lead-salt QW VCSEL"

Contributed talks

Y. Cao, S. Yu, X. Jin, D. Ding, J. Wang, S. Johnson, and Y.-H. Zhang, Arizona State University
"Room Temperature CW Operation of 2.1 um Quantum Well Lasers Grown on GaSb"

3. MBE for Quantum Information

Co-chairmen: Richard Mirin, NIST (mirin@boulder.nist.gov)
Nitin Samarth, Penn State (nsamarth@psu.edu)

This workshop will focus on new materials and devices for Quantum Information. Materials such as dilute magnetic semiconductors and quantum dots will be discussed. Important topics of discussion will include what advances need to be made in MBE growth in order to advance the area of Quantum Information.

List of Invited Speakers

Prof. Jeremy Levy, University of Pittsburg
"Oxide-Semiconductor Materials for Quantum Computation"
Prof. Michael Flatté, University of Iowa
1. An Introduction to Quantum Information Technologies: A Range From "You Can Buy It Now" to "Can It Ever Be Done?"
2. Molecular Beam Epitaxy Challenges from Quantum Information Technologies
Dr. Tom Reinecke, Naval Research Laboratory
"Semiconductor Nanostructures for Quantum Information Technology"
Dr. David Pappas, National Institute of Standards and Technology
"Epitaxial materials for solid state quantum computing applications"

The workshop will consist of talks in the morning, followed by a panel discussion after lunch. The goal of this workshop is to examine critical issues that MBE needs to address in order to expedite progress in realizing solid state quantum computers.

NAMBE 2003 Program

Monday, September 29, 2003

8:10-10:10: Quantum Structures I

Chair: Norman Cheng (University of Illinois)

MA-1: Enhancement of one dimensionality by stacking effect of self-organized In0.53Ga0.47As quantum wires grown on (221)B-oriented InP substrates by MBE
S. Shimomura, K. Hyodo, A.Shigenobu,Y. Ohno, T. Kitada, and S. Hiyamizu
Osaka University, Japan

MA-2: Temperature Stabilized 1.55 μm Photoluminescence in InAs Quantum-Dots grown on InP
Z. H. Zhang and K. Y. Cheng
University of Illinois at Urbana-Champaign

MA-3: Improvement on the InAs quantum dot size distribution by employing high temperature GaAs(100) substrate treatments
N. Saucedo-Zeni, A. Yu. Gorbatchev, A. Lastras-Martinez, and V.H. Méndez-Garcia
Universidad Autonoma de San Luis Potosi, Mexico

MA-4: Extending the Emission of InAs/GaAs Self-Assembled Quantum Dots Beyond 1.3 μm Using Capping Effects
B. J. Riel, P. J. Poole, Z. R. Wasilewski, and S. Raymond
National Research Council-Canada

MA-5: Study of Structural and Optical Properties of Quantum Dots-in-a-Well Heterostructures
P. Rotella, G. von Winckel, S. Raghavan, A. Stintz, and S. Krishna
University of New Mexico

MA-6: Heterostructures for Achieving Very Large Responsivity in InAs/GaAs Quantum Dot Infrared Photodetectors
S. Chakrabarti[a)], A.D. Stiff-Roberts[a)], P. Bhattacharya[a)], and S. Kennerly[b)]
[a)]University of Michigan; [b)]Army Research Laboratory

Enhancement of one dimensionality by stacking effect of self-organized $In_{0.53}Ga_{0.47}As$ quantum wires grown on (221)B-oriented InP substrates by MBE

S. Shimomura, K. Hyodo, A.Shigenobu,Y. Ohno, T. Kitada, and S. Hiyamizu

Department of Physical Science, Graduate School of Engineering Science, Osaka University, Toyonaka, Osaka 560-8531, Japan

Recently, we have reported high-density self-organized $In_{0.53}Ga_{0.47}As/In_{0.52}Al_{0.48}As$ quantum wire (QWR) structures with 1.3 μm range light emission can be fabricated on (221)B-oriented [15.8° off (111)B toward (110)] InP substrates by molecular beam epitaxy (MBE). The (221)B InGaAs QWRs have high uniformity (photoluminescence (PL) full width at half maximum (FWHM) = 17 meV) but small one-dimensionality resulting in small PL polarized degree ($P = I_{//} - I_{\perp} / I_{//} + I_{\perp} = 0.13$), where $I_{//}$ ($I_{\perp}$) is the intensity of PL polarized along (vertical to) the wire direction. In this work, we grew stacked (221)B $In_{0.53}Ga_{0.47}As$ QWRs structures separated with much thinner InAlAs barrier layers and achieved larger one-dimensionality.

We grew the stacked (221)B InGaAs QWR structures consist of three $In_{0.53}Ga_{0.47}As$ QWR layers and two thin $In_{0.52}Al_{0.48}As$ barrier layers. An Interface of $In_{0.52}Al_{0.48}As$ on $In_{0.53}Ga_{0.47}As$ ($In_{0.53}Ga_{0.47}As$ on $In_{0.52}Al_{0.48}As$) was is corrugated at a period of 25 nm (20 nm) and amplitude of 0.9 nm (0.8 nm). Hence, QWR confinement potential is induced by the thickness modulation of the $In_{0.53}Ga_{0.47}As$ well layers. The $In_{0.53}Ga_{0.47}As$ QWR layers was nominally 3.3 nm thick and three kind of thin barrier layers with Lb = 1,2,3 nm were inserted to allow electrons (hole) in each InGaAs layer penetrate to the adjacent QWR layers. The QWR sample with three InGsaAs layers (3.3 nm) thick and (20-nm-thick) $In_{0.52}Al_{0.48}As$ barrier layers was also grown as a reference sample. Polarization dependence of PL(12K) spectra from the (221)B stacked InGaAs QWRs samples and a reference (221)B InGaAs QWRs are shown in Fig.2. Single PL peak was observed from each sample and it was polarized in the wire direction. For instance, PL peak energy was gradually decreased with decreasing, L_b, and a PL peak of the sample with L_b =2 nm was observed at 1239 nm which was 11 nm longer than that of the reference QWRs. Increase of red shifts increased overlapping of the carrier wave functions between the adjacent InGaAs wells. The sample with L_b = 2 nm showed smaller PL-FWHM of 12 meV and a larger polarized degree of P = 0. 20 compared with those of the reference sample (Fig. 3).

Corresponding author : S. Shimomura

E-mail:shimomura@mp.es.osaka-u.ac.jp,Phone:+81-6-6850-6457,Fax:+81-6-6845-4632

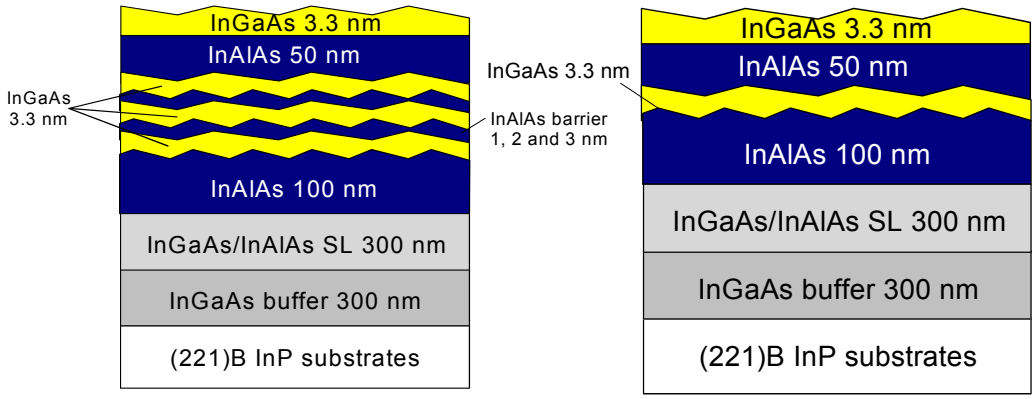

Fig. 1: Schematic illustration of stacked and reference self-organized (221)B InGaAs/InAlAs QWRs

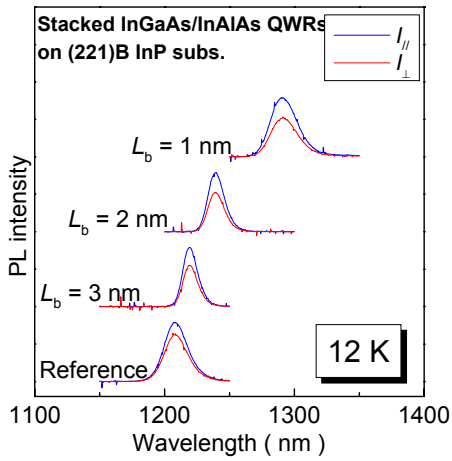

Fig. 2: Polarization dependence of PL spectra from the stacked (221)B InGaAs/InAlAs QWRs with L_b =1, 2 and 3 nm and a reference (221)B InGaAs/InAlAs QWRs

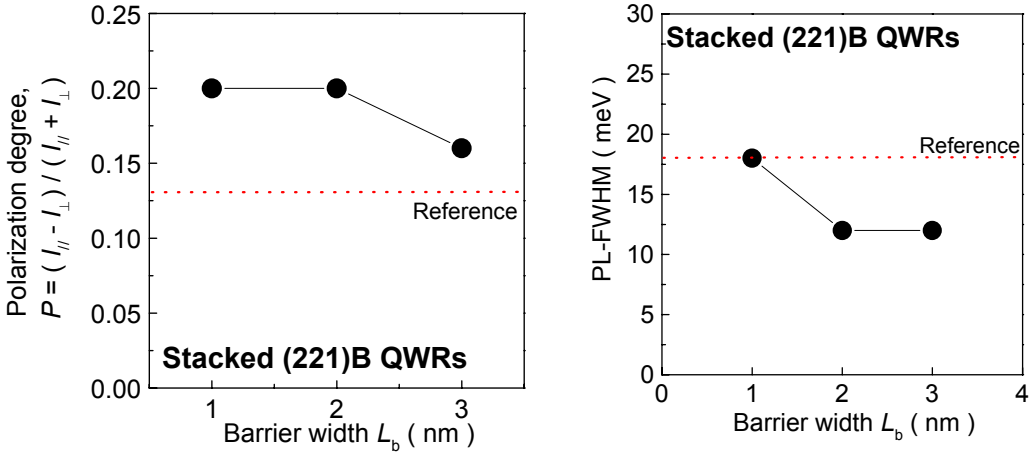

Fig.3 (a) Polarized degree and (b) PL-FWHM of PL peaks for the stacked (221)B InGaAs/InAlAs QWRs as a function of barrier width L_b.

Temperature Stabilized 1.55 μm Photoluminescence in InAs Quantum-Dots Grown on InP

Z. H. Zhang and K. Y. Cheng
Department of Electrical and Computer Engineering, and Micro and Nanotechnology Laboratory
University of Illinois at Urbana-Champaign, 208 N. Wright St., Urbana, IL 61801
Phone: 217-333-4053, Fax: 217-244-6375, Email: zzhang8@uiuc.edu

Quantum dot (QD) lasers have been proven to have some unique device characteristics such as a low threshold current density, a weak threshold current dependence on temperature, and a moderate chirp property. In order to utilize the QD laser for optical communications, QD structures with emission wavelengths near 1.55 μm are required. Since it is difficult to realize 1.55 μm emission in InAs/GaAs QD system, attentions are shifted to the InP based InAs QD system.

The emission wavelength of semiconductor lasers varies with temperature due to a temperature-dependent band gap energy. Wohlert et al. demonstrated a temperature stabilized photoluminescence (PL) near 1.6 μm in InGaAs quantum wire (QWR) structures grown on InP [1]. In this study, we report the observation of a temperature stabilized PL emission centered near 1.55 μm in InAs QDs and the origin of this phenomenon is discussed. The InAs self-assembled QDs were grown on $In_{0.52}Al_{0.24}Ga_{0.24}As$ buffer layers lattice matched to InP. On-axis [100] InP wafers were used as substrates. Atomic force microscopy (AFM) and PL measurements have been used to characterize the InAs QDs. Through the control of growth parameters, such as As overpressure, substrate temperature, and QD layer thickness, InAs QDs with high density up to 5×10^{10} cm^{-2} have been achieved, as shown in Fig. 1. This is the highest InAs QD density achieved on (100) on-axis InP substrates. Nevertheless, higher dot density was observed in InAs QDs grown on high index (311)B InP substrates [2]. Room-temperature and 77K PL measurements show the temperature stabilized emission near 1.55 μm (Fig. 2). It should be noticed that the 77K emission peak (~1.15 μm) from the InAlGaAs barrier layer has a conventional red-shift when temperature increases. To study the origin of this temperature stabilized emission, two groups of samples were prepared. In the first group, InAs QDs with different layer thickness were deposited to investigate the effects of the overall strain. In the other group, GaAs layers with different thickness were introduced immediately after the deposition of InAs QD layer to balance the strain caused by the formation of QDs. Figures 3 and 4 show the PL emission wavelength shift between room-temperature and 77K as functions of InAs layer thickness and GaAs layer thickness, respectively. The fact that the InAs QD with larger layer thickness resulted in a smaller wavelength shift, or even a blue-shift in the case of 6.5 ML InAs, indicates that the temperature stabilized emission originates from the strain interactions between compressive strained InAs QDs and InAlGaAs barrier layers. When the InAs QD induced compressive strain is balanced by the tensile strained GaAs upper barrier layer, as shown in Fig. 4, the trend of emission wavelength shows the conventional red-shift with the increasing of temperature. Comparing with QWRs, which also show a temperature stabilized PL, the InAs QD samples have no polarization preference due to their symmetric dot shape. It is believed that the incorporation of temperature stabilized InAs QDs into laser structures will have great potentials for optical communication applications.

[1] D. E. Wohlert, S. T. Chou, A. C. Chen, K. Y. Cheng, and K. C. Hsieh, Appl. Phys. Lett. **68**, 2386, 1996

[2] H. Saito, K. Nishi, and S. Sugou, Appl. Phys. Lett. **78**, 267, 2001

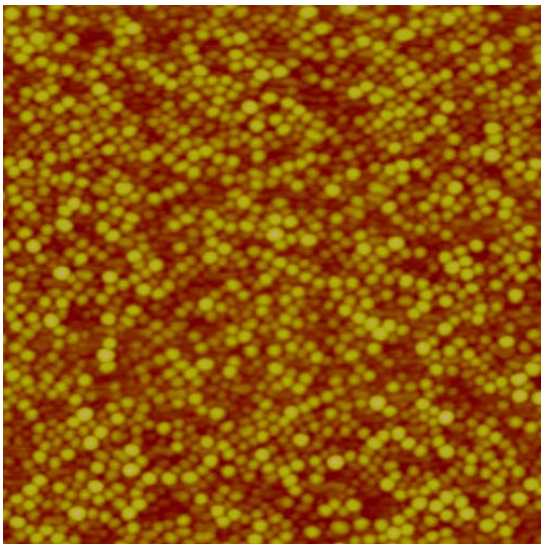

Figure 1. Atomic force microscopy image of InAs QDs grown on InAlGaAs/InP. The size of the image is 2μm×2μm. The dots density is about 5×10^{10} cm^{-2}.

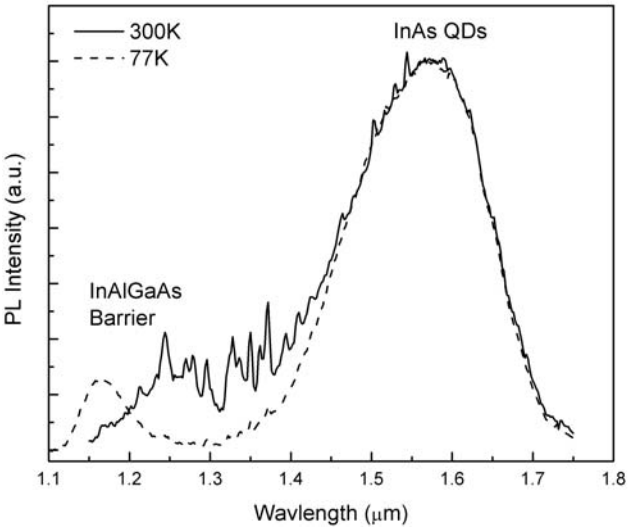

Figure 2. Room temperature and 77K photoluminescence spectra of InAs QDs grown on InAlGaAs/InP. The InAs thickness was 5.5 ML. There is no PL wavelength shift between 300K and 77K for InAs QDs. The peak PL wavelength for InAlGaAs has a 900Å shift between 300K and 77K.

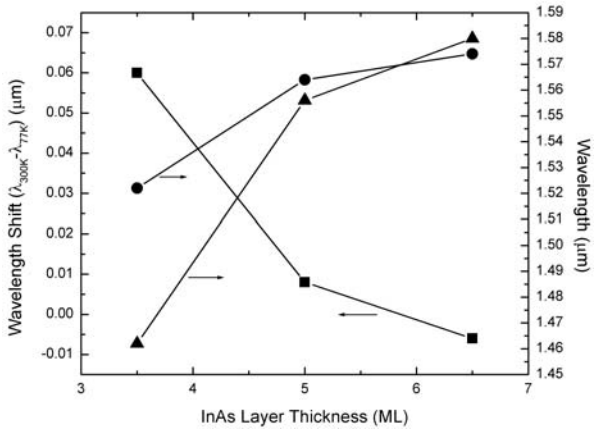

Figure 3. PL wavelength shift between 300K and 77K as a function of InAs layer thickness. The wavelengths of these samples at 300K and 77K are also included as a reference. Solid square: wavelength shift; solid circle: wavelength at 300K; solid triangular: wavelength at 77K.

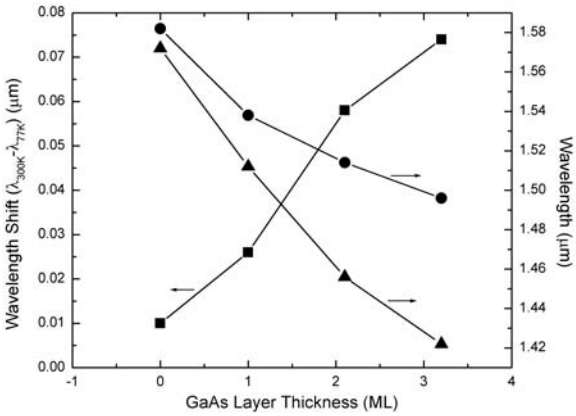

Figure 4. PL wavelength shift between 300K and 77K as a function of GaAs strain-balance layer thickness. The wavelengths of these samples at 300K and 77K are also included as a reference. Solid square: wavelength shift; solid circle: wavelength at 300K; solid triangular: wavelength at 77K.

Improvement on the InAs quantum dot size distribution by employing high-temperature GaAs(100) substrate treatments.

N. Saucedo-Zeni, A.Yu. Gorbatchev, A. Lastras-Martínez and V.H. Méndez-García*.
Instituto de Investigación en Comunicación Óptica, Universidad Autónoma de San Luis Potosí, Av. Karakorum 1470, Lomas 4ª. Sección, San Luis Potosí, S.L.P., México 78210. Tel: +52 444 8250183, Fax: +52 444 8250198, e-mail: vmendez@cactus.iico.uaslp.mx

Nowadays, Quantum Dots (QDs) self-assembling by Stranski-Krastanov (SK) growth mode is an established technique for the preparation of dislocation-free zero-dimensional structures. However, the spontaneous nature makes difficult to control size, density and size homogeneity of QDs. Controlling their arrangement at SK growth mode would have a powerful impact on the effectiveness of QDs based electronic and optical devices. In this work we report on the effects of exposing the GaAs substrate a high temperature, under a molecular Si-flux (Sample B) and under no Si flux (Sample C) on the self-assembling of InAs QDs. For the growth, a Riber 32 MBE system was used employing SI-GaAs(100) substrates. After the oxide desorption process, a 0.5 μm-thick GaAs buffer layer was grown at 600ºC. Immediately after that, the substrate temperature was raised up to 650ºC and then, the As_4 shutter was closed for 10 seconds. Sample B was irradiated with Si during this interval. Sample C was kept with no As or Si flux during this time interval. After this procedure, the As_4 shutter was opened again and the substrate temperature was lowered to ~500ºC in order to start InAs QDs deposition. A conventional InAs QDs growth was made for comparison purposes (Sample A). For Samples A and B an equivalent thickness of 2.1 InAs monolayers (MLs) were grown, while for Sample C 3.4 MLs was deposited. In all samples, InAs growth was interrupted after deposition of 0.4 MLs, after the 2D-3D transition. Fig. 1 shows the RHEED specular spot intensity evolution for Samples B and C during the substrate exposure at high temperature with no As flux. We observed for both samples an abrupt drop in the RHEED intensity just after the As_4 shutter was closed, and a subsequent recovery once the As_4 flux was reestablished. Also the initial RHEED pattern did not show any visible changes with high temperature treatment (insets of Fig. 1). Therefore, there seems that this treatment did not induce significant differences in the samples. However, when InAs deposition started, important changes on the InAs nucleation were observed. For instance, the 2D-3D transition which is frequently observed at 1.7 MLs, was delayed for 1.3 MLs with respect to Sample C. On the other hand, in Fig. 2 we show the atomic force microscopy (AFM) images for the studied samples along with their respective QDs size histograms. Considerable differences on the QDs morphology are observed. For the Si treated sample (Sample B), the diameter distribution shows almost the same standard deviation (σ=8Å) as the conventional QDs growth (Sample A), but the islands average diameter is larger (12nm for Sample A, and 18nm for Sample B). Moreover, for Sample C a significant improvement on the InAs QDs size distribution can be clearly observed (see Fig. 2(c)). We obtained for this sample a diameter standard deviation of σ=5Å, while the average diameter of the QDs is 24nm. Heights also observed to experience a significant reduction on their standard deviation. Average heights were 3, 4.3 and 5.3 nm for Samples A, B and C, respectively. Therefore, the former results indicate that, by applying the thermal treatments described previously to the GaAs substrate, it is possible to tailor the size distribution of the InAs QDs which is a current demand on QDs based technology. Finally, as a consequence of the changes on size distribution, photoluminescence (PL) spectroscopy at 17 K revealed a redshift in the emission energy for samples subjected to the high-temperature treatments (Samples B and C). *Also at Facultad de Ingeniería, UASLP.

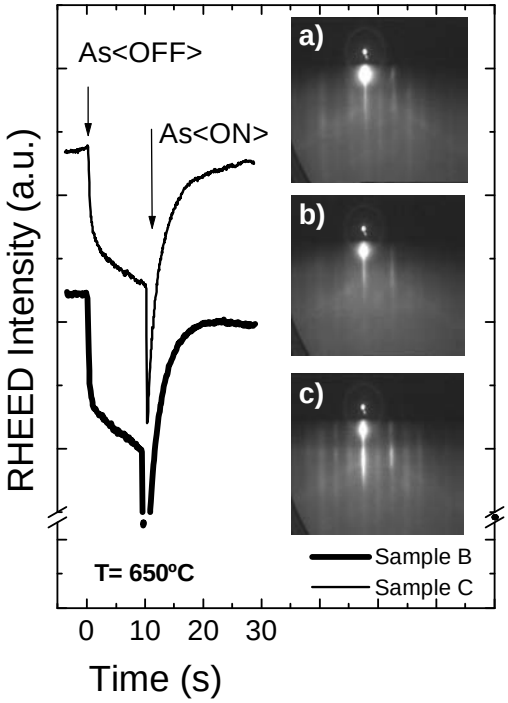

Fig. 1. RHEED specular spot intensity behavior observed when the As_4 shutter was closed at 650°C. Insets show the respective RHEED patterns observed (a) before the high temperature treatment, (b) once the As_4 shutter was closed and, (c) when the As_4 shutter was opened again.

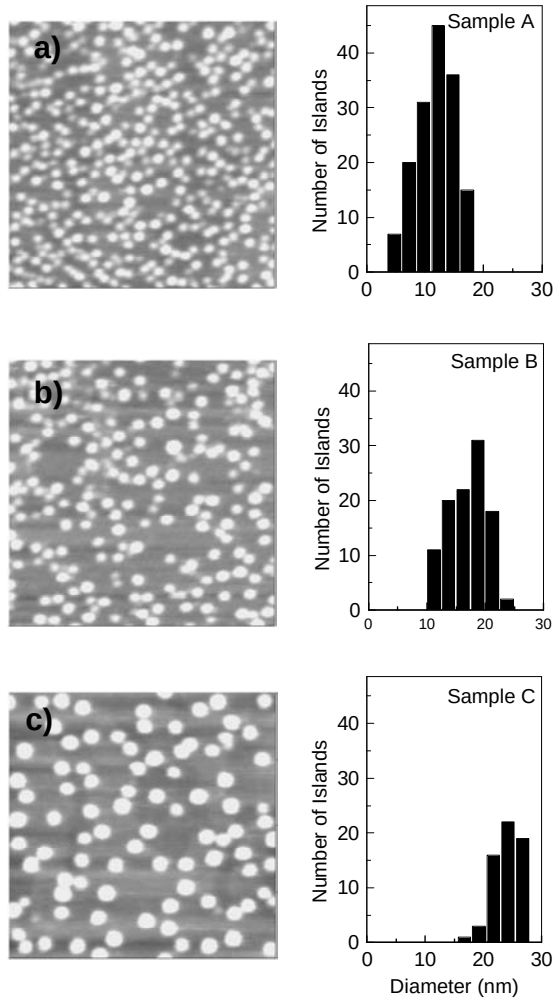

Fig. 2. 400×400 nm^2 AFM images and InAs QDs diameter histograms grown (a) conventionally (Sample A), (b) on GaAs substrate subjected for 10 s to a high temperature and irradiated with Si-flux (Sample B) and, (c) on GaAs substrate subjected at 650°C without any flux (Sample C).

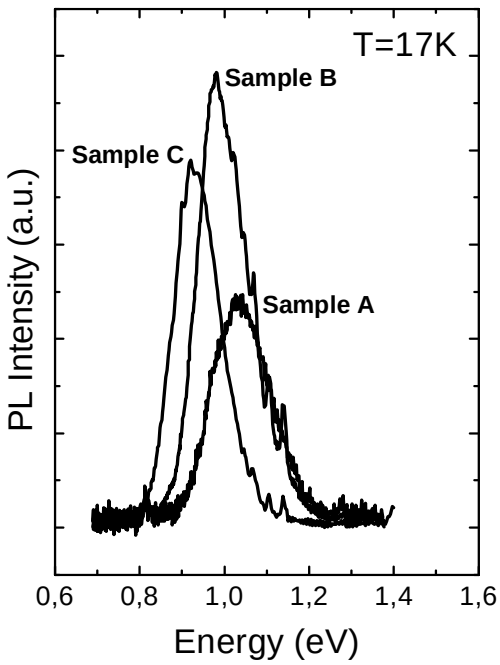

Fig. 3. Photoluminescence spectra from samples shown in Fig. 2. The gradual increase on the dimensions of the InAs QDs was reflected in the redshift of the emission peak observed for Samples B and C.

Extending the Emission of InAs/GaAs Self-Assembled Quantum Dots Beyond 1.3 µm Using Capping Effects

B. J. Riel, P. J. Poole, Z. R. Wasilewski, S. Raymond
Institute for Microstructural Sciences, National Research Council, Ottawa, Ontario, Canada K1A 0R6.

Adjusting the growth control parameters during the deposition and annealing of strained material has been extensively explored. To obtain highly uniform self-assembled quantum dot (QD) ensembles and tailor designed energy levels, the size and shape of QDs can be engineered using the following growth control parameters: (1) the amount of deposited strained material, (2) the growth temperature, (3) the arsenic pressure, and (4) the deposition rate and anneal time which together determine the total time over which the QDs evolve [1]. This has allowed for the designing of the ground state emission of InAs/GaAs QDs over a range of more than 200 nm.

The expertise acquired at the Institute for Microstructural Sciences of the National Research Council of Canada in the growth of self-assembled InAs QDs on GaAs by molecular beam epitaxy (MBE) has recently been successfully transferred to chemical beam epitaxy (CBE) growth using TMIn, TEGa and pre-cracked arsine. Equivalently excellent material displaying well resolved excited state structures has been produced as shown in Fig. 1.

We studied CBE grown InAs/GaAs QDs as a function of GaAs growth rate, arsenic pressure, and substrate temperature during capping. Adjustment of these conditions produced significant emission shifts observed in room temperature photoluminescence (PL): Fig. 2 shows the effects of varying the GaAs growth rate; Fig. 3 shows the effects of varying the substrate temperature; and Fig. 4 is an example of a PL spectrum of a highly uniform QD ensemble optically active beyond 1.3 µm. This last sample was produced by optimising the growth parameters for each step in the QD formation process, namely the deposition of the strained material, the annealing (evolution) of the QDs, and the capping of the QDs. This exploits the rapid gas switching in CBE which allows for sudden changes in group III and group V fluxes.

We will present microscopy of uncapped QDs and photoluminescence of capped quantum dots grown in nominally identical conditions demonstrating the effects of the growth rate, arsenic pressure, and substrate temperature during the overgrowth of nominally pure InAs QDs with GaAs. We will discuss the effects of the mechanisms by which QDs are modified during the capping procedure, and compare the capping effects in the InAs/GaAs and InAs/InP systems.

[1] B.J. Riel et al, J. Crystal Growth 236 (2002) 145.

Bruno J. Riel: (613) 993-4177, bruno.riel@nrc.ca

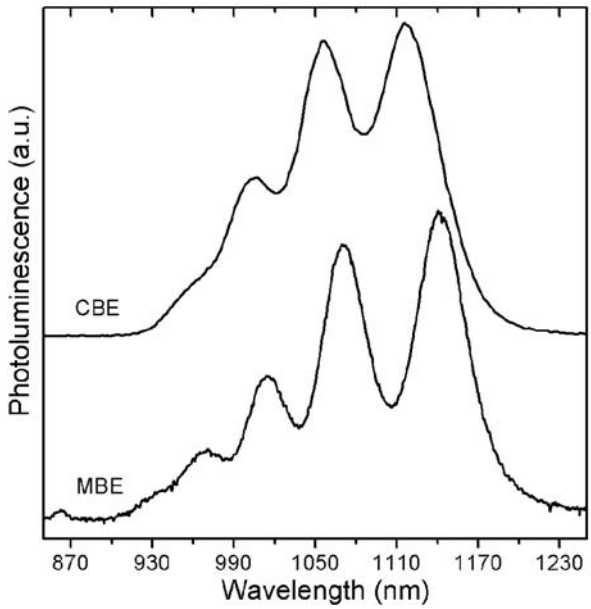

Figure 1: Comparison of similarly grown MBE and CBE InAs-QD/GaAs samples. The PL was measured at 77K. The spectra were normalized to the same intensity.

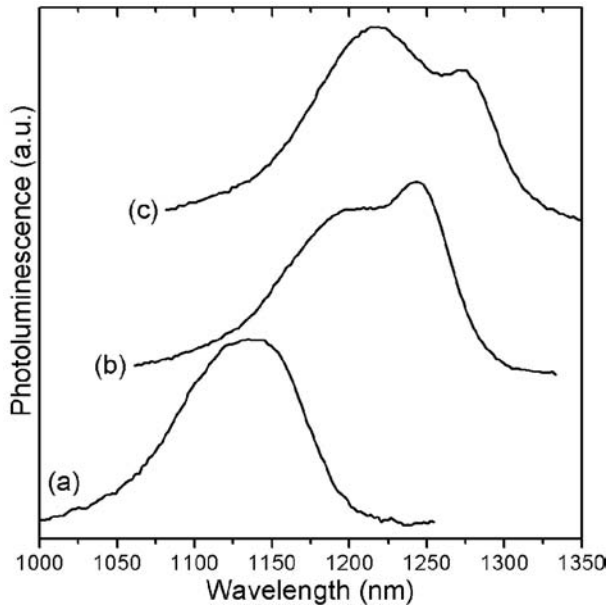

Figure 2 : Evolution of the QDs as a function of GaAs growth rate during capping, approximately: (a) 2 Å/s, (b) 5 Å/s, and (c) 10 Å/s. The PL was measured at room temperature. The spectra were normalized to the same intensity.

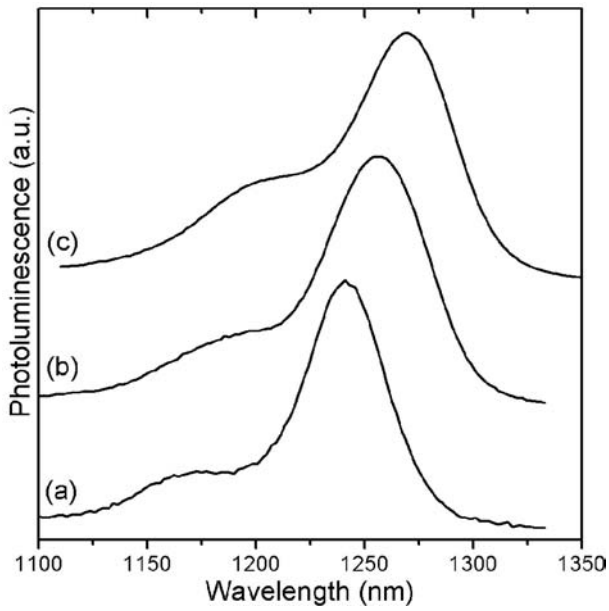

Figure 3 : Evolution of the QDs as a function of substrate temperature during capping: (a) 500 °C, (b) 480 °C, and (c) 455 °C. The PL was measured at room temperature. The spectra were normalized to the same intensity.

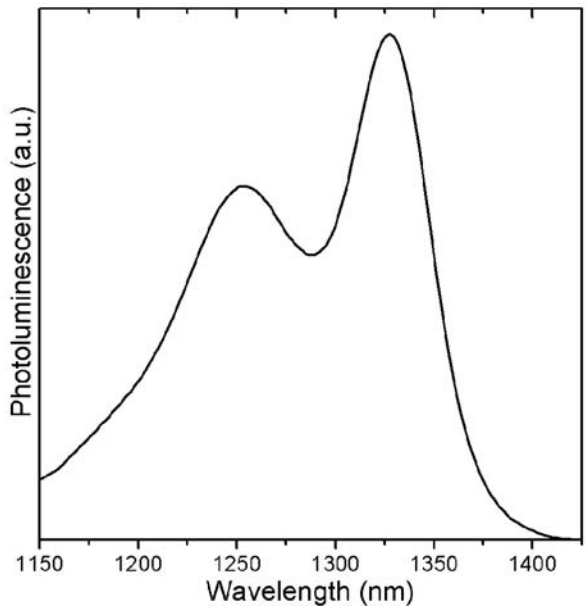

Figure 4: QD ground state and first excited state emission. The PL was measured at room temperature.

Student Paper

Study of Structural and Optical Properties of Quantum Dots-in-a-Well Heterostructures

P. Rotella, G. von Winckel, S. Raghavan, A. Stintz, S. Krishna*
Center for High Technology Materials, ECE Dept.,
University of New Mexico, Albuquerque, NM

Recent research has shown a great deal of progress for quantum dot detectors. However, current quantum dot detectors do not have a dial-in recipe for the operating wavelength of the detector. This lack of precise control is due to the dependence of the operating wavelength on the dot dimensions, which are not easily controlled during epitaxial growth. One method to help control the absorption wavelength is to use a quantum dots-in-a-well (QDWELL) structure. In the QDWELL structure, InAs dots are placed in an InGaAs quantum well, which in turn is placed in a GaAs barrier. By varying the thickness of the InGaAs well, the operating wavelength can be tailored. When the well width is increased, the higher energy states in the heterostructure move closer to the electron ground state in the dot. This decrease in the energy between the dot and well leads to an increase in peak operating wavelength of the sample. The operating wavelength can also be increased by decreasing the dot size. Smaller dots can be grown by reducing the growth temperature during the molecular beam epitaxy process, with the intention of pushing the ground state closer to the well state.

In this study, we investigate the effects of the operating wavelength by changing the dimensions of the well on both sides of the quantum dots. Seven samples are studied where the thickness below the quantum dot layer (t_{bot}) varies from 10 to 70 Angstroms, and from 40 to 60 Angstroms on top of the quantum dot layer (t_{top}). Photoluminescence, Absorption and cross sectional transmission electron microscopy (XTEM) were performed on these samples to determine their structural and optical properties. Figure 1 shows the XTEM image of the sample with the widest well (1388) and it is clearly seen that the InAs dot is confined to the upper half of the InGaAs well. The base and the height of the dot is about 13 nm and 5 nm, respectively. Figure 2 (a) shows the photoluminescence spectra of the seven samples. Figure 2(b) is a table of the peak PL energy, and the difference of energy in the conduction band (CB) between the GaAs conduction band edge and the InAs QD ground state for the seven samples. A 60:40 CB rule was used in the calculation. It is to be noted that the maximum variation in the peak energy for the samples is about 35 meV. Although this variation does not seem large, the difference between an atmospheric wall detector at 7.2 μm (sample 1199) and an atmospheric window detector at 10.06 μm (sample 1420) is less than 50meV. The photocurrent spectra of these two detectors are shown in Fig. 3. This shows that we can control the peak-operating wavelength of the DWELL detectors by varying the parameters of the heterostructure. Structural and optical properties of all the samples will be discussed in detail in the presentation.

Work supported by DOE Basic Energy Sciences Grant DE-FG03-02ER46014

* Corresponding Author: skrishna@chtm.unm.edu

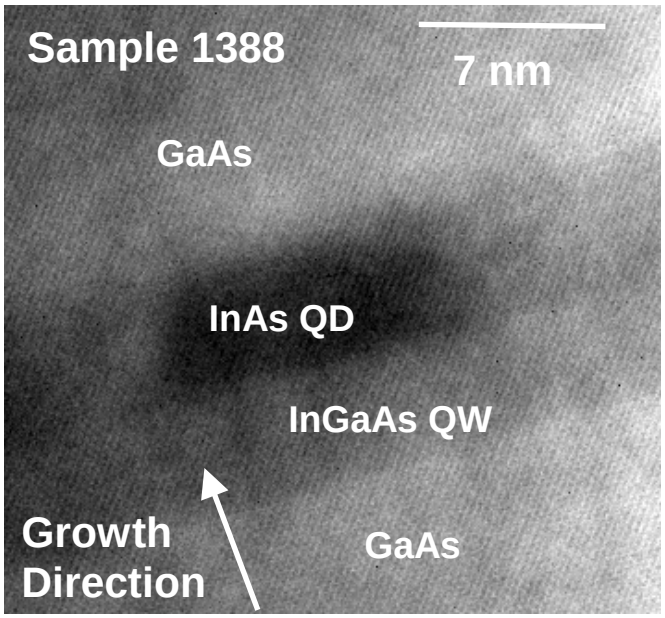

Figure 1: Cross sectional transmission electron microscopy image of a single InAs quantum dot in a 12 nm $In_{0.15}Ga_{0.85}As$ quantum well.

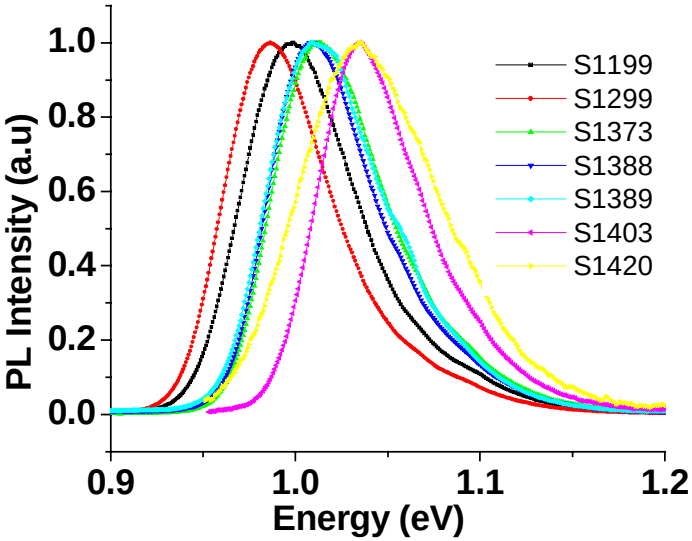

Sample #	t_{bot}(nm)	t_{top}(nm)	T_{dots}(C)	Peak energy (eV)	$E_{GaAs} - E_{dot}$ (eV)
1199	1	6	490	1.242	0.1068
1299	3	6	480	1.257	0.0978
1373	5	6	480	1.225	0.117
1388	6	6	480	1.229	0.1146
1389	5	6	475	1.229	0.1146
1403	7	4	480	1.198	0.1332
1420	5	6	475	1.198	0.1332

Figure 2: Photoluminescence spectra of the seven samples with different well widths and growth temperatures

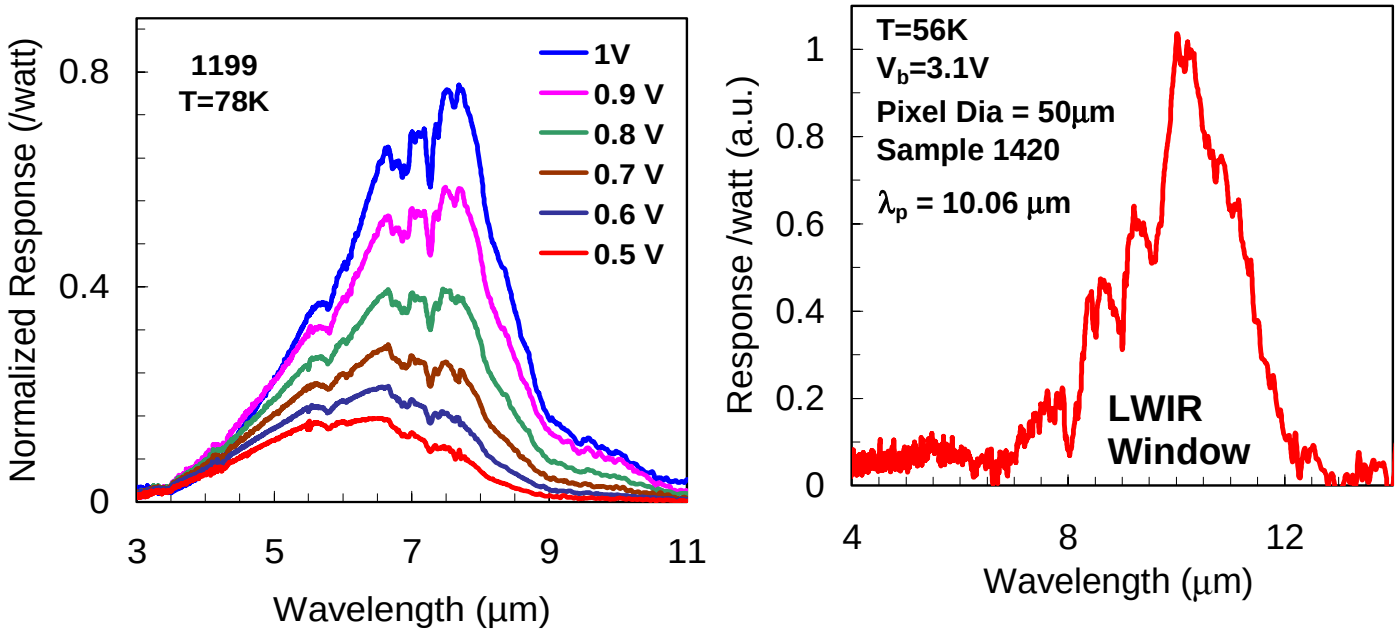

Figure 3: Normalized spectral response of the DWELL detector with (a) 7 nm QW and (b) 12 nm QW

Heterostructures for Achieving Very Large Responsivity in InAs/GaAs Quantum Dot Infrared Photodetectors

S. Chakrabarti[a)], A.D. Stiff-Roberts[a)], P. Bhattacharya[a), 1], and S. Kennerly[b)]

a) Solid State Electronics Laboratory, Department of Electrical Engineering and Computer Science, University of Michigan, Ann Arbor, MI 48109-2122

b) Sensors and Electron Devices Directorate, Army Research Laboratory, Adelphi, MD 20783

Abstract[2]

Quantum dot infrared photodetectors (QDIPs) utilizing intersubband transitions in the quantum dot (QD) conduction band are a relatively new technology for detection in the mid-wave and long-wave infrared ranges[3]. The three-dimensional quantum confinement of electrons in QDIPs yields unique device characteristics such as inherent sensitivity to normal-incidence radiation, low dark current, and high-temperature operation. While QDIPs theoretically surpass the performance of other IR photodetectors[4,5], the expected superior performance has not been demonstrated consistently, particularly in terms of responsivity, a measure of the generated photocurrent for a given incident photon power. In order to realize the full potential of QDIPs, the responsivity must be increased from ~mA/W or less to ~A/W, especially for low-background applications, where responsivity is the most relevant figure of merit (as opposed to the detectivity – a normalized signal-to-noise ratio). In this paper, we describe the molecular beam epitaxial (MBE) growth and device characteristics of two InAs/GaAs QD heterostructures which demonstrate an increase in the measured QDIP responsivity by two to three orders of magnitude.

In the first heterostructure, we incorporate as many as 70 QD layers to enhance intersubband absorption. In order to inhibit the generation/propagation of dislocations, 50 nm GaAs barriers, grown with temperature cycling (490-590°C), are incorporated between the QD layers of the n-i-n device heterostructure. XTEM measurements show little or no defect generation/propagation, and photoluminescence measurements indicate that the emission linewidth (FWHM) remains relatively constant (≈ 60 meV) as the number of QD layers is increased to 70. QDIPs fabricated with this heterostructure exhibit a peak absorbance at 8.9 µm. Under V_{bias} = 2.0 V the measured responsivity is 0.12 A/W at 175 K, which is ~ 100 times greater than that measured in a 10-layer QD device[6]. This is also one of the highest operating temperatures reported for a QDIP. Measured dark currents at 175 K and 2V bias are as low as 10^{-7} A/cm^2 and D* = 4.5×10^7 cmHz$^{1/2}$/W.

In the second type of QDIP, a periodic heterostructure is used as the barrier material in which minibands are created[7]. These minibands provide two advantages: they provide more states which the photoexcited electrons from the QD states can occupy, and they allow efficient miniband conduction of the photoexcited electrons to the contact. The entire active region is grown at ~ 500°C to increase the density of dots grown directly on AlAs. This 'superlattice' QDIP has yielded a responsivity of 2.5 A/W and a conversion efficiency of 71 % at a bias of -1.5 V at 78 K. The responsivity, therefore, is 20 times larger than that for the 70-layer device, and these detectors exhibit state-of-the-art performance for QDIPs. The growth and properties of these devices will be described and discussed.

---

[1] Email: pkb@eecs.umich.edu, Phone: (734) 763-6678, Fax: (734) 763-9324. [2] This work is supported by ARO and DARPA. [3] E. Towe and D. Pan, IEEE J. Select. Top. Quant. Electron., **6**, 408 (2000). [4] V. Ryzhii, Semicond. Sci. Technol., **11**, 759 (1996). [5] J. Phillips, J. Appl. Phys., **91**, 4590 (2002). [6] A. D. Stiff, et. al., IEEE J. Quant. Electron., **37**, 1412 (2001). [7] L. Rebohle, et. al., Appl. Phys. Lett., **81**, 2079 (2002).

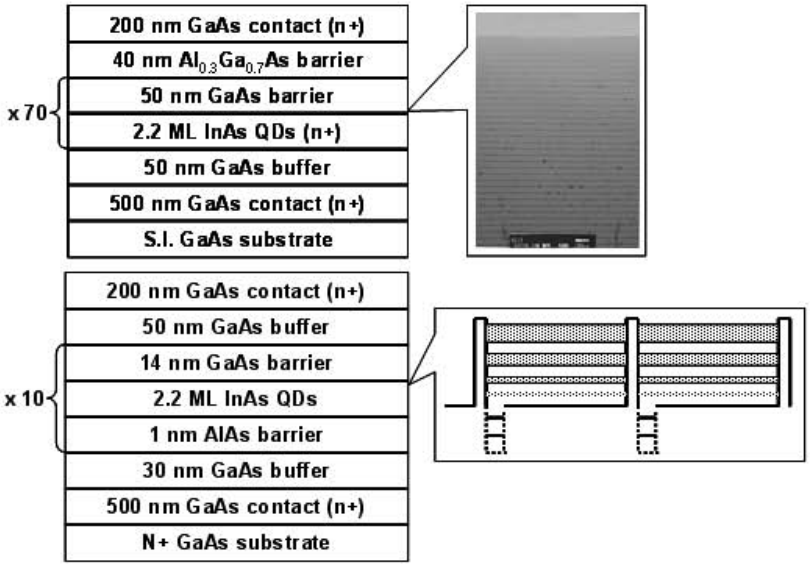

Figure 1. Device heterostructure schematics for (top) 70-layer InAs/GaAs QDIP and (bottom) superlattice QDIP. The top inset shows a XTEM image of the 70-layer QD stack, while the bottom inset shows a schematic of the superlattice QDIP conduction band.

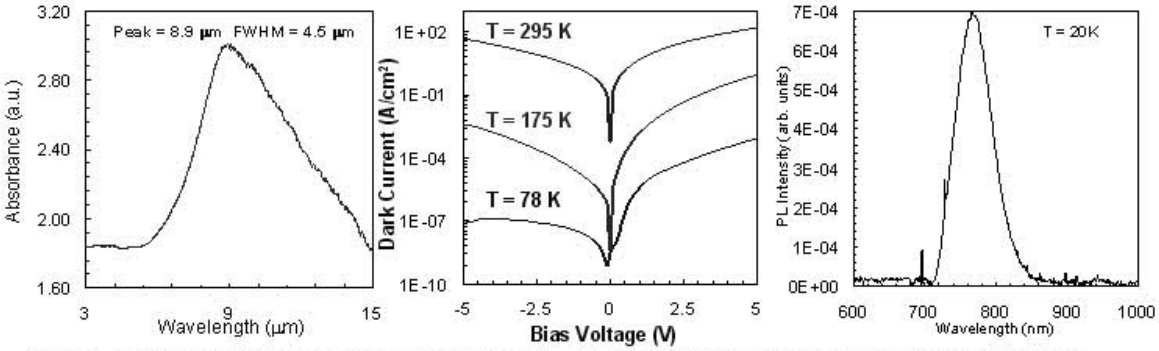

Figure 2. (left) Room-temperature FTIR absorbance spectrum and (middle) dark current I-V curves for 70-layer QDIP. (right) PL spectrum of InAs QDs grown on AlAs for the superlattice QDIP.

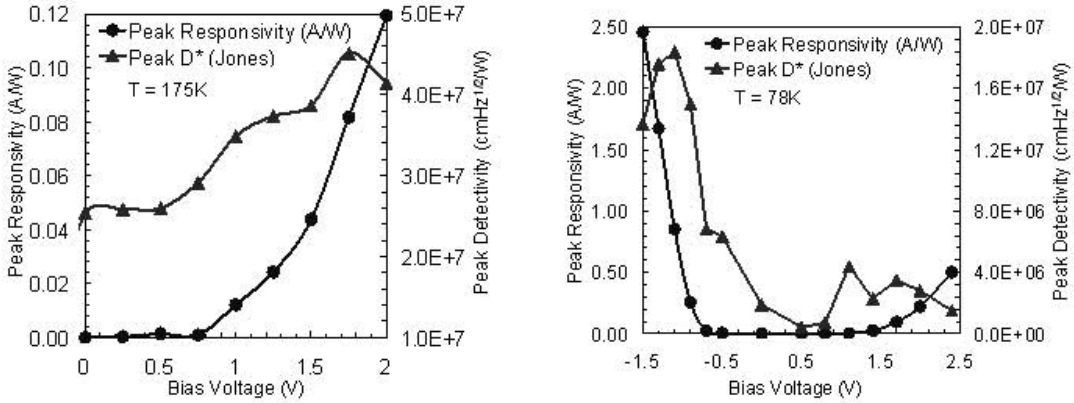

Figure 3. Peak responsivity and detectivity for (left) 70-layer QDIP and (right) superlattice QDIP.

NAMBE 2003 Program

Monday, September 29, 2003

10:30-12:10: Gallium Nitride-Based Growth and Devices

Chair: Shane Johnson (Arizona State University)

MB-1: Periodically Poled GaN Grown by Molecular Beam Epitaxy
Hock M. Ng, Nils G. Weimann, Manish Bhardwaj, and Aref Chowdhury
Bell Laboratories, Lucent Technologies

MB-2: The Effect of Ga-rich Growth Conditions on the Optical Properties of GaN Films Grown by Plasma-assisted Molecular Beam Epitaxy
A.V. Sampath, G. A. Garrett, C. J. Collins, P. Boyd, J. Y. Choe, P. G. Newman, H. Shen, M. Wraback, and R.J. Molnar*
U.S. Army Research Laboratory; *MIT Lincoln Laboratory

MB-3: Efficient p-type doping of GaN films by MBE
A. Bhattacharyya, W. Li, C. Thomidis, T. D. Moustakas, and David J. Smith*
Boston University; * Arizona State University

MB-4: Lateral photocurrent spectroscopy investigation of excitonic absorption in AlGaN/GaN multiple quantum wells grown by molecular beam epitaxy
I. Friel, C. Thomidis, Y. Fedyunin, and T. D. Moustakas
Boston University

MB-5: Polarization-doped 3D electron slabs in graded III-V Nitride heterostructures: MBE growth, physics, and demonstration of the PolFET
D. Jena, S. Heikman, D. Buttari, A. Jimenez, S. Rajan, H. Xing, J. S. Speck, and U. K. Mishra
University of California, Santa Barbara

North American Molecular Beam Epitaxy Conference (NAMBE), Sept. 28 – Oct. 2, 2003, Keystone, CO.

Periodically Poled GaN Grown by Molecular Beam Epitaxy

Hock M. Ng, Nils G. Weimann, Manish Bhardwaj, and Aref Chowdhury
Bell Laboratories, Lucent Technologies
600 Mountain Ave., Murray Hill, NJ 07974, U.S.A.

Periodically poled structures play an important role in frequency conversion applications such as second harmonic generation by quasi-phase matching (QPM) [1]. The most common material for QPM thus far is $LiNbO_3$ which is periodically poled by applying high electric fields. However, the transparency region for $LiNbO_3$ is 350 nm - 5 μm while that of GaN is 365 nm – 13.6 μm. This transparency range can be further extended in the ultraviolet region by employing $Al_xGa_{1-x}N$ which has a bandgap of 6 eV (200 nm) for x=1. In order to obtain QPM in GaN, one of the requirements would be to fabricate a periodically poled structure.

We demonstrate periodically poled GaN (PPGaN) structures grown by plasma-assisted molecular beam epitaxy (MBE). Polarity-controlled growth of wurtzite GaN can be achieved by the presence or absence of an AlN buffer layer grown on (0001) sapphire substrate. Ga-polar GaN is obtained when an AlN buffer layer is first grown at high temperature (700-750 °C) followed by GaN growth. However, if GaN is directly grown on the sapphire substrate at similar high temperatures, the resulting crystal polarity is N-polar. Therefore, we can grow structures with alternating crystal polarity that is periodic in the lateral direction if a suitable patterned template is provided.

The fabrication of PPGaN involved two growth and one photolithography step as shown schematically in Figure 1. In the first growth step, a thin AlN buffer layer (~ 30 nm) was grown followed by a 50 nm layer of GaN to prevent oxidation of the AlN surface upon removal from the growth chamber. A stripe pattern was generated on the sample by photolithography and the unmasked regions were etched down to the sapphire layer. The sample was then cleaned and reintroduced into the growth chamber for the second growth of GaN. During the second growth, the periodically poled structure was automatically generated since Ga- and N-polar GaN grew on GaN/AlN and directly on sapphire, respectively. A scanning electron microscope image of the completed sample is shown in Figure 2. The polarity of the GaN layers was confirmed by observing different reconstruction patterns in reflection high-energy electron diffraction (RHEED) on control samples. Further confirmation of the sample polarity was also obtained by performing chemical etching in KOH solution. Preliminary results on second harmonic generation will also be presented at the conference.

[1] J. A. Armstrong, N. Bloembergen, J. Ducuing, and P. S. Pershan, “Interaction between lightwaves in a nonlinear dielectric,” *Phys. Rev.*, **127**, 1918 (1962).

Corresponding author: Hock M. Ng, E-mail: hmng@lucent.com, Tel: (908) 582-2072

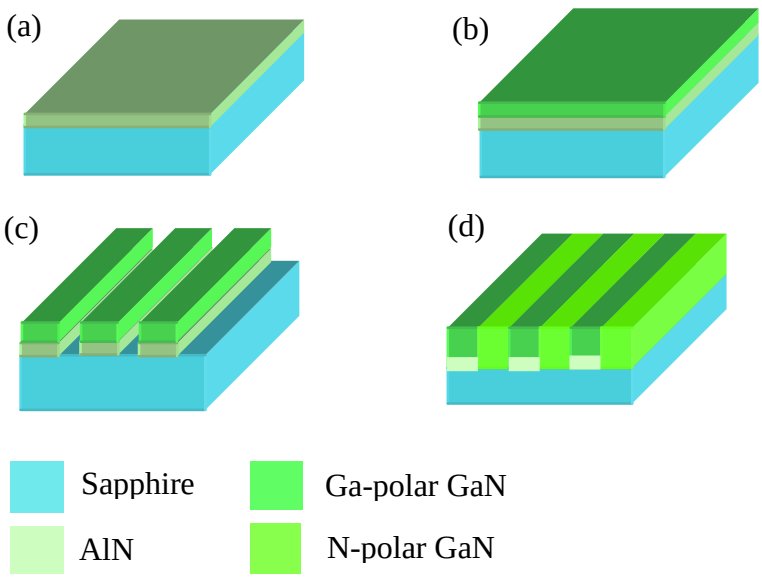

Figure 1: Process steps for fabricating PPGaN include (a) growth of AlN layer on sapphire substrate, (b) growth of GaN cap layer, (c) photolithography and plasma etching to expose striped regions of the sapphire substrate, and (d) subsequent growth of thick GaN.

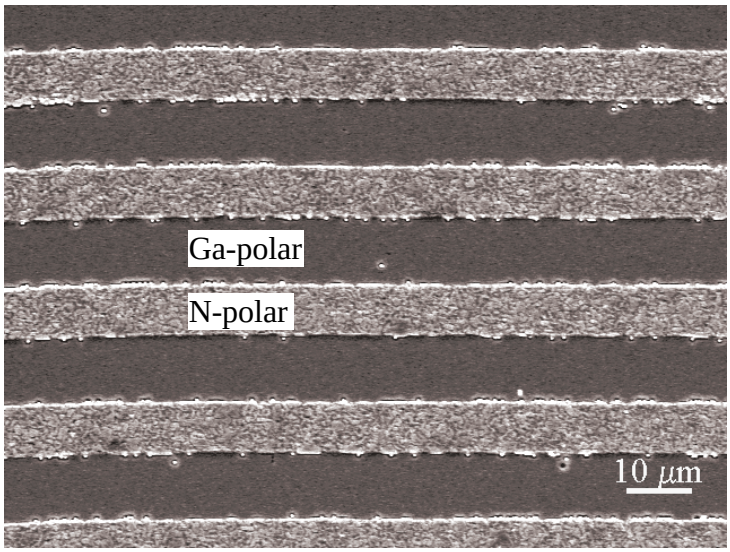

Figure 2: Scanning electron microscope image of a PPGaN sample with a periodicity of 17.2 μm

THE EFFECT OF GA-RICH GROWTH CONDITIONS ON THE OPTICAL PROPERTIES OF GAN FILMS GROWN BY PLASMA-ASSISTED MOLECULAR BEAM EPITAXY.

A.V. Sampath, G. A. Garrett, C. J. Collins, P. Boyd, J. Y. Choe, P. G. Newman, H. Shen, M. Wraback
U.S. Army Research Laboratory, AMSRL-SE-EM, 2800 Powder Mill Road, Adelphi MD, 20783

R.J. Molnar
Massachusetts Institute of Technology, Lincoln Laboratory, 244 Wood Street, Lexington MA, 02420-9108

While it is well known that high quality III-Nitride material is deposited by plasma-assisted molecular beam epitaxy (PA-MBE) only under III-rich conditions, the extent of III-flux required for optimal film growth is unclear. Some work has been reported on this subject with respect to the impact of Ga-rich growth conditions on the structural properties of GaN [1] as well as the performance of AlGaN/GaN 2DEGs [2], but the conclusions have differed. In this paper, we focus on the dependence of the optical properties of the material on the III/V flux ratio. Specifically, we report on the photoluminescence (PL) intensity and the lifetime of photogenerated carriers in homoepitaxially grown GaN films as a function of the Ga flux employed during growth. The samples investigated consisted of ~1.2 micron-thick GaN films grown homoepitaxially under Ga-rich growth conditions by PA-MBE on ~ 80 micron thick GaN templates grown by the hydride vapor phase epitaxy method. The films were deposited under Ga-rich conditions with Ga flux varying from 0.9 to 1.0 $x10^{-6}$ torr while the N-plasma conditions (300W, 0.6 sccm) were held constant. In addition, all of the films were deposited on pieces of the same GaN template to eliminate its effect on the results. AFM studies of the samples found that the surface roughness of samples deposited at intermediate (9.2E-7 torr) and high (1E-6 torr) flux were similar, while films deposited at low Ga flux (9E-7 torr) were considerably rougher. Metal Ga droplets were not observed in any of the films grown under these conditions.The room temperature PL spectra were measured using a HeCd laser with its intensity held constant to enable quantitative comparison. Figure 1 shows that the peak PL intensity in the films grown at the intermediate Ga flux were approximately 3.5x more intense than films grown at the higher or lower fluxes investigated. Similarly, the lifetime of photo-generated carriers measured by time-correlated single photon counting in films grown at the higher Ga flux were found to be ~2x smaller than what is observed for films grown at the intermediate flux (Fig. 2). These results are attributed to the formation of defects under Ga-rich growth conditions that act as nonradiative recombination centers in these materials, and are important for the development of PA-MBE grown optoelectronic devices.

[1] C.D. Lee, A. Sagar, R. Feenstra, C.K. Inoki, T.S. Kuan, W.L. Sarney, L. Salamanca-Riba, Appl. Phys. Lett, **79**, (2001) 3428.
[2] C.R. Elsass, C. Poblenz, B. Heying, P. Fini, P.M. Petroff, S.P. DenBaars, U.K. Mishra, J.S Speck, J. Cryst. Growth, **233**, (2001) 709.

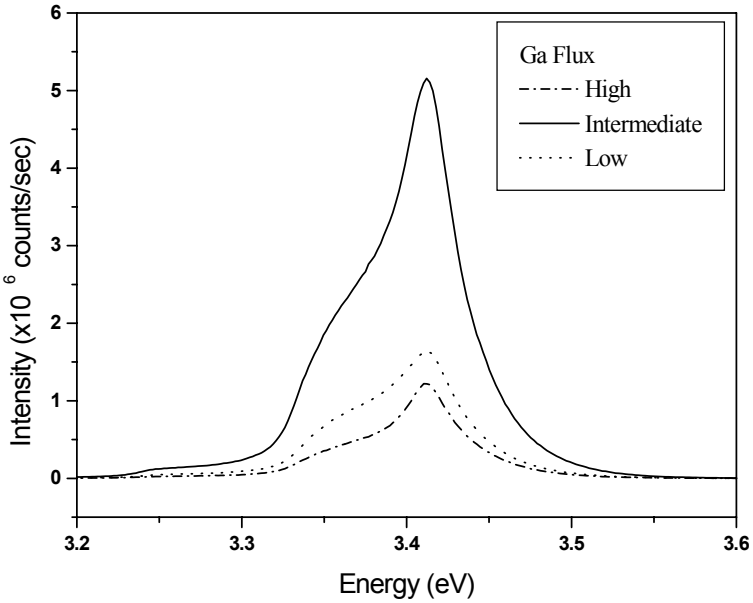

Figure 1. Room temperature CW photoluminescence intensity in GaN as a function of Ga flux for three representative fluxes.

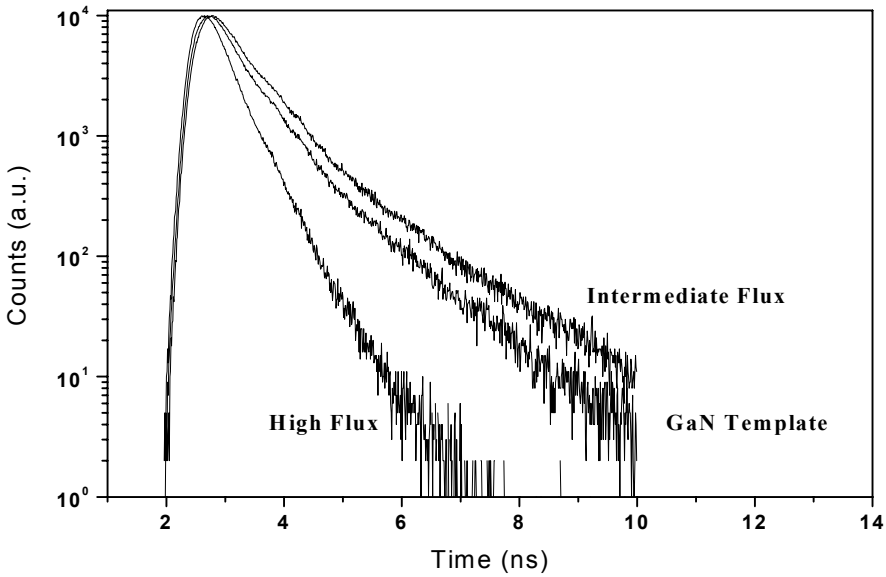

Figure 2. Comparison of photoluminescence lifetimes in GaN for different Ga fluxes.

Efficient p-type doping of GaN films by MBE

A. Bhattacharyya*, W. Li, C. Thomidis and T. D. Moustakas
Department of Electrical Engineering, Boston University, Boston MA, 02215, USA
David J. Smith
Center for Solid State Science and Department of Physics and Astronomy, Arizona State University, Tempe, AZ, USA

The efficient P-type doping of GaN and its alloys with InN and AlN is still one of the most challenging problems during the fabrication of both electronic and optical devices based on this class of materials. This is partly due to the problems associated with the deep nature of Mg acceptors as well as to compensation during doping of wide band-gap semiconductors, which cause a reduction in hole mobility. Reports in the literature indicate that the room-temperature resistivity of Mg doped P-type films grown either by MOCVD or MBE has been typically more than 1 ohm-cm.

In this paper we report enhanced efficiency of Mg doping during growth of GaN films by plasma assisted molecular beam epitaxy. These films were grown in Varian GenII system with standard effusion cells and an Applied-Epi RF plasma source for nitrogen activation. The investigated films were grown with Ga BEP up to 1.2E-6 Torr, RF plasma power of 450 Watts, and a substrate temperature of 770C. The Mg flux was varied from 2.0E-8 to 1.2E-7 Torr. The films were studied by SIMS analysis, room and low temperature Hall effect, Fourier Transform spectroscopy and photoluminescence measurement.

Our data show strong correlation between Mg-incorporation and ratio of III-V fluxes. We have obtained films with room-temperature hole concentrations ranging from 1.0E+17 to 2.0E+18 /cm^3, with corresponding mobilities ranged from 30 to 6 cm^2/Vs. The best resistivity obtained was around 0.2 ohm-cm, which is a significant improvement on the typical values reported in the literature. Furthermore FTS transmission measurements indicate that the films with hole concentrations 1.0E+18/cm^3 exhibit an abrupt band-edge with no evidence of band-tailing. This is of vital importance when these films are used as part of vertically emitting LEDs, LDs and UV photodetector structures.

We have also conducted detailed PL measurements on these samples. It is well known that highly doped as-deposited films by MOCVD or MBE generally exhibit weak luminescence at room temperature. Upon annealing at high temperature for dopant activation, the MOCVD films show a strong and broad blue luminescence spectrum. In this paper we report highly doped GaN films that exhibit a narrow band-edge luminescence as well as D-A transitions attributed to Mg doping. The peak positions and relative intensities have been correlated to the Mg doping levels in these films.

References:

1. Peter Kozodoy, Huili Xing, Steven P. DenBaars, Umesh K. Mishra, A. Saxler, R. Perrin, S. Elhamri, and W. C. Mitchel, J. Appl. Phys. **87**, 1832 (2000)
2. Keunjoo Kim and Joseph G. Harrison, J. Vac. Sci. Technol. A **21**, 134 (2003)

*e-mail: anirban@bu.edu

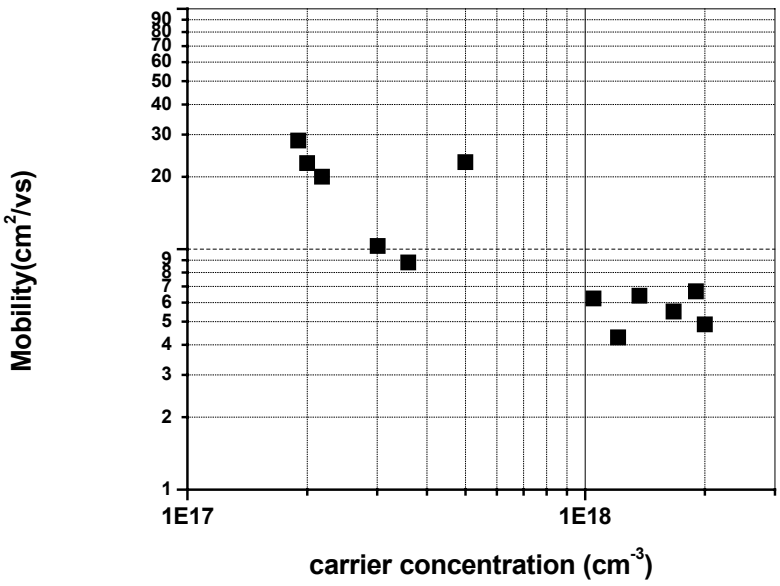

Fig 1: Carrier-concentration vs. mobility measurements for typical Mg doped films

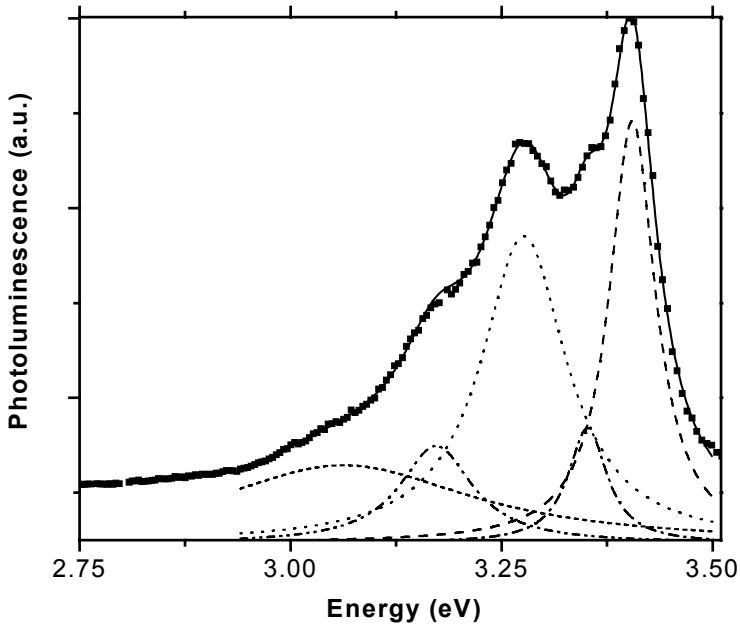

Fig 2: PL spectra of a GaN sample heavily doped with Mg

Title: Lateral photocurrent spectroscopy investigation of excitonic absorption in AlGaN/GaN multiple quantum wells grown by molecular beam epitaxy

Authors: I. Friel, C. Thomidis, Y. Fedyunin, T. D. Moustakas.
Department of Physics and Department of Electrical and Computer Engineering, Boston University.
(**Contact:** ifriel@bu.edu)

Abstract: We report on the use of lateral photocurrent (LPC) spectroscopy as a simple and sensitive method to investigate the excitonic transitions in III-nitride bulk materials and quantum wells. The technique is demonstrated on a 15 period $Al_{0.2}Ga_{0.8}N$/GaN multiple quantum well (MQW) structure grown homoepitaxially by plasma-assisted molecular beam epitaxy on a 4 µm thick (0001) HVPE GaN template, and the results compared to photoluminescence (PL) measurements. The nominally undoped MQW structure was grown in the group-III rich regime without growth interruption. The well and barrier widths were estimated from XRD measurements to be 4 and 16 monolayers (MLs) thick respectively. Rudimentary ohmic contacts for the LPC measurements were formed by deposting In into two deeply scribed lines, resulting in electrical contact to both the MQWs and the bulk GaN template (Fig. 1). The electric field used to collect the photocurrent was estimated to be 2.7 Vcm^{-1}, which ensures that the electronic properties of the system are essentially unperturbed.

The LPC spectra were taken using standard phase-sensitive detection techniques over the range 9 to 300 K and compared with PL spectra taken over the same temperature range. Strong excitonic absorption was observed in the LPC measurements up to room temperature in both the bulk GaN layer and the MQW structure. The LPC spectrum taken at 160 K is shown in Fig. 2 as an example, along with curve fits to the data. We find that the bulk GaN peak is best fit with a Lorentzian lineshape, indicating predominantly homogeneous broadening, whereas the MQW peak is best fit with a Gaussian lineshape, indicating predominantly inhomogeneous broadening. Only a single peak due to transitions in the MQW is observed unambiguously in the data, which we attribute to the ground state heavy-hole (hh) exciton.

The PL peak energies of the MQW were found to be strongly Stokes-shifted with respect to the absorption peaks of the LPC spectra, indicating the presence of disorder-induced band-tail states. Furthermore, the PL integrated intensity of the MQW transition was found to be strongly quenched as the temperature was increased. The data was well modeled by assuming two non-radiative mechanisms with activation energies of $E_{a1} = 33 \pm 6$ meV and $E_{a2} = 165 \pm 33$ meV (Fig. 3). We attribute the higher energy quenching mechanism as being due to excitons thermally excited out of the quantum well. In this case, excitons excited into the barrier layers are field-ionized very efficiently by the large electric fields (of the order of $MVcm^{-1}$) present in III-nitride heterostructures due to polarization effects. The lower energy quenching mechanism is attributed to delocalization of excitons from band-tail states caused by interface roughness fluctuations. This increases the population of free excitons, which are then able to migrate in the planes of the MQWs allowing the holes to annihilate on charged threading dislocations (TDs). We have calculated the change in electron and hh confinement energies in the investigated MQW resulting from variations in the well width. This was done by numerically solving the effective mass Hamiltonian, including the potential variation created by the polarization sheet charges at the well/barrier interfaces. Assuming a localization energy of 33 ± 6 meV, as suggested by the PL intensity analysis, the calculation predicts a fluctuation in the well width of 0.7 ± 0.2 ML. This indicates that for narrow wells in AlGaN/GaN MQW structures, even small well width fluctuations can lead to relatively large changes in confinement energy. Nonetheless, this may be beneficial in AlGaN/GaN MQWs, since, in analogy with InGaN/GaN MQWs, where In-rich quantum dots leads to exciton localization, so interface roughness can lead to exciton localization, and therefore the probability of non-radiative recombination of the exciton with TDs is reduced.

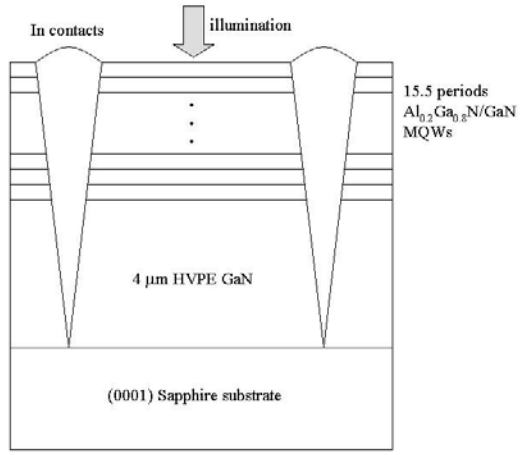

Fig. 1 – Schematic of the structure investigated and contact geometry used for LPC measurements.

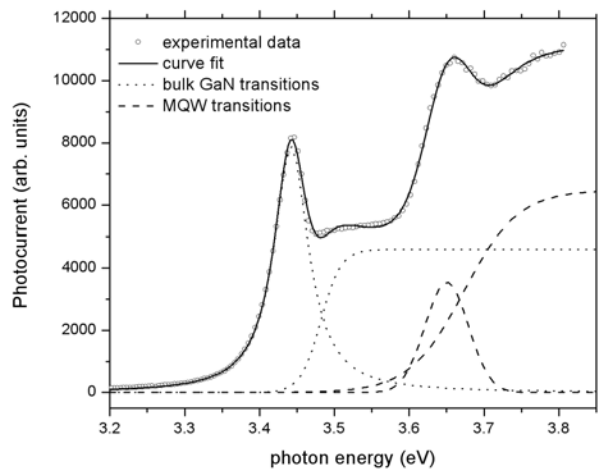

Fig. 2 – LPC spectrum taken at 160 K and curve fitting results

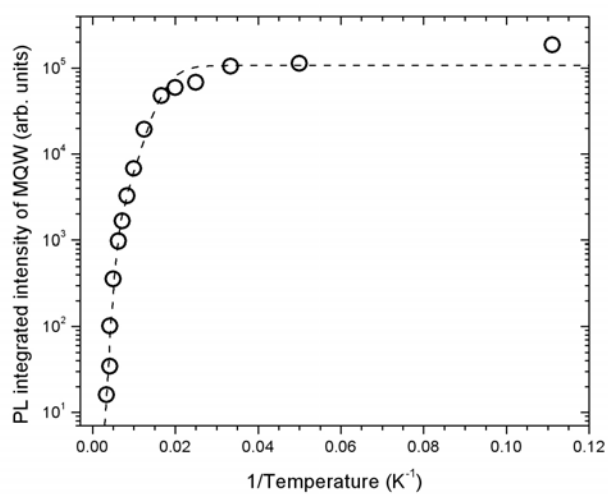

Fig. 3 – Arrhenius plot of integrated PL intensity from $Al_{0.2}Ga_{0.8}N/GaN$ MQWs. The dashed line is a fit which assumes two thermally activated non-radiative channels.

Polarization-doped 3D electron slabs in graded III-V Nitride heterostructures: MBE growth, physics, and demonstration of the PolFET

D. Jena[+], S. Heikman, D. Buttari, A. Jimenez, S. Rajan, H. Xing, J. S. Speck, and U. K. Mishra
Department of Electrical and Computer Engineering & Materials Dept,
University of California, Santa Barbara, CA 93106, USA.
([+]Email: djena@engineering.ucsb.edu)

*Abstract (Submitted for **NAMBE 2003**)*
MESFET/JFET technology using III-V Nitride semiconductors, especially GaN, has not received enough attention due to the low mobility of heavily doped GaN channels[1-3]. An exciting alternative to traditional impurity doping that allows us to circumvent the low-conductivity problem of the channel is to use polarization doping for Nitride-based MESFETs, which is demonstrated in this work. We recently demonstrated[4] polarization-doped three-dimensional electron slabs (3DES) in linearly graded AlGaN/GaN semiconductor layers grown by RF-plasma-N_2 source MBE. The 3DES carriers generated by exploiting the large polarization fields[5] in wurtzite III-V Nitride semiconductors in this technique have superior transport properties over donor (Si)-doped 3D-carriers. In particular, the *absence* of ionized-impurity scattering results in an enhancement of carrier mobility. The low-temperature mobility is further enhanced, which has enabled us[6] to observe Shubnikov de-Haas oscillations of the 3DES carriers revealing the effective mass, quantum scattering time, and the alloy scattering potential of AlGaN. The room temperature conductivity is much higher than Si-doped layers, which makes it attractive as the channel material of FETs. In this work, we demonstrate such a MBE-grown polarization-doped channel Junction-FET (JFET), the PolFET.

The structure and the energy band-diagram of the device are shown in Figure I. The structure is grown by RF-plasma-N_2 source Gen-II MBE system at UCSB under nominal metal-rich conditions[7]. Fe-doped semi-insulating GaN on c-plane sapphire grown by MOCVD[8] was used as the template. The structure (Figure 1(b)) consisted of 100nm of undoped GaN, followed by 100nm of 0→30% linearly graded AlGaN, followed by a 50nm p-GaN cap doped with Mg of nominal concentration N_A~10^{19}/cm^3. The structure results in a 3DES channel of mobile charge density n~10^{18}/cm^3 and mobility μ~700cm^2/V.s (as compared to a Si-doped channel with n~10^{18}/cm^3 and mobility μ~200cm^2/V.s)[3] at room temperature. The PolFET was fabricated by Ti/Al/Ni/Au ohmic contact formation, mesa isolation, Pd/Au/Ni gate, and reactive-ion-etching (RIE) of the access regions. Figure 1(a) shows the top-view and 1(b) shows the cross section of the fabricated PolFET.

Figure 2(a) depicts the DC I_{DS}-V_{DS} curves and 2(b) shows the transconductance for different gate voltages for the PolFET. The maximum current I_{DS}(max)=430mA/mm and maximum transconductance g_m(max)=67ms/mm are higher than previously reported values of similar doping and gate lengths. Channel pinch-off is obtained at a gate voltage of V_g=-6V. The source and drain contact resistance to the 3DES channel of the PolFET is in the range of 0.3-0.5Ωmm. Frequency-dependent measurements yielded f_T=8.45GHz and f_{max}=10.9GHz for a gate length of 0.7μm. The gate-drain breakdown voltage was measured to be 60V for a cutoff-current of 1mA/mm. In summary, the PolFET with a polarization-doped channel compares well to the traditional impurity-doped channel FETs, and hold much promise for further improvement.

[1] M. A. Khan, A. R. Bhattarai, J. N. Kuznia, and D. T. Olson, Appl. Phys. Lett. **63** 1214 (1993).
[2] R. Gaska et. al., Appl. Phys. Lett. **78** 769 (2001).
[3] L. Zhang *et al.*, IEEE Trans. El. Dev. **47** 507 (2000).
[4] D. Jena *et. al.*, Appl. Phys. Lett, **81** 4395 (2002).
[5] F. Bernardini, V. Fiorentini, and D. Vanderbilt, Phys. Rev. B **56** R10024 (1997).
[6] D. Jena *et. al.,* Phys. Rev. B **67** 153306 (2003).
[7] B. Heying *et. al.*, J. Appl. Phys. **88** 1855 (2000).
[8] S. Heikman, S. Keller, S. P. DenBaars, and U. K. Mishra, Appl. Phys. Lett. **81**, 439 (2002).

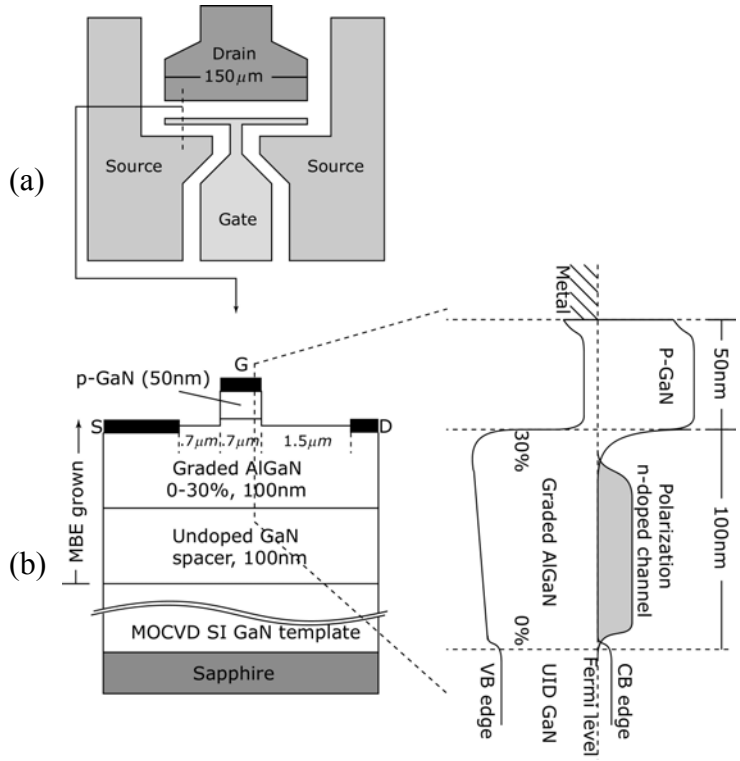

Figure I

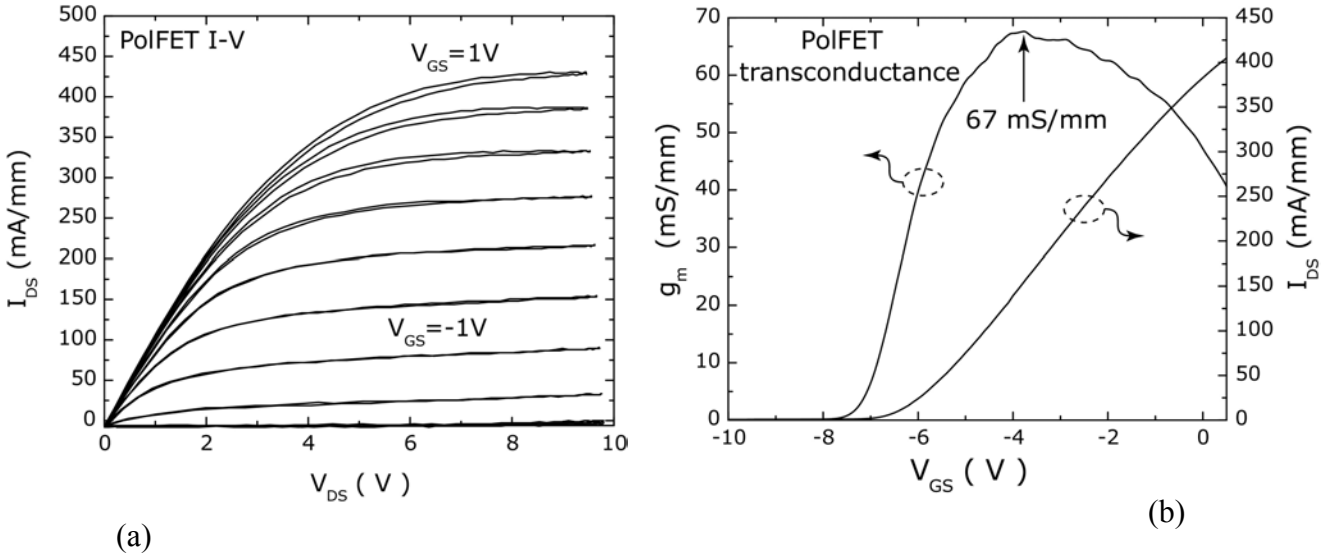

Figure II

NAMBE 2003 Program

Monday, September 29, 2003

1:30-3:30: Quantum Structures II

Chair: Archie Holmes (University of Texas at Austin)

MC-1: Photoluminescence properties of CdSe quantum dots grown on ZnSe and $Zn_{0.97}Be_{0.03}Se$ by Molecular Beam Epitaxy
Xuecong Zhou[1], Martin Muñoz[1], Shiping Guo[1], Maria C. Tamargo[1], Yi Gu[2], Igor L. Kuskovsky[2], and G. F. Neumark[2]
[1]The City College of New York; [2]Columbia University

MC-2: Free carrier compensation of semi-metallic ErAs particles embedded in an InGaAs matrix
Daniel C. Driscoll[a], Micah P. Hanson[a], Mihail Suhkotin[b], Elliott Brown[b], and Arthur C. Gossard[a]
[a]University of California, Santa Barbara; [b]University of California, Los Angeles

MC-3: Growth and electrical properties of GaSb/ErSb composites
M. H. Hanson, D.C. Driscoll, J. Zimmerman, and A.C. Gossard
University of California, Santa Barbara

MC-4: The Selective Growth of InP Nanowires by Chemical Beam Epitaxy
P.J. Poole, J. Lefebvre, and J. Fraser
National Research Council-Canada

MC-5: Photoconductive characteristics in a trench-type InGaAs quantum wire
K.-Y.Jang[1,2,3], T.Sugaya[1,2], A.Shinoda[2,4], C.-K. Hahn[1,2], M. Ogura[1,2], and K. Komori[1,2]
[1]National Institute of Advanced Industrial Science and Technology(AIST); [2]CREST, Japan Science and Technology Corporation (JST); [3]Japan Science for the Promotion of Science (JSPS)-Domestic Research Fellow; [4]Shibaura Institute of Technology, Japan

MC-6: Si-based Quantum Dot LED grown by MBE
M. Jo[1], N. Yasuhara[1], K. Kawamoto[1], and S. Fukatsu[1, 2]
[1]The University of Tokyo, Japan; [2]PRESTO, Japan Science and Technology Corporation (JST), Japan

Photoluminescence properties of CdSe quantum dots grown on ZnSe and $Zn_{0.97}Be_{0.03}Se$ by Molecular Beam Epitaxy

Xuecong Zhou[a,*], Martin Muñoz, Shiping Guo, and Maria C. Tamargo[b,*]
The City College of CUNY, 138th St. & Convent Ave., New York, NY 10031
**The Graduate Center of CUNY, New York, NY 10016*
Yi Gu, Igor L. Kuskovsky, and G. F. Neumark
Columbia University, New York, NY 10027

We have previously grown[1] CdSe quantum dots (QDs) on ZnSe and $Zn_{0.97}Be_{0.03}Se$ by Molecular Beam Epitaxy (MBE). Also we have investigated[2] the steady state PL intensity at room temperature (RT) and 77 K for these two QDs samples. It was observed that the steady state PL intensity from the CdSe QDs on ZnSe measured at RT is much stronger than that from CdSe QDs on $Zn_{0.97}Be_{0.03}Se$ while they are similar at 77 K. To better understand this phenomenon, we have performed time-resolved photoluminescence (TRPL) measurements on both samples as a function of temperature, in the range of 77 K to RT. We attributed the dominant non-radiative processes at high temperatures in the CdSe/$Zn_{0.97}Be_{0.03}Se$ QDs to the oxygen incorporation in the $Zn_{0.97}Be_{0.03}Se$ layer (possibly due to the reactivity of Be). In the following we will propose another more probable explanation for the strikingly different temperature dependences of the PL lifetime for these two samples based on the size and composition of these QDs.

We developed a method to estimate the capped CdSe/$Zn_{0.97}Be_{0.03}Se$ QDs size and composition, based on photoluminescence (PL) and photoluminescence excitation (PLE) as well as Raman spectroscopy measurements. Our analysis suggests that both the size and the composition of the QDs may affect the PL emission energy. Furthermore, assuming spherical QDs, we obtained QD diameters in the range of 4.8 nm to 6.5 nm with Cd composition in the range of 50%-57%. Meanwhile, we performed contactless electroreflectance (CER) measurements on the CdSe/ZnSe QDs, and observed transitions due to the QDs and the wetting layer. In this case, assuming lens shaped QDs, we extracted the QDs diameter to be around 19.0 nm, the height about 3.24 nm. Raman spectroscopy measurement suggest that Cd composition is > 90%. We propose that the presence of Be in the barrier makes the QDs size smaller but enhances the amount of Zn intermixing in the QDs. The CdSe/$Zn_{0.97}Be_{0.03}Se$ QDs are very small, exhibit 0-dimensional quantum confinement, consistent with the temperature dependent TRPL results where the PL lifetime for the CdSe/$Zn_{0.97}Be_{0.03}Se$ QDs is about 232 ps at 77 K and remains nearly constant up to 150 K. Due to the Zn intermixing in the QDs as well as the small size of the QDs (low ionization energy), then the PL lifetime goes down to about 83 ps at RT where the non-radiative processes dominate. In the case of CdSe/ZnSe QDs, the QDs size is large, showing a two-dimensional behavior. In this case, the temperature dependent TRPL results show the PL lifetime for CdSe QDs grown on ZnSe is about 255 ps at 77 K and increases with increasing temperature, consistent with 2-dimensional confinement. Due to the very small amount of Zn intermixing in the QDs as well as the large size of the QDs (very high ionization energy), the PL lifetime increases steadily all the way to about 453 ps at RT without effect of the non-radiative processes. Additional investigations to further quantify the size and composition of the QDs are being pursued.

---

a.Also in Physics Department. Email: cong999@yahoo.com
b.Correspondence author. Email: tamar@sci.ccny.cuny.edu
1.S. P. Guo, X. Zhou, O. Maksimov, and M. C. Tamargo, J. Vac. Sci. Technol. B **19**(4), Jul/Aug 2001
2.X. Zhou, S. P. Guo, M. C. Tamargo, and Y. C. Chen, J. Elect. Mat. (To be published).

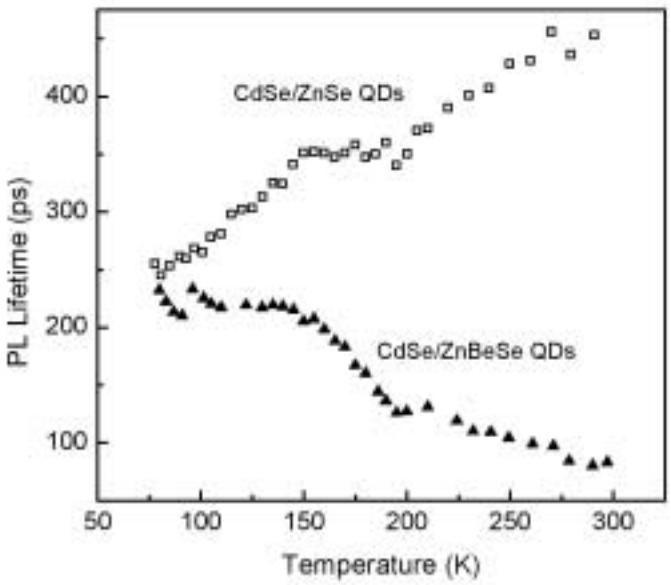

Fig. 1 Temperature dependence of photoluminescence (PL) lifetime for CdSe/ZnSe QDs and CdSe/$Zn_{0.97}Be_{0.03}Se$ QDs.

Table 1. Comparison of results for CdSe/ZnSe QDs and CdSe/$Zn_{0.97}Be_{0.03}Se$ QDs

Structures	Exp. Method	Assumed QD shape	QDs size (nm)	Cd composition in QDs
CdSe/$Zn_{0.97}Be_{0.03}Se$ QDs	PL/PLE	Spherical	4.8-6.5 (diameter)	50%-57%
CdSe/ZnSe QDs	CER	Lens shaped	19 (diameter), 3.24 (height)	> 90% (Raman)

Free carrier compensation of semi-metallic ErAs particles embedded in an $In_{0.53}Ga_{0.47}As$ matrix

Daniel C. Driscoll[a], Micah P. Hanson[a], Mihail Suhkotin[b], Elliott Brown[b], Arthur C. Gossard[a]

[a]*Materials Department, University of California, Santa Barbara, CA 93106-5050*
[b] *Electrical Engineering Department, University of California, Los Angeles, California 90095*

Corresponding Author: Daniel C. Driscoll (dand@engineering.ucsb.edu)
Tel: 805-893-8154 Fax: 805-893-8971

We report on the enhanced resistivity obtained by beryllium doping composite epitaxial materials consisting of layers of semi-metallic ErAs particles embedded in an $In_{0.53}Ga_{0.47}As$ matrix. These structures are grown by molecular beam epitaxy on (100)-oriented semi-insulating InP:Fe substrates at 490°C, as measured by a pyrometer. This material may serve as a fast photoconductor for terahertz photomixer devices at longer wavelengths than low temperature grown GaAs [1,2] or ErAs:GaAs [3-5]. Materials for photomixer devices require high dark resistivities and breakdown voltages to withstand the high bias voltages as well as sub-picosecond photocarrier lifetimes in order to operate into the terahertz spectrum. In the ErAs:InGaAs material, the ErAs particles act as fast carrier recombination centers, while the $In_{0.53}Ga_{0.47}As$ matrix allows for photoexcitation at wavelengths of 1.55μm[6].

The composite material layer sequence is shown schematically in Figure 1b. The 2.5 nm of InGaAs above and below each layer of ErAs particles is doped with Be (doping concentration ranges from 0 to $1x10^{20}$ cm^{-3}). The addition of ErAs particles into an InGaAs matrix increases the electron charge density. As the size of the ErAs islands increases, the room temperature free electron concentration decreases, as shown in Figure 1a. By doping these materials with beryllium acceptors in the vicinity of the particles, partial compensation of the free electrons imparted to the InGaAs by the ErAs particles is possible, as shown in Figure 2. The room temperature electron concentration of an ErAs superlattice sample with 1.75 ML ErAs per layer can be reduced by a factor of ~1500 by compensating with Be at a concentration of $1x10^{-20}$ cm^{-3}.

1 S. Verghese, K.A. McIntosh, and E.R. Brown, Appl. Phys. Lett. **71**, 2743 (1997).
2 F.W. Smith, A.R. Calawa, C.L. Chen, M.J. Manfra, and L.J. Mahoney, IEEE Electron Device Lett. **9**, 77 (1988).
3 C. Kadow, A.W. Jackson, A.C. Gossard, S. Matsuura, and G.A. Blake, Appl. Phys. Lett. **76**, 3510 (2000).
4 C. Kadow, A.W. Jackson, A.C. Gossard, J.E. Bowers, S. Matsurura, and G.A. Blake, Physica E **7**, 97 (2000).
5 C. Kadow, S.B. Fleischer, J.P. Ibbetson, J.E. Bowers, A.C. Gossard, J.W. Dong, and C.J. Palmstrom, Appl. Phys. Lett. **75**, 3548 (1999).
6 M. Sukhotin, E. R. Brown, A. C. Gossard, D. C. Driscoll, and M. Hanson, Appl. Phys. Lett. **82**, 3116 (2003).

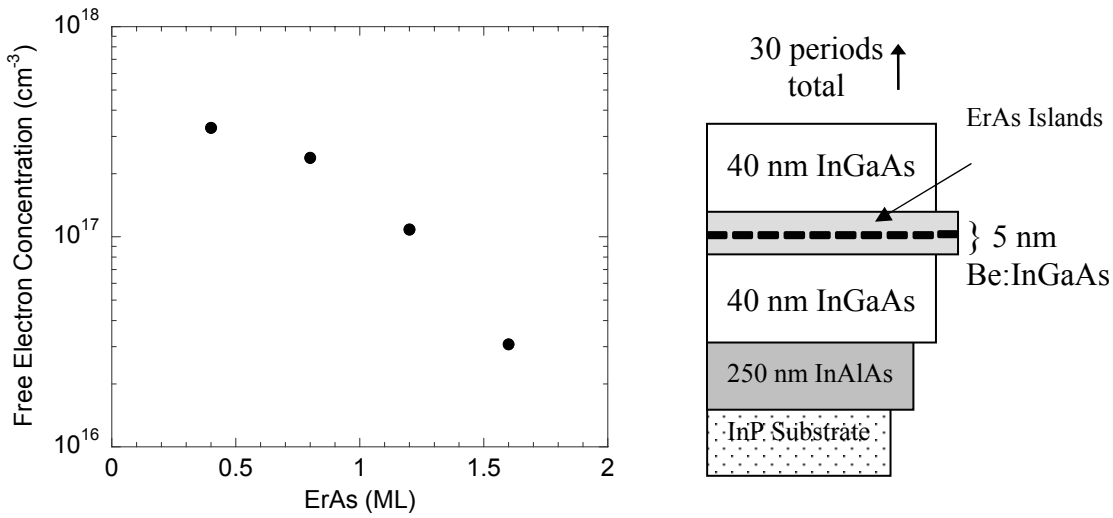

(a) **(b)**

Figure 1: (a) Room temperature three-dimensional electron charge plotted as a function of ErAs deposition for a sample with no Be doping. Increasing ErAs deposition results in larger particles which impart fewer electrons to the conduction band. (b) Sample structure.

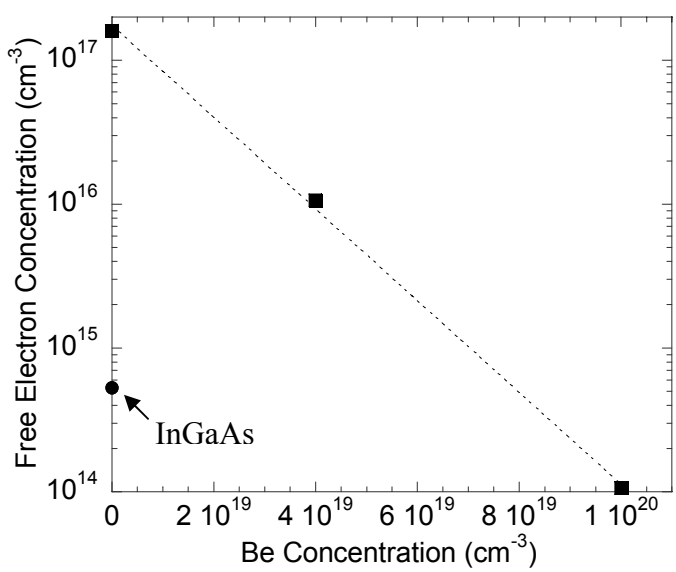

Figure 2: Room temperature three-dimensional electron charge as a function of Be doping concentration for a 30 period superlattice sample with 1.75 ML of ErAs per layer. A sample with no ErAs (as-grown InGaAs) is also plotted as a reference. At the optimal doping of 1x20 cm^{-3}, the free electron concentration is reduced by a factor of ~ 1500 as compared to a sample with no Be doping and 1.75 ML of ErAs per layer, and by a factor of ~5 as compared to the reference InGaAs sample.

Growth and electrical properties of GaSb/ErSb composites

M. H. Hanson*, D.C. Driscoll, J. Zimmerman, A.C. Gossard
Materials Department, University of California, Santa Barbara 93106-5050

We report the growth of GaSb/ErSb semiconductor/metal composites by molecular beam epitaxy (MBE). The 0.73 eV band gap of GaSb host material allows strong absorption at the technologically significant wavelength of 1.55 µm. The semimetallic band structure of ErSb [1] and the extremely small lattice mismatch of less than 0.1% with GaSb make ErSb a good choice for GaSb based metal/semiconductor composite structures. Growth of high quality complete layers of ErSb on GaSb by MBE has previously been demonstrated [2]. In our research we examine the growth regime prior to the formation of a complete film. In this regime the ErSb spontaneously forms nanometer size particles. We study the properties of superlattices consisting of layers of ErSb particles separated by GaSb. Previously, GaAs/ErAs superlattices have been used to reduce electrical conductivity and carrier lifetimes in GaAs [3].

From the atomic force microscopy (AFM) images of ErSb deposited on a GaSb surface shown in Fig. 1, we can see that ErSb grows in an island growth mode similar to what has been observed for ErAs on both GaAs [3] and InGaAs [4]. The heights of these particles remain relatively constant, between 10Å and 16Å, for both 1 monolayer (ML) and 0.5 ML depositions. As the deposition increases from 0.5 ML to 1 ML the islands merge to form larger particles. Reflective high energy electron diffraction, x-ray diffraction, and AFM show that smooth epitaxial GaSb can be grown over depositions of up 2 ML of ErSb. Superlattices of GaSb/ErSb were grown on relaxed AlSb buffers nucleated on semi-insulating GaAs substrates. Hall measurements were then performed on the superlattices to determine the effective bulk electrical properties. A reference GaSb layer was measured to be p-type with a charge of 3.5×10^{16} cm^{-3} and mobility of 600 cm^2/Vs. Fig. 2a shows hole concentration vs. 1/kT for various ErSb depositions in a 30 period GaSb/ErSb superlattice, with a 20 nm repeat unit, as well as the GaSb reference sample. It is observed that as the deposition, and therefore the size of ErSb particles, decreases, the density of holes in the material also decreases until 0.5 ML. From 0.5 ML to 0.1 ML the carrier concentration remains relatively independent of deposition. In Fig. 2b the total thickness of the layer is kept constant by adjusting both the number and spacing of the ErSb layers. We find that as the spacing between ErSb layers decreases so too does the hole density. When the layer spacing is reduced to 5 nm, the hole concentration is reduced by factor of 40 relative to the reference GaSb sample. This is consistent with an increase in the overlap between depletion regions that surround the metal particles. It is therefore possible to tune the hole concentration from the undoped reference level of 3.5×10^{16} cm^{-3} down to 8.5×10^{14} cm^{-3} by adjusting the deposition and spacing of ErSb layers.

These results raise the possibility that ErSb/GaSb superlattices may act as a fast photoconductor at the fiber optic communications wavelength of 1.55 µm. Such a material would be desirable for use in devices such as fast photodetectors and photomixers [5].

1. Q. G. Sheng, B. R. Cooper, S. P. Lim, J. Appl. Phys. **73**, 5409 (1993)
2. A. Guivarc'h, Y. Ballini, Y. Toudic, M. Minier, P. Auvray, B. Guenais, J. Ccaulet, B. Le Merdy, B. Lambert, and A. Regreny, J. Appl. Phys. **75**, 2876 (1994)
3. C. Kadow, A.W. Jackson, A.C. Gossard, J.E. Bowers, S. Matsuura, G.A. Blake, Physica E **7** 3510 (2000)
4. D. C. Driscoll, M. P. Hanson, E Mueller, A. C. Gossard, J. of Crystal Growth **251**, 243 (2003)
5. E. R. Brown, F. W. Smith, and K. A. McIntosh, J. Appl. Phys. **73**, 1480 (1993)

* Corresponding author. tel.: (805) 893-7055; fax: (805) 893-8971; E-mail: micah@engineering.ucsb.edu

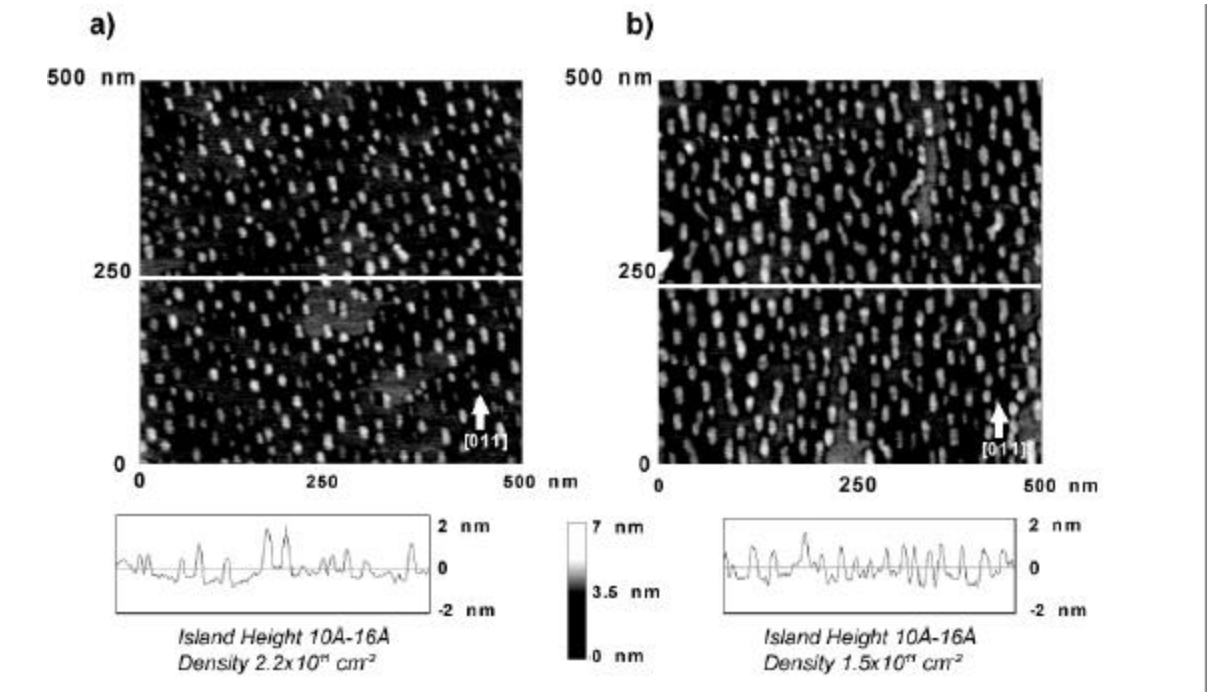

Fig. 1 a) AFM image of 0.5 ML of ErSb on a GaSb surface **b)** AFM image of 1 ML of ErSb on a GaSb surface

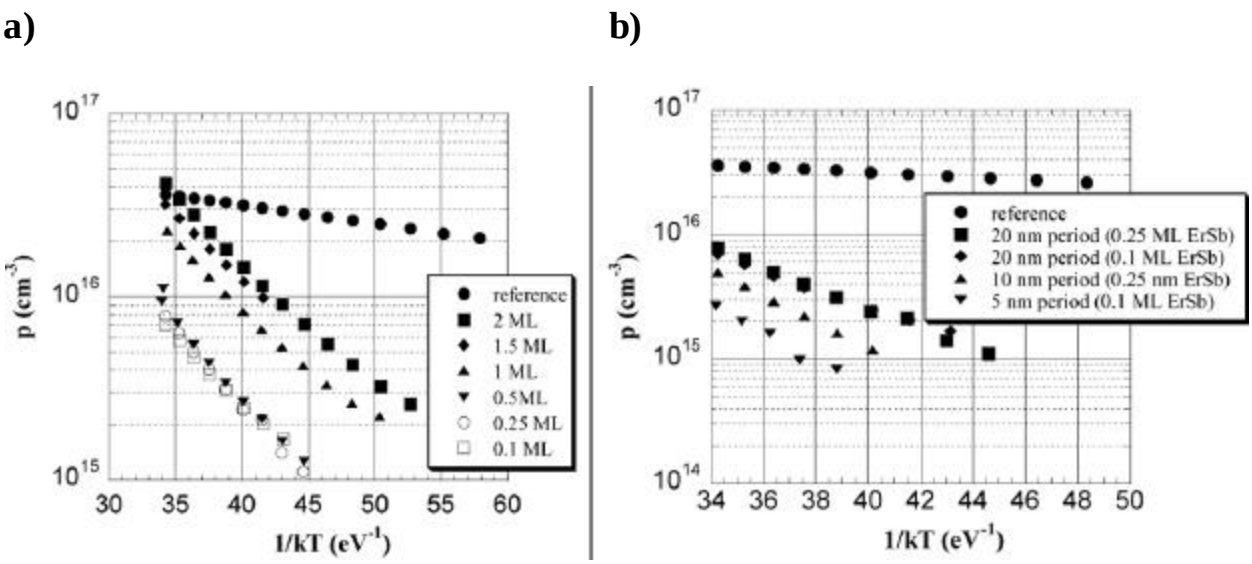

Fig. 2 a) Hole concentration vs. 1/kT for various depositions of ErSb in a 30x20 nm superlattice **b)** Hole concentration vs. 1/kT for various GaSb/ErSb superlattice periods. The total thickness of the sample was held constant at 620 nm.

The Selective Growth of InP Nanowires by Chemical Beam Epitaxy

P.J. Poole, J. Lefebvre, and J. Fraser

Institute for Microstructural Sciences, National Research Council, Ottawa, Ontario K1A 0R6, Canada

Dramatic advances have been made in the last few years in the study of one-dimensional structures, with the efforts on carbon nanotubes being particularly visible. There are still some important issues to be solved in this material system, particularly in controlling the electronic properties, which depend on the chirality of the tubes. In parallel there have been significant advances in the growth of nanowires from more conventional semiconductor materials such as SiC, Si, GaAs, InAs, InP and GaP. These materials, unlike the carbon nanotubes, can have their electronic properties easily tailored through the use of bandgap engineering and electrical doping. This has allowed the fabrication of diodes, field effect transistors, light emitting diodes, detectors and biochemical sensors.

The growth of these semiconductor nanowires has almost exclusively used a metal particle (usually gold or iron) to act as a seed utilising the vapour-liquid-solid (VLS) growth mechanism. Efforts have been made to grow the wires in specific locations by positioning the seed particles using an atomic force microscope, or using electron-beam lithography.

In this paper, we describe the growth of InP nanowires with diameters as small as 40 nm using selective area Chemical Beam Epitaxy. This growth process differs from other reports in that it does not use the VLS method. It does not require the use of a seed particle, and allows nanowires to be positioned in very well defined locations on a wafer with well-defined orientations. The (001) InP wafers used in this study were first coated with a 20 nm thick SiO_2 layer before being patterned using electron-beam lithography. Small windows, of the order of 40 to 100 nm in diameter, were opened in the oxide by reactive ion etching, exposing the InP surface. The growth conditions used resulted in complete selectivity, meaning that growth only occurred within the windows opened in the SiO_2 mask. Following the growth of InP, which corresponded to a thickness of 123 nm for a planar unpatterned substrate, single nanowire pairs were observed growing from each opening.

Figure 1 shows SEM images of typical nanowires grown using the technique described above. The nanowire pairs are aligned along the two possible (111)A directions available for the (001) InP surface. They are 600 nm long and have a diameter of 40 nm. Figure 2 shows low temperature photoluminescence measurements of a single nanowire pair where a thin InAs layer is incorporated within each nanowire. Clear excited state emission is observed as the excitation density is increased, indicating the quantum dot like behaviour of the InAs/InP nanowire system.

The growth mechanism for the formation of these nanowires will be discussed.

philip.poole@nrc.ca
Tel: (613) 993 7172

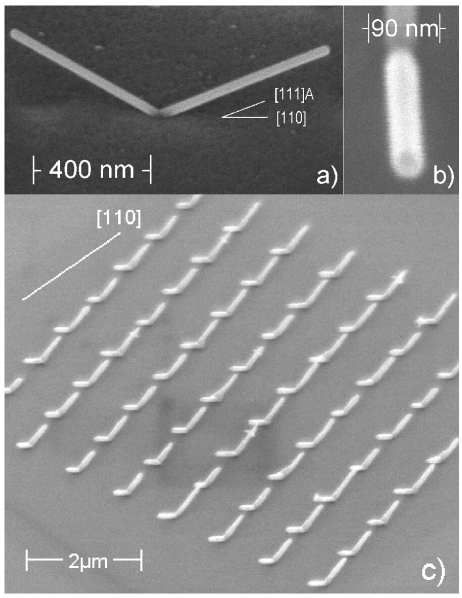

Figure 1. Scanning electron microscope images of InAs/InP nanowires. a) single nanowire pair, where the nanowires point in the two available <111>A directions, b) looking down the length of a single nanowire, c) an array of 64 nanowire pairs

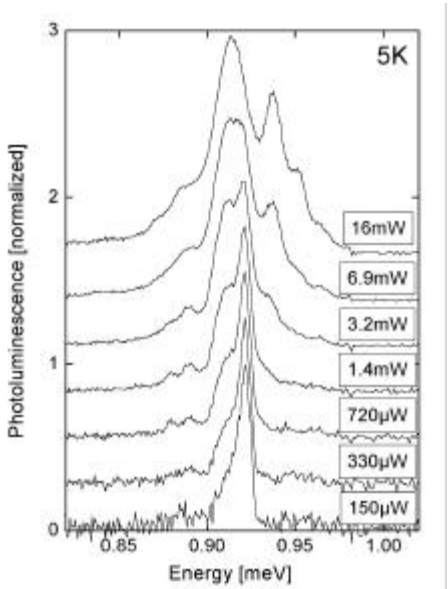

Figure 2. 5K photoluminescence spectra from a single nanowire pair as a function of excitation density, with a spotsize of around 20µm. The spectra have been normalized to the intensity at 921 meV.

Photoconductive characteristics in a trench-type InGaAs quantum wire

K.-Y. Jang[1,2,3)], T. Sugaya[1,2,a)], A. Shinoda[2,4)], C.-K. Hahn[1,2)], M. Ogura[1,2)] and K. Komori[1,2)]

[1)] National Institute of Advanced Industrial Science and Technology (AIST)
[2)] CREST, Japan Science and Technology Corporation (JST)
1-1-1 Umezono, Tsukuba, 305-8568 Japan
[3)]Japan Science for the Promotion of Science (JSPS)-Domestic Research Fellow,
[4)]Shibaura Institute of Technology, Japan

[a)] Corresponding Author; Tel.81-29-861-5466, Fax.81-29-861-5602, e-mail. t.sugaya@aist.go.jp

We have recently demonstrated a novel trench-type InGaAs quantum wire (QWR) grown on a V-grooved InP (311)A substrate by hydrogen-assisted molecular beam epitaxy.[1] QWR-FETs formed from trench-type InGaAs QWRs show a pronounced negative differential resistance (NDR), with a high peak-to-valley current ratio (PVR) and a low onset voltage.[2] The NDR effects are important in terms of their possible applications to high speed switching and memory devices, and also for the view point of fundamental interest. In this report, we demonstrate photoconductive characteristics of the trench-type QWR-FET, which indicate the NDR effects based on a carrier transfer from the InGaAs QWR layer to the sidewall quantum wells (QWs).

Figure 1 shows a clear NDR effect of the trench-type QWR-FET with a high PVR (= 4.3) at a low onset voltage (V_{NDR} = 0.2 V). We have confirmed that the carriers flow only through the QWR layer at low drain voltage by the low-temperature magnetoresistance measurement.[3] In order to investigate the distribution of the electrons in the trench-type QWR structure, we measured the photoconductivity at two different drain (V_{DS}) voltages at 24 K. In Fig, 2, we show the intensity characteristics of the photoconductivity as a function of the wavelength of the spectral-resolved incident light in the trench-type QWR-FET. The intensity peaks at around 1450 nm in both spectra originate from (100) QWs, which is thought to be due to the strongly excited photoconductive measurement by the incident light. In the static *I-V* measurement as shown in Fig. 1, the current will not flow in the (100) QW regions, because almost (100) QW regions are etched away and the depletion layer spread from the etched surfaces.[3] In the spectrum for the drain voltage of 0.2 V, distinct intensity peak is observed at around 1300 nm, which originate from the InGaAs QWR.[1] This result indicates that the carriers in the fundamental level of the QWR are predominant in the drain voltage region lower than V_{NDR}. In the spectrum for V_{DS} = 0.3V, the peak of QWR is negligible, indicating the carriers transfer from QWR level to other quantum levels. There are two possible quantum levels to which carriers can transfer, one is the level in the InAlAs barrier layer and another is in the sidewall (111)A and (331)B QWs (in Fig.3(b)). Since the conduction band offset between InGaAs QWR to the InAlAs barrier layer is 0.46 eV, the onset voltage of 0.2 V is too low to be explained by the carrier transfer to the InAlAs. The QWR and the QWs are structurally connected and embedded in the barrier layer. We calculated the sub-band energy level based on the actual geometry of the QWR taken from the cross-sectional TEM image (in Fig. 3(b)) by numerically solving the two dimensional single band Schrodinger equation using finite- element method. The energy separation of electrons between the QWR and QWs is estimated to be as large as 84 meV, which is consistent with the V_{NDR} in the trench-type QWR-FET. The electron mobility in the QWs is thought to be extremely low because of its thin (2.5 nm) and low crystal quality.[1] The NDR characteristics can be occur due to the carrier transfer from the high mobility QWR layer to the low-mobility QW regions. In Fig. 3, we show the schematic illustration of NDR mechanism in our trench-type QWR-FET. The channel electrons flow in the QWR at lower drain voltage, and are transferred to the low mobility sidewall QWs at the drain voltage larger than V_{NDR}.

[1] T.Sugaya, M.Ogura, Y.Sugiyama, K.Matsumoto, K.Yonei, and T.Sekiguchi, Appl. Phys. Lett. **78,** 76 (2002).
[2] K.-Y. Jang, T. Sugaya, C.-K. Hahn, A. Shinoda, , M. Ogura and K. Komori, 14th IPRM'02 conference proceeding, pp. 581-584 (2002).
[3] T.Sugaya, J.P.Bird, D.K.Ferry, M.Ogura, Y.Sugiyama, and K.-Y.Jang, Appl. Phys. Lett. **80,** 434 (2002).

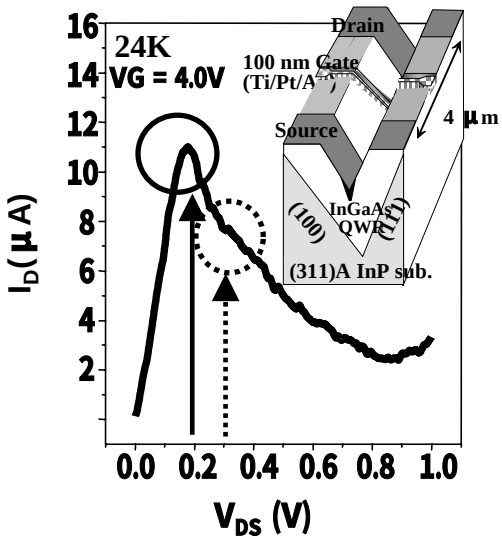

Figure 1. I_d-V_{ds} characteristics of a trench-type QWR-FET at 24 K with the gate length of 100 nm. NDR spectrum is clearly observed at V_G = 4.0V.

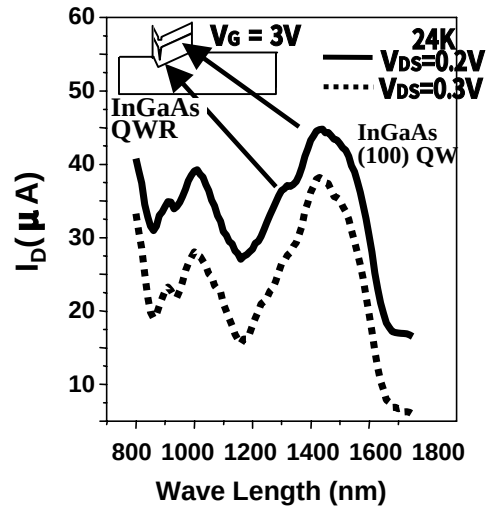

Figure 2. Photoconductivity characteristics of QWR-FET at 24K. The spectrum for V_{DS} = 0.3 V is shifted downward by 10 μA.

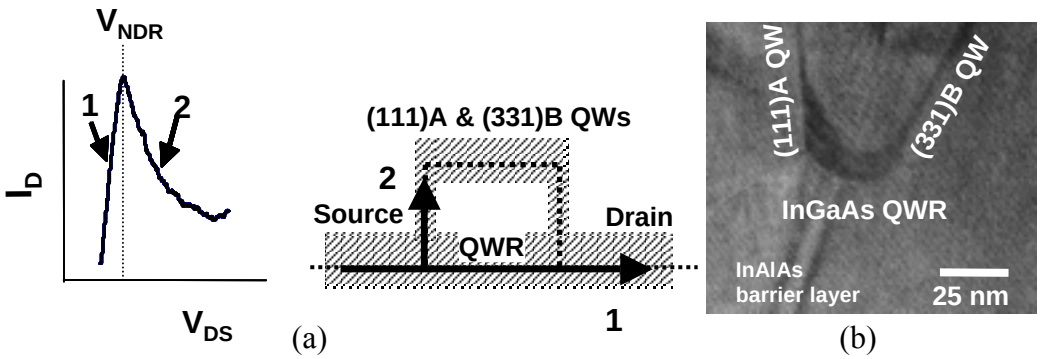

Figure.3. (a) The NDR mechanism in the trench type InGaAs QWR-FET. The current path is transferred from InGaAs QWR (1) to side QWs (2) with increasing drain voltage. (c) Cross-sectional TEM image of QWR and side QWs in the structure.

Si-based Quantum Dot Light Emitting Diode grown by MBE

M. Jo[1], N. Yasuhara[1], K. Kawamoto[1] and S. Fukatsu[1, 2]

[1]Graduate School of Arts and Sciences, The University of Tokyo
Komaba, Meguro, Tokyo 153-8902, Japan
[2]PRESTO, Japan Science and Technology Corporation (JST)
Kawaguchi, Saitama 332-0012, Japan
Phone: +81-3-5454-6754 Fax: +81-3-5454-4311 E-mail: cfkatz@mail.ecc.u-tokyo.ac.jp

To create a Si-based light emitter has been a common target of research in the materials science community. In this context, compound semiconductor quantum dots embedded in Si (hereafter referred to as super quantum dots (SQDs)) have emerged as a new class of Si-based, self-assembling nanostructure that allows a realistic Si-based light emitter if one can establish a type-I potential well due to the direct band-gap, compound semiconductors within the Si matrix. In spite of such expectation, theory predicts that the band line-up of column-III-V SQDs should be of type-II and an indirect band-gap is established due to the low-lying conduction-band valleys of Si. However, our recent study shows that a built-in electric dipole developing at the CSQD/Si heterointerface provides a short-ranged potential trap for electrons, which offers the possibility of utilizing localized electron-hole pairs to produce efficient luminescence in a Si-based quantum-confined structure that would be otherwise susceptible to grown-in, dissipative pathways.

In this work, we report on the observation of intense electroluminescence (EL) from strained column III-V SQDs. A quantum efficiency of the order of 0.1% was obtained at low temperature (10 K), demonstrating an efficient Si-based light emitting diode (LED) containing QDs in the active layer.

Strained III-V compound SQDs embedded in Si were grown by solid-source Si molecular beam epitaxy (MBE) on Si(001). Column-III-V materials were codeposited over a column-V stabilized Si surface under a slightly column-V-rich condition. The growth temperature was in the range 150-500°C. The column-III-V SQDs were found to grow in much the same way as those for representative QDs such as InAs/GaAs and Ge/Si. A maximum dot density of $10^{10}cm^{-2}$ was achieved for a few monolayers equivalent of SQDs, which was sufficient to produce intense luminescence in the near-infrared.

The Si cap layers of SQDs were spontaneously n-typed doped due to the surface segregation of column-V species during MBE growth. As a result, p-n junction diodes are routinely obtained simply by using a p-type substrate. The EL spectrum was inhomogeneously-broadened and extended over the sub-band-gap region of Si. Tight-binding calculation shows that this energy broadening has to do with the interface-localized electrons rather than the quantum-confined holes. The interface localization of electrons due to the built-in dipole at the SQD/Si interface characterizes SQDs and effectively suppresses the energy dissipation due to nonradiative pathways.

EL from SQDs was so intense that standard lab detectors of meager sensitivity (i.e., Ge and InGaAs operating at room temperature) were capable of recording the spectrum at a good S/N ratio. This is contrasted with SiGe/Si quantum wells that is less emissive and hard to be detected likewise. An attempt of direct imaging on an infrared camera was successful. The 0.1-% quantum efficiency obtained for SQD-LED is comparable to those of commercially available column-III-V LEDs.

Interestingly, light amplifying characteristics that promise a Si-based semiconductor optical amplifier (SOA) were observed for SQDs under pulsed, visible laser excitation. An edge-emitting sample containing SQDs was configured in an oscillator-pump geometry. Amplified spontaneous emission was observed with increasing pump power. In the time-domain, a very fast decay was observed in the initial stage of excitation, which indicates the establishment of population inversion of interface localized electron-hole pairs.

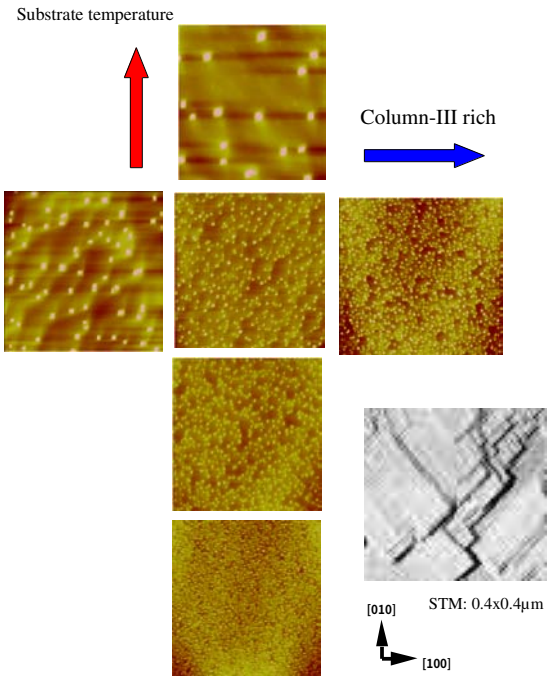

FIG.1 5μmx5μm AFM scans of InSb SQDs grown on Si(001). Inset is an STM image taken in UHV.

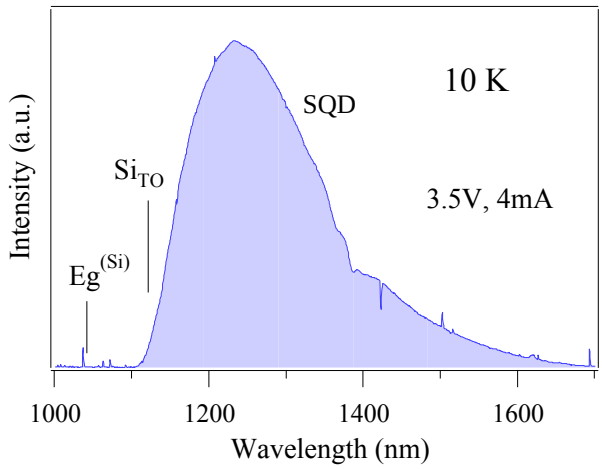

FIG.1 10-K EL spectrum of GaSb/Si SQDs.

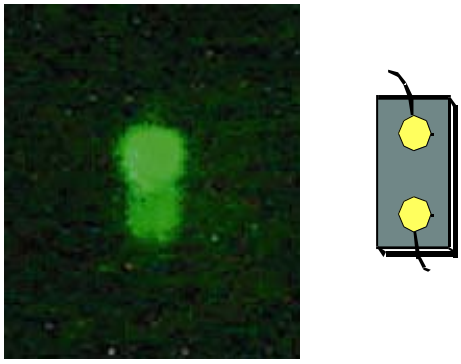

FIG.3 A near-infrared image of an SQD-LED at 10 K captured by an infrared camera. Note that the upper electrode is in operation.

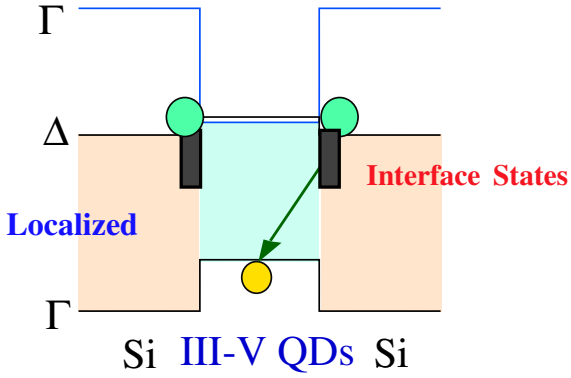

FIG.4 Potential diagram appropriate for SQD .The built-in electric dipole produces a trapping potential for the electrons. Radiative recombination occurs across the type-II interface.

NAMBE 2003 Program

Poster Session 1: Monday, September 29, 2003, 3:30-500

P1-1: Magneto-Photoconductive Characterization of Quantum States of Barrier Shallow Donors in MBE Grown GaAs/AlGaAs Heterostructures
A. Naweed, W. D. Goodhue, W. J. Gorveatt, R. Giles, J. Waldman and V. Menon#
University of Massachusetts Lowell; # Princeton University

P1-2: Probing the Electronic Structures of III-V-Nitride Semiconductors by X-ray Photoelectron Spectroscopy
T.S. Lay[1], W.T. Kuo[1], L.P. Chen[1], Y.H. Lai[2], W.H. Hung[2],J.S. Wang[3], J.Y. Chi[3], D.K. Shih[4], H.H. Lin[4], C.M. Chuang[5], K.H. Chen[5]
[1]National Sun Yat-Sen University; [2]National Synchrotron Radiation Research Center,Taiwan; [3]Industrial Technology Research Institute,Taiwan; [4]National Taiwan University; [5]Institute of Atomic and Molecular Sciences, Academia Sinica

P1-3: Mg segregation in Mg-GaN MBE growth: A Simulation Investigation
Irena Stanley and Rama Venkat
University of Nevada, Las Vegas

P1-4: Epitaxial Growth on Gas Cluster Ion Beam Processed GaSb Substrates Using Molecular Beam Epitaxy
K. Krishnaswami[a], W.D. Goodhue[a], L.P. Allen[b], C. Santeufemio[b], X. Liu[c], M.C. Ospina[c], B. Zhu[a],J. Whitten[c], C. Sung[c], H. Dauplaise[d], D. Bliss[d], G. Dallas[e], D. Bakken[e], and K.S. Jones[f]
[a] Photonics Center, University of Massachusetts, Lowell; [b] Epion Corporation; [c] Center for Advanced Material, University of Massachusetts;[d] Air Force Research Laboratory/SNHC;[e] Galaxy Compound Semiconductors; [f] Department of Materials Science, University

P1-5: Optical and electrical characteristics of C60/GaAs
Masaaki Ogawa, Kazuki Nomoto, Yousuke Kida and Yoshiji Horikoshi
Waseda University, Japan

P1-6: Strong Lateral Confinement in Self-Organized InGaAs/InAlAs quantum wires grown on a (221)A oriented InGaAs ternary alloy substrate by MBE
K. Miyagawa, D. Suma, T. Kitada, S. Shimomura and S. Hiyamizu
Osaka University, Japan

P1-7: Stability of Pseudomorphic InGaAs Layers during annealing
A. Riposan, G.K.M. Martin, and J. Mirecki Millunchick
University of Michigan

P1-8: Contact-less Electroreflectance of CdSe/ZnSe Quantum Dots grown by MBE
Martín Muñoz, Shiping Guo, Xuecong Zhou, Maria C. Tamargo, Y.S Huang#, C. Trallero-Giner*, and A. H. Rodríguez*
City College of the City University of New York; # National Taiwan University of Science and Technology; * Universidad de La Habana San Lazaro y L, Cuba

P1-9: MBE growth of ZnO using initial Zn layer and MgO buffer layer on Si (111) substrates
Miki Fujita, Noriaki Kawamoto, Masanori Sasajima and Yoshiji Horikoshi
Waseda University, Japan

P1-10: Compositional Analysis of Graded AlxGa(-x)As Layers by X-ray Energy Dispersive Spectrometry
K. Mahalingam, R. Wheeler, K. G. Eyink, and S. T. Fenstermaker
Air Force Research Laboratory

P1-11: Low Temperature Si Growth on Si (001): Impurity Incorporation and Limiting Thickness for Epitaxy
J.-M. Baribeau, X. Wu, D.J. Lockwood, L. Tay, and G. I. Sproule
National Research Council-Canada

Magneto-Photoconductive Characterization of Quantum States of Barrier Shallow Donors in MBE Grown GaAs/AlGaAs Heterostructures

A. Naweed* and W. D. Goodhue
Photonics and Optoelectronic Device Center, University of Massachusetts Lowell, Lowell, MA 01854

W. J. Gorveatt, R. Giles and J. Waldman
Submillimeter-Wave Technology Laboratory, University of Massachusetts Lowell, Lowell, MA 0185

V. Menon
Department of Electrical Engineering, Princeton University, Princeton, NJ

Fax: (978) 934-4994; E-mail: William_Goodhue@uml.edu

A 'shallow donor,' consisting of an electron bound to an impurity ion in a semiconducting material, exhibits a hydrogen-atom-like character. Modern crystal growth techniques, such as molecular beam epitaxy (MBE), allow realization of barrier shallow donors where the electron and the donor ion are spatially separate, despite being bound together by their mutual coulomb interaction. Here we report results of far-infrared (FIR) magneto-spectroscopy of such barrier donor states in Si-doped GaAs/AlGaAs quantum well structures. The shallow donor transitions, induced by FIR radiation in the presence of a magnetic field, are studied by means of photoconductivity, a tool that has so far remained unexplored in barrier donor identification despite its obvious success in characterization of bulk and quantum well donors. Unlike previous investigations (see, e.g., Refs. 1-2), only barriers have been doped in the present work, thereby promoting formation of only barrier donor species. High-resolution and high signal-to-noise ratio photoconductive spectra has been obtained that reveals a variety of shallow donor transitions, including those suggestive of binding of in-well electrons to Si dimers in the barrier. Experimental results are compared with theoretical calculations based on a variational approach within the effective mass theory. Apart from underlining the significance of impurity redistribution in heterostructures (Fig. 1), our results also indicate that, in contrast to widespread belief, impurity incorporation into the host crystal during MBE growth may have a non-random origin. The feasibility of observing shallow donor transitions in a single period quantum well structure is also reported.

References:

1. E. Glaser et al., Phys. Rev. B **36**, 8185 (1987).
2. Y. J. Wang et al., J Electron. Mater. **20**, 71 (1991).

* Present Address: Department of Physics, Oklahoma State University, Stillwater, OK 74078

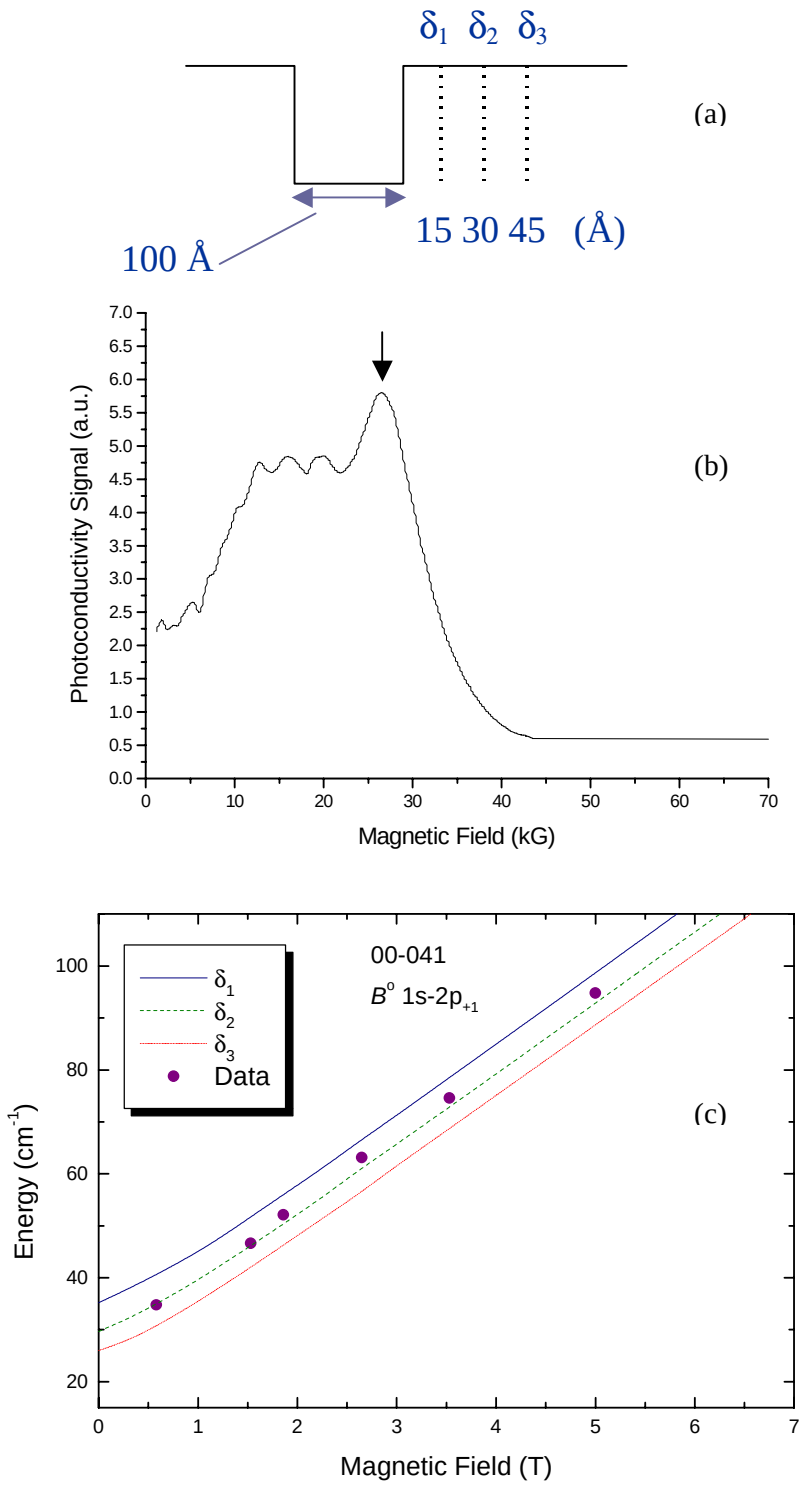

Fig. 1. (a): The investigated structure consisting of a 100 Å quantum well. The distance between each sheet doped layer in the barrier is 15 Å and the first layer is located 15 Å away from the edge of the well. (b): Sample's magneto-photoconductive response obtained with a FIR laser wavelength of 158.5 μm (63.09 cm^{-1}). The 1s-$2p_{+1}$ transition is indicated by the arrow. (c): Plot of peak positions of 1s-$2p_{+1}$ transitions as a function of applied magnetic filed. Filled circles represent experimental data. Curves represent theoretically determined transition energies for donors located in different monolayers. The experimental data appears to agree well with theoretical curve describing the second doped layer.

Probing the Electronic Structures of III-V-Nitride Semiconductors by X-ray Photoelectron Spectroscopy

T.S. Lay[1,*], W.T. Kuo[1], L.P. Chen[1], Y.H. Lai[2], W.H. Hung[2],
J.S. Wang[3], J.Y. Chi[3], D.K. Shih[4], H.H. Lin[4], C.M. Chuang[5], K.H. Chen[5]

[1]*Institute of Electro-Optical Engineering, National Sun Yat-Sen University, Kaohsiung 804, Taiwan*

[2]*National Synchrotron Radiation Research Center, Hsinchu, Taiwan*

[3]*Opto-Electronics and System Labs., Industrial Technology Research Institute, Hsinchu, Taiwan*

[4]*Department of Electrical Engineering, National Taiwan University, Taipei, Taiwan*

[5]*Institute of Atomic and Molecular Sciences, Academia Sinica, Taipei, Taiwan*

(*Corresponding author: E-mail: tslay@mail.nsysu.edu.tw; Tel: 886-7-525-4458, Fax: 886-7-525-4499)

InGaAsN/GaAs structure provides an alternative material system to InGaAsP/InP for photonic devices in λ = 1.3-1.6 μm fiber communication. MBE and MOCVD have been widely adopted to prepare the InGaAsN/GaAs structures. Recently, high quality diode laser performances, such as λ = 1.3 μm edge-emitting lasers and VCSELs have been demonstrated [1]. Further understanding the InGaAsN microscopic properties will improve the bandgap engineering and device fabrications. The incorporation of N, which has a much larger electronegativity and smaller atom size compared to As, makes the InGaAsN electronic structure an interesting topic to investigate the bandgap properties. The nearest-neighbor bonding configuration of the isovalent nitrogen in InGaAsN, i.e, In-N or Ga-N rich, has a strong influence on the band gap [2]. X-ray photoelectron spectroscopy (XPS), which provides a direct method to probe the core-level photoelectron, is often used to investigate the chemical bondings and electronic structures. However, the very dilute N mole fraction and surface oxidation of InGaAsN make the N(1s) spectra measurement much more difficult. In this paper, we are able to observe the N(1s) signal of the InGaAsN with 2-3% mole fraction of nitrogen by using high-resolution synchrotron radiation light source and low-energy Ar^+ sputtering. The N(1s) data are summarized in Fig. 1. The XPS data were measured from the MBE-grown InGaAsN, GaAsN, and InAsN samples, and the MOCVD-grown InN and GaN samples. For InAsN, the N(1s) peak is corresponding to the N(1s) peak at binding energy (E_b) ~ 397.0 eV from InN sample. For GaAsN, the N(1s) peak is close the N(1s) peak at E_b ~ 398.0 eV from GaN sample. As to the InGaAsN samples, the N(1s) signal shows a major peak corresponding to In-N bonding, and a minor component of Ga-N bonding. The data suggest that the MBE-grown InGaAsN has an In-N rich configuration. Detailed analysis as well as the Ga(3d), In(3d), As(3d) data will be elucidated in the presentation.

[1] H. Riechert, "GaInNAs/GaAs based long-wavelength edge emitters and VCSELs," Proceedings of 14th IPRM, Stockholm, Sweden, pp. 19-22, 2002.

[2] K. Kim and A. Zunger, "Spatial correlations in InGaAsN alloys and their effects on band-gap enhancement and electron localization," Phys. Rev. Lett., **86**, pp. 2609-2612, 2001.

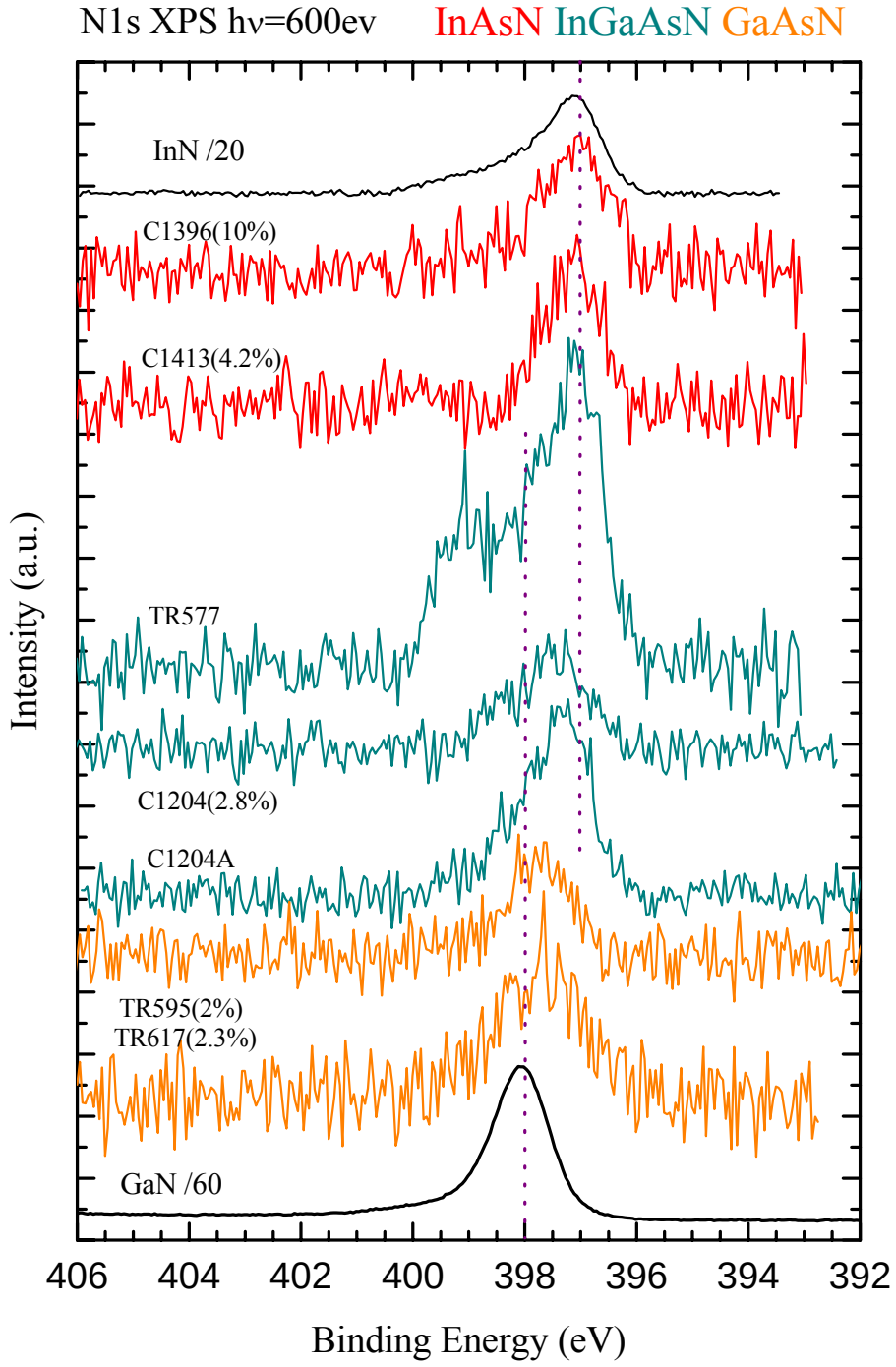

Fig. 1. XPS data from top to bottom curves are the N(1s) spectra corresponding to (a) InN; (b) InAsN: C1396 and C1413; (c) InGaAsN: TR577, C1204, and C1204A; (d) GaAsN: TR595 and TR617; (e) GaN, respectively. The curves are level shifted for clarity.

***Mg* Segregation in *Mg-GaN* MBE Growth: A Simulation Investigation**

Irena Stanley, Rama venkat

Department of Electrical and Computer Engineering

University of Nevada, Las Vegas, NV 89154-4026

(702) 895 1094; (702) 895 4075

venkat@ee.unlv.edu

A rate equation model including all physically relevant surface processes is developed for the study of *Mg* segregation in *Mg* doped *GaN* MBE growth. The simulations were carried for various growth temperatures in the range of 600-750 ^{o}C with constant flux rates of *Mg*, *Ga* and *N* such as $5.5\times10^{13}\,atoms/cm^2s$, $1.1\times10^{14}\,atoms/cm^2s$ and $8.3\times10^{14}\,atoms/cm^2s$ respectively. In the model, the segregation of *Mg* atoms was allowed from the lower layer to the upper layer of the growing crystal. For the given flux rates, it is found that *Mg* segregates to the surface with the increase in temperature. Above 750 ^{o}C a dopant depleted zone is formed below the surface layer due to the difference between *Mg* atoms segregating into and out of the layer. The segregation energy is found to be 2.9 eV. Results obtained from our simulations are in qualitative agreement with the experimental data reported in the literature.[1-3]

[1] S. Guha *et. al.*, "*Mg* in *GaN*: Incorporation of a volatile species at high temperatures during Molecular Beam Epitaxy", Appl. Phys. Lett., 71 (12), 1685, (1997).

[2] J. M. Myoung *et. al.*, "Effects of growth temperature on *Mg*-doped *GaN* epitaxial films grown by plasma assisted Molecular Beam Epitaxy", J. Vac. Sci. Technol. A, 18 (2), 450, (2000).

[3] J. M. Myoung *et. al.*, "Effect of growth temperature on the properties of *p*-type *GaN* grown by plasma-assisted Molecular beam epitaxy", J. Cryst. Growth, 182, 241, (1997).

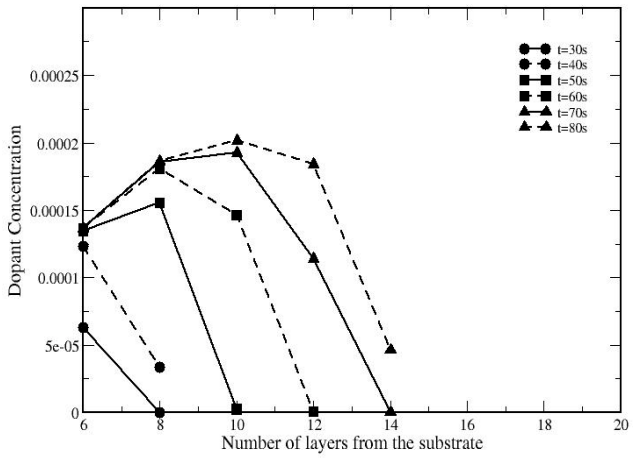
Dopant Concentration
Number of layers from the substrate
t=30s
t=40s
t=50s
t=60s
t=70s
t=80s

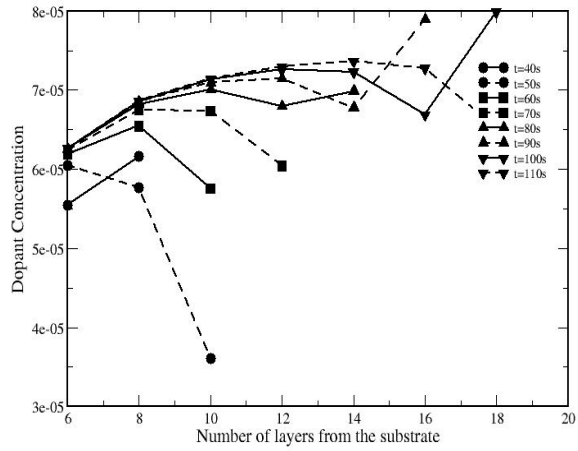
Dopant Concentration
Number of layers from the substrate
t=40s
t=50s
t=60s
t=70s
t=80s
t=90s
t=100s
t=110s

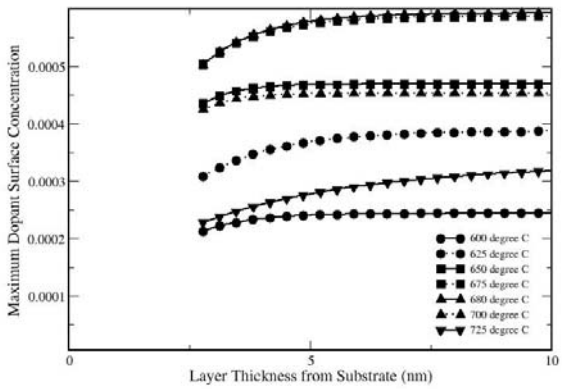
Maximum Dopant Surface Concentration
Layer Thickness from Substrate (nm)
600 degree C
625 degree C
650 degree C
675 degree C
680 degree C
700 degree C
725 degree C

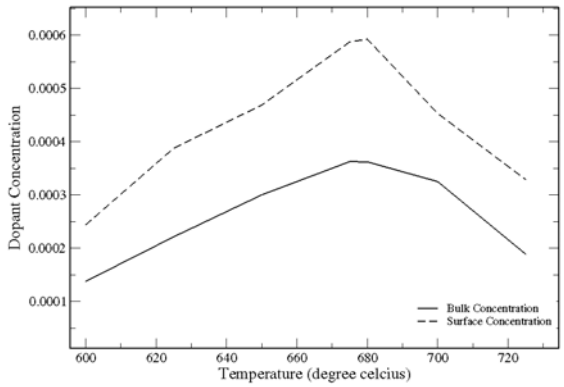
Dopant Concentration
Temperature (degree celcius)
Bulk Concentration
Surface Concentration

Epitaxial Growth on Gas Cluster Ion Beam Processed GaSb Substrates Using Molecular Beam Epitaxy

K. Krishnaswami[a], W.D. Goodhue[a*], L.P. Allen[b], C. Santeufemio[b], X. Liu[c], M.C. Ospina[c], B. Zhu[a], J. Whitten[c], C. Sung[c], H. Dauplaise[d], D. Bliss[d], G. Dallas[e], D. Bakken[e], and K.S. Jones[f]

[a] Photonics Center, University of Massachusetts, Lowell, MA 01854, USA
[b] Epion Corporation, Billerica MA. 01821, USA
[c] Center for Advanced Material, University of Massachusetts, Lowell, MA 01854, USA
[d] Air Force Research Laboratory/SNHC, Hanscom AFB, USA
[e] Galaxy Compound Semiconductors, 9922 East Montgomery #7, Spokane, WA 99206, USA
[f] Department of Materials Science, University of Florida, Gainesville, FL 32611, USA

In order to bring low-power epitaxy-based GaSb electronics and electro-optics to market, high-quality GaSb substrates with atomic surface smoothness and without sub-surface damage are required. Gas Cluster Ion Beam (GCIB) processing, a novel final polishing technique, has been shown to improve the surface finish of chemical-mechanical polished (CMP) two-inch (100) GaSb wafers by smoothing and removal of CMP induced surface and sub-surface damage[1]. In addition, specific mixtures of GCIB gases have been shown to produce thin engineered oxide layers that are easily desorbed in our Molecular Beam Epitaxy (MBE) system.

A CMP polished substrate of deliberate average quality was processed using a dual-energy single-gas GCIB process that included a moderate energy (10kV) oxygen based etch step followed by a low energy (3kV) oxygen based smoothing step with a relatively low total GCIB dose of 4.5×10^{15} ions/cm^2. Half the wafer was masked such that the same substrate contained both CMP and GCIB polished surfaces. AFM images with a resolution of $10 \times 10 \mu m^2$ show that the surface roughness was not significantly altered by this process. However, X-Ray Photon Spectroscopy (XPS) measurements made on the two surface regions showed that the composition of surface oxides were significantly different. The oxide layers on the two regions of this substrate were simultaneously and successfully desorbed in the MBE growth chamber (monitored by observing the RHEED patterns from the surface) by raising the substrate temperature to 560ºC. Starting with a homoepitaxial layer of GaSb, five periods of GaSb/AlGaSb layers were grown on both surfaces simultaneously in an Sb rich environment with a substrate temperature of 470ºC. TEM images of the substrate/epi interface show that the CMP finished region contained defects which propagated to the first AlGaSb barrier layer while the GCIB finished region showed no such defects.

The goal of this work is to determine if the GCIB technique is capable of preparing "epi-ready" surfaces. Currently, GaSb substrates with varying degrees of surface and sub-surface damage are being processed with a variety of GCIB process schedules. This includes dual-energy dual-gas species to identify oxide constituents for MBE applications and increased total dose for reduced surface roughness. For the first time, desorption of the GCIB grown oxide within the MBE growth chamber is conclusively shown. The characteristics of MBE epilayers grown on these surfaces will be presented.

This project was supported by DARPA's ABCS program #F49620-01-1-0514 and The Department of the Army, contract #DAAH01-03-CR018.

* Corresponding author: william_goodhue@uml.edu; (978) 934-3785

---

[1] L.P. Allen, T.G. Tetrault, C. Santeufemio, M. Tabat, X. Li, W. Goodhue , C. Sung, D. Bliss, and K.S. Jones, "Gas Cluster Ion Beam Smoothing of CMP Damaged GaSb(100) Substrates," Proc. of the International Conference on Alternative Substrate Technology, (September 14-17, 2002, Cancun, Mexico) p. 34. *Accepted for publication in the Journal of Electronic Materials, June 2003.*

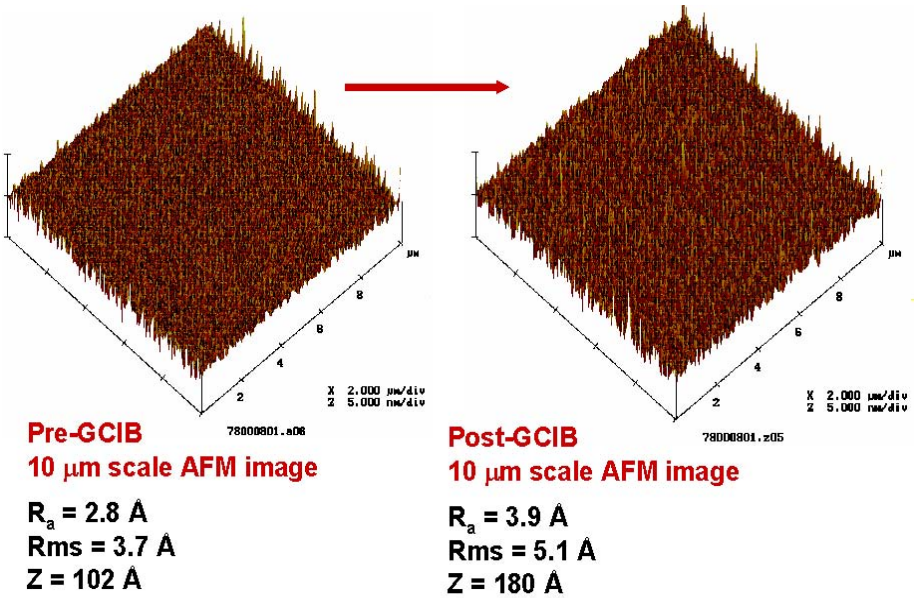

Figure 1 AFM images of CMP polished and GCIB polished GaSb, pre- and post-GCIB respectively, on a 10x10μm^2 resolution. The GCIB process was dual-energy single-gas specie process did not significantly alter the surface roughness.

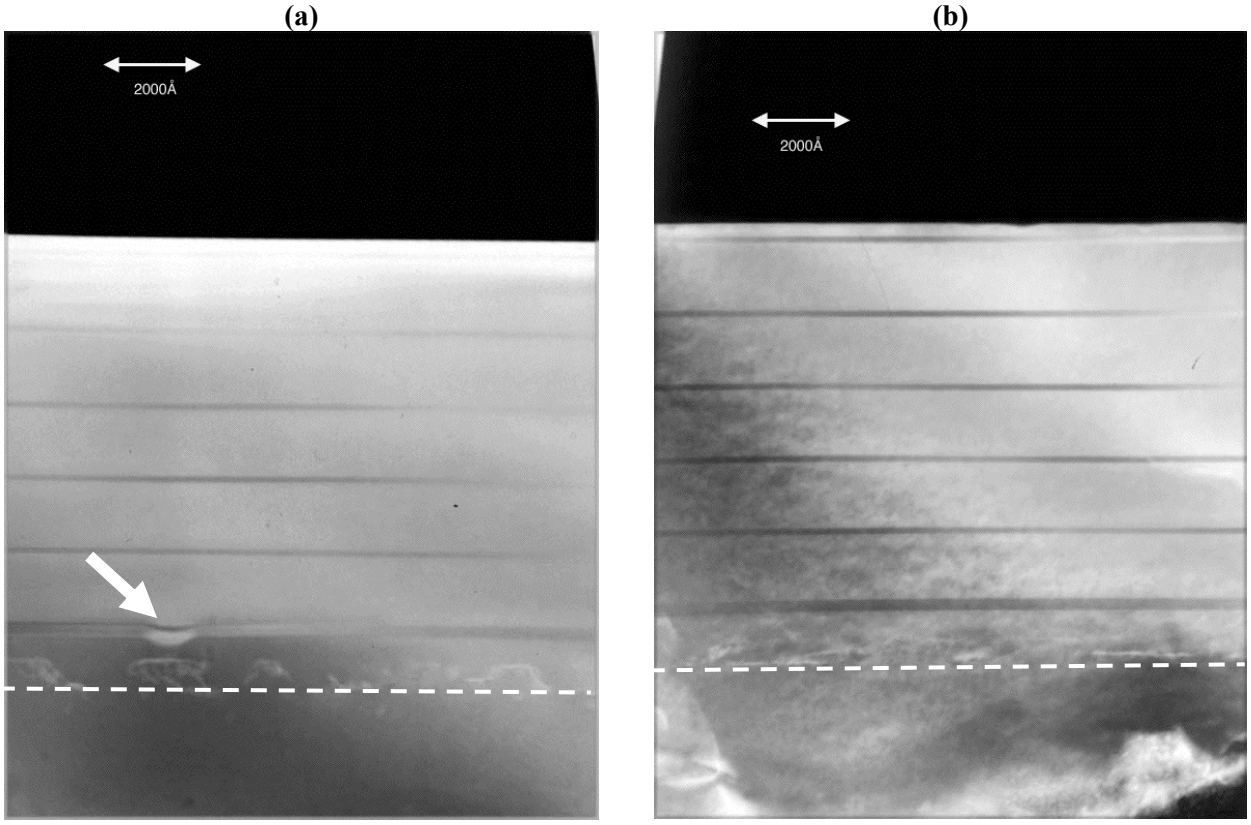

Figure 2 TEM images of: a) CMP and b) CMP/GCIB polished substrates with GaSb and AlGaSb epitaxial layers with thicknesses ~1400Å and 120Å respectively. The arrow indicates a pitted area in the first interface layer of the CMP finished substrate which disappears by the second layer and the dashed lines indicate the substrate/epi interface. The GCIB processed part of the wafer was free of such defects.

Optical and electrical characteristics of C_{60}/GaAs

Masaaki Ogawa[2], Kazuki Nomoto[1,2], Yousuke Kida[1,2] and Yoshiji Horikoshi[1,2]

[1]School of Science and Engineering, Waseda University, 3-4-1 Okubo, Shinjuku-ku, Tokyo 169-8555, Japan

[2]Kagami Memorial Laboratory for Materials Science and Technology, Waseda University, 2-8-26 Nishiwaseda, Shinjuku-ku , Tokyo 169-0051, Japan

Phone:+81-3-5286-3176, Fax:+81-3-3209-3450

E-Mail:syoumei39@toki.waseda.jp

Discovery of C_{60}, as the third modification of carbon bodies; diamond and graphite, and its synthesis on a microscopic scale have stimulated very intensive research efforts, due to its fascinating chemical and physical properties. However, there are few reports investigating the characteristic of C_{60} in semiconductors and C_{60}/semiconductor heterostructures.

In this study, we have grown C_{60} layers on GaAs (111)B substrates by molecular beam epitaxy(MBE). C_{60} δ–doped GaAs and AlGaAs/GaAs quantum well layers are also grown on GaAs. By C_{60} doping, both GaAs and quantum wells become almost semi-insulating, indicating that the C_{60} δ–doping introduces high density of recombination centers to GaAs. However, it should be pointed out that the C_{60} δ–doping at the center of the quantum well resulted in a blue shift in the quantum well photoluminescence(PL) suggesting that the C_{60} δ–doping layer acts as barriers in the quantum wells.

Next we discuss the characteristics of C_{60} layers grown on GaAs (111)B substrates. 150-500nm thick C_{60} layers are grown on the substrates at room temperature. The C_{60} cell temperature is fixed at 380℃ and the layer thickness is varied by changing the deposition time. For the 150nm-thick C_{60} layer, the growth time is approximately 3 hours. The substrate is either uniform or partially covered by SiO_2 mask. Figure1 shows surface morphologies of the grown wafers. At this growth temperature, the C_{60} growth takes place even on the mask, i.e., the grown thickness is quite uniform over the whole wafer. However, the surface of C_{60} layer grown on the SiO_2 mask is much rougher than that grown on the open areas. The PL emission from the C_{60} layer is observed only in the open areas as shown in Fig.2.

Figure 3 shows the PL spectrum of C_{60} islands. The 866-nm peak is corresponding to the edge emission of GaAs while the other peaks(630nm, 660nm and 726nm) are from C_{60} islands. Since these peaks coincide well with those observed in cubic C_{60} crystals, the C_{60} layer grown on the GaAs(111)B surface is crystalline C_{60}. These results indicate that although the lattice constant of C_{60} crystal is much larger than that of GaAs, some substrate effects are operative in this heterostructure.

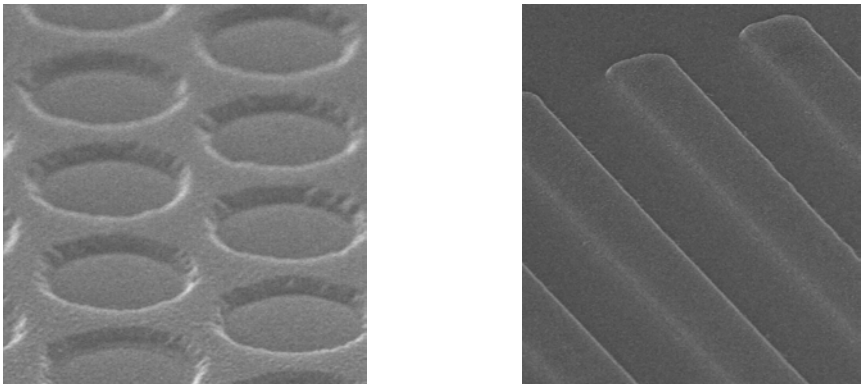

(a)C_{60} islands (2μm diameter) (b) 3μm Line&Space

Fig.1 SEM photograpns

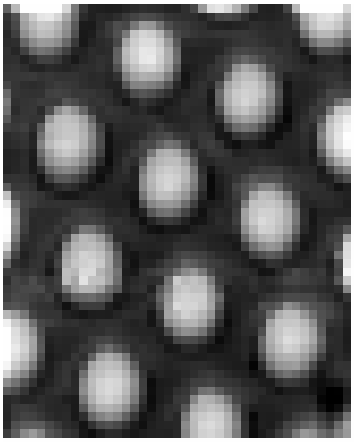

Fig.2 Micro-photoluminescence pattern of C_{60} islands

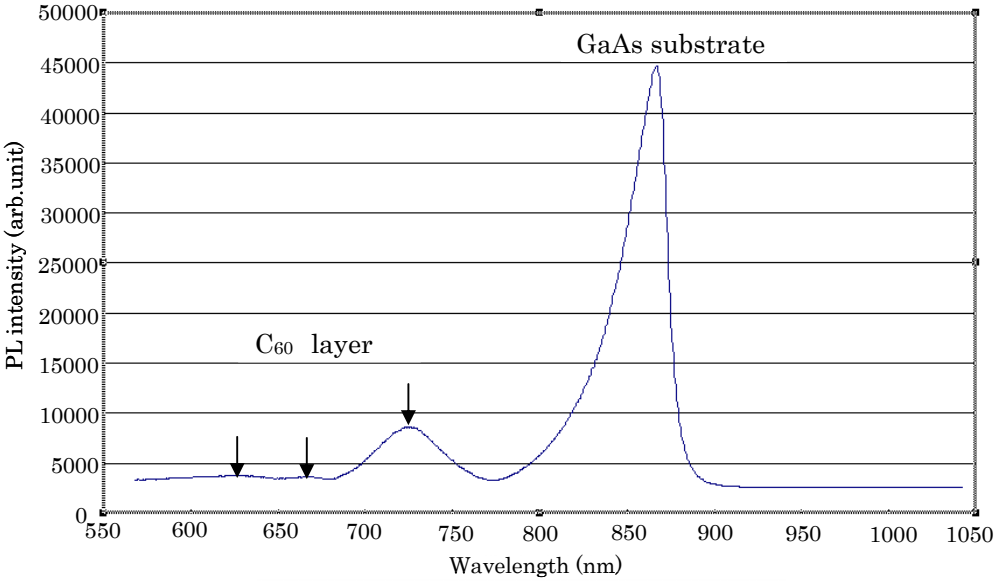

Fig.3 PL spectrum of C_{60} islands

Strong lateral confinement in self-organized $In_{0.26}Ga_{0.74}As/In_{0.26}Al_{0.74}As$ quantum wires grown on a (221)A-oriented $In_{0.26}Ga_{0.74}As$ ternary alloy substrate by MBE

K. Miyagawa, D. Suma, T. Kitada, S. Shimomura and S. Hiyamizu
Department of Physical Science, Graduate School of Engineering Science, Osaka University, Toyonaka, Osaka 560-8531, Japan

Previously we reported that quite uniform self-organized $In_{0.2}Ga_{0.8}As/GaAs$ quantum wires (QWRs) can be grown on a (221)A-oriented GaAs substrate by molecular beam epitaxy (MBE). The full-width at half maximum (FWHM) of the QWRs was as small as 5.8 meV at 12K, that is the best data reported so far for QWRs. The lateral confinement energy of the QWR, however, is rather small (~20 meV) because of a small band-offset energy (ΔEg) of 170 meV between $In_{0.2}Ga_{0.8}As$ and GaAs. $In_xGa_{1-x}As$ ternary alloy substrates enable us to grow a $In_xGa_{1-x}As/ In_xAl_{1-x}As$ heterostructure with larger band discontinuity. In this work, we grew self-organized $In_{0.26}Ga_{0.74}As/In_{0.26}Al_{0.74}As$ QWRs on a (221)A-oriented $In_{0.26}Ga_{0.74}As$ ternary alloy substrate by MBE and much enhanced lateral confinement energy was obtained.

The (221)A $In_{0.26}Ga_{0.74}As$ substrate was sliced off from an InGaAs bulk crystal which was grown with a GaAs seed crystal by the Bridgeman method. $In_{0.26}Ga_{0.74}As/In_{0.26}Al_{0.74}As$ QWs with well widths (L_w) of 0.8, 2 and 3 nm were grown on the (221)A InGaAs substrate at a temperature (T_s) of 570°C under a V/III ratio[As_4/Ga] of 20 by MBE (Fig.1). The AFM image showed the surface of the InGaAs top layer was corrugated and its step edges lay in the [1-10] direction. This corrugation has a 1.0-nm vertical amplitude and a 20-nm lateral period. Surface of the $In_{0.26}Al_{0.74}As$ layer was flat. Photoluminescence (PL) peaks were observed at 675 nm and 845 nm for the QWR layer with a nominal thickness of 0.8 nm and 2 nm, respectively. The luminescence was strongly polarized along the wire direction and the polarization degree, $P = (I_{//} - I_{\perp})/(I_{//} + I_{\perp})$, was as high as 0.36 which was much larger than that (0.23) observed for the previous (221)A $In_{0.2}Ga_{0.8}As/GaAs$ QWRs. Observed PL-FWHMs of the present QWRs were very large (54 and 35.5 meV), which is probably due to rather poor crystal quality of the InGaAs ternary ally substrates. PL excitation (PLE) spectrum was observed at 12K (Fig.4). In the PLE spectrum (detected at 1467 meV) from the 2-nm-thick QWR layer at 12K, the first peak was observed at 30 meV higher energy from the detection energy and other seven peaks were observed in the energy range of more than 130 meV. These results indicate that self-organized $In_{0.26}Ga_{0.74}As/In_{0.26}Al_{0.74}As$ QWRs grown on the (221)A $In_{0.26}Ga_{0.74}As$ substrate have much higher lateral confinement energy.

[1]T. Nitta et al., J.Vac.Sci.Technol.B19(5),1824(2001)

Corresponding author : K. Miyagawa
Phone:+81-6-6850-6457,Fax:+81-6-6850-6457,E-mail:miyagawa@d310.mp.es.osaka-u.ac.jp

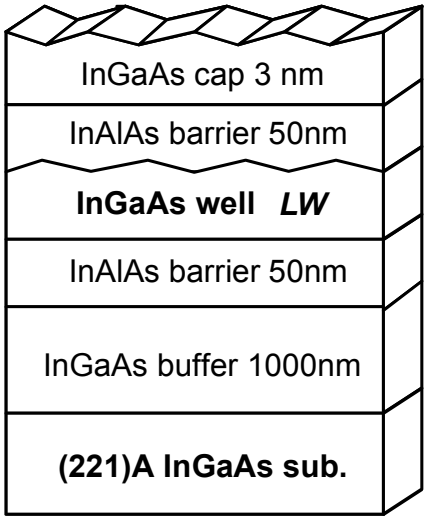

Fig.1 Schematic illustration of self-organized $In_{0.26}Ga_{0.74}As/In_{0.26}Al_{0.74}As$ QWRs grown on a (221)A $In_{0.26}Ga_{0.74}As$ substrate

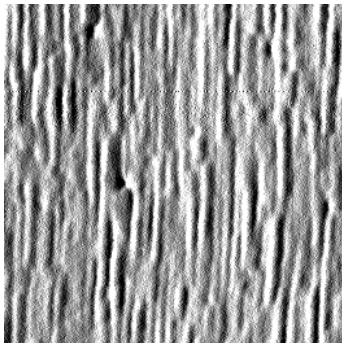

Fig.2 AFM surface image of a 3.0-nm-thick $In_{0.26}Ga_{0.74}As$ cap layer

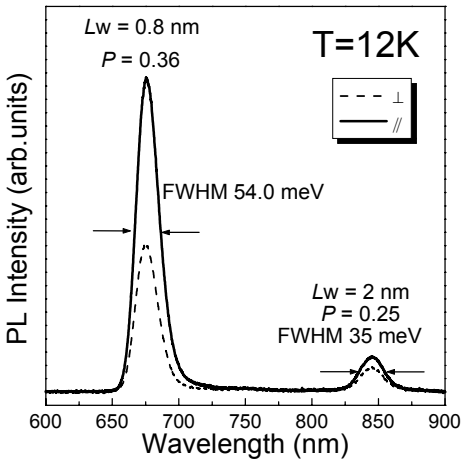

Fig.3 Polarized PL spectra of the self-organized $In_{0.26}Ga_{0.74}As/In_{0.26}Al_{0.74}As$ QWRs grown on a (221)A $In_{0.26}Ga_{0.74}As$ substrate

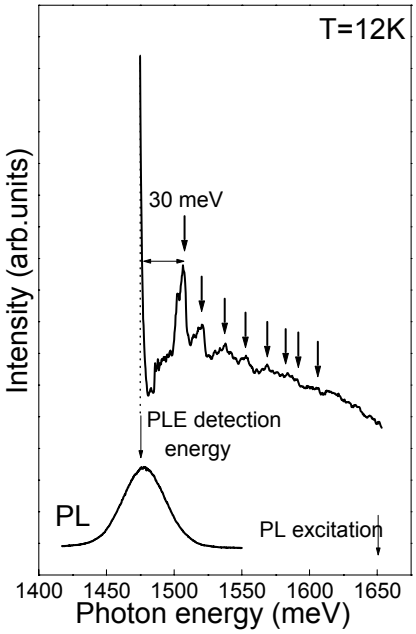

Fig.4 PL and PLE spectra of the self-organized $In_{0.26}Ga_{0.74}As/In_{0.26}Al_{0.74}As$ QWRs grown on a (221)A $In_{0.26}Ga_{0.74}As$ substrate

Stability of Pseudomorphic InGaAs Layers during annealing

A. Riposan, G.K.M. Martin, J. Mirecki Millunchick
Department of Materials Science and Engineering, University of Michigan,
2300 Hayward, Ann Arbor MI 48104-2316

MBE grown III-V compound semiconductor alloys are widely used in the fabrication of optoelectronic and microelectronic devices, many of which require flat pseudomorphic layers for the growth of quantum wells or barriers. Although growth interruptions are commonly used to enhance interface abruptness, the surfaces of strained layers may also roughen during annealing. We investigate the stability of strained $In_xGa_{1-x}As$ layers during annealing. Pseudomorphic $In_{0.27}Ga_{0.73}As/GaAs$ and $In_{0.81}Ga_{0.19}As/InP$ films were grown and annealed under various conditions ($460<T<538$ºC and $6x10^{-6}<$ As BEP$<16x10^{-6}$ torr). These compositions corresponds to the same compressive misfit strain of 1.9%. The surface morphology was examined *in situ* by Scanning Tunneling Microscopy (STM) and *ex situ* by Tapping Mode Atomic Force Microscopy (AFM). The surface composition was examined by X-ray photoelectron spectroscopy (XPS).

The surfaces of pseudomorphic Ga-rich alloys destabilize upon annealing (Fig. 1). At the end of growth, the morphology consists of wide flat terraces with wavy step edges, and a large density of 2D islands (Fig. 1a). Large 3D islands form on top of the initially flat surface upon short annealing time (Fig. 1b). With increasing annealing time, the islands are reabsorbed into the surface (Fig. 1c). At the same time, cusps form at the step edges, which inject 2D vacancies into the terraces and lead to the deterioration of the step structure (Fig. 1c). The step instability competes with the formation and the dissolution of 3D islands as mechanisms of energy reduction, depending on the annealing conditions. The 3D islands form to relieve strain energy, while their dissolution leads to a decrease in the surface energy of the alloy. The island dissolution becomes favorable due to changes in the surface composition during annealing, as measured by XPS. At the same time, undulating steps can reduce the surface energy compared with surfaces with straight steps.

The morphology of pseudomorphic In-rich layers with the same misfit strain is more stable during annealing. Initially rough step edges straighten upon annealing under high As overpressures, and no 3D island formation is observed (Fig. 2). These may be effects of the surface energy of high In concentrations. At lower overpressures, the steps develop jagged edges, as opposed to the cusping observed on the Ga-rich surfaces.

The differences observed in these systems are related to dissimilarities in the surface reconstruction. The surface reconstruction of the Ga-rich layers consists of highly disordered regions and small domains of nx3 and $\sqrt{2}(2x4)$ (Fig. 3a). For the same misfit strain, the In-rich surfaces consist mostly of domains of 4x3 and $\sqrt{2}(2x4)$ reconstructions (Fig. 3b). The reconstruction domains are larger on these surfaces, and their relative coverage changes during annealing. The increased order in the reconstruction of In-rich layers may increase the line tension of the steps, impeding the cusping.

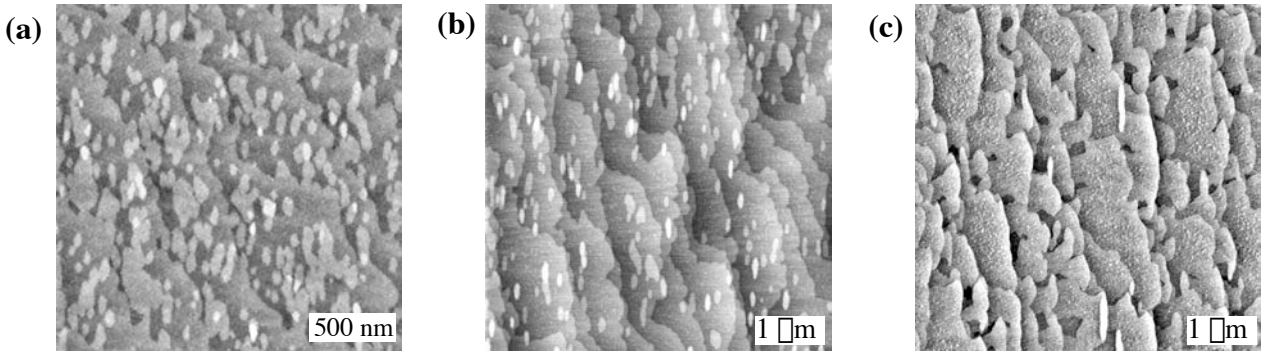

Fig. 1: AFM showing the surface morphology of $In_{0.27}Ga_{0.73}As/GaAs$ layers, grown to h=25 ML at T=487°C and BEP=16x10^{-6} torr (a), and annealed at T=487°C and BEP=6x10^{-6} torr for 5 min (b) and 25 min (c). The height scale is 5 nm.

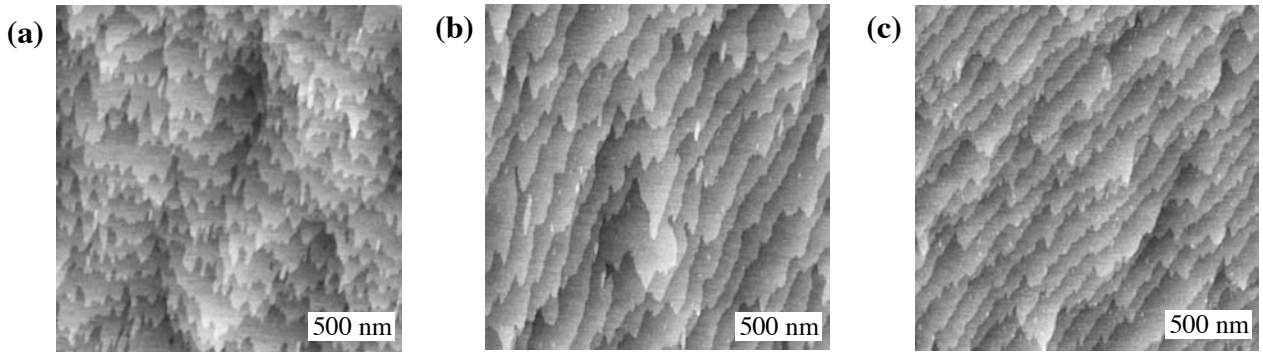

Fig. 2: AFM showing the surface morphology of $In_{0.81}Ga_{0.19}As/InP$ layers, grown to h=25 ML at T=460°C and BEP=12x10^{-6} torr (a), and annealed for 5 min (b) and 25 min (c). The height scale is 5 nm.

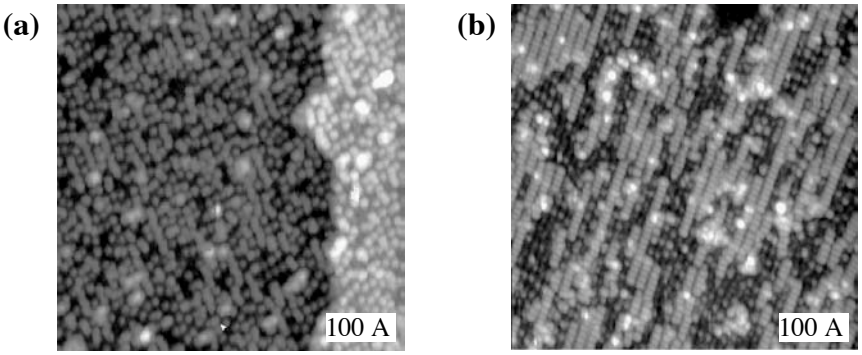

Fig. 3: STM images showing the surface reconstruction of (a) h=25 ML $In_{0.27}Ga_{0.73}As/GaAs$ grown at T=487°C and BEP=16x10^{-6} torr, and (b) h=25 ML $In_{0.81}Ga_{0.19}As/InP$ grown at T=460°C and BEP=12x10^{-6} torr.

Contact-less Electroreflectance of CdSe/ZnSe Quantum Dots Grown by Molecular Beam Epitaxy

Martín Muñoz[1], Shiping Guo, Xuecong Zhou, and Maria C. Tamargo

Chemistry Department, City College of the City University of New York

Convent Ave. at 138th Street, New York, NY 10031.

Y. S. Huang
Department of Electronic Engineering, National Taiwan University of Science and

Technology, Taipei 106, Taiwan, Republic of China.

C. Trallero-Giner, and A. H. Rodríguez
Departamento de Física Teórica, Facultad de Fisica, Universidad de La Habana

San Lazaro y L, 10400 La Habana, Cuba

The interband transitions of a capped CdSe quantum dots structure have been investigated using contact-less electroreflectance. The electroreflectance spectrum shows transitions originating from all the relevant portions of the sample including the quantum dots and the wetting layer. The transitions of the two dimensional layers have been modeled using an envelope approximation calculation which takes into account the bi-dimensional strain in the wetting layer. A good agreement was found between the experimental values for the transitions and the calculated ones. From atomic force microscopy measurements a lens shape was observed for the uncapped quantum dots. Taking into account the lens shape geometry and assuming that the effective height-to-radius ratio is preserved, the size of the capped quantum dots was determined using the observed electroreflectance transitions, in the framework of the effective mass approximation.

[1] Correspondence Author, e-mail: mmunoz@sci.ccny.cuny.edu.

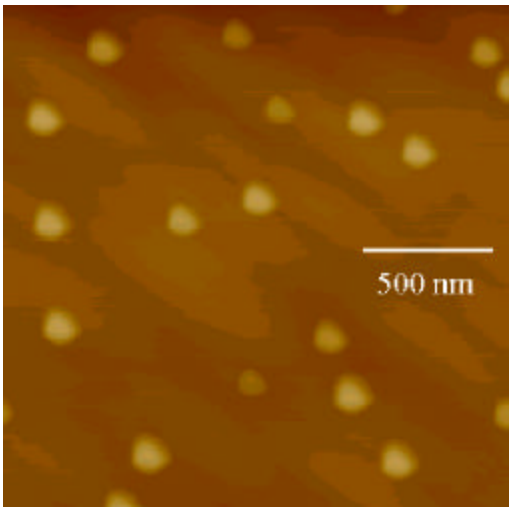

Fig. 1 AFM image (2x2 m) of uncapped CdSe quantum dots deposited on ZnSe.

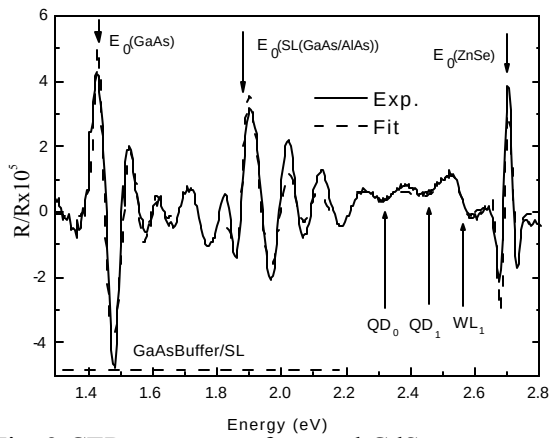

Fig. 2 CER spectrum of capped CdSe quantum dot structure. Solid and dashed lines represent the experimental data and fit, respectively. The arrows indicate the energies obtained from our fit scheme.

Table 1. Experimental and calculated interband energies.

Transition	Experiment (eV) (±0.005)	Theory (eV)	PL (eV) (±0.002)
E_0(GaAs)	1.428 (1.422[a])		
SL(GaAs/AlAs) 1C-1H	1.873	1.876	
QD_0 $\|1,0\rangle_e$ $\|1,0\rangle_{hh}$	2.320	2.320	2.319
QD_1 $\|1,1\rangle_e$ $\|1,1\rangle_{hh}$	2.455	2.455	
WL_1 1C-1H	2.560	2.560[b]	
E_0(ZnSe)	2.700	2.700[c]	

MBE growth of ZnO using initial Zn layer and MgO buffer layer on Si(111) substrates

Miki Fujita, Noriaki Kawamoto, Masanori Sasajima and Yoshiji Horikoshi
School of Science and Engineering, Waseda University, 34-1 Okubo, Shinjuku-ku, Tokyo 169-8555, Japan
Kagami Memorial Laboratory for Materials Science and Technology, Waseda University, 2-8-26 Nishiwaseda, Shinjuku-ku , Tokyo 169-0051, Japan
Phone:+81-3-5286-3176, Fax:+81-3-3209-3450
E-Mail:miki-f@ruri.waseda.jp

ZnO is one of the most attractive materials for use in short wavelength optical devices due to its direct wideband gap (3.37eV at room temperature) and large exciton binding energy (60meV). In most studies, sapphire substrates are used for ZnO growth. However, sapphire is electrically insulating material. Electrically conductive Si substrate is useful when the material is applied to injection devices. The growth of epitaxial ZnO films on Si substrate is, however, known to be a difficult task, because the Si substrate surface is easily oxidized. Therefore, to prevent the Si substrate surface from being oxidized in the initial stage of ZnO growth is the most important issue for ZnO growth on Si substrate. We have attempted to grow ZnO films on Si substrates by two methods: (i) initial Zn layer deposition followed by its oxidation, and (ii) thin MgO buffer layer deposition prior to the growth. All the layers are deposited on Si(111) substrates by molecular beam epitaxy (MBE) using a radio frequency (RF) radical cell. Figure 1 shows the layer structures for these two growth sequences.

In the first growth sequence (i), an initial Zn layer is deposited on Si(111) surface with (7×7) reconstruction and then oxidized at 50℃. Then thin ZnO buffer layer is grown at 400℃, and finally 1μm thick ZnO layer is grown at 575℃. The ZnO films with thin MgO buffer layer (ii) are grown by depositing a few monolayer Mg at 350℃ on (7×7) reconstructed Si(111) surface. After oxidizing the Mg layer, the main ZnO layer is grown at 575℃.

The microscopic images of grown layer surfaces are shown in Fig.2. The ZnO films grown by using initial Zn layer exhibit straight lines along the principal axes of Si(111) surface. They are probably due to the cracks caused by the difference in thermal expansion coefficients. This phenomenon is alleviated considerably by introducing a thin MgO buffer layer as shown in Fig.2(b). X-ray diffraction measurements reveal that (0001)-oriented ZnO films are grown on Si(111) substrates in both cases. The $2\theta/\omega$,and ω scan spectra are demonstrated in Fig.3. Two peaks shown in XRD $2\theta/\omega$ spectrum in the ZnO sample grown using initial Zn layer is probably caused by these cracks. The samples with thin MgO buffer layer show no double peaks and the FWHM value for both $2\theta/\omega$, and ω scan are quite sharp. The photoluminescence emission intensity is also improved by using thin MgO buffer layer as shown in Fig.4.

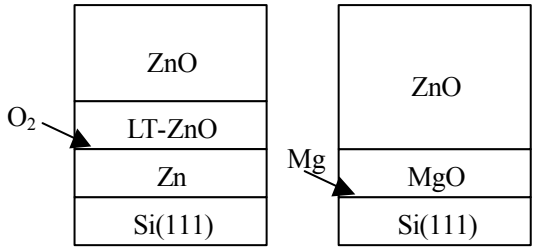

(a) initial Zn layer (b) MgO buffer layer

Fig. 1 structures

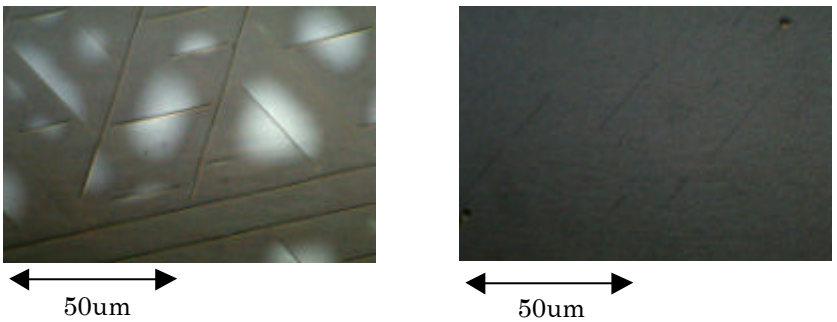

(a) initial Zn layer (b) MgO buffer layer

Fig.2 microscopic images

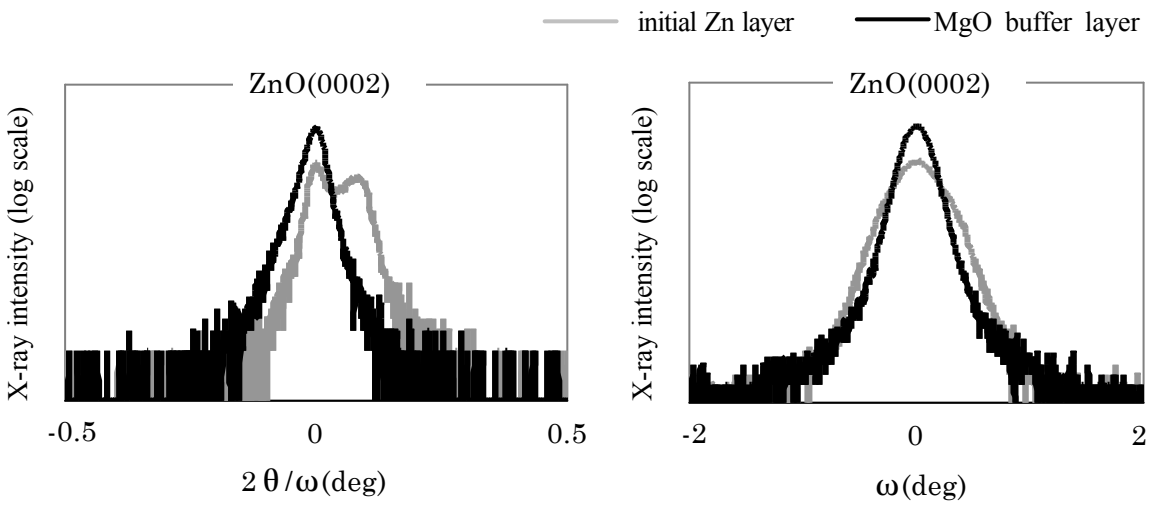

Fig.3 XRD spectra

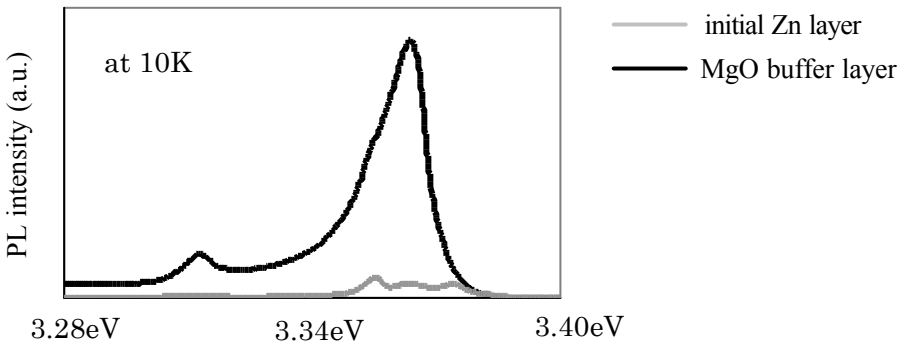

Fig.4 PL spectra

Compositional Analysis of Graded $Al_xGa_{(-x)}As$ Layers by X-ray Energy Dispersive Spectrometry

K. Mahalingam, R. Wheeler, K. G. Eyink, and S. T. Fenstermaker
Air Force Research Laboratory, Materials & Manufacturing Directorate
AFRL/MLPS, 3005 P St., Wright-Patterson AFB, OH 45433-7707

Compositionally graded $Al_xGa_{(1-x)}As$ layers are important materials for graded-index wave guide applications, wherein the index of refraction varies continuously with Al content. Successful application of these materials requires characterization techniques that can accurately quantify both, the shape of the graded profile and its composition. The use of techniques such as SIMS and Auger electron spectroscopy (AES) pose problems due to insufficient spatial resolution and inaccuracies in composition due to smearing from adjacent layers.

In this study we employ the X-ray energy dispersive spectrometry (XEDS) technique to characterize a variety of $Al_xGa_{(1-x)}As$ layers with linear, parabolic and sinusoidal grading in the Al content. The individual layers were grown by molecular beam epitaxy, with film thickness and composition monitored in-situ by spectroscopic ellipsometry (SE). The XEDS measurements were obtained using field emission gun transmission electron microscope (FEG TEM), to exploit the small probe size (high spatial resolution) and high brightness (improved sensitivity) associated with the FEG source. The Al/Ga composition profiles were determined based on the Cliff-Lorimer (CL) equations, assuming the thin-foil criterion. The so called “k-factors” in the CL equations (k_{Al-As} , k_{Ga-As} and k_{Al-Ga}), required for calculating the composition profiles, were determined from pre calibrated $Al_xGa_{(1-x)}As$ layers. Further details on the comparison between XEDS results with those obtained from other techniques will be presented. The application of XEDS to identify film growth related problems, such as flux transients, will also be discussed.

Note: Poster presentation preferred

Corresponding Author:

Krishnamurthy Mahalingam
E-mail: krishnamurthy.mahalingam@wpafb.af.mil
Phone: (937) 255-4474 Ext. 3245

Supporting Data

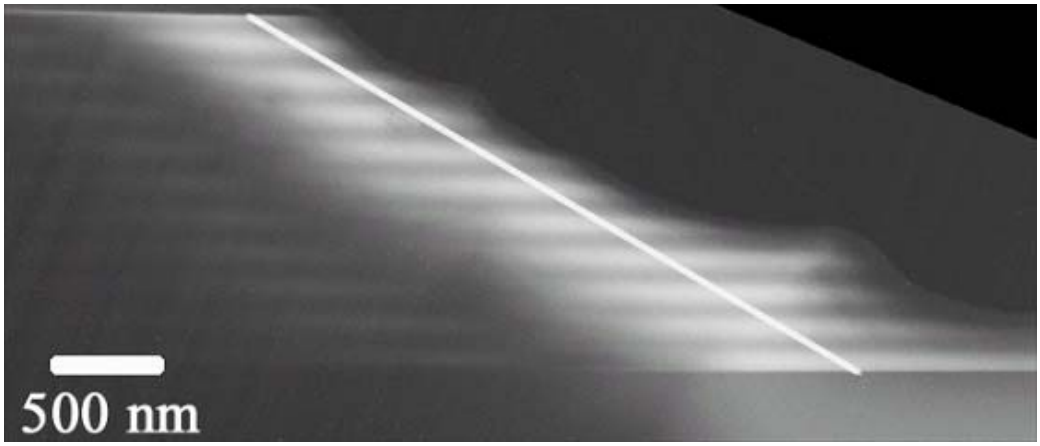

Figure 1 A 200 dark-field TEM image of a 10-period sinusoidal-graded $Al_xGa_{(1-x)}As$ layer.

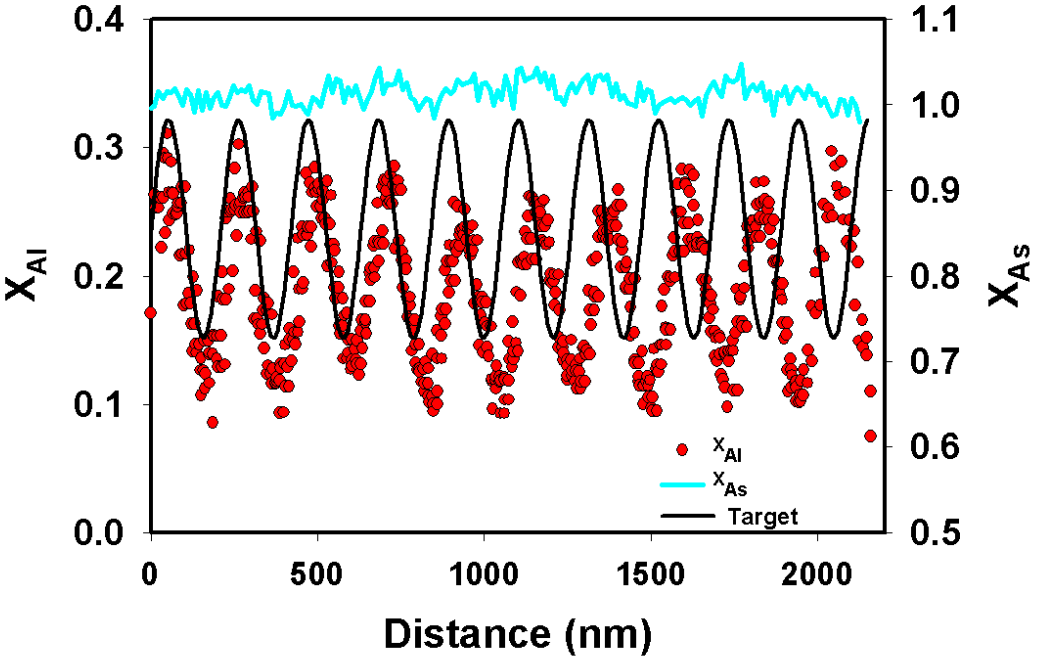

Figure 2 The Al and As concentration profile for the ten periods of the sinusoidal-graded $Al_xGa_{(1-x)}As$ layer (along the line shown in Fig. 1).

Low Temperature Si Growth on Si (001): Impurity Incorporation and Limiting Thickness for Epitaxy

J.-M. Baribeau, X. Wu, D.J. Lockwood, L. Tay, G. I. Sproule*

Institute for Microstructural Sciences, National Research Council Canada,
Ottawa, K1A 0R6, Canada

Structural studies of Si grown at low temperature on Si(001) have revealed the existence of a limiting thickness for epitaxial growth *h* for that system.[1,2] As temperature is decreased, breakdown of epitaxy is observed at increasingly smaller thickness. Although the temperature dependence of *h* has been studied by several authors[1,3-5], the mechanism that leads to epitaxy breakdown is not fully understood and the concomitant impurity incorporation has not been much investigated. Here we report a study of the structural evolution and impurity incorporation in low-temperature Si MBE.

A number of wafers were prepared by depositing Si on 100 mm Si(001) wafers in a V80 VG Semicon MBE system. For these experiments, the growth rate was fixed at 0.2 nm/s and the temperature varied in the range 177– 414 ^{o}C. The Si wafer preparation consisted of a dilute HF dip to remove the native oxide and to leave a H-passivating layer that was desorbed in UHV at 600 ^{o}C prior to growth. For comparison, a-Si films were also prepared under similar growth conditions by depositing Si directly on substrates that had not received the above surface preparation. The layers thus grown were studied by TEM, SIMS, and Raman scattering.

Fig.1 is a <110> cross-section TEM image of a sample grown at 374 ^{o}C. At this fairly high temperature, after the initial (~ 50 nm thick) perfect epitaxial growth, epitaxy breakdown occurs and is characterized by a columnar structure along the [001] growth direction. The TEM image also shows planar defects (twins) formed in {111} planes (indicated by arrows) after the epitaxy breakdown. The formation of twins in the film is clearly evident in the diffraction pattern of the film (see inset, Fig. 1) The SIMS impurity profile for this sample is shown in Fig. 2. The depth at which defects are first observed is correlated with a peak in the H concentration. This is consistent with H atoms segregating to the surface in the crystalline phase and being incorporated there once extended defects start to nucleate in the film. The O and C incorporation is low until the film crystallinity has strongly deteriorated. A similar film evolution is seen at lower growth temperatures, but occurring earlier on (i.e., at smaller thicknesses) during deposition. The limiting thickness *h* is shown in Fig. 3 in an Arrhenius plot. Our data is in good agreement with published results and consistent with an activation energy of 0.47 eV. This would lend support to a recent model that links the breakdown of epitaxy to the supersaturation of the growing layer with hydrogen.[6]

The impurity profiles in a-Si films exhibit a close similarity to those obtained on epitaxial c-Si grown at the same temperature (see Fig. 4 for an example for a growth at 335 ^{o}C). While similar saturation levels near the surface are not surprising as they reflect the Si flux to impurity flux ratio, the similarity found deeper in the film is somewhat surprising and indicates an impurity uptake in the a-Si phase more characteristic of defective c-Si than bulk a-Si. Raman scattering results on these samples showing the evolution of the layer growth and the Si bond configuration with growth temperature will be presented.

1. D.J. Eaglesham, H.-J. Gossmann and M. Cerullo, Phys. Rev. Lett. **10**, 1227 (1990).
2. H. Jorke, H.-J. Herzog and H. Kibbel, Phys. Rev. B **40**, 2005 (1989).
3. M.V.R. Murty and H.A. Atwater, Appl. Phys. Lett. **62**, 2566 (1994).
4. W.J. Varhue, J.L. Rodgers, P.S. Audrey and E. Adams, Appl. Phys. Lett. **68**, 349 (1996).
5. A.I. Nikiforov, B.Z. Kanter and O.P. Pchelyakov, Thin Solid Films **336**, 179 (1998).
6. J. Thiesen, H.M. Branz and R.S. Crandall, Appl. Phys. Lett. **77**, 3589 (2000).

* *Corresponding author. e-mail jeanmarc.baribeau@nrc.ca, Tel. 613 993 8249, Fax 613 941 4667*

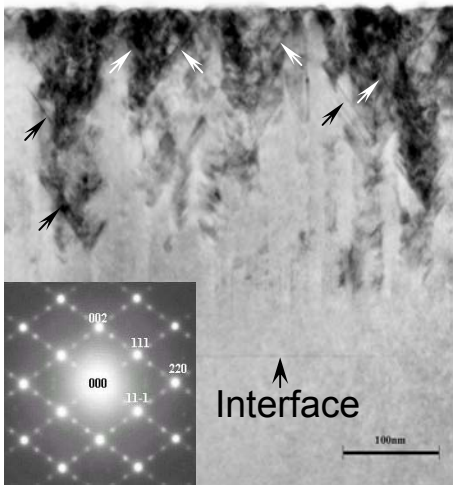

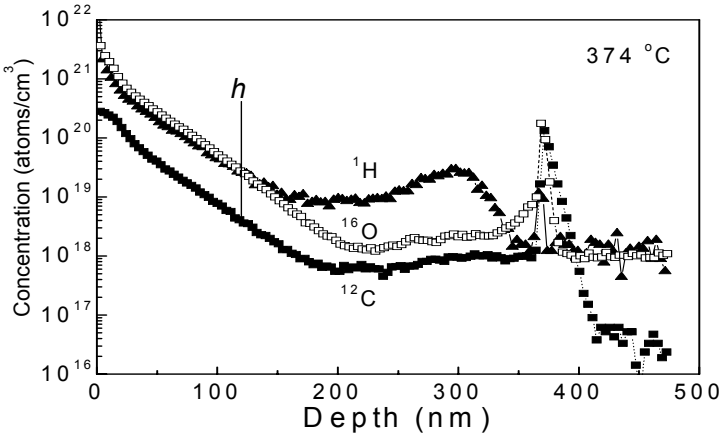

Fig 1. (left) Cross sectional TEM micrograph of a Si film deposited at 374 °C with a selected area diffraction pattern taken from the defected region. Fig. 2 (right) SIMS impurity profiles for the same sample.

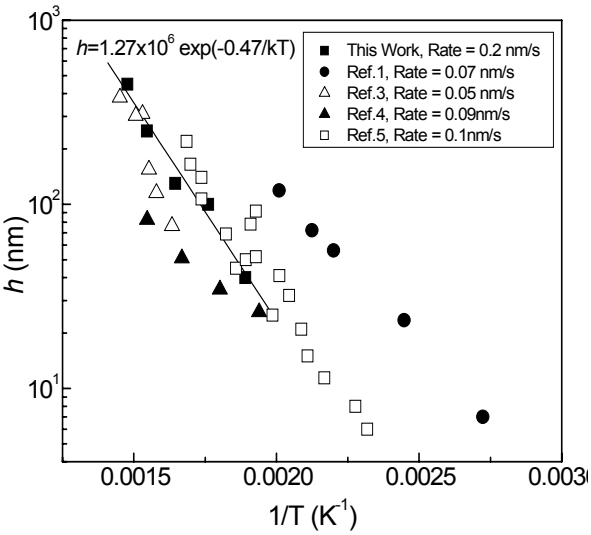

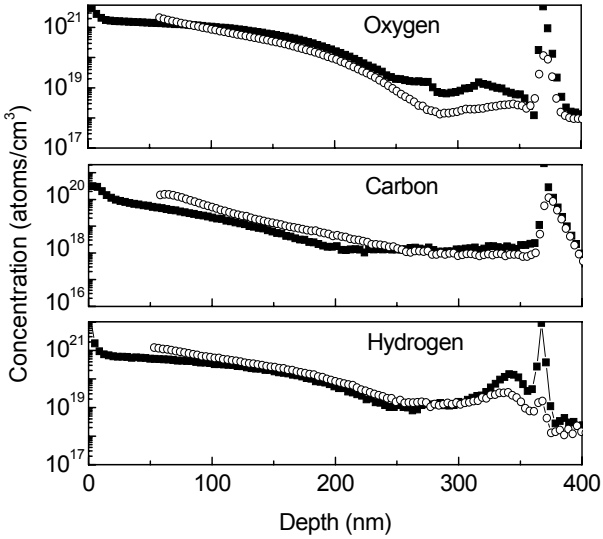

Fig 3. (left) Limiting thickness for epitaxy *h* for Si deposition on Si (001). Fig. 4 (right) Comparison of impurity profiles in Si films deposited on Si(100) epitaxially (open circles) or in the amorphous phase (full squares). Growth temperature was 335 °C. The ease conparison the profiles from the epitaxial film have been shifted so that the film/substrate interfaces appear at the same depth for both samples.

NAMBE 2003 Program

Tuesday, September 30, 2003

8:00-10:00: Special Topics in MBE Growth and Characterization

Chair: Hock Ng (Lucent)

TA-1: Studies of Oxide Desorption from GaAs Substrates via Ga_2O_3 to Ga_2O Conversion by Exposure to Ga Flux
Z. R. Wasilewski, J.-M. Baribeau, M. Beaulieu, X. Wu, G. I. Sproule, and J. W. Fraser
National Research Council-Canada

TA-2: Mn and Be co-doped GaAs for high hole concentration by LT-MEE
Koji Onomitsu, Hideo Fukui, Takashi Maeda, and Yoshiji Horikoshi
Waseda University, Japan

TA-3: Sb-Mediated Growth of Si and Be Doped AlGaAs by Molecular Beam Epitaxy
S. R. Johnson*, Yu. G. Sadofyev, K. Franzreb, Y. Cao, D. Ding, N. Samal, S. A. Chaparro, J. Wang, J. Xu, S. Q. Yu, and Y.-H. Zhang
Arizona State University

TA-4: Composition Verification of AlGaAs Epitaxial Layers using Inductively Coupled Plasma Optical-Emission Spectroscopy
K. A. Bertness, T. E. Harvey, A. J. Paul, L. H. Robins, G. C. Turk, T. A. Butler, and M. L. Salit
National Institute of Standards and Technology

TA-5: Single-phase growth studies of GaP on Si by solid-source MBE
X.Yu, P.S. Kuo, K Ma, M. M. Fejer, and J. S. Harris Jr.
Stanford University

TA-6: Intermixing and As Incorporation in GaAs/GaSb Multilayers
C. Dorin, C. Wauchope, and J. Mirecki Millunchick
University of Michigan

Studies of Oxide Desorption from GaAs Substrates via Ga_2O_3 to Ga_2O Conversion by Exposure to Ga Flux

Z. R. Wasilewski*, J.-M. Baribeau, M. Beaulieu, X. Wu, G. I. Sproule, J. W. Fraser
Institute for Microstructural Sciences, National Research Council Canada, Ottawa, Ontario K1A 0R6, Canada

Standard thermal desorption of native oxides from GaAs substrates can lead to very considerable roughening of the surface. Typically, very high densities of surface pits are formed, many of which are deeper than 10 nm.[1] For many epitaxial structures such morphology is not acceptable. Although combination of smoothing superlattices and thick GaAs buffer layers can effectively planarize the surface, their deposition takes time, consumes elements, and could be undesirable for a variety of other reasons. Recently, an alternative method of oxide desorption, which can lead to a much smoother surface has been proposed.[2] Rather than desorbing the oxide by ramping the substrate temperature above 580 °C under As flux, the oxide was removed via a Ga_2O_3 to Ga_2O conversion by exposure of the substrate surface to a Ga flux at 440 °C. In the present work we aim at gaining a better understanding of the processes involved during both methods of oxide desorption, as well as assessing the practicality of the latter approach in day-to-day work. We use a Ga flux of 4.4×10^{14} $cm^{-2}s^{-1}$, which would result in a 0.2 nm/s GaAs growth rate. The oxide conversion procedure was carried out with the wafer at 480 °C and Ga delivered to the surface in 1 s pulses spaced every 16 s. The progress of oxide removal was monitored with synchronized RHEED and Desorption Mass Spectrometry (DMS) tuned to the Ga_2O signal (Fig. 1). The experiments were performed on rotating substrates (~ 60 RPM) to ensure uniform temperature and Ga exposure across the wafer. The surface morphologies were examined ex-situ with AFM (Fig. 2), while the quality of the interface between the substrate and GaAs epi-layers was assessed with SIMS, TEM and SEM. The supply of 80-100% of the Ga needed for complete conversion results in an RMS roughness of less than 0.3 nm, provided that the remaining oxide is removed in the standard fashion. Although an even larger under-supply of Ga to the surface can result in greatly improved morphology, we find the procedure to be considerably less tolerant of an oversupply of Ga. In this case accumulated Ga droplets are hard to planarize with subsequent epitaxy, even if completely converted to GaAs mounds. We present other practical implications ensuing from this study, and discuss the insights into the general processes governing oxide removal gained from analysis of the dynamic response of RHEED and DMS signals, as well as from AFM measurements of partially removed oxides.

[1] A. Ballestad, B. J. Ruck, J. H. Schmid, M. Adamcyk, E. Nodwell, C. Nicoll, and T. Tiedje, Phys. Rev. B **65,** 205302 (2002) and references therein.
[2] Y. Asaoka, J. Cryst. Growth **251,** 40 (2003).

* Corresponding author: e-mail: zbig.wasilewski@nrc.ca

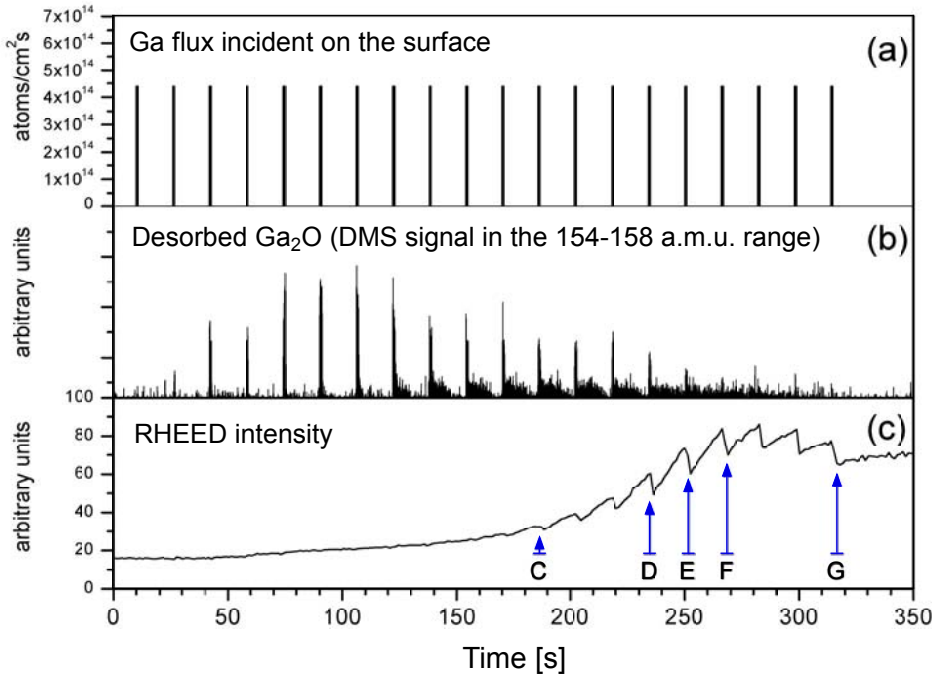

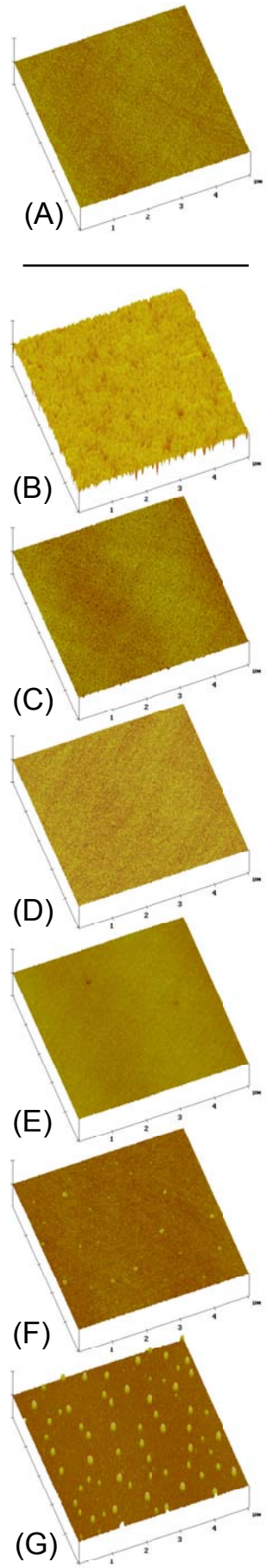

Figure 1. DMS and RHEED recordings showing the process of oxide removal at 480 °C by converting stable Ga_2O_3 into volatile Ga_2O with exposure to Ga flux. (a) Ga flux incident on the surface vs. time - total of 20 pulses, each 1s long. (b) DMS count of desorbing Ga_2O vs. time - note that the first two pulses produce very little Ga_2O, also note the appearance of a component with longer decay time at the later stages (c) RHEED diffraction spot intensity vs. time - note the instant drop of intensity during Ga exposure followed by strong intensity recovery. The arrows schematically show the amount of Ga delivered to the surface at 480 °C for the samples shown in Fig. 2 with corresponding labels.

Figure 2. AFM images of 5x5 μm area of substrate surface before oxide removal (A), and after oxide removal (B)-(G). The vertical scale total length is 50 nm. Surface (B) has been obtained by standard oxide removal procedure, where the substrate is ramped under As overpressure to temperature 630 °C. Surfaces (C)-(G) were obtained by (i) bringing the substrate temperature to 480 °C, (ii) supplying Ga to the surface in 1s pulses in absence of As, (iii) ramping the substrate to 600 °C and annealing for 600s in the presence of As. The amount of Ga supplied to the surface for each of the cases (C)-(G) is schematically indicated with an arrow and corresponding letter in Fig. 1. The RMS roughness and Max depth or height of localized features are:

Panel	RMS	Max
A	0.30 nm	
B	2.19 nm	-24.9 nm
C	0.40 nm	-2.2 nm
D	0.24 nm	
E	0.24 nm	-2.2 nm
F	0.65 nm	+1.9 nm
G	2.31 nm	+6.5 nm

Mn and Be co-doped GaAs for high hole concentration by LT-MEE

Koji Onomitsu [1,2], Hideo Fukui[1,2], Takashi Maeda[1,2] and Yoshiji Horikoshi[1,2]

[1]School of Science and Engineering, Waseda University, 3-4-1 Okubo, Shinjuku-ku, Tokyo 169-8555, Japan

[2]Kagami Memorial Laboratory for Materials Science and Technology, Waseda University, 2-8-26 Nishiwaseda, Shinjuku-ku , Tokyo 169-0051, Japan

Phone:+81-3-5286-3176, Fax:+81-3-3209-3450

E-Mail:onomitsu@horikosi.elec.waseda.jp

Mn doped GaAs is attractive material as a dilute magnetic semiconductor. It is reported that the Curie temperature (Tc) can be raised by increasing the hole concentration as well as Mn concentration. However, the hole concentration due to the Mn doping tends to saturated at approximately ~$10^{20}/cm^3$. Therefore, some additional doping is needed to achieve high hole concentration. In addition, since the growth of heavily Mn doped GaAs layers is performed under high As pressure at low temperatures, point defects such as As-anti sites and interstitial As are inevitably formed in the crystal. In the present work, we have investigated the effect of co-doping of Mn-Be and also the effect of modified doping to raise the total hole concentration. Also by applying the migration-enhanced epitaxy (MEE) at low temperatures under optimized As pressure, we have grown the layer with low point defect concentration.

Figure 1 compares the carrier concentration and resistivity for Mn doped and Be doped samples with the simultaneously Mn-Be co-doped sample. Both Mn doped and Be doped samples exhibit hole concentrations higher than $1x10^{19}/cm^3$ at room temperature. In contrast, the Mn-Be co-doped sample shows remarkable decrease in its hole concentration, and the resistivity increases. The corresponding hole mobility is also decreased. These results indicate that the complex defects of Mn and Be are formed, and deteriorate the electrical characteristic of GaAs. Two structures have been studied in order to alleviate the complex defect. First, Be-AlGaAs/Mn-GaAs modulation doped heterostructures are grown in order to increase the total hole concentration in the Mn doped GaAs layer. Spatially separated doping of Mn and Be in GaAs is also performed. In this experiment, 177 pairs of Be doped GaAs (8 monolayers)/ Mn doped GaAs (8 monolayers) separated by undoped GaAs (2 monolayers) are grown by low temperatures MEE. In both cases, considerable increase in the hole concentration is achieved. The latter results are shown in Fig. 2. Because the hole concentration increases and the mobility shows no decrease for this sample, it is expected that the complex defect concentration is decreased considerably. Figure 2 (d) shows the magnetic Hall resistance of separation-doped sample. Although the magnetic characteristic is still observed only at low temperatures, the increase of Tc can be expected by optimizing the structure.

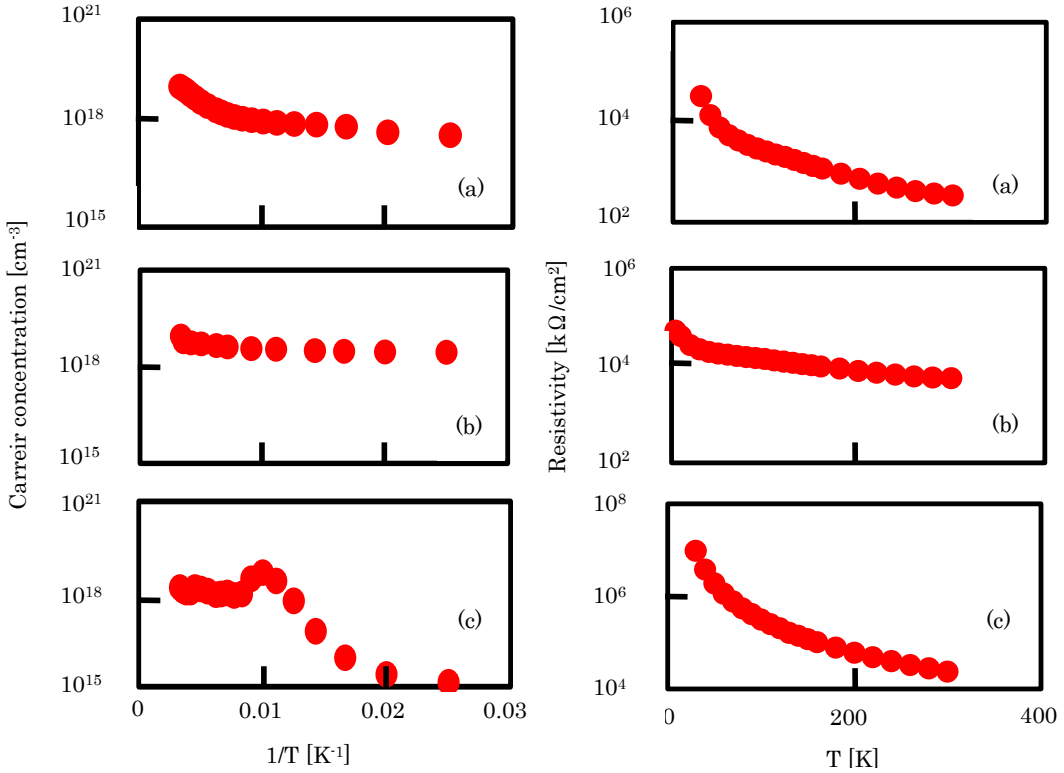

Fig.1 Carrier concentration and resistivity of

(a) Mn doped sample (b) Be doped sample (c) Co-doped sample

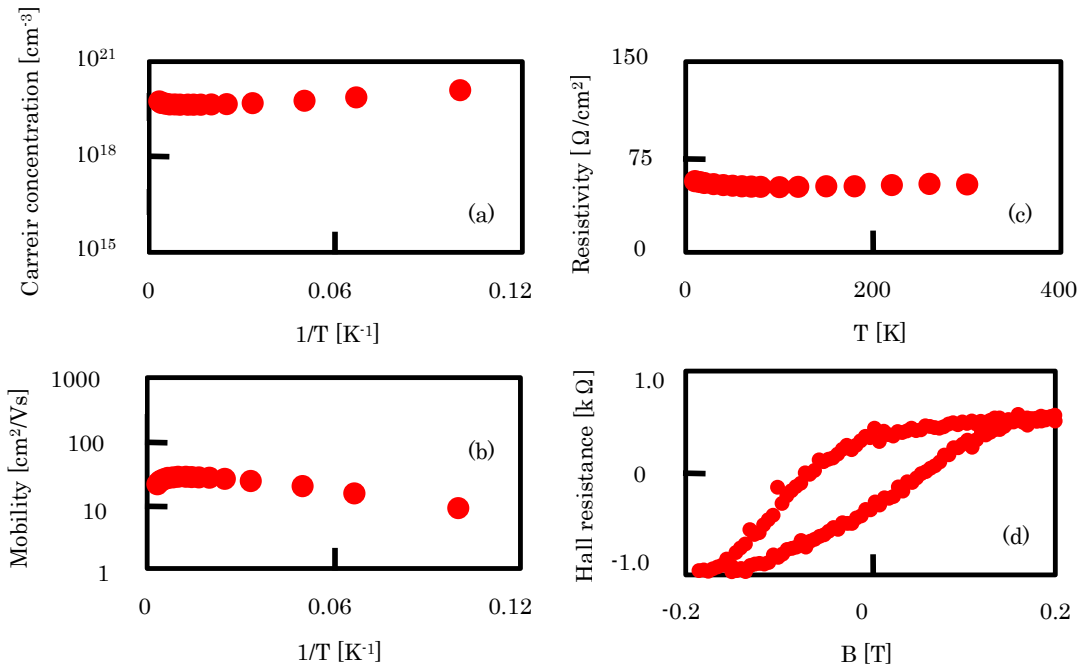

Fig.2 (a)~(c) : The electrical characteristics, and (d) : Magnetic hall resistance of separation doped sample

Sb-Mediated Growth of Si and Be Doped AlGaAs by Molecular Beam Epitaxy

S. R. Johnson*, Yu. G. Sadofyev, K. Franzreb, Y. Cao, D. Ding, N. Samal,
S. A. Chaparro, J. Wang, J. Xu, S. Q. Yu, Y.-H. Zhang
Center for Solid State Electronics Research, Department of Electrical Engineering,
Arizona State University, Tempe, AZ 85287-6206

The molecular beam epitaxy (MBE) growth of AlGaAs layers in the forbidden temperature region (620–680 °C) gives rise to poor surface morphology [1-4]. Lower growth temperatures result in a smooth surface morphology, but with less than optimal electrical properties compared to material grown at higher temperatures. At higher growth temperatures the sticking coefficient of Ga is less than unity, resulting in poor composition control. Kaspi et al [5] proposed the use Sb as a surfactant to facilitate the growth of smoother AlGaAs in the forbidden temperature gap where the Ga sticking coefficient is close to unity.

In this work we study the Sb-mediated growth of AlGaAs layers doped with Be and Si with emphasis on optimizing the electrical and optical properties for device applications. Several samples were grown at 580, 610, 640, 670, 700, and 720 °C using Sb/III flux ratios of 0.00, 0.005, 0.01, and 0.02 with As/III overpressures of 1.5 for lower growth temperatures and 2.0 for higher growth temperatures. The samples were grown on (100) semi-insulating (SI) GaAs substrates, starting with a 30 nm GaAs buffer layer, followed by 200 nm of undoped $Al_{0.65}Ga_{0.35}As$ and 1000 nm of Si (or Be) doped $Al_{0.65}Ga_{0.35}As$, capped with a 10 nm thick n (or p) GaAs contact layer. The contact layer thickness was chosen to be thick enough to provide electrical contact to AlGaAs layer and yet thin enough not to obscure the surface morphology of the under lying AlGaAs layer. The samples were investigated using atomic force microscopy (AFM), Hall effect in the Van der Pauw contact geometry, X-ray diffraction (XRD), and secondary ion mass spectroscopy (SIMS).

The root mean square surface roughness (RMS) measurements by AFM for the various Sb/III flux ratios and growth temperatures are shown in Fig. 1. For growth in the forbidden temperature zone, the smoothing effect of the Sb surfactant is evident and the amount of Sb flux required for smoothing increases with substrate temperature. The XRD measurements reveal that 40% of the Sb is incorporated at 580 °C. Fig. 2 shows the temperature dependence of the Sb incorporation rate as determined by SIMS measurements on the samples grown with a Sb/III flux ratio of 0.02. The Sb mole fraction (left-hand axis) and the Sb sticking coefficient (right-hand axis) decrease by two orders of magnitude, resulting in a Sb concentration of 2×10^{18} cm^{-3} at 700°C. Even at the highest growth temperatures Sb is incorporated as an isoelectronic dopant.

The electron mobility given by room temperature Hall effect measurements is shown in Fig. 3 for the Si doped $Al_{0.65}Ga_{0.35}As$ samples in this study. The electron mobility increases with growth temperature and is enhanced by Sb co-doping. It appears that the optimal Sb co-doping levels occur at a Sb/III flux ratio of about 0.005 to 0.01 over the 640 to 700 °C growth temperature range, which results in Sb co-doping levels in the mid 10^{18} cm^{-3} range. At the highest growth temperature (720 °C) the decrease in the mobility is caused by an increase in the Al mole fraction from 0.65 to 0.70 due to a reduction in the Ga sticking coefficient from close to unity at 700 °C to about 0.8 at 720 °C. We also grew Be-doped, Sb-mediated $Al_{0.65}Ga_{0.35}As$ layers with 1.5×10^{18} cm^{-3} hole-concentrations, and experienced the same smoothing effects as in n-type AlGaAs. However, unlike the n-type material, Sb co-doping reduced the hole-mobilities.

*Corresponding author: Tel: 480-965-2565, Fax: 480-965-0775, E-mail: shane.johnson@asu.edu

References

[1] H. Morkoç, T.J. Drummond, W. Kopp, R. Fischer. J. Electrchem. Soc. **129**, 824 (1982).

[2] W.I. Wang, S. Judaprawira, C.E.C. Wood, L.F. Eastman. Appl. Phys. Lett. **38**, 708 (1981).

[3] R.A. Stall, J. Zilko, V. Swaminathan, N. Schumaker. J. Vac. Sci. Technol. **B3**, 524 (1985).

[4] K. Ohta, T. Kojima, T. Nakagawa. J. Cryst. Growth **95**, 71 (1989).

[5] R. Kaspi, K. R. Evans, D.C. Reynolds, J. Brown, M. Skowronski. Mat. Res. Symp. Proc. **379**, 79 (1995).

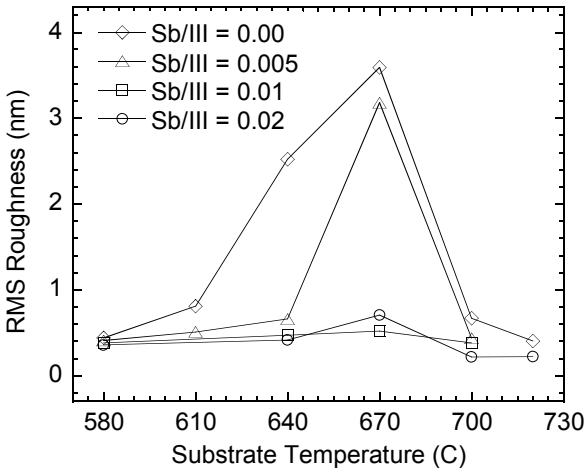

Fig. 1. Root mean square (RMS) surface roughness for 1 μm thick $Al_{0.65}Ga_{0.35}As$ layers grown at various Sb fluxes and substrate temperatures.

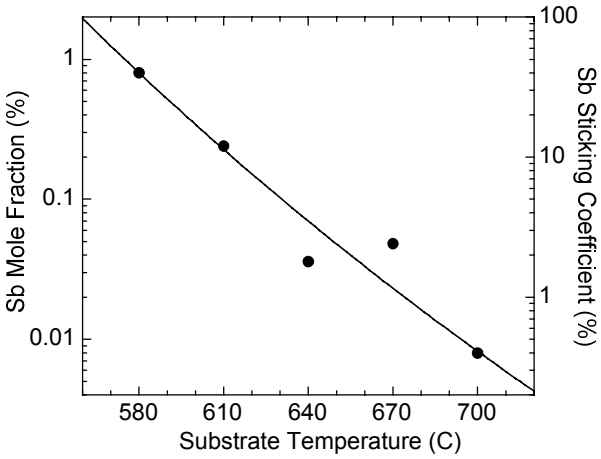

Fig. 2. Sb mole fraction and sticking coefficient derived from SIMS and XRD data for Si doped $Al_{0.65}Ga_{0.35}As$ layers grown at different temperatures and a Sb/III flux ratio of 0.02.

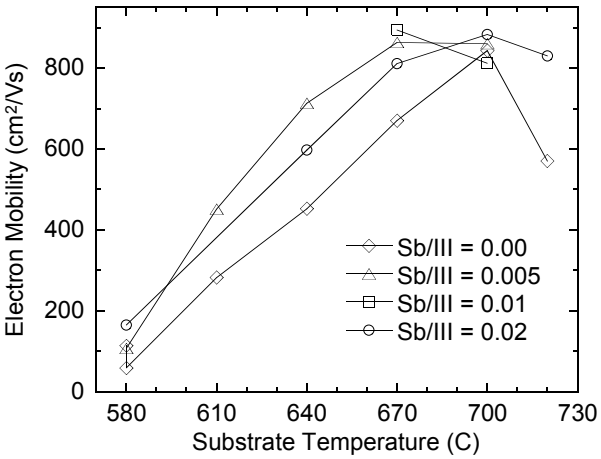

Fig. 3. Electron mobility of 1 μm thick Si-doped $Al_{0.65}Ga_{0.35}As$ layer grown at various Sb fluxes and substrate temperatures.

Composition Verification of AlGaAs Epitaxial Layers using Inductively Coupled Plasma Optical-Emission Spectroscopy *

K. A. Bertness,** T. E. Harvey, A. J. Paul, L. H. Robins, G. C. Turk, T. A. Butler, and M. L. Salit,
National Institute of Standards and Technology, Boulder, CO, and Gaithersburg, MD

We have applied an analytical chemistry method, inductively coupled plasma optical-emission spectroscopy (ICP-OES), to increase measurement accuracy for the composition of AlGaAs epitaxial thin films. ICP-OES results were compared with determination of composition from photoluminescence (PL) spectra based on a newly developed correlation equation [1] between peak luminescence energy and film composition. This correlation was based on electron microprobe analysis and growth rate measurements using reflection high-energy electron diffraction (RHEED). Although ICP-OES is a destructive method, it has high absolute accuracy with results directly traceable to the mole. The AlGaAs films used in this study were grown by molecular beam epitaxy to a thickness of 3 μm. The composition was determined near the time of film growth from RHEED oscillation measurements of the individual AlAs and GaAs growth rates using methods[2] designed to optimize the accuracy and precision of this technique. The films were characterized after growth using PL and ICP-OES on adjacent pieces from the same wafer. PL measurements included lateral uniformity assessment and temperature corrections for deviations from a standard sample temperature of 298.3 K. ICP-OES specimens were prepared by dissolving the AlGaAs film in a mixture of sulfuric acid, hydrogen peroxide, and water. In order to avoid contamination from the GaAs substrate, the films were either transferred first to silicon substrates using epitaxial lift-off or grown on Ge substrates. We observed that for most specimens, the three methods of Al mole fraction measurement agree to within their stated uncertainties, ranging from 0.0015 to 0.012. The largest deviations between the RHEED and PL measurements were most likely due to drift in Ga flux over time. This work was part of a program to offer standard-reference AlGaAs films on GaAs for use in establishing standardized measurement of composition in III-V semiconductor alloys.

[1] L. H. Robins, J. T. Armstrong, R. B. Marinenko, A. J. Paul, J. G. Pellegrino, and K. A. Bertness, *J. Appl. Phys.* **93,** 3747-59 (2003).

[2] T. E. Harvey, K. A. Bertness, R. K. Hickernell, C. M. Wang, and J. D. Splett, *J. Cryst. Growth* **251,** 73-9 (2003).

* This abstract is a contribution of an agency of the U.S. government and is not subject to copyright.
** Corresponding author: NIST, Mail Stop 815.04, 325 Broadway, Boulder, CO 80305, 303-497-5069, bertness@boulder.nist.gov

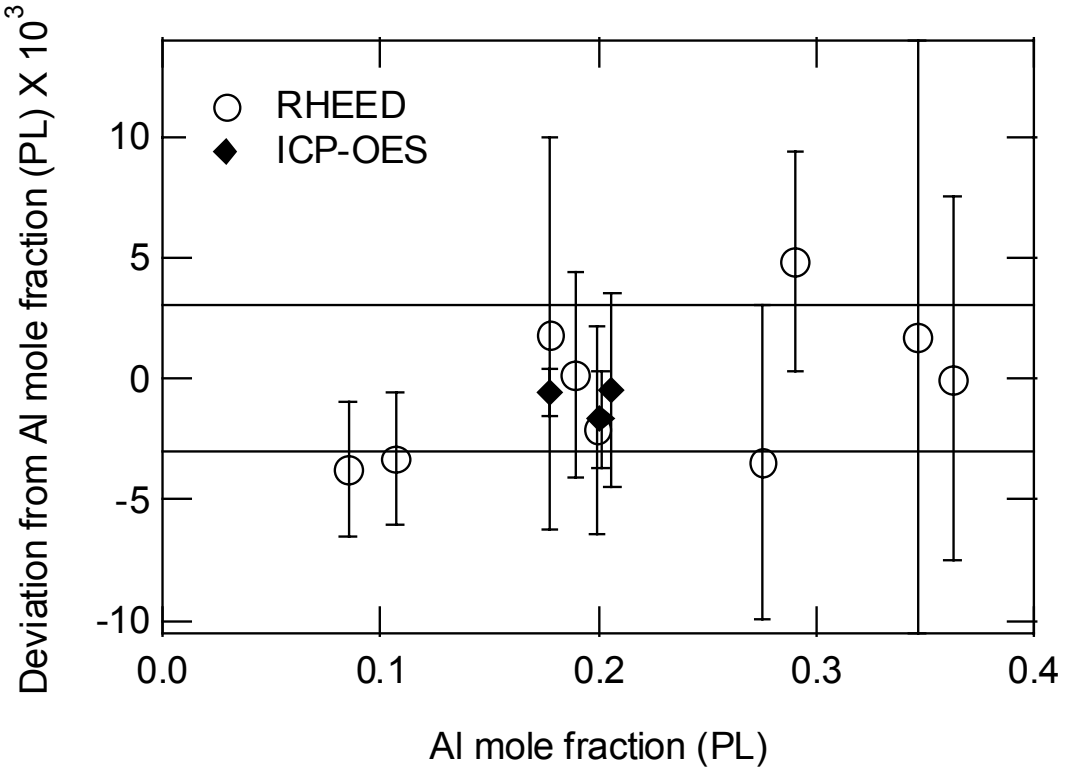

Deviation of the Al mole fraction of AlGaAs films as determined by RHEED and ICP-OES relative to the Al mole fraction value as determined by PL. The horizontal bars indicate the uncertainty limits of +/- 0.003 for the planned AlGaAs standard reference materials with mole fraction near 0.2.

Single-phase growth studies of GaP on Si by solid-source MBE

X.Yu, P.S. Kuo, K Ma, M. M. Fejer and J. S. Harris Jr.
Solid-State and Photonics Laboratory: CIS-X 126
Stanford University, Stanford, CA 94305-4075
phone: (650) 725-6911 fax: (650) 723-4659
email: xjyu@snow.stanford.edu

Several zincblende semiconductors, such as GaP and GaAs, have desirable characteristics for nonlinear optical frequency mixing, including the wide transparency range, large nonlinear susceptibility, and high thermal conductivity. However, the isotropic nature of these materials precludes birefringent phasematching. Various techniques have been developed to achieve quasi-phasematching (QPM) in these materials. One highly promising technique is all-epitaxial growth of orientation-patterned GaAs, which has recently been used to demonstrate frequency mixing [1~3]. Compared with GaAs, GaP has even more attractive properties, including a wide transparency range down to the visible 0.6~11um, and twice as large a thermal conductivity as compared to GaAs. Application of GaP to nonlinear optics has become an interesting research field. In order to get an orientation-patterned GaP film, GaP/Si/GaP heteroepitaxy must be used to create an inverted or antiphase GaP layer~~s~~ on a GaP substrate. Si, which is lattic-matched to GaP, is used as a non-polar layer to allow nucleation of the antiphase film. To utilize the wide-availability of Si substrates, the two phases of GaP, which differ by a 90° in-plane rotation about [001], both need to be grown on a Si substrate. Here, we report a growth study of GaP films grown by solid-source molecular beam epitaxy on (001) Si substrates oriented 4° off towards [110].

Growth studies were carried out as a function of the growth temperature, V/III ratio, and prelayers. The growth results were characterized by Reflective High-energy Electron Diffraction (RHEED), Atomic Force Microscopy (AFM) and X-ray Diffraction (XRD).

The nucleation temperature has been identified as the controlling factor for phase selection. Figure 1 showed the RHEED pattern for different nucleation temperatures using a phosphorus prelayer on a Si substrate. With a nucleation temperature above 575°C, the GaP film showed a 2×4 reconstruction, which indicated the phase with a 4° offset towards (111)A. However, at a low temperature, typically with substrate temperature around 350°C, the 4×2 reconstruction showed a 90° in-plane rotation with respect to the high temperature phase.

We found that the V/III flux ratio affected the film quality. A comparison by AFM of the surface quality under different flux ratios is shown in Figure 2. A high flux ratio, V/III=8×, at 500°C showed a surface roughness as high as 30nm. A low flux ratio about 3× greatly improved the surface smoothness. We found that a high flux ratio was needed for low temperature nucleation, but continued growth at this temperature resulted in a rough GaP film. Thus a two-step growth was used to get good low-temperature-phase films, that is, after a 200Å thick GaP film nucleated at 350°C, a thick film was deposited at a 700°C growth temperature, which was also shown in Figure 1.

In conclusion, two GaP phases can be grown on a Si (001) substrate with a 4° miscut. The high temperature phase was grown with a low flux ratio, and the low temperature phase was grown using a two-step growth.

References

1. C. B. Ebert, L. A. Eyres, M. M. Fejer, and J. S. Harris, J. Cryst. Growth., 201/202, 187-193 (1999).
2. S. Koh, T. Kondo, M. Ebihara, T. Ishiwada, H. Sawada, H. Ichinose, I. Shoji, and R. Ito, Jpn. J. Appl. Phys., Part 2 38, L508 (1999).
3. L. A. Eyres, P. J. Tourreau, T. J. Pinguet, C. B. Ebert, J. S. Harris, and M. M. Fejer, L. Becouarn, B. Gerard, and E. Lallier. Appl. Phy. Lett. 79(7), 904-906 (2001).

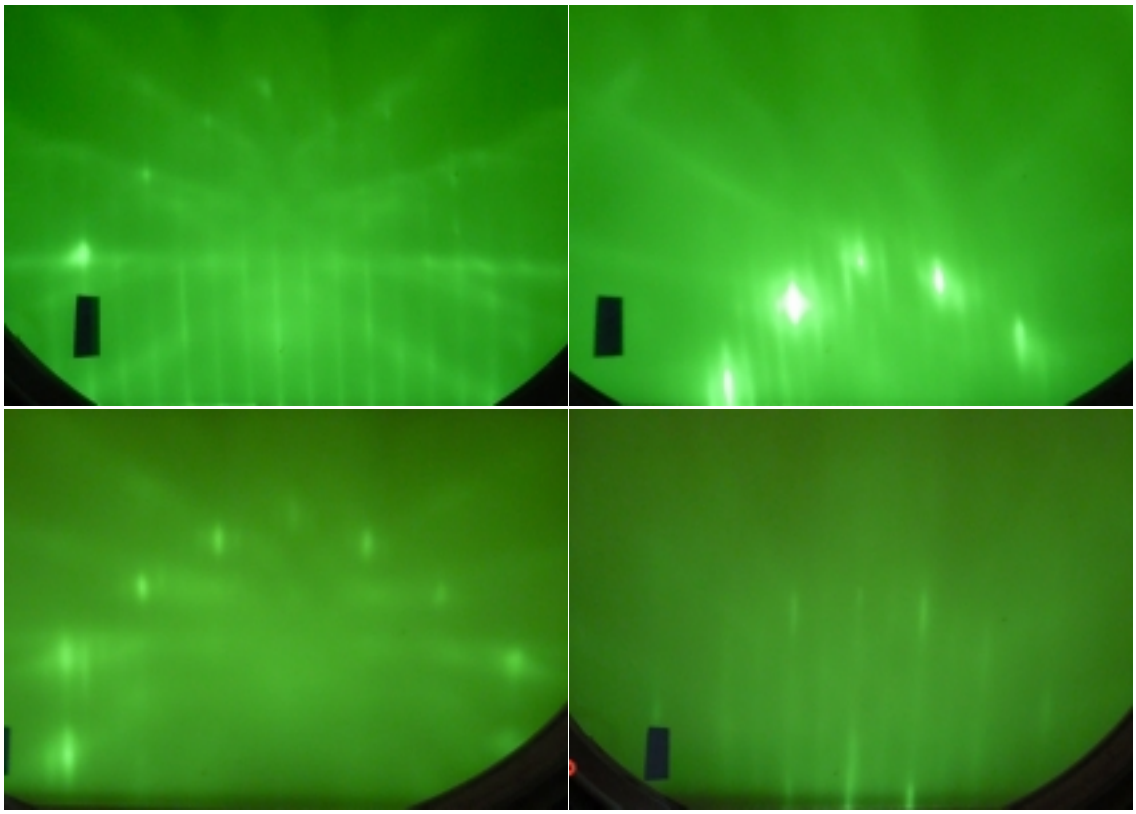

Figure 1. RHEED image of GaP grown on Si

1. One-step growth at 575°C, flux ratio P/Ga=3.5×, 2×4 reconstruction
2. Two-step growth, nucleate at 350°C, grown at 700°C, flux ratio P/Ga=10×, 4×2 reconstruction

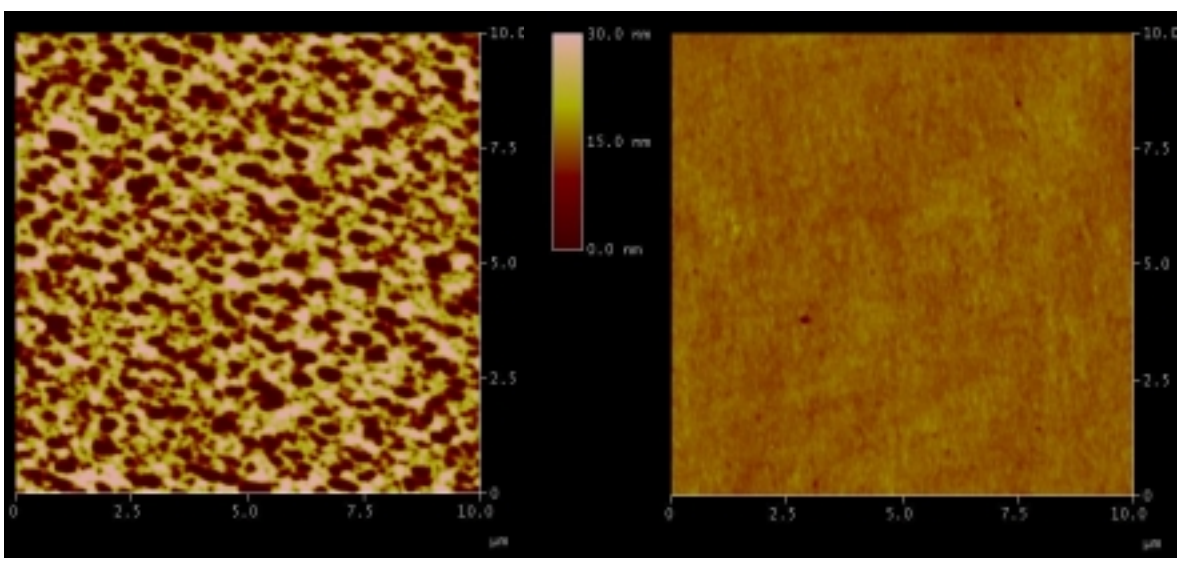

Figure 2. AFM image of 4000 Å GaP on Si at 500°C growth
V/III flux ratio: (a) P/Ga=8×; (b) P/Ga=3×

Intermixing and As Incorporation in GaAs/GaSb Multilayers

C. Dorin, C. Wauchope[*] and J. Mirecki Millunchick,
Department of Materials Science and Engineering, University of Michigan, Ann Arbor, MI 48109-2136
[*]Electron Microbeam Analysis Laboratory, University of Michigan, Ann Arbor, MI 48109-2136

GaAsSb is a promising material for high speed frequency bipolar transistors (HBT), long wavelength lasers and infrared detectors. However, the material quality is a concern since the abruptness of the interfaces, the degree of intermixing, the anion cross incorporation and the homogeneity of the material greatly affect the performance of these devices. One way to control the composition is either to change the As species or deposit multilayer structures rather than random alloys.

This paper discusses the As incorporation and As sticking coefficient in GaAsSb random alloys and GaAs/GaSb short period superlattices (SPS) deposited by Molecular Beam Epitaxy (MBE) as a function of As species, growth temperature and SPS thicknesses. Random alloys of GaAsSb/InP deposited with As_4 species result in a fully relaxed and dislocated GaSb film. Decreasing the group V flux is not significantly increasing the As incorporation. Alloys grown with As_2 species result in $GaAs_{0.49}Sb_{0.51}$ high quality films. Figure 1 is the (224) reciprocal space map of such a GaAsSb random alloy deposited with (a) As_4 and with (b) As_2, showing the improved As incorporation and film quality for the As_2 case. Multilayer structures are also compared as a function of As species. Figure 2a is a cross section TEM (XTEM) image of a $GaAs_{2ML}/GaSb_{2ML}$ SPS grown at T = 400°C with As_4. The film is defective and posses lateral composition modulation. Figure 2b is the XTEM image of the same SPS structure but deposited with As_2. The interfaces are flat, the sample shows marked improvement in crystalline quality and no phase separation is observed.

To further study the As incorporation, a series of multilayer structures is deposited at different temperatures and with different SPS thicknesses. As incorporation increases as the growth temperature increases. The As sticking coefficient was found to be temperature dependent, but did not significantly change for different SPS individual layers thicknesses. Figure 3 plots the As sticking coefficient σ_{As} as a function of temperature for $GaAs_{2ML}/GaSb_{2ML}$ SPSs. σ_{As} is constant for growth temperatures of 370°C $\leq$T$\leq$420°C and is increasing 430°C $\leq$T$\leq$465°C. Spontaneous phase separation is observed as well in structures deposited in temperature range of 430°C $\leq$T$\leq$465°C. The changes in the microstructure versus growth temperature are explained using a kinetic model that considers Sb surface segregation. Optical properties of these structures are discussed as well.

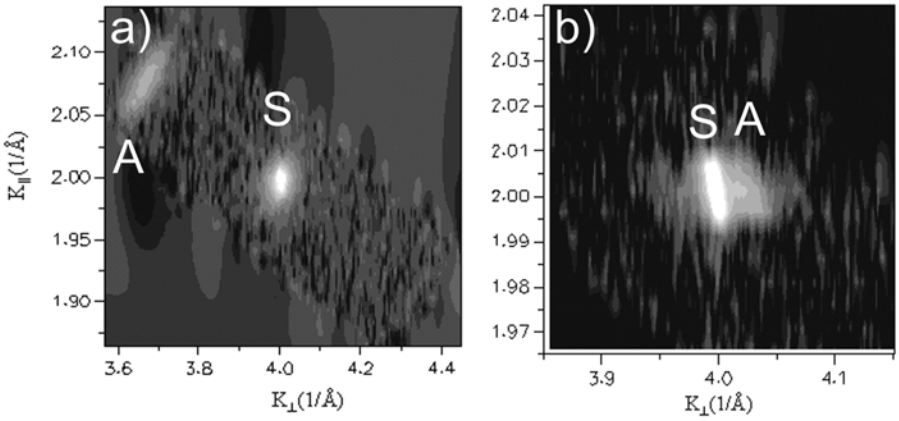

Figure 1: (224) Reciprocal Space Maps for GaAsSb alloys grown with As_4 (1a) and As_2 (1b) at T = 400°C.

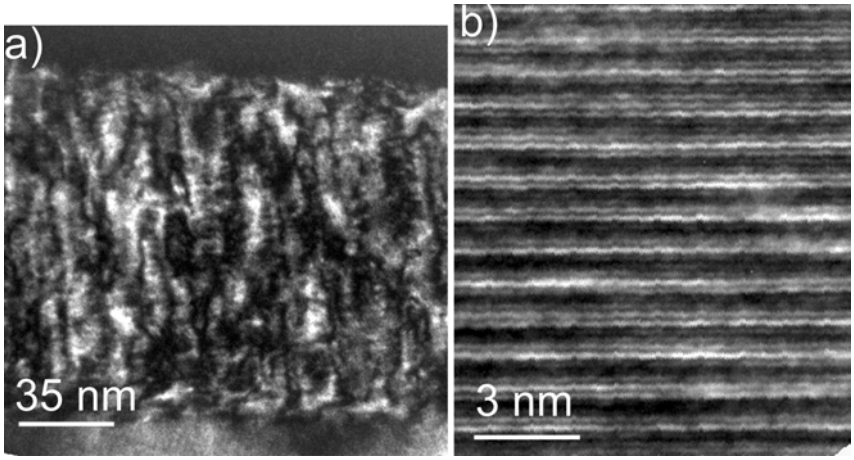

Figure 2: (002) dark filed cross section TEM of $GaAs_{2ML}/GaSb_{2ML}$ grown with As_4 and T = 400°C and with As_2 and at T = 420°C (2b).

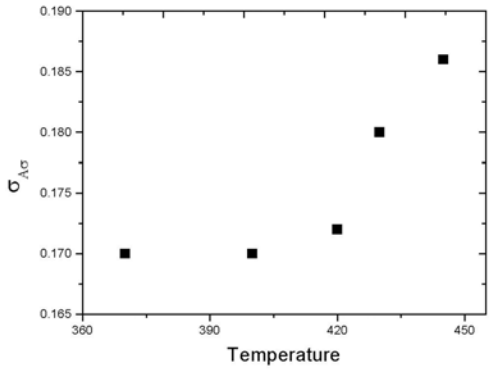

Figure 3: As sticking coefficient σ_{As} as a function of temperature for $GaAs_{2ML}/GaSb_{2ML}$ SPSs grown with As_2.

NAMBE 2003 Program

Tuesday, September 30, 2003

10:20-12:00: Highly-Strained Materials: Growth and Characterization

Chair: Rod Beresford (Brown University)

TB-1: Dislocation Structure and Surface Roughness of InAslAs graded buffer layers grown on InP for 6.05 and 6.0 angstrom applications
A.M. Noori*, R.S. Sandhu*,§, S.L. Hayashi*,§, E.D. Meserole*, A. Cavus§, C. Monier§, R.Hsing§, D. Sawdai§, M. Wojtowicz§, T. R. Block§, A. Gutierrez-Aitken§, and M.S.Goorsky*
*University of California,Los Angeles; §Northrop Grumman Space Technology

TB-2: Real-time strain evolution during growth of InAlAs/GaAs metamorphic buffer layers
C. Lynch, R. Beresford, and E. Chason
Brown University

TB-3: Effect of Buffer Layer on InSb Quantum Wells Grown on GaAs (001) Substrates
T.D. Mishima, J.C. Keay, N. Goel, M.A. Ball, S.J. Chung, M.B. Johnson, and M.B. Santos
University of Oklahoma

TB-4: Defect-Controlled Selective Epitaxial Growth of GaAs on Si substrate with Strained Short Period Superlattices
Takuto Tsuji, Hiroo Yonezu#, and Naoki Ohshima*
Takuma National College of Technology; #Toyohashi University of Technology; *Yamaguchi University

TB-5: Material Properties and Performance of Metamorphic Optoelectronic Integrated Circuits Grown by Molecular Beam Epitaxy on GaAs Substrates
W. Hoke, R. Leoni, C. Whelan, T. Kennedy, A. Torabi, P. Marsh, Y. Zhang, C. Xu*, and K.C. Hsieh*
Raytheon RF Components; *University of Illinois

Dislocation Structure and Surface Roughness of $In_xAl_{1-x}As$ Graded Buffer Layers Grown on InP for 6.05Å and 6.0Å Applications.

A.M. Noori*, R.S. Sandhu[*,§], S.L. Hayashi[*,§], E.D. Meserole[*], A. Cavus[§], C. Monier[§], R. Hsing[§], D. Sawdai[§] ,M. Wojtowicz[§], T. R. Block[§], A. Gutierrez-Aitken[§], and M.S. Goorsky[*]

*Department of Materials Science and Engineering, University of California, Los Angeles, Los Angeles, CA 90095 USA

[§]Northrop Grumman Space Technology, One Space Park, Redondo Beach, CA 90278 USA

Abstract

In this study, metamorphic compositionally graded $In_xAl_{1-x}As$ layers grown on InP by molecular beam epitaxy with a final indium mole fraction of x=1.0 (6.05 Å) and x = 0.85 (6.0 Å) are investigated. The metamorphic InP/$In_xAl_{1-x}As$/InAs or InP/$In_xAl_{1-x}As$/$In_{.85}Al_{.15}As$ graded system provides a virtual substrate with semi-insulating properties for the growth of InAs based device structures, which cannot be achieved through lattice-matched growth; in contrast, the GaAs/$In_xAl_{1-x}As$/InP is an alternate approach used in MHEMT technology to circumvent the use on InP substrates. In the $In_xAl_{1-x}As$ system, the activation energy for dislocation glide follows the same trend as the melting temperature in the pseudo-binary phase diagram. At x>0.52, the melting temperature is approximately constant with respect to composition, and therefore the dislocation velocity throughout this composition is approximately the same as InAs. The high misfit dislocation velocity in this system (as compared to $In_xGa_{1-x}P$ or Si_xGe_{1-x}) allows the grading to be accomplished with a thin layer (~1μm) while still achieving complete strain relaxation and low threading dislocation densities, following the model established by Fitzgerald *et al.* [Mat. Sci. and Eng. B67 (1999) 53-61]. To examine the effects of temperature on strain relaxation and surface morphology, a sequence of samples were produced with the indium mole fraction graded from x=0.52 to x=0.64, 0.79, and 1.0 with a constant grading rate. The evolution of the strain relaxation, threading dislocation density, and surface morphology were evaluated by triple axis x-ray diffraction (TAD), transmission electron microscopy (TEM), etch pit density (EPD) and atomic force microscopy (AFM). The misfit dislocation interactions and the threading dislocation density was found to be strongly dependent on substrate temperature, and threading densities as low as 10^6 cm^{-2} were achieved, as measured by plan-view TEM and EPD. The final surface roughness can be controlled by the growth temperature of a constant composition cap layer. The surface roughness at the end of growth was removed by implementing a very low removal rate (<30nm/min) chemical-mechanical polishing step.

Figures

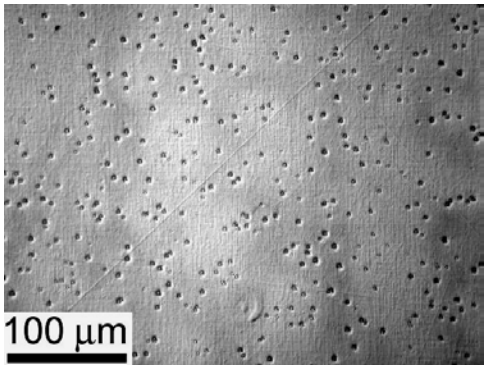

Figure 1- Nomarski interference micrograph of EPD measurements done on a 6.0 Å graded buffer layer, showing threading dislocations (3×10^5 cm^{-2}).

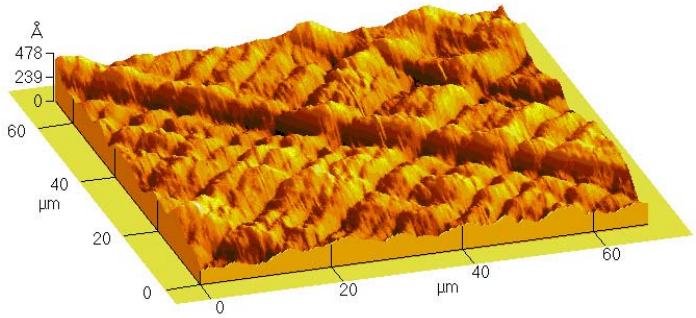

Figure 2- (65 µm)^2 AFM image of 6.05 Å graded buffer layer surface exhibiting crosshatch morphology. The root-mean-square roughness of the sample is 5.8 nm.

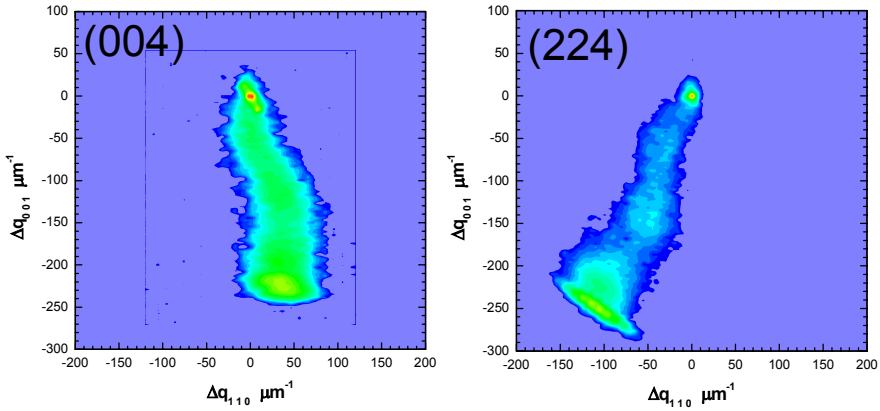

Figure 3- Triple axis reciprocal space maps of symmetric (*left*) and asymmetric (*right*) InP/$In_xAl_{1-x}As$/InAs reciprocal lattice points. The relaxation varies slightly throughout the graded layer; 96% (± 2%) at x=0.64, 99% at x=0.79, and 93% at x=1.0.

Real-time strain evolution during growth of $In_xAl_{1-x}As/GaAs$ metamorphic buffer layers

C. Lynch*, R. Beresford, and E. Chason
Division of Engineering, Box D, Brown University, Providence, RI 02912

Growth of high In content high-electron-mobility transistors on GaAs substrates is desirable due to the lower cost and higher availability of GaAs substrates over InP. The use of metamorphic buffer layers allows the large misfit between $In_{0.53}Ga_{0.47}As$ and GaAs to be accommodated by transitioning the lattice parameter from GaAs (5.653 Å) to that of InP (5.869 Å), or even larger values. Successful device growth on the metamorphic buffer requires control over the final surface roughness and dislocation density (to maintain a high resistivity in the buffer and to avoid extending dislocations into the active region). To control these effects, it is critical to understand the strain relaxation behavior. Although the final layer strains may be determined after growth, the real-time behavior must be studied *in situ*. We present real-time strain relaxation measurements during MBE growth of $In_xAl_{1-x}As/GaAs$ metamorphic buffer layers.

Film strain evolution is monitored *in situ* by a multibeam optical stress sensor (MOSS), which measures the curvature induced in the substrate by a biaxially strained thin film. The wafer curvature is determined by measuring the deflection of a parallel array of laser beams reflected off of the film surface. The change in spacing of the beams is related to the substrate curvature, which can then be used to determine the stress in the film. Continuously recording the deflected beam spacing during growth allows us to study the dynamic evolution of strain; this method offers information that would be unavailable by *ex situ* strain measurement techniques.

In this work we measured the film strain evolution during growth of step-graded and continuously graded $In_xAl_{1-x}As/GaAs$ buffer layers (Fig. 1). The step-graded buffer layer grows pseudomorphically at the onset of each new layer, followed by rapid strain relaxation beginning at layer thicknesses below the critical thickness for single layers of the same strain. The strain relaxation in each layer saturates at approximately 70-80% of the initial layer misfit until the subsequent layer is deposited. The continuously graded buffer layer relaxes more slowly than the step graded layer. Both buffer layers eventually reach comparable stress levels after the final grading step. The roughnesses of the final surfaces were characterized by atomic force microscopy. In addition, the evolution of the surface roughness can be studied using the magnitude of oscillations in the intensity of the reflected beams (Fig. 2). These intensity oscillations arise due to constructive and destructive interference of reflections from interfaces. The use of this work to develop strategies for optimizing the growth of metamorphic buffer layers, including minimizing buffer layer thickness, residual strain, and surface roughness will be discussed.

* Candace_Lynch@brown.edu

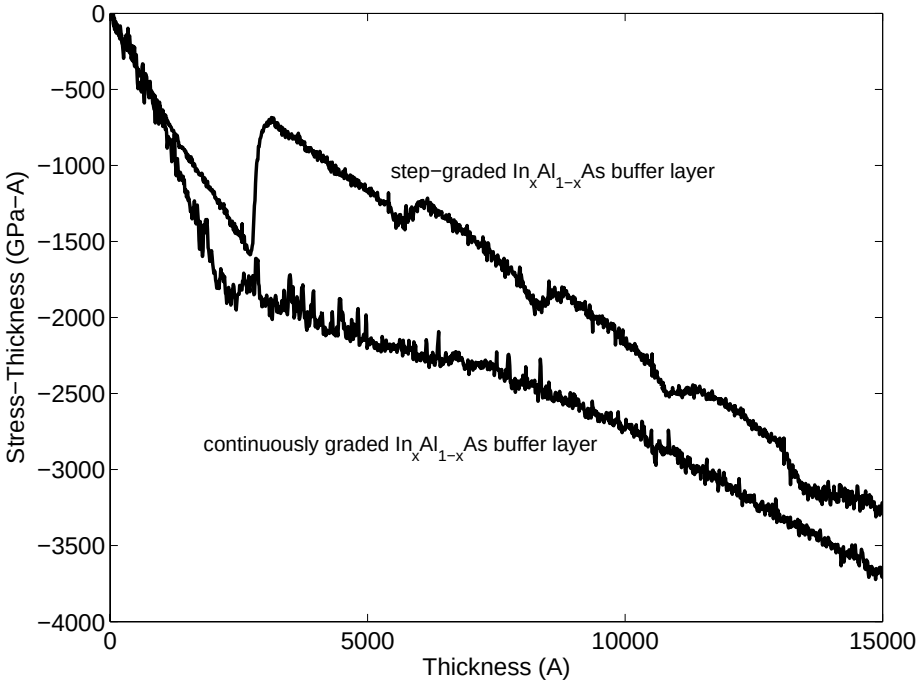

Fig. 1. Real-time measurement of the stress-thickness product during MBE growth of $In_xAl_{1-x}As$/GaAs metamorphic buffer layers.

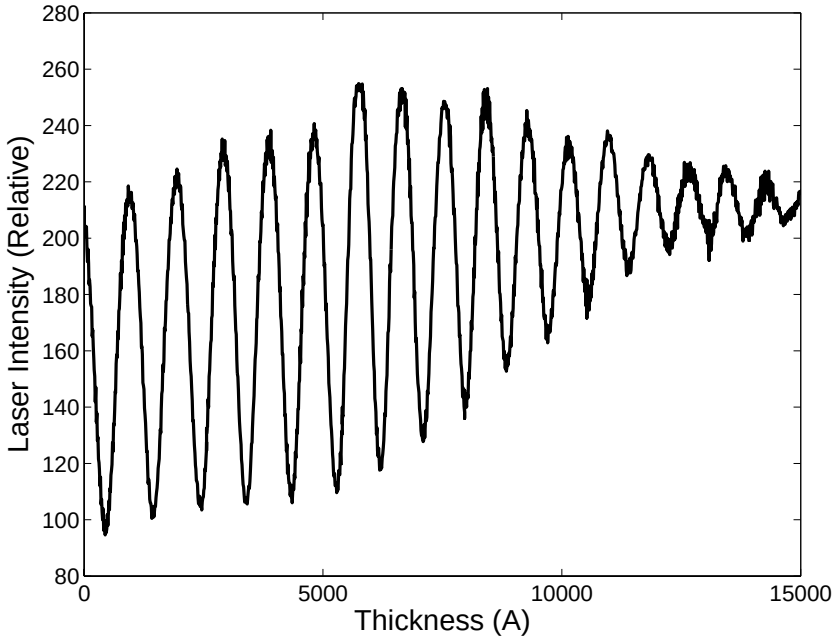

Fig. 2. Oscillations in the reflected beam intensity recorded during growth. The amplitude change is an indication of surface roughness.

Effect of Buffer Layer on InSb Quantum Wells Grown on GaAs (001) Substrates

T.D. Mishima, J.C. Keay, N. Goel, M.A. Ball, S.J. Chung, M.B. Johnson, and M.B. Santos
Department of Physics and Astronomy, and Center for Semiconductor Physics in Nanostructures, University of Oklahoma, 440 West Brooks, Norman, OK 73019
Tel: (405) 325-3961 Fax: (405) 325-7557 e-mail: mishima@ou.edu

InSb quantum wells (QWs) with remotely doped $Al_xIn_{1-x}Sb$ barriers have been studied with the goal of realizing novel devices, such as mesoscopic magnetoresistors [1] and spin transistors [2,3], that take advantage of a small electron effective mass or a large spin orbit coupling. To maximize the performance of such devices, a low defect density in the QW and atomically flat/abrupt interfaces between the QW and barrier layers are highly desirable. For InSb QWs, these requirements can be demanding, because lattice-matched III-V insulators are not available as a substrate material. Due to its high-quality but reasonable-price, GaAs is thought to be one sensible choice, in spite of a large lattice mismatch of ~14.6% between the QW and substrate.

In this study, we use transmission electron microscopy (TEM) to investigate structural defects of InSb QW samples on GaAs (001) substrates. For these samples, InSb or AlSb is used as nucleation layer material, while the subsequent buffer layer structure is identical. We obtained a higher low-temperature mobility for AlSb-nucleated samples with a lower micro-twin density. Our results strongly suggest that minimizing the density of micro-twins is one key factor to improve the InSb QW based devices.

Figs. 1(a) and (b) are cross-sectional TEM images of InSb- and AlSb-nucleated samples, respectively. Around the QW region of the InSb-nucleated sample in Fig. 1(a), one can see straight-line contrasts. Dark field images taken with a micro-twin spot (e.g., inset of Fig. 1(a)) reveal that they are derived from micro-twins. On the other hand, for the AlSb-nucleated sample in Fig. 1(a), the dominant defect at the QW region is dislocations with additional contribution of micro-twins. In Figs. 2(a) and (b), we show a micro-twin and a dislocation propagating through a QW, respectively. There is an offset between the sections of the QW on each side of the micro-twin in Fig. 2(a), while the dislocation in Fig. 2(b) causes no visible offset when viewed with the same magnification. Figs. 3(a) and (b) are plan-view TEM images for the two different types of QW samples. Micro-twins are seen as rectangular features in these images. Both samples exhibit a higher density of micro-twins in the $[\bar{1}10]$ direction than in the [110] direction. The micro-twin density ratio (number per unit length along /number per unit length along [110]) is further from unity in the InSb-nucleated sample than in the AlSb-nucleated sample. As shown in Fig. 4, the low-temperature mobility ratio is also further from unity for the InSb-nucleated sample. We will discuss, in more detail, the dependence of defects and mobility on buffer-layer structure and composition.

[1] S.A. Solin, D.R. Hines, A.C.H. Rowe, J.S. Tsai, Yu. A. Pashkin, S.J. Chung, N. Goel, M.B. Santos, Appl. Phys. Lett. 80, 4012 (2002).
[2] G.A. Khodaparast, R.E. Doezema, S.J. Chung, K.J. Goldammer, M.B. Santos, IPAP Conf. Series **2**, 245 (2001).
[3] N. Goel, K. Suzuki, S. Miyashita S.J. Chung, M.B. Santos, and Y. Hirayama, Bull. Am. Phys. Soc. **48**, 102 (2003).

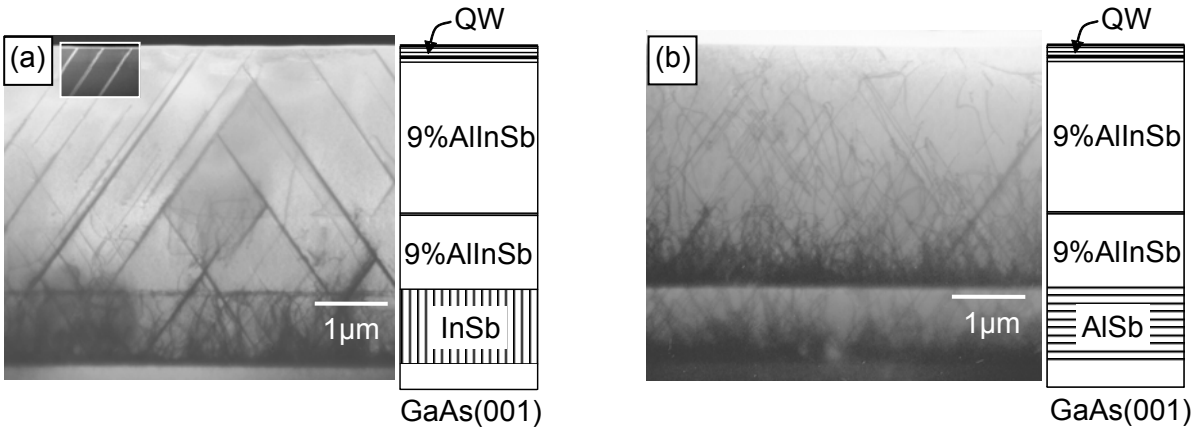

Fig. 1. Cross-sectional TEM (X-TEM) images for (a) InSb- and (b) AlSb-nucleated QW samples. Corresponding layer sequences are shown on the right side. Inset in (a) is a dark field image taken with a micro-twin spot, in which micro-twins appear as bright contrasts.

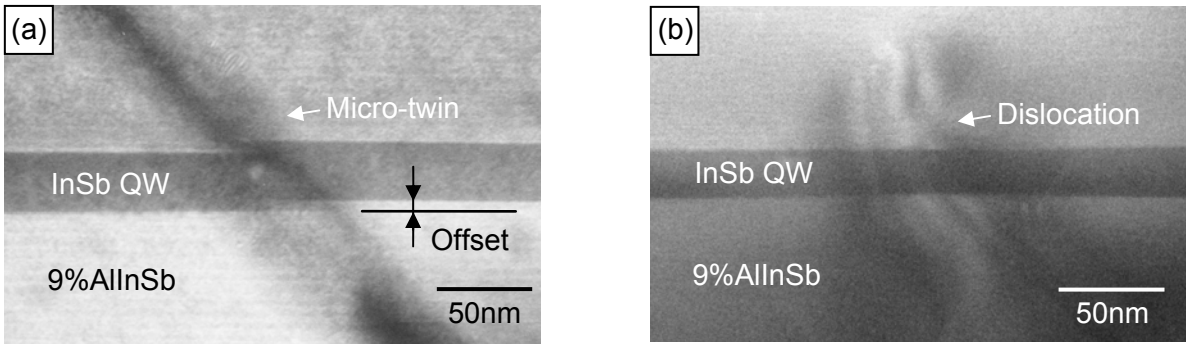

Fig. 2. X-TEM images of (a) a micro-twin and (b) a dislocation propagating through an InSb QW. Note an offset on the QW in (a).

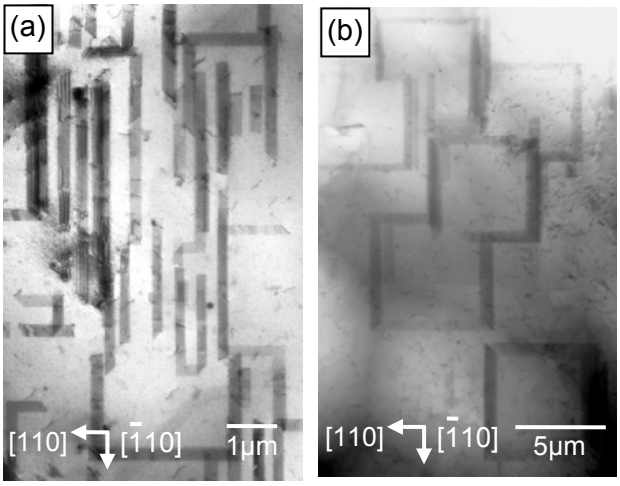

Fig. 3. Plan-view TEM images of (a) InSb- and (b) AlSb-nucleated QW samples.

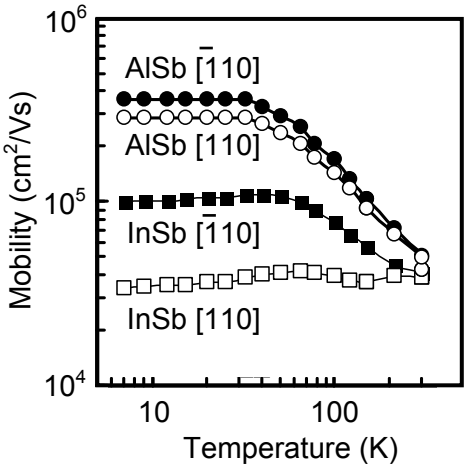

Fig. 4. Mobilities for the InSb- and AlSb-nucleated QW samples.

Defect-Controlled Selective Epitaxial Growth of GaAs on Si substrate with Strained Short-Period Superlattices

Takuto Tsuji, Hiroo Yonezu†, and Naoki Ohshima‡

Department of Telecommunications, Takuma National College of Technology,
Kohda 551, Takuma-cho, Mitoyo, Kagawa 769-1192, Japan
Phone : +81-875-83-8562, Fax : +81-875-83-8590, E-mail : tsuji@dt.takuma-ct.ac.jp

1. Introduction

The selective epitaxial growth of III-V compound semiconductors on Si is necessary for optoelectronic integrated circuits (OEICs). However, a large number of threading dislocations are generated in the III-V compound layers selectively grown on Si due to the differences in physical properties and crystal structures between III-V compounds and Si[1]. Recently, we have effectively suppressed the generation of threading dislocations in GaAs-on-Si and InP-on-Si by introducing strained short-period superlattices (SSPSs) and a GaP buffer layer [2], [3]. Thus, the selective epitaxial growth of GaAs/SSPSs/GaP on Si is interesting for realization of small GaAs optical devices on Si ICs. One of the key issues in the selective epitaxial growth is to grow a GaP layer on Si and we have succefully grown the GaP layer on Si by migration-enhanced epitaxy(MEE) without crystalline defects[4]. Therefore, we attempted the selective epitaxial growth of GaAs/SSPSs/GaP/Si structure by molecular beam epitaxy(MBE) under atomic hydrogen irradiation.

2. Experimental

The surface of Si(100) substrates misoriented by 4° toward [011] azimuth was covered with a 60-nm-thick dry-SiO_2 mask, because the dry-SiO_2 mask is excellent for evaporation characteristic of III-V compound semiconductors absorbed on the mask surface[4]. The dry-SiO_2 mask was patterned with square holes of 3×3, 5×5, 20×20[μm^2] and 3×3[mm^2]. The GaP layer was selectively grown on the patterned-Si substrates about 300[nm] at 550°C by MEE under atomic irradiation[4]. After the growth of the GaP, the multi-$(GaAs)_m(GaP)_n$ SSPSs were selectively grown on the GaP/Si at 550°C by MBE with H. The number of monolayers (m,n) were changed in the order of (1,3), (1,1), (3,1) and (7,1). The thickness of (1,3), (1,1) and (3,1) layers was 200[nm] and that of (7,1) layer was 150 [nm], respectively. The GaAs layer was finally grown at 600°C around 1[μm] thickness with H. The hydrogen back pressure was kept at 3.5×10^{-5}[Torr] during the selective growth. A schematic structure of the sample is shown in Fig. 1.

The surface was observed in-situ during the selective epitaxial growth by reflection high-energy electron diffraction (RHEED). The selective epitaxial layers were evaluated by scanning electron microscopy (SEM) and transmission electron microscopy (TEM).

†H. Yonezu is with Department of Electrical and Electronic Engineering, Toyohashi University of Technology, Japan

‡N. Ohshima is with Department of Advanced Materials Science and Engineering, Yamaguchi University, Japan

3. Results and Discussion

Streaked patterns were observed throughout with no apparent change to 3D spot patterns during the selective epitaxial growth of the GaAs/SSPSs/GaP/Si.

A bird-view SEM image of the GaAs/SSPSs/GaP/Si selectively grown on Si substrate is shown in Fig. 2. It is clear that the structure was selectively grown on circular patterned Si area under atomic hydrogen irradiation.

Fig. 3 shows cross-sectional TEM image of the GaAs/SSPSs/GaP/Si structure near the edge of masked region. It is also confirmed from the TEM observation that the GaAs/SSPSs/GaP/Si structure was grown selectively on unmasked Si area and the thickness of each layer is slightly increased near the edge of unmasked region, as shown in Fig. 3.

Fig. 4 shows the cross-sectional TEM image of the GaAs/SSPSs/GaP/Si structure grown on 20×20 [μm^2] squared hole Si area. It was found that the generation of threading dislocations was successfully suppressed in the GaAs/SSPSs/GaP/Si grown on 20×20 [μm^2] small growth area.

The distibution of dislocations in each layer was investigated by taking tilted TEM image of the GaAs/SSPSs/GaP/Si structure. The TEM specimen were tilted about 30° toward the [100] direction. As shown in Fig. 5, a lot of misfit dislocations were observed, which lay at all the hetero-interfaces. Most of these dislocations were lying along the <110> directions. Therefore, it is clarified that the lattice mismatch between GaAs and Si was relaxed in a stepwise fashion by introducing the misfit dislocations in the <011> directions.

4. Conclusion

The selective epitaxial growth of GaAs/SSPSs/GaP/Si was perfoemed by MBE under atomic hydrogen irradiation. As a result, GaAs/SSPSs/GaP/Si structure was selectively grown on Si substrate. During the growth, 2D growth was entirely maintained. Therefore, the generation of threading dislocations due to 3D growth was effectively suppressed and the density of the threading dislocations was successfully reduced by inserting the multi-SSPSs and the GaP into hetero-interface of the GaAs-Si.

References

[1] M. Tamura, A. Hashimoto, J. Kasai, and A. Nishida, J. Cryst. Growth **147**, 264 (1995).

[2] Y. Takagi, H. Yonezu, T. Kawai, K. Hayashida, K. Samonji, N. Ohshima , and K. Pak, J. Cryst. Growth **150**, 677 (1995).

[3] K. Samonji, H. Yonezu, Y. Takagi, K. Iwaki, N. Ohshima, J. K. Shin, and K. Pak, Appl. Phys. Lett. **69**, 100 (1996).

[4] T. Tsuji, H. Yonezu, M. Yokozeki, Y. Takagi, Y. Fujimoto, and N. Ohshima, Jpn. J. Appl. Phys. **36**, 5431 (1997).

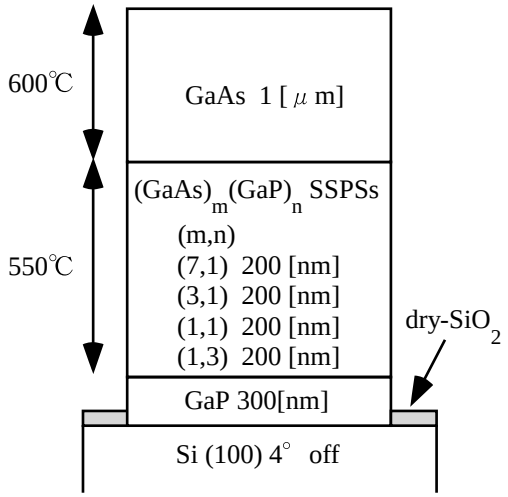

Fig. 1 Schematic of the GaAs/SSPSs/GaP/Si structure selectively grown by MBE.

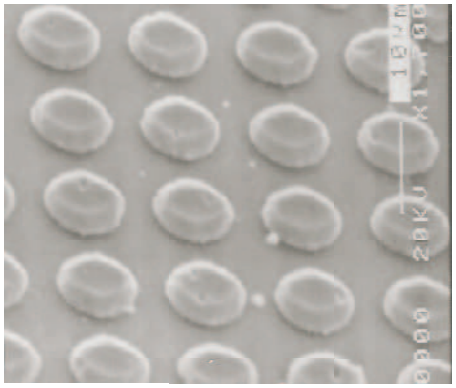

Fig. 2 Bird-view SEM image of the selectively grown GaAs/SSPSs/GaP on circular patterned-Si substrate.

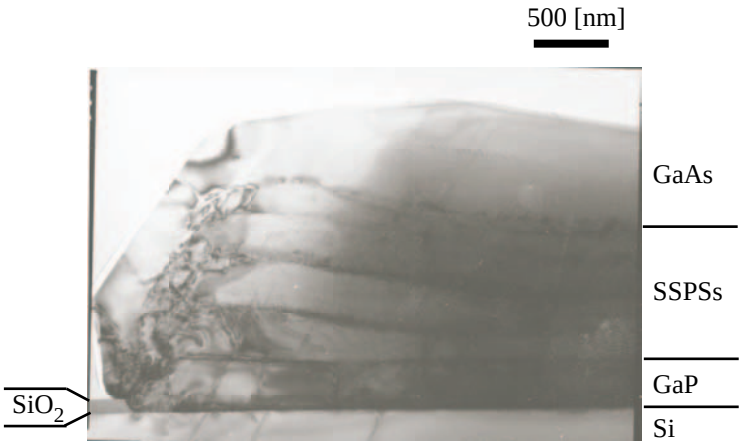

Fig. 3 Cross-sectional TEM image of the selectively grown GaAs/SSPSs/GaP/Si on 20×20 [μm^2] unmasked Si substrate near the edge of the masked region.

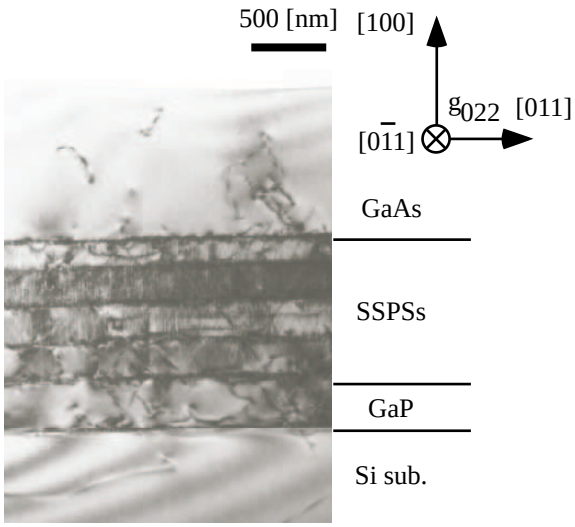

Fig. 4 Cross-sectional TEM image of the GaAs/SSPSs/GaP/Si grown selectively on 20×20 [μm^2] Si area.

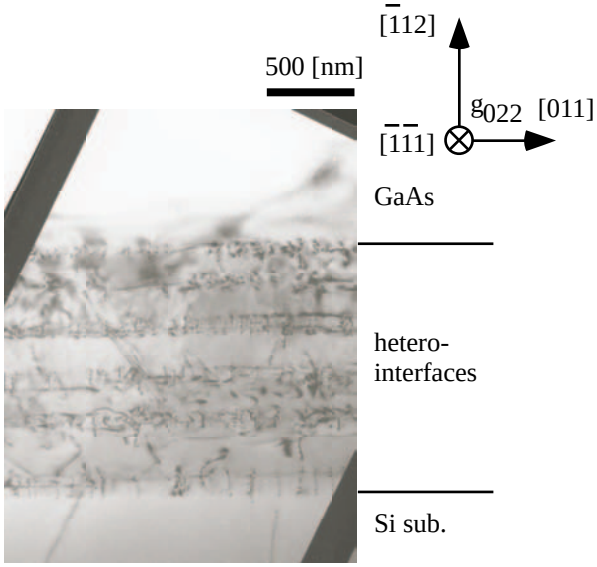

Fig. 5 Tilted TEM image of the GaAs/SSPSs/GaP/Si selectively grown on 20×20 [μm^2] Si area.

Material Properties and Performance of Metamorphic Optoelectronic Integrated Circuits Grown by Molecular Beam Epitaxy on GaAs Substrates

W. Hoke, R. Leoni, C. Whelan, T. Kennedy, A. Torabi, P. Marsh, Y. Zhang
Raytheon RF Components, 362 Lowell St., Andover, MA 01810

C. Xu and K.C. Hsieh
Microelectronics and Material Research Laboratory, University of Illinois

Considerable success has been achieved in applying metamorphic growth technology for the deposition of high quality device structures on GaAs substrates. This effort is motivated by the lower cost and larger diameter of GaAs substrates compared to other III-V substrates as well as its availability in conducting and semi-insulating forms. Furthermore the arbitrary grading of the lattice constant enables new or optimized device structures. The high quality of device layers is made possible by the metamorphic buffer layer that contains most of the dislocations necessarily formed in altering the lattice constant. Consequently the density of dislocations reaching the critical device layers near the surface is low for many device geometries. Additionally the strain-driven surface roughness from metamorphic growth is typically considerably less than the thinnest layers in most device structures.

Metamorphic electronic and optical devices have been demonstrated. A natural extension of the technology is to integrate both types of devices in a single layer stack to reduce parasitics compared to a hybrid combination. In this effort molecular beam epitaxy was used to deposit in a single growth run the device layers for a metamorphic HEMT traveling wave amplifier (TWA) and PIN photodiode containing 53% indium content. The PIN diode layers, with total thickness of 1.5 microns, were grown on top of the HEMT. Figure 1 shows cross sectional TEM micrographs of the structure and a higher magnification of the HEMT layers with the transition to the PIN structure. The dislocations are predominantly localized in the buffer layer indicating that the thick PIN layers are not significantly straining the underlying HEMT structure. The HEMT layers exhibit well-defined, planar interfaces. Several plan view TEM micrographs were taken from which the surface dislocation density is estimated to be $1x10^6$ cm^{-2}.

The combined growth of the metamorphic HEMT and PIN layers did not significantly degrade the separate performance of either structure. After etching off the PIN layers, the room temperature electron mobility of the HEMT was 10,100 cm^2/Vs. The transistor properties were also comparable to our conventional MHEMT. The current density at 0 gate voltage, Idss, was 610 mA/mm and the transconductance was 900 mS/mm. Unpackaged metamorphic photodiodes with a 12 micron optical window had responsivities of 0.5 A/W and a –3dB bandwidth of 28 GHz. As shown in Figure 2, the frequency performance compares well to non-metamorphic InP photodiodes with the same optical window diameter. Finally the performance of the OEIC is illustrated in Figure 3. With the PIN photodiode and HEMT TWA integrated on the same wafer, a larger bandwidth is obtained compared to a hybrid circuit due to reduced parasitics associated with interconnects. Furthermore an integrated buffer amplifier for matching provides a power gain of 6 dB which further demonstrates the advantages of monolithic integration.

Contact: Bill Hoke, Phone: 978-684-8581; FAX: 978-684-5345; whoke@rrfc.raytheon.com

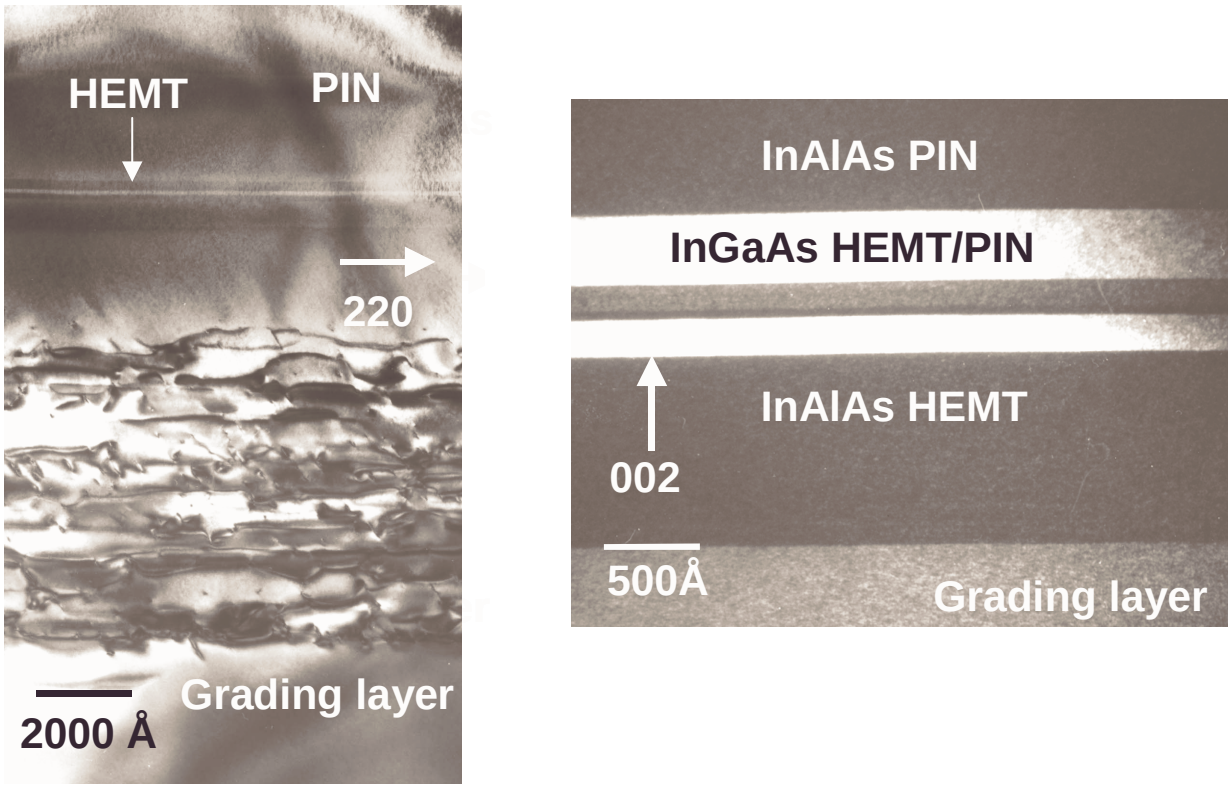

Figure 1. Left: Cross sectional TEM of metamorphic HEMT/PIN layer stack. Right: Higher magnification of the HEMT layers and transition to the PIN layers.

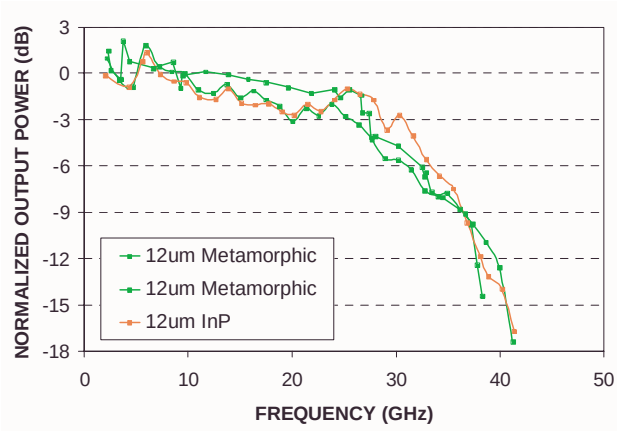

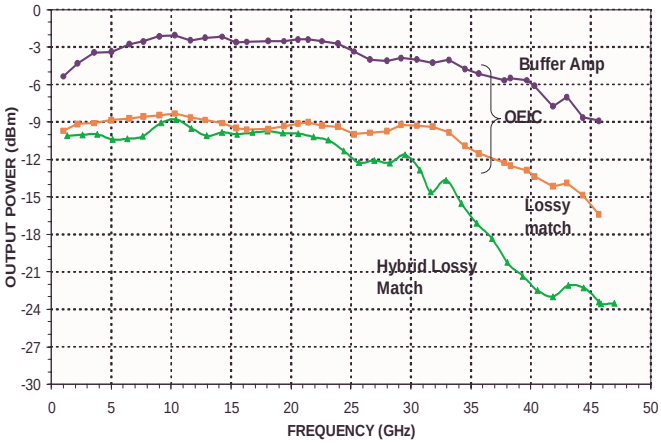

Figure 2 (Left). Unpackaged frequency performances of two metamorphic PIN photodiodes compared to an unpackaged InP PIN diode. The optical windows of all three diodes was 12 µm.

Figure 3 (Right). Frequency performance of three metamorphic photoreceiver configurations. The photodiode-amplifier connections are made with a hybrid lossy match, a monolithic lossy match, or a buffer amplifier. The measurements were made with the same 1.55 µm optical input power.

NAMBE 2003 Program

Tuesday, September 30, 2003

1:30-3:10: Materials for Spintronics and Quantum Information

Chair: Gary Wicks (University of Rochester)

TC-1: MBE growth of high Curie temperature GaMnAs films
R P Campion, K W Edmonds, L Zhao, K Wang, B L Gallagher, and C T Foxon
University of Nottingham, United Kingdom

TC-2: Influence of Defects on Structural and Magnetic Properties of GaMnAs
J. Sadowski[1, 2, 3], J. Kanski[4], P. Svedlindh[5], V. Stanciu[5], J. Z. Domagala[3], J. Bak -Misiuk[3], A. Mikkelsen[2], C. Glover[6], and E. Hankiewicz[7]
[1]Copenhagen University, Denmark; [2] Lund University, Sweden; [3]Polish Academy of Sciences, Poland; [4]Chalmers University of Technology, Sweden; [5]Uppsala University, Sweden; [6]Australian National University, Australia; [7]Iowa State University, USA

TC-3: Reduced interface reaction during the epitaxial Fe growth on InAs for high efficiency spin injection
Kanji Yoh[1], Hiroshi Ohno[1], Kazuhisa Sueoka[1], and Manfred E. Ramsteiner[2]
[1]Hokkaido University, Japan; [2]Paul Drude Institute of Solid State Electronics, Germany

TC-4: Epitaxial Growth of a Spin-Polarized Ferromagnetic Oxide on Silicon: EuO/Si (001)
D.G. Schlom[1], V. Vaithyanathan[1], J. Lettieri[1], S.B. Ogale[2], S.K. Eah[3], J. Levy[3], J. Stephens[4], V. Sih[4], and D.D. Awschalom[4]
[1]Penn State University; [2]University of Maryland; [3]University of Pittsburgh; [4]University of California, Santa Barbara

TC-5: Epitaxial growth of two-dimensional Al(111) films on Si(111) – applications in quantum computing
D. A. Hite, R. W. Simmonds, K. M. Lang, R. McDermott, J. M. Martinis, and D. P. Pappas
National Institute of Standards and Technology

MBE growth of high Curie temperature GaMnAs films

R P Campion, K W Edmonds, L Zhao, K Wang, B L Gallagher and C T Foxon.
School of Physics and Astronomy, University of Nottingham, Nottingham NG7 2RD

Abstract:

There is increasing interest in dilute magnetic semiconductors, with predictions of room temperature ferromagnetic behaviour in several different systems. Many groups have investigated GaMnAs films grown at low temperature by Molecular Beam Epitaxy (MBE). Films are grown with low arsenic to gallium ratio to avoid the incorporation of antisite defects. Post growth annealing can be used to improve both the material properties and the Curie temperature [1].

For some time Curie temperatures was limited to 110K [2], but we have recently increased this to considerably higher values (160K). To achieve this aim, we investigated the growth of GaMnAs films as a function of growth temperature, growth rate and Mn flux. For a given growth rate, at high Mn fluxes or high growth temperatures, a three-dimensional (3D) growth mode is observed by reflection high-energy electron diffraction (RHEED), but at lower Mn fluxes or reduced growth temperature a two-dimensional (2D) growth mode is observed, as previously reported [3]. We have mapped the transition region over a range of Mn fluxes from 0 to 8 x 10^{-9}Torr for temperatures in the range 175 to 300°C. Ferromagnetic transition temperatures up to 90K are obtained for un-annealed thin films grown close to this 2D to 3D transition region. The samples have very high metallic conductivities for a wider range of Mn concentrations than has been previously observed (1.5 to 8%) with very low compensation [4]. After post-growth annealing, the best samples show a Curie temperature of ~160K [5], significantly higher than previously reported values [2]. Using this method, we have been able to grow ultra-thin (5nm) samples, which show metallic behaviour down to 4K for relatively low (2%) Mn concentration.

In this paper we will concentrate on the MBE growth conditions required to obtain high quality dilute ferromagnetic semiconductors in the GaMnAs system.

References

[1] S J Potashnik et al, Appl. Phys. Lett., **79, 2001** 1495

[2] F Matsukura, H Ohno, A Shen and Y Sugawara, Phys Rev, **B57, 1998** R2037

[3] R P Campion, K W Edmonds, L X Zhao, K Y Wang, C T Foxon, B L Gallagher and C R Staddon

[4] K.W. Edmonds, K.Y. Wang, R.P. Campion, A.C. Neumann, C.T. Foxon, B.L. Gallagher. P.C. Main, Appl. Phys. Lett., **81, 2002** 3010

Corresponding author: R. P. Campion, School of Physics and Astronomy, University of Nottingham, Nottingham NG7 2RD, UK

Phone: +44 115 9515189, Fax: +44 115 9515180, email: richard.campion@nottingham.ac.uk

INFLUENCE OF DEFECTS ON STRUCTURAL AND MAGNETIC PROPERTIES OF GaMnAs

J. Sadowski[1*, 2, 3], J. Kanski[4], P. Svedlindh[5], V. Stanciu[5], J. Z. Domagala[3], J. Bąk-Misiuk[3], A. Mikkelsen[2], C. Glover[6], E. Hankiewicz[7]

[1] *Niels Bohr Institute, Copenhagen University, DK-2100 Copenhagen, Denmark*

[2] *MAX-Lab, Lund University, Po. Box. 118, 221 00 Lund, Sweden*

[3] *Institute of Physics, Polish Academy of Sciences, 02-668 Warszawa, Poland*

[4] *Chalmers University of Technology, 412 96 Göteborg,. Sweden*

[5] *Uppsala University, 751 21 Uppsala, Sweden*

[6] *Department of Electronic Materials Engineering, Australian National University, Canberra, ACT, Australia.*

[7] *Ames Laboratory, Iowa State University, USA*

III-V magnetic semiconductors are extensively studied by many research groups due to their fascinating properties associated with carrier induced ferromagnetic ordering of Mn spins. GaMnAs though very easy to obtain by low temperature Moleculer Beam Epitaxy (LT MBE) is a very complex material in point of view of both: crystallographic structure and magnetic/magnetotransport properties. Since GaMnAs can only be obtained by LT MBE method it contains a large variety of defects know to occur in LT GaAs. Moreover, other defects, not present in LT GaAs occur in GaMnAs only (for example Mn interstitials). Thus it is very important to identify the most abundant defects in GaMnAs and their influence on properties of this compound. Until recently only As antisites were supposed to play a crucial role in GaMnAs [1]. Recent experiments demonstrated the very important role of Mn interstitials [2]. It's now believed that low temperature post growth annealing techniques which improve transport and magnetic properties of GaMnAs are associated with removal of Mn interstitials. However, as demonstrated by several groups also As, antisites influence significantly properties of GaMnAs. This is evident that concentration of As antisites (as is well know for LT GaAs) is set by the MBE growth conditions such as substrate temperature, and As/Ga overpressure. The temperature window for MBE growth of homogeneous (without MnAs precipitates) GaMnAs compound is narrowing with increasing Mn content, being relatively wide for Mn content up to about 5.5%, and quite narrow for Mn compositions higher than 6%. This is reflected in the magnetotransport properties of GaMnAs. Until recently the optimum Mn composition for highest Tc and lowest resistivity was close to 5.5%. Recently the optimized annealing procedures made possible to overcome this limit and even GaMnAs containing 6% - 9% Mn exhibit excellent properties (in terms of Tc and conductivity). In this work we investigate the influence of different defects on magnetic, structural and transport properties of GaMnAs. A wide variety of experimental techniques Such as: SQUID magnetometry, Hall effect measurements, XRD, EXAFS, photoemission, X-ray Absorption/Emission Spectroscopy, Scanning Tunneling Microscopy, Electron Spin Resonance were used to investigate GaMnAs samples with different concentration of defects.

[1] *K. M. Yu, W. Walukiewicz, T. Wojtowicz, I. Kuryliszyn, X. Liu, Y. Sasaki, and J. K. Furdyna, Phys. Rev. B* ***65****, 201303 (2002)*

[2] *P. A. Korzhavyi, I. A. Abrikosov, E. A. Smirnova, L. Bergqvist, P. Mohn, R. Mathieu, P. Svedlindh, J. Sadowski, E. I. Isaev, Yu. Kh. Vekilov, and O. Eriksson, Phys. Rev. Lett.* ***88****, 187202 (2002)*

* Corresponding author, e-mail: sadow@maxlab.lu.se

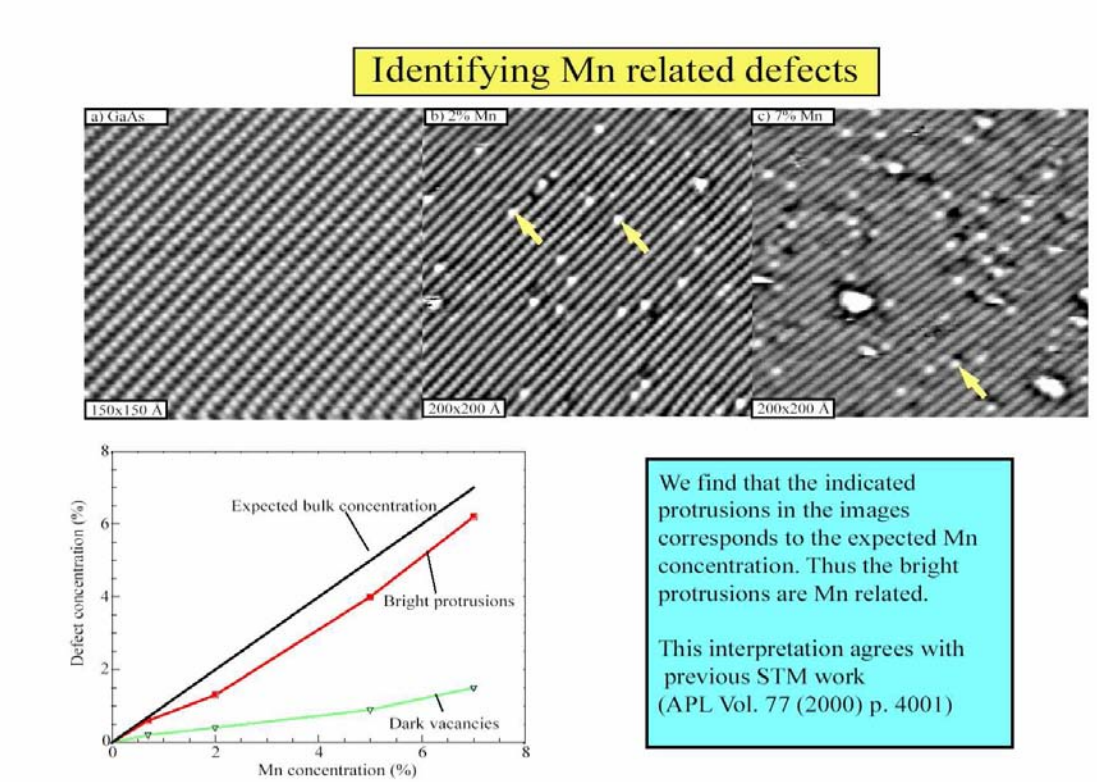

Fig. 1 Cross sectional STM pictures of:

- high temperature GaAs buffer layer (left image)
- $Ga_{0.98}Mn_{0.02}As$ layer (central image)
- $Ga_{0.93}Mn_{0.07}As$ layer (right image)

Reduced interface reaction during the epitaxial Fe growth on InAs for high efficiency spin injection

Kanji Yoh[1], Hiroshi Ohno[2], Kazuhisa Sueoka[2], and Manfred E. Ramsteiner[3]

[1]Research Center for Integrated Quantum Electronics, Hokkaido University, Sapporo, 060-8628 Japan
[2]Graduate School of Engineering, Hokkaido University, Sapporo, 060-8628 Japan
[3]Paul Drude Institute of Solid State Electronics, Berlin, 060-8628 Germany

Spin-injection from ferromagnetic metals into semiconductors is one of the key technologies to achieve spintronics [1] in the future. In spite of its potential importance, there have been keen discussions on whether or not an efficient spin injection into semiconductor is possible at all. Experimentally, spin injection from high Tc ferromagnetic metals into semiconductor has been reported by several groups[2] in Fe/GaAs system where electrons tunnel through a Schottky barrier which would limit the drain current drastically. Besides, those tunneling barriers, which might work as a spin filter, are believed to be the very reason which enables spin-injection through ferromagnet/semiconductor junction. One of the key conditions to allow high efficiency spin injection was proven to be the reduced interface diffusion and redaction at the ferromagnet and semiconductor interface. We have tried to compare the two growth temperature schemes 23℃ and 175℃ for the substrate temperature during the growth. The Reflection High Energy Electron Diffraction (RHEED) and Secondary Ion Mass Spaectroscopy (SIMS) characterization have been performed. Then, spin polarization efficiency was estimated by measuring the degree of circular polarization of the electroluminescence and the high efficiency of 20% in degree of circular polarization was verified with the low temperature sample.

The RHEED observation revealed that the low temperature(23℃) growth yields 3D-like growth at the initial stage compared with the high temperature (175℃) growth sample. However, the smoothe 2D growth is recovered in both cases after 300Å of the Fe growth which is followed by 30Å of Au cap layer. On the other hand, the SIMS measurement revealed that the high temperature sample have increased diffusion of As and In into the Fe layer which suggests that the lower temperature growth is preferred to reduce possible interface reaction while high temperature sample seems to be preferred to obtain better crystal quality of Fe thin film at least at the initial stage. The polarization experiment was possible in only low temperature growth samples because no electroluminescence was observed in high temperature sample probably due to increased interface states.

Spin polarization of Fe/InAs sample grown at 23℃ was measured by measuring the circular polarization in the surface direction as shown in Fig.3. A clear electro-luminescence was detected from the top of the sample by the InSb photo-detector. The electro-luminescence (EL) data showed clear spin injection when compared with EL of non-magnetic samples and photoluminescence of InAs substrate despite the theoretical controversy[3][4] on spin injection. Observed circular polarization efficiencywas estimated to be ~12%[5]. The $^{+}$ and components of the luminescence were measured by switching the angle of the quarter-wave plate. Fig.3 shows the external magnetic field dependence of the polarization efficiency calculated by the measured results of the $^{+}$ and components intensity of the luminescence P_L. Considering the opposite polarization behavior from the non-magnetic sample(EL) and the bare InAs substrate (PL), which is due to the Zeeman effect, the net polarization in the Fe electrode is estimated to be much higher, approaching a theoretical limit of 20% with the present experimental condition. These results clearly indicate that the spin injection in the FM/SC hybrid system is possible without a tunneling barrier.

References

[1] S.Datta and B.Das; Appl.Phys.Lett. 56 (1990) 665
[2] H.J.Zhu et al, Appl.Phys.Lett. 80 (2001) 016601
[3] P.C. van Son et al, Phys.Rev.Lett. 58 (1987) 2271
[4] O.Wunnicke et al, Phys.Rev.B 65 (2002)24136(R)
[5] H.Ohno et al, Jpn.J.Appl.Phys.Vol.42 (2993) pp.L1-L3 Part 2, No.2A, 1 February 2003

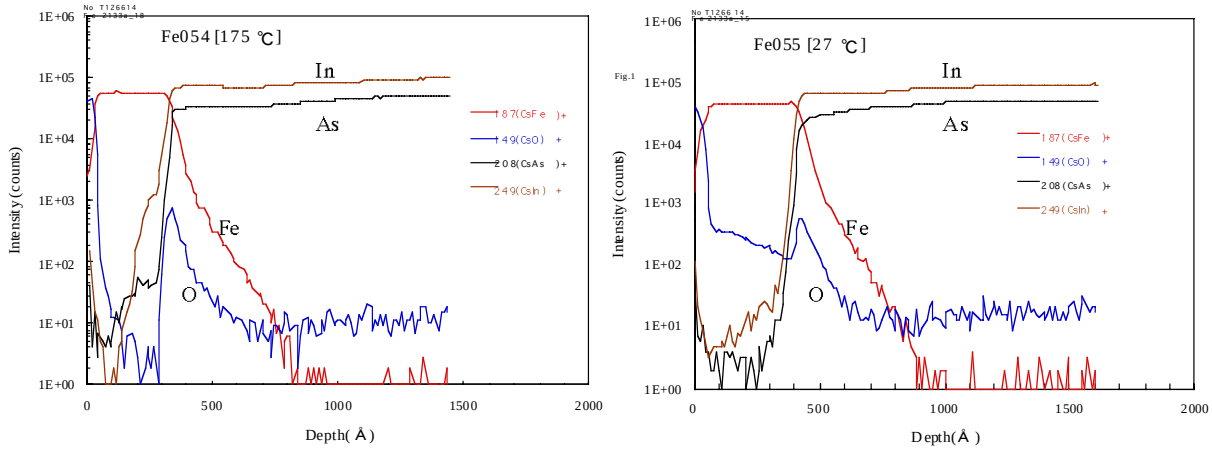

(a) (b)

Fig.1 SIMS profile of Fe/InAs samples grown at (a) 175°C and (b) 23°C. Increased diffusion of In and As in Fe layer is observed in (a) 175°C sample.

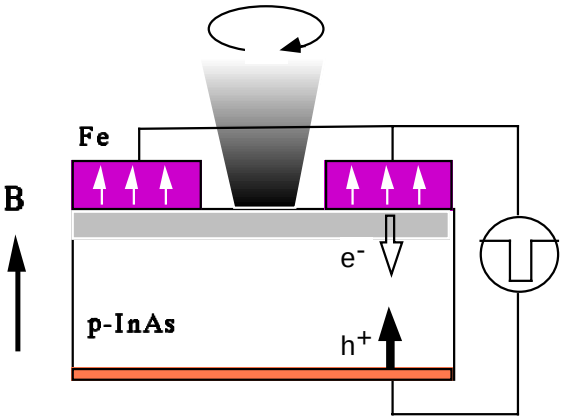

Fig.2 Schematic vertical structure of the device

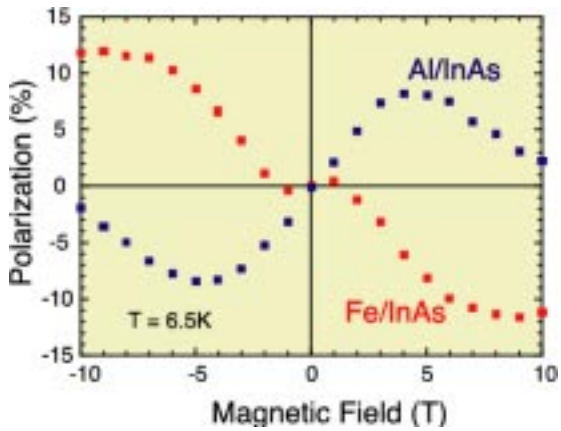

Fig.3 Spin polarization of electroluminescence light.

EPITAXIAL GROWTH OF A SPIN-POLARIZED FERROMAGNETIC OXIDE ON SILICON: EuO/Si (001)

D.G. Schlom*, V. Vaithyanathan, and J. Lettieri

Department of Materials Science and Engineering
Penn State University

S.B. Ogale

Department of Physics
University of Maryland

S.K. Eah and J. Levy

Department of Physics and Astronomy
University of Pittsburgh

J. Stephens, V. Sih, and D.D. Awschalom

Department of Physics and Center for Spintronics and Quantum Computation
University of California, Santa Barbara

EuO is a ferromagnetic semiconductor that in bulk can exhibit an insulator-metal transition at its Curie temperature (69 K) with a huge change in resistivity. Resistivity changes at the insulator-metal transition of up to 12 orders of magnitude with changing temperature, up to 6 orders of magnitude for an applied magnetic field, and up to 10 orders of magnitude for an applied pressure have been reported. It also exhibits a Faraday rotation that is among the largest of any known material (up to 7.5×10^5 °/cm). Of relevance to spintronics, recent studies on bulk EuO have shown that the charge carriers in the ferromagnetic state of EuO are nearly 100% spin polarized.[1] Additionally, of all binary oxides that may be thermodynamically stable in contact with silicon, the only magnetic one is EuO. This unique set of properties, coupled with the weak spin-orbit coupling for electrons in silicon and the relatively long transverse decoherence times (T_2) observed for bound states in silicon,[2] motivates the epitaxial integration of EuO with silicon for spintronic applications. The lattice mismatch between (001) Si and (001) EuO is 5.6%. This, together with the relative ease of oxidation of europium have made it possible for us to grow epitaxial EuO on silicon using the fully epitaxial sequence EuO / SrO / $SrSi_2$ / Si (001), where the $SrSi_2$ layer is formed by reacting half a monolayer of strontium with silicon at 700 °C and the SrO buffer layer, grown at close to room temperature, may be as thin as one monolayer. These films were grown by reactive molecular beam epitaxy. The entire epitaxial stack is capped with a protective aluminum layer to allow *ex situ* characterization of the grown layer. *In situ* RHEED and *ex situ* x-ray diffraction, shown in Figs. 1 and 2, confirm epitaxial growth and indicate a cube-on-cube orientation relationship between the layers, i.e., EuO (001) // SrO (001) // Si (001) and EuO [100] // SrO [100] // Si [100]. Magnetic measurements, shown in Fig. 3, reveal that the epitaxial EuO films are ferromagnetic with a Curie temperature of 68 K, close to the bulk value. The saturation magnetic moment of EuO is found to be 4.7 μ_B per Eu atom. The magneto-optical response of EuO, studied by polar Kerr effect at a wavelength of 1.3 μm, is comparable to bulk EuO. By mixing EuO with BaO, we have grown lattice-matched epitaxial (Ba,Eu)O / $SrSi_2$ / Si (001) at close to room temperature. This lattice-matched solid solution has a Curie temperature of about 20 K.

---

* Contact Information: schlom@ems.psu.edu, Tel: (814) 863-8579, Fax: (814) 863-0618

[1] P.G. Steeneken, L.H. Tjeng, I. Elfimov, G.A. Sawatzky, G. Ghiringhelli, N.B. Brookes, and D.-J. Huang, Phys. Rev. Lett. **88**, 047201 (2002).

[2]. J. P. Gordon and K. D. Bowers, Phys. Rev. Lett. **10**, 368 (1958).

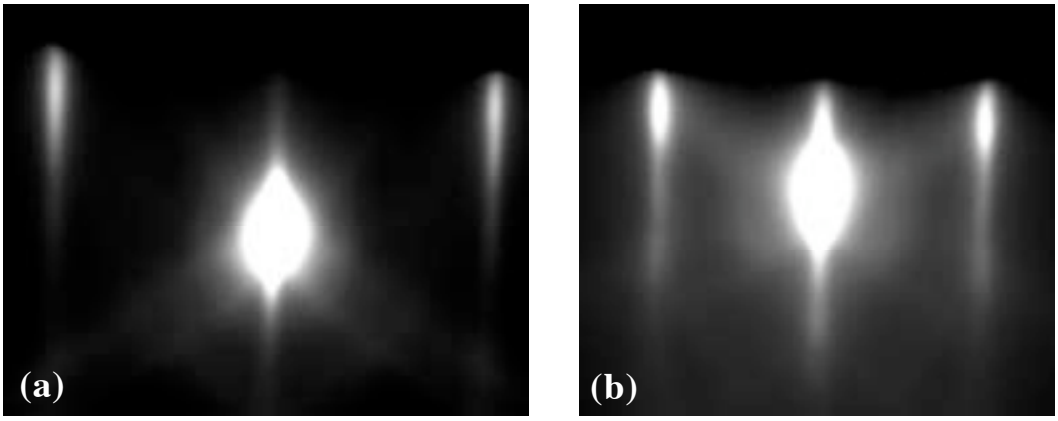

Fig. 1. RHEED images along the (a) [100] and (b) [110] azimuth of a 1 μm EuO / 13 Å SrO / $SrSi_2$ / (001) Si film.

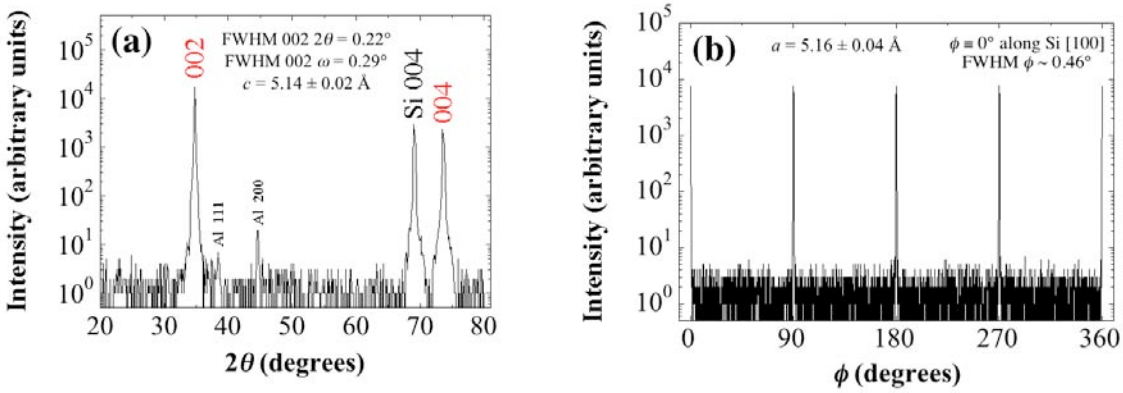

Fig. 2. Four-circle x-ray diffraction scans of a 1400 Å Al / 1 μm EuO / 13 Å SrO / $SrSi_2$ / (001) Si epitaxial film: (a) θ-2θ and (b) φ-scan of the EuO 202 peak. Despite the significant lattice mismatch, the 002 peak of the EuO film has a rocking curve width of 0.29°.

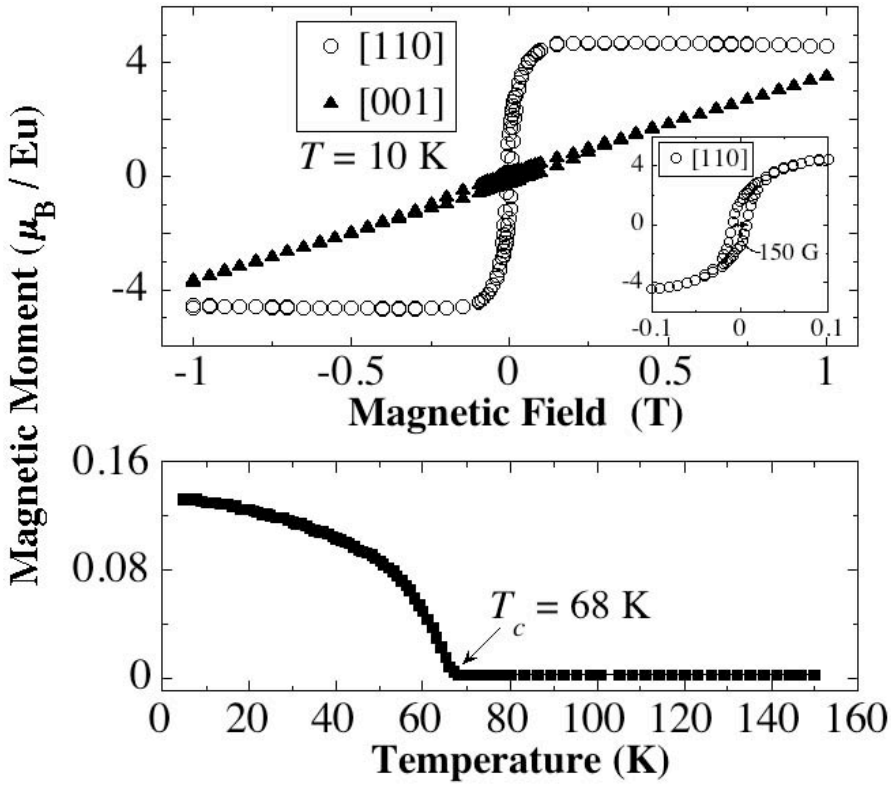

Fig. 3. (a) In-plane $B \parallel [110]$ and out-of-plane $B \parallel [001]$ hysteresis loops taken at $T = 10$ K of a 1300 Å Al / 660 Å EuO / 13 Å SrO / $SrSi_2$ / (001) Si epitaxial film. Inset depicts zoomed in [110] data showing remnance of ~1.5 μB per Eu atom and coercivity of ~150 G. (b) Zero-field warming curve with the sample oriented along the [110] direction reveals a Curie temperature of ~68 K.

Epitaxial growth of two-dimensional Al(111) films on Si(111) – applications in quantum computing

D. A. Hite, R. W. Simmonds, K. M. Lang, R. McDermott, J. M. Martinis and D. P. Pappas

National Institute of Standards and Technology, Boulder, CO 80305

Abstract

The importance of epitaxial materials in various applications is becoming increasing evident. For example, applications in quantum computing require low noise tunnel junctions that may only be achievable with advanced growth techniques. Specifically, the status of the NIST Josephson phase qubit is characterized by Rabi oscillations with coherence times ~ 40 ns with corresponding quality factors of Q ~ 2000. It is imperative that these figures of merit be improved in order to perform a qubit operation. Recently, spurious microwave resonances have been ubiquitously observed and identified as a dominant decoherence mechanism of the Rabi oscillation 'amplitude' [1]. These resonances are believed to originate from the microstructural defects in the insulating tunnel barrier and/or related interfacial regions. Our present effort is to use natively oxidized aluminum as the tunnel barrier. With advanced growth procedures, we have been able to use flat, epitaxial aluminum base electrodes for these quantum computing applications.

In itself, the ability to grow metal films on semiconductor substrates that are atomically flat and uniform, and that have sharp, non-intermixed interfaces is a new and interesting phenomenon. In this work, we use high quality Al films epitaxially grown on the Si(111)-(7 × 7) surface as the foundation for the qubit device. An initial seed layer of Al is deposited at 120 K and consequently annealed to 450 K. This technique results in an atomically flat Al film forming a metastable structure, where interfacial diffusion and reactive epitaxy have been inhibited [2]. During each step in the junction trilayer growth process, we have investigated the structure *in situ* by AES, AED and LEED in order to optimize the growth parameters and thereby process these samples into high quality epitaxial Josephson junctions and phase qubits. In this talk, we will present new results showing the relationship between the growth conditions of the junctions and the quantum coherence of the devices.

[1] R. W. Simmonds, K. M. Lang, D. A. Hite, D. P. Pappas and J. M. Martinis, submitted to *Science*.

[2] L. Aballe, C. Rogero, P. Kratzer, S. Gokhale, and K Horn**,** *Physical Review Letters* **87**, 156801 (2001).

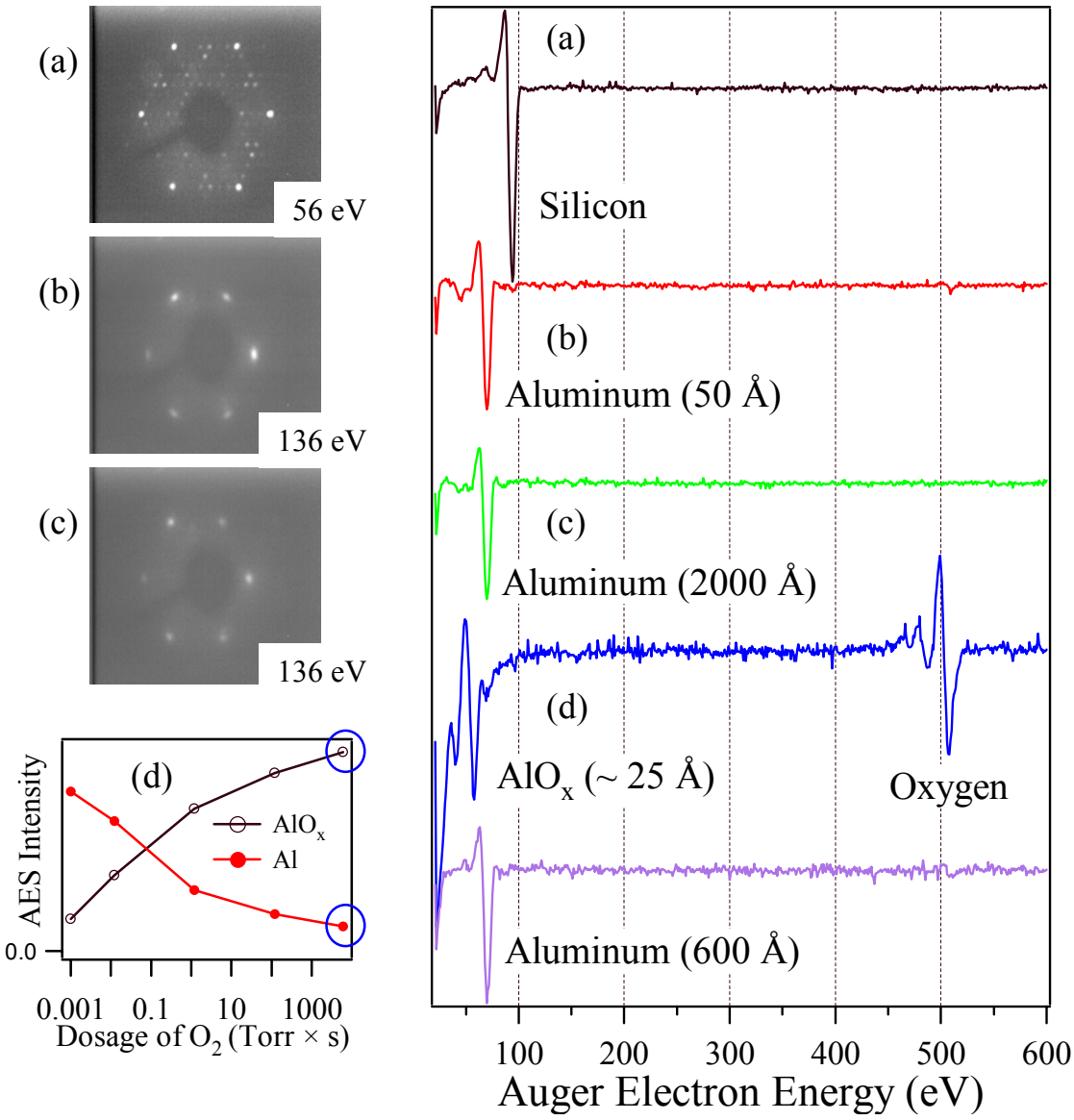

In this study, we start with (a) the clean, highly ordered and stable Si(111)-(7 × 7) reconstructed surface, and then deposit a seed layer of Al (~5 nm) at 120 K. (b) This seed layer is then annealed to 450 K in order to obtain a high quality epitaxial film of Al/Si(111) without intermixing at the interface. We then use (c) Al homo-epitaxy at room temperature to complete the base electrode to 200 nm. The tunnel barrier is made by the native aluminum oxide formed at room temperature (d) and subsequently annealed. Finally, the trilayer is completed using an aluminum counter electrode and processed into devices using standard photolithographic techniques.

NAMBE 2003 Program

Poster Session 2: Tuesday, September 30, 2003, 3:30-500

P2-1: Integrated In-Situ Monitoring of MBE Processes
R. Hartmann, P. Chow, and T. Barnacle
SVT Associates

P2-2: Growth of Be-doped GaInP/GaAs HBTS by all Solid-source Multiwafer Production MBE
A. Wilk, M. Zaknoune, S. Godey, P. Gérard, S. Dhellemmes, C. Chaix, and F. Mollot
RIBER and IEMN

P2-3: High Material Quality of 830nm Laser device Grown by SSMBE for Printing Applications
I. C. Hernandez, G. K. Kuang, and M. McElhinney
Lasertel, Inc.

P2-4: Investigation of radiative and non-radiative centers in Al-doped ZnSe grown by molecular beam epitaxy
D. C. Oh[a], J. S. Song[b], J. H. Chang[c], T. Takai[a], F. Lu[d], T. Hanada[a], M. W. Cho[a], and T. Yao[a]
[a]Tohoku University, Japan; [b]Korea Maritime University; [c]NeosemiTech Corp., Korea; [d]Fudan University, China

P2-5: Flux Profile Modeling : Monte Carlo Simulation and Numerical Computation
Bharat Reddy Pemmireddy[1], Ramprasad Vijayagopal[1], Rama Venkat[1], Hwa Cheng[2], and Rich Bresnahan[2]
[1]University of Nevada, Las Vegas; [2]Applied Epi-Veeco

P2-6: Solid-Source Molecular Beam Epitaxy (SSMBE) growth of GaInNAs on InP substrate
Junxian Fu, Seth Bank, Mark Wistey, James S. Harris, Jr
. Stanford University

P2-7: Optimisation of SiGe/Si hetero-interface in GSMBE aided by RHEED intensity oscillations
X.B. Li and J. Zhang
Imperial College London, United Kingdom

P2-8: Molecular beam epitaxial growth of antimony compounds on indium-free GaSb substrates
J.B. Héroux, C. Pei and W. I. Wang
Columbia University

P2-9: Real-time Ion Count from Nitrogen Plasma Source
Mark A. Wistey, Seth R. Bank, Homan B. Yuen, Lynford L. Goddard, and James S. Harris
Stanford University

P2-10: Regrowth of Extrinsic Contacts for High-Speed InP-based HBT Devices
V. Gambin, D. Mensa, M. Lange, A. Cavus, D. Sawdai, T. Block, A. Gutierrez-Aitken, and A.Oki
Northrop Grumman Space Technology

P2-11: Optical Properties of Very Low Temperatures Grown Compound Semiconductor by MBE
K. L. Chang, J. H. Epple, K. Y. Cheng, and K. C. Hsieh
University of Illinois at Urbana-Champaign

Integrated In-Situ Monitoring of MBE Processes

R. Hartmann, P. Chow, T. Barnacle (all SVT Associates)
Corresponding author: Ralf Hartmann, SVT Associates, 7620 Executive Drive, Eden Prairie MN, USA
Phone: +1 952 934 2100 x 223, Fax: +1 952 934 2737, Email: hartmann@svta.com

Nitride material systems (III-N_x-V_{1-x} alloys) pose many challenges to MBE deposition processes because of the strong dependence of the band gap on the nitrogen content. In the GaN_xAs_{1-x} system for example the band gap is reduced by more than 100meV per atomic percent of nitrogen [1]. Optimum device performance and high yield thus require accurate composition control better than 0.1%. The MBE growth of InGaAsSbN films is especially challenging due to the fact that the relative sticking coefficient of all the group V fluxes is highly temperature dependent. Thus temperature stability is a very critical process parameter. The wafer temperature also affects the crystalline quality of the grown material. Another challenging task is the deposition of the mirror stacks in the fabrication of InGaAsN VCSEL [2]. The tight thickness requirements dictate the use of in-situ process control to account for changes in material deposition rates.

SVT Associates has developed a broad range of in-situ monitoring tools that can enhance MBE processes. The development of an advanced temperature measurement system (In-Situ 4000 Process Monitor) specifically designed for MBE provides two-color pyrometry and two channels of narrowband reflectometry in a single instrument. The unique feature of the In-Situ 4000 is its ability to simultaneously measure both the substrate temperature and the film growth rate. It automatically compensates for emissivity variations caused by interference effects of the growing thin film layers resulting in a "real temperature" reading [3]. It also meets the accuracy requirements for accurate film thickness for reproducible growths of the mirror stacks needed for laser devices.

Another novel system is our atomic absorption based flux controller (AccuFlux™) for all MBE deposition processes. The excellent sensitivity of the AccuFlux Process Controller is better than 0.002 Å/s (corresponding to 0.1% composition changes) and allows closed-loop feedback control of atomic fluxes.

We have also established a very reliable, automated monitoring technique using in-situ RHEED for surface probing on an atomic level. The diffraction pattern is digitized with a CCD camera based acquisition system. Comprehensive image processing algorithms extract lattice constants providing insight into strain evolution. This information is routinely used to ensure lattice matching [4].

Desorption Mass Spectroscopy (DMS) is commonly used for our substrate temperature system calibration. Quantitative loss analysis of Ga provides important information for accurate thickness determination during nucleation layer growth [5] and composition analysis.

MBE process control has proven to be essential for high quality growth. Employment of sensors in a redundant mode and for calibration purposes is necessary for reliable feedback control in production systems. Implementation of these tools has demonstrated their inherent benefits in the development and optimization of state-of-the-art MBE processes.

References

[1] M. Kondow: Jpn. J. Appl. Phys., Part 2 **33**, L1056, 1994
[2] Chalmers, K. Lear, K. Killeen: Appl. Phys. Letters, **62**, pp 1585-1590, 1993
[3] F. Boebel et al.: J. Vac. Sci. Technology B, **12**(2), pp 1207-1210, 1994
[4] A. Nemcsics, F. Riesz: Cryst. Res. Technol., **36** (8-10), pp 1011-1017, 2001
[5] G. Koblmueller, P.Pongratz, et al.: Appl. Phys. Letters, **80**(13), pp 2281-2283, 2002

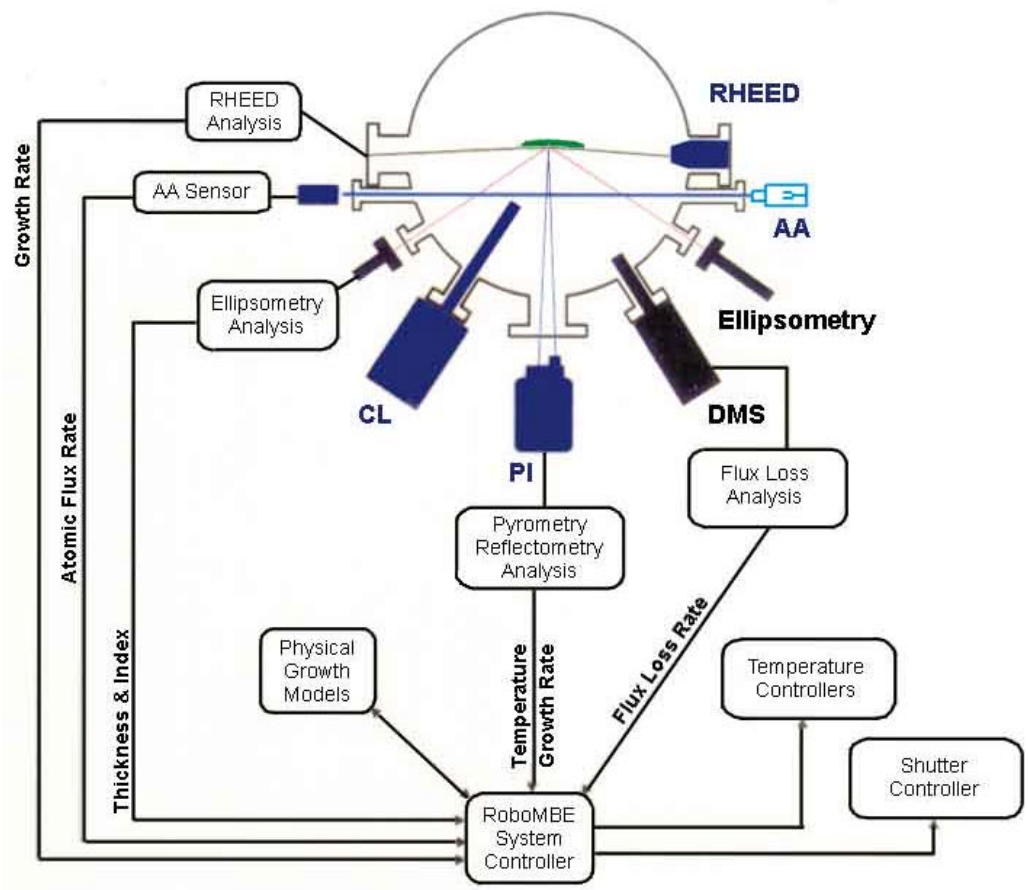

Fig. 1: In-Situ Monitoring Systems of MBE Processes

GROWTH OF Be-DOPED GaInP/GaAs HBTs BY ALL SOLID-SOURCE MULTIWAFER PRODUCTION MBE

A. Wilk, M. Zaknoune, S. Godey, P. Gérard, S. Dhellemmes, C. Chaix, F. Mollot
a) RIBER, 133 bd National, 92503 Rueil-Malmaison, France
b) IEMN, avenue Poincaré, BP 69, 59652 Villeneuve d'Ascq Cedex, France

Abstract

The rapid set-up of the MBE growth process for GaInP/GaAs HBTs in an all solid-source RIBER49 production MBE system is reported. The first 100x100 µm² large area test structures enable to determine the static gain, which is above 200. RF measurements on 8x10 µm² devices exhibit a cut-off frequency f_T of 34 GHz. Most publications concerning production of such devices are related to MOCVD grown material. In this paper we demonstrate that MBE is a very efficient method for high volume production of GaInP/GaAs HBT. In particular we emphasize on the fact that the MBE growth process for production of benchmark HBT devices is both high yield and easy to implement in a very short time. Further work will focus on the metallurgical and electrical Emitter/Base interface.

Uniformity and quality of grown material

In a production situation, one of the first issues is the uniformity : for thickness, composition and doping. Consequently, in a first step towards the final device, it is important to demonstrate that all these parameters meet the requirements of HBT manufacturers. We started the study with the growth of structures such as AlGaInP/GaInP QWs demonstrating both thickness and composition uniformities of the III element fluxes on 13x2" platen (Figure 1 shows a wavelength uniformity of ± 3 Å). The V-element uniformity is an important issue and has been demonstrated by means of the growth of InAsP/InP QWs on different platen types (13x2" and 5x3") to show wavelength variation of ± 5 Å (Figure 2). Finally the doping uniformity was studied. It is not only a function of the Be and Si flux profiles over the platen but it depends also on growth rate, temperature and more faintly on V/III flux ratio uniformity (at high doping level). Because the device performance uniformity is widely dependant on this particular aspect, we have characterized the Be and Si doping of GaAs and GaInP materials. Standard measured doping uniformities of 1.4 % on 3x4" platens are shown in figure 3 for Si-doped AlGaAs and GaAs.

GaInP/GaAs interface study

Only 2 months after the first layers performed on the system we have grown a first HBT structure. The Be doping level of the Base is as high as 4.10^{19} cm^{-3} and its thickness is 400 Å. A 50 Å GaInP etch-stop layer has been introduced in the Sub-Collector.

The key element of the HBT structure is the Emitter/Base interface, consequently in order to optimize it we need to study the following parameters : spacer thickness (varying from 20 to 40 Å), interface material (including GaP and AlInP), growth temperatures (Be-doped Base, undoped spacer and GaInP Emitter) and As & P valve/shutter commutation between GaAs and GaInP. First, in order to study the metallurgical GaInP/GaAs interface, asymmetric AlGaAs/GaAs/GaInP SQWs were grown. The measured PL energy (figure 4) was compared to envelop function calculations of the nominal structure. We can notice that the memory effect of As is weak since a growth interruption shorter than 5" is enough to obtain the nominal PL energy, without any P exposition prior the growth of GaInP. Furthermore low temperature (10 K) PL measurements (figure 5) have been performed on PN junction (Base/Emitter diodes). A typical PL spectrum exhibits 3 distinct peaks : the lowest energy peak is related to the GaAs (around 1.5 eV), the highest one is related to GaInP (~ 1.98 eV). In between, a high intensity peak at 1.59 eV is correlated to the GaAs(Be)/GaInP(Si) interface. Indeed radiative recombination between holes from the GaAs base and electrons from the GaInP emitter occurs. Depending on the electrical junction position, the junction electric field is responsible for the reduction of PL intensity : in the case of junction shifting towards the Emitter (Be diffusion in the GaInP), the electric field is going to separate e^- and h^+, consequently decreasing the radiative recombination in the GaInP emitter (h^+ well in GaAs close to the interface providing an emission at 1.6 eV). As a confirmation, on every spectrum, high intensities measured at 1.6 eV correspond to the lowest ones at 1.98 eV and vice-versa. In addition I(V) measurements on processed PN junction (160 series) exhibit poor ideality factor. The same measurements have to be done on the 185-188 diodes. Their behavior is completely different compared to 160;161;165 samples. It appears that the insertion of a thin layer at the interface has a consequence on the PL intensity. The barrier provided by the AlInP disturbs the electric field and favors radiative recombination in the GaInP emitter as shown for samples 187 and 188.

GaInP/GaAs HBT first results

The 100x100 µm² large area test structures enable the measurement of static gain, which is above 200 as shown by the Gummel plot in figure 6. 8x10 µm² devices yields RF measurements with a cut-off frequency f_T of 34 GHz (figure 7). From the Gummel plot and the measured slope (1.38 for I_b and 1.08 for I_c) we can see that the metallurgical interface and the electrical junction are well suited for high performance HBT operation. An additional characteristic of the transistor is its breakdown voltage of 10 V, a typical value for GaAs.

Conclusion

Presented device results are the first obtained on this system and look very promising. A detailed study of the Emitter/Base interface, which is a key element of the structure, will permit a better understanding of the growth mechanism concerning the Be-diffusion from GaAs to GaInP and the necessity to tailor the metallurgical interface. We have shown that in a short time period MBE is able to produce benchmark HBT and can successfully compete with MOCVD.

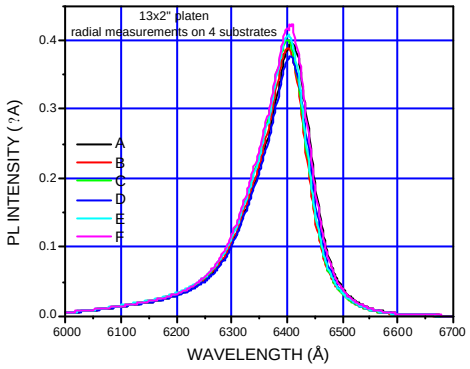

Fig. 1 : AlGaInP/GaInP QWs, PL measurements

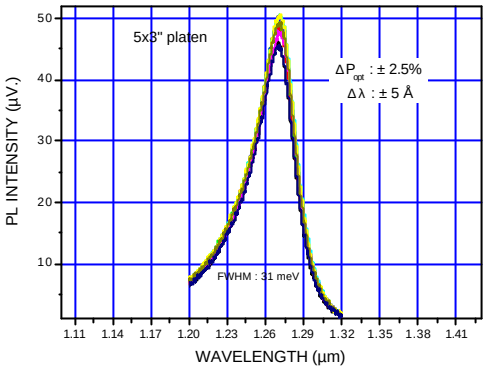

Fig. 2: InAsP/InP QWs, PL measurements

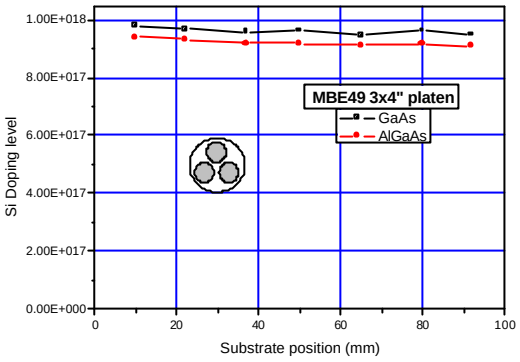

Fig. 3 : GaAs & AlGaAs Si-doping uniformity on 4" substrate

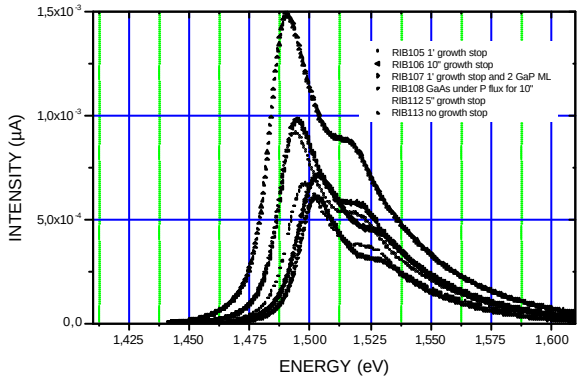

Fig.4 : RTPL GaAs/GaInP/AlGaAs asymmetric single QW

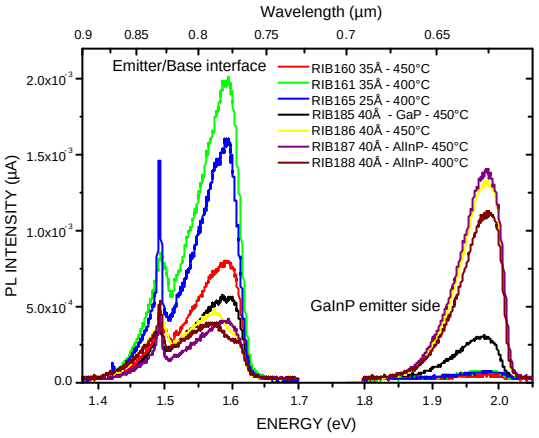

Fig. 5: PL measurements on GaAs(Be)/GaInP(Si) diodes

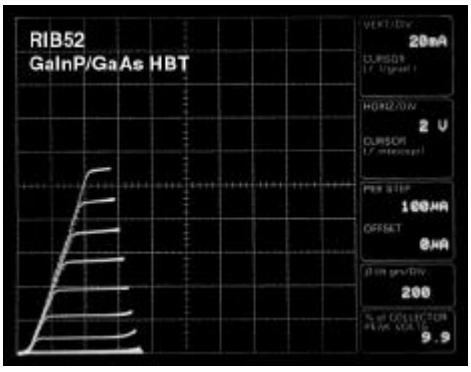

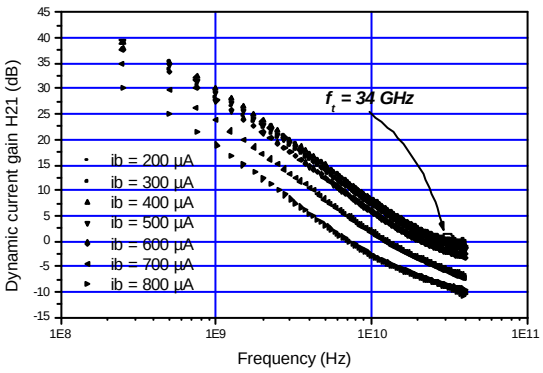

Fig. 6 & 7 : DC & RF measurements performed on the first HBT structure

High Material Quality of 830nm Laser device Grown by SSMBE for Printing Applications

I. C. Hernandez*, G. K. Kuang, M. McElhinney

Lasertel Inc., 7775 N. Casa Grande Hwy, Tucson, AZ 85743, USA

Molecular Beam Epitaxy has been employed almost entirely for growth of arsenic compounds due to the lack of a suitable solid phosphorous source. Advanced Phosphide Epitaxy has only been performed basically by Metal Organic Vapor Deposition (MOCVD) and phosphide based Gas-Source MBE. SSMBE is capable to grow GaInAsP and AlGaInP layers structures without using toxic gases as source material [1].

The key of SSMBE is valved cracker cell for elemental Arsenic and Phosphorous. This cell is formed by three zones: white P, red P and cracker zone. By changing the temperature of the cracker zone we can optimize the red and withe phosphorous rate released from the cell [2-3].

The material was grown in GEN III reactor on 2-inch GaAs wafers doped with Si. Substrate Growth Temperature by pyrometer was 510 °C. Cracker temperature was kept at 850 °C. This temperature is not too low, so we can avoid high accumulation of white P on the wall of the chamber and from other side is not to high to break Phosphorous Oxide which could release Oxygen with subsequent incorporation into the grown layers.

To verify the material quality, wafers were processed with different cavity lengths and 56μm emitter size. The obtained Internal Quantum Efficiency (η_i) is 92.8 % while Internal Optical Loss (α_i) is 0.87cm^{-1} at 25 °C (Fig.1).

LIV measurements at different temperatures were made in order to calculate T_0. Obtained values for T_0 for three different chips are 210, 223 and 245 °K which indicate very good thermal stability (Figs. 1-3).

From this data we can conclude that SSMBE is suitable MBE growth method to get high quality phosphorous-based material [4].

References:

1. M. Pesa, M. Toivonen, P. Savolainen, J. Kongas, R. Murison, T Panarello. All-Solid-Source MBE Growth Of AlGaInAsP- Based Optoelectronic Devices. 10th Intern. Conf. On Indium Phosphide and Related Materials 11-15 May 1998.
2. W.E. Hoke, P.J. Limonais, and A. Torabi. Reduction of Oxygen contamination in InGaP and AlGaInP films grown by Solid Source Molecular Epitaxy. J. Vac. Sci. Technol. B 16(6) Nov/Dec 1998.
3. W.E. Hoke, P.J. Limonais. Practical Aspects of Soid Source Molecular Beam Epitaxial Growth of Phosphorous-containing films. J. Vac. Sci. Technol. B 17(5), Sep/Oct 1999.
4. I. Hernandez and A. Ovtchinnikov. Epitaxial Formula Makes Better Lasers. Photonic Spectra, October 2001, pp. 151-156.

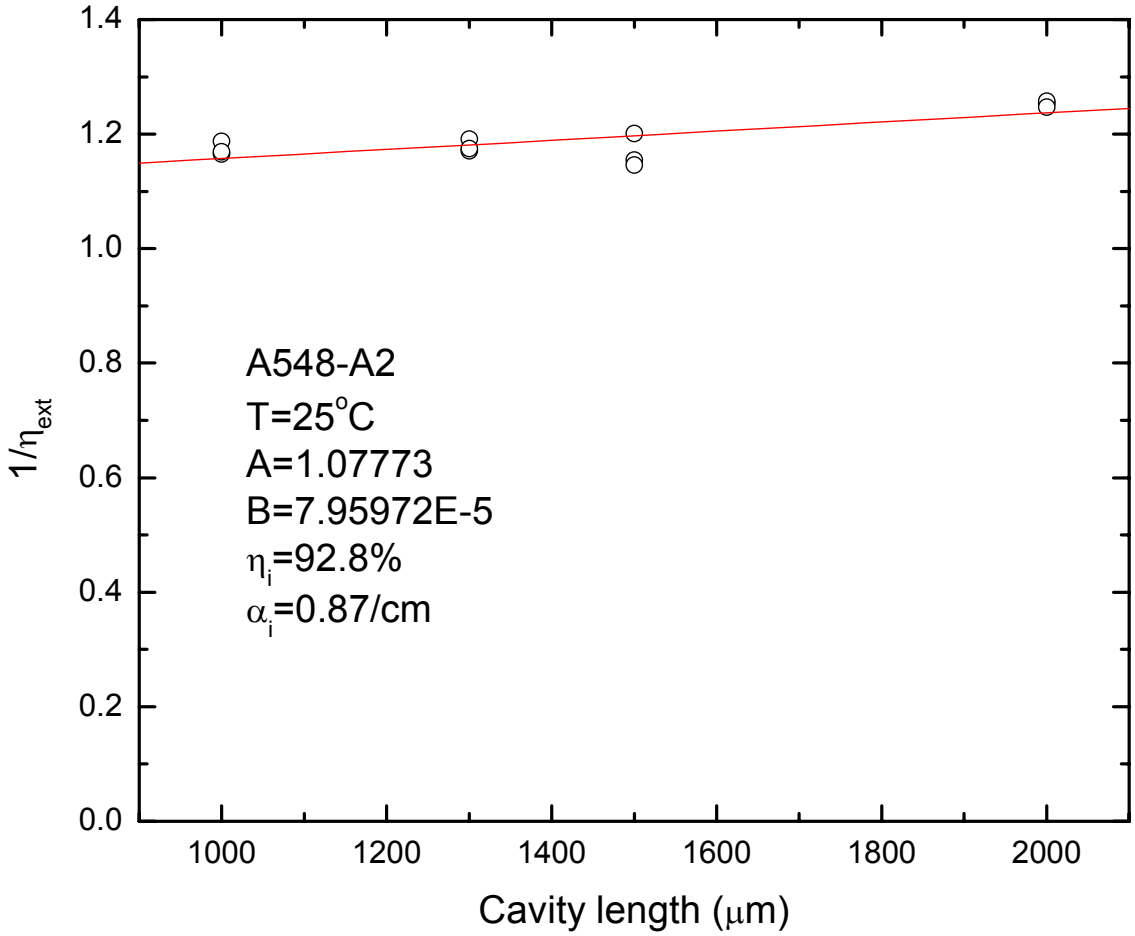
1.4
1.2
1.0
0.8
0.6
0.4
0.2
0.0
1/ηext
A548-A2
T=25°C
A=1.07773
B=7.95972E-5
ηi=92.8%
αi=0.87/cm
1000
1200
1400
1600
1800
2000
Cavity length (μm)

Figure 1

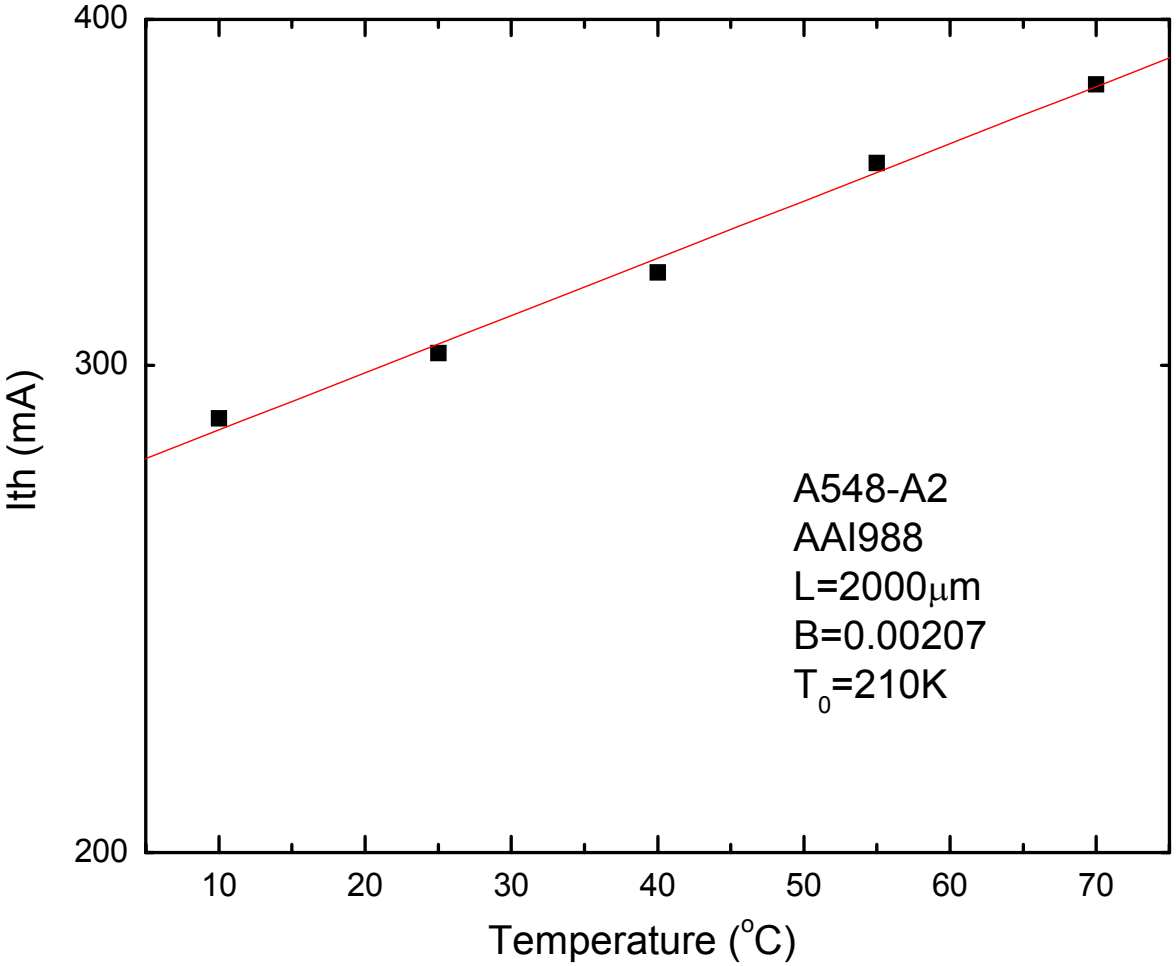
400
300
200
Ith (mA)
10
20
30
40
50
60
70
Temperature (°C)
A548-A2
AAI988
L=2000μm
B=0.00207
T0=210K

Figure 2

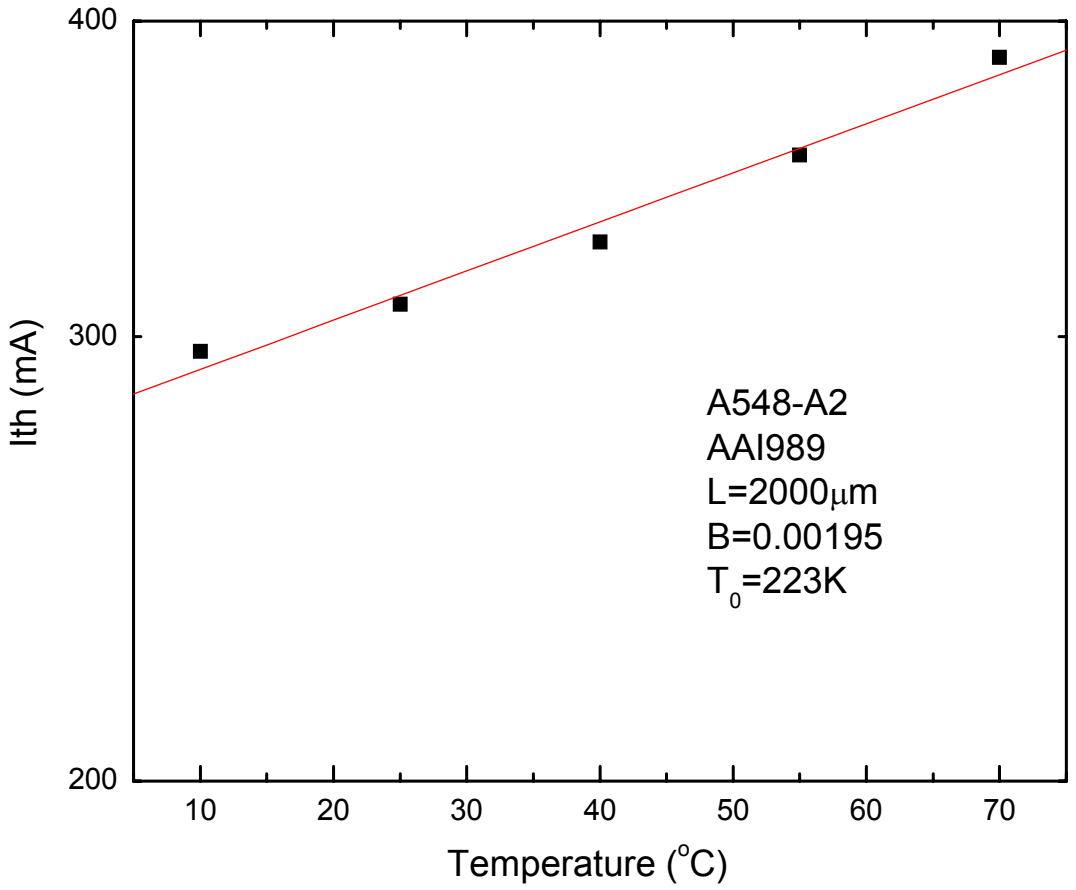
400
300
200
Ith (mA)
10
20
30
40
50
60
70
Temperature (°C)
A548-A2
AAI989
L=2000μm
B=0.00195
T0=223K

Figure 3

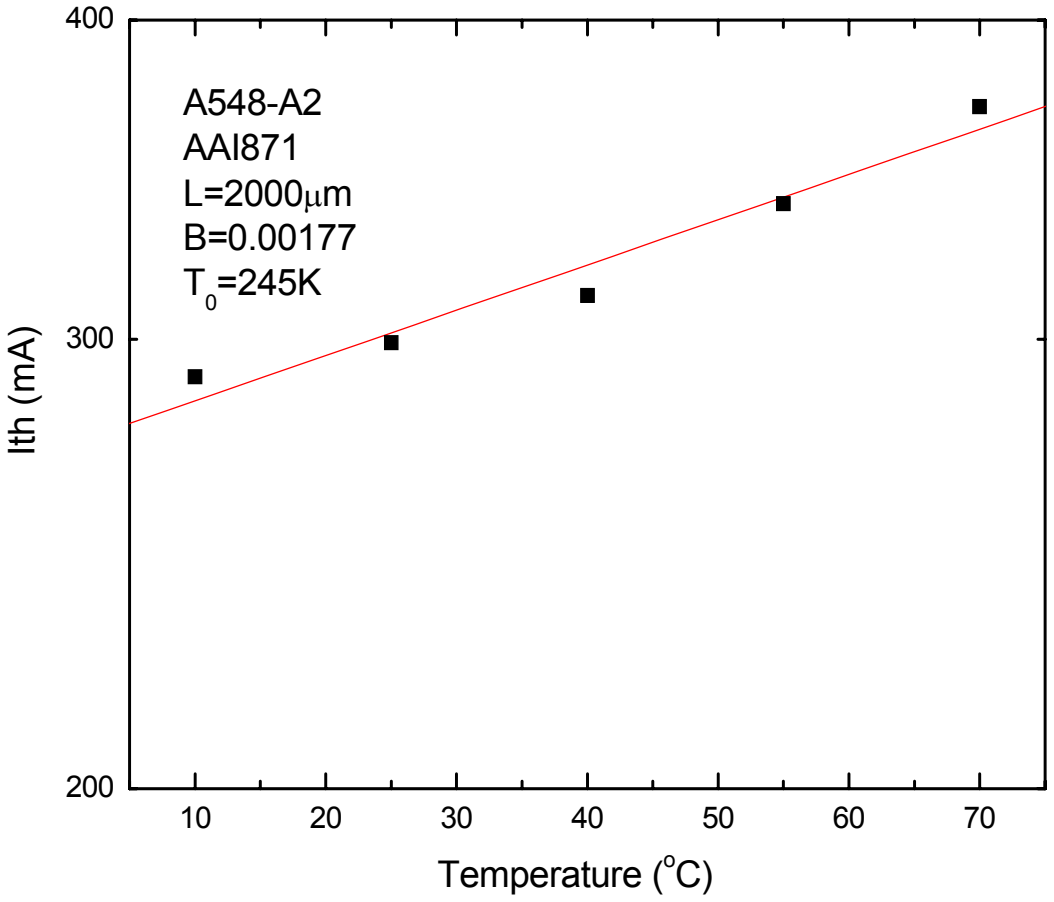
A548-A2
AAI871
L=2000μm
B=0.00177
T0=245K
Ith (mA)
400
300
200
10
20
30
40
50
60
70
Temperature (°C)

Figure 4

Investigation of radiative and non-radiative centers in Al-doped ZnSe grown by molecular beam epitaxy

D. C. Oh[a, *], J. S. Song[b], J. H. Chang[c], T. Takai[a], F. Lu[d], T. Hanada[a], M. W. Cho[a], and T. Yao[a]

[a]*Institute for materials research, Tohoku university, Katahira 2-1-1, Aoba-ku, Sendai, 980-8577, Japan*
[b]*Department of applied physics, Korea maritime university, 1 Dongsam-dong, Yeoungdo-koo, Pusan, 606-791, Korea*
[c]*NeosemiTech corporate, 357-13 Dangha-dong, Seo-koo, Incheon, 151-818, Korea*
[d]*Department of physics, Fudan university, 220 Handan road, Shanghai, 200433, P. R. China*
[a, *]*Corresponding author – e-mail : ohdongch@imr.tohoku.ac.jp Tel : 81-22-215-2074 FAX : 81-22-215-2073*

The identification and characterization of various defects in ZnSe have been extensively carried out to improve visible light emitting devices. Those defect states, native or introduced by dopants, strongly affect the efficiency of radiative recombination and induce carrier compensation. Recently, the molecular beam epitaxy (MBE) growth of high quality Al-doped ZnSe with the electron concentration of 5×10^{18}cm^{-3} has been reported.[1] Owing to availability of high-purity elemental form and low chemical reactivity, Al is an ideal source material for n-type dopant of ZnSe in MBE. However, attempts to realize higher electron concentration by introducing higher doses of Al result in the saturation or even the decrease of electron concentration. Nevertheless, there is rather little knowledge about deep trap centers which act as non-radiative centers or induce carrier compensation in Al-doped ZnSe.

In this work, a series of Al-doped ZnSe samples were grown on semi-insulating (001) GaAs substrate by MBE. The electron concentration and the electron mobility were investigated by Hall measurement. Radiative and non-radiative centers were investigated by photoluminescence (PL), deep level transient spectroscopy (DLTS), optical deep level transient spectroscopy (ODLTS), and photocapacitance (PHCAP).

As shown in Fig. 1, the spectra of Al-doped ZnSe are much different from that of undoped ZnSe. The near-band edge (NBE) emission intensity is much weak. Deep-level emission is observed around 2.25eV, which shows oscillatory structures because of the interference effect. The deep level which causes the 2.25eV emission is positioned at 0.55eV from the valence band maximum. The intensity of this deep level emission shows the tendency to increases as Al cell temperature increases. The deep level emission of Al-doped ZnSe is tentatively assigned to a point defect such as Al donor complex.

DLTS results show two negative peaks at the temperature range of 65K (D1) and 225K (D2), indicating the presence of two majority electron traps. The electron trap, D1 and D2 are estimated to be positioned to be 0.2eV and 0.8eV below conduction band minimum, respectively. The capture cross-section of D2 is estimated to have the large value of $1\times10^{-7}\sim2\times10^{-7}$cm^2, differently from what have been reported in ZnSe,[2,3] which is ascribed to heavy doping.

Subsequently, ODLTS and PHCAP characteristics are investigated in order to study non-radiatve centers near conduction band maximum. As a result, we could succeed in elucidating the radiative and non-radiative centers which contribute to carrier compensation in Al-doped ZnSe.

[1] T. Takai et al, Phys. Stat. Sol. (b) **229**, 381 (2002)
[2] T. Miyajima et al, J. Appl. Phys. **67**, 1389 (1990)
[3] G. Karczewski et al, J. Appl. Phys. **75**, 7382 (1994)

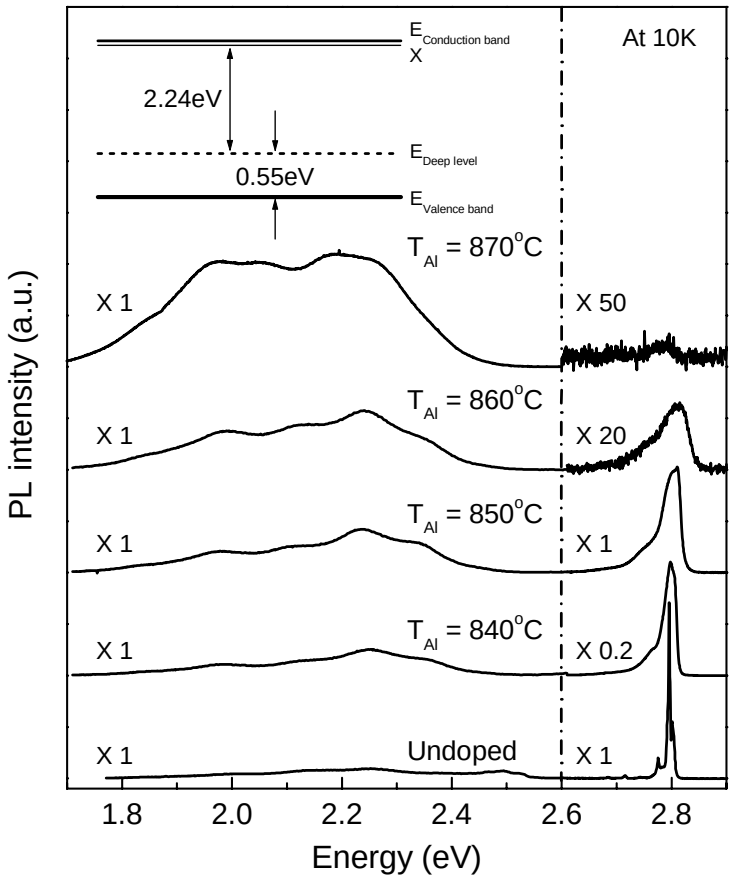

Fig. 1 PL spectra for undoped ZnSe and Al-doped ZnSe at 10K.

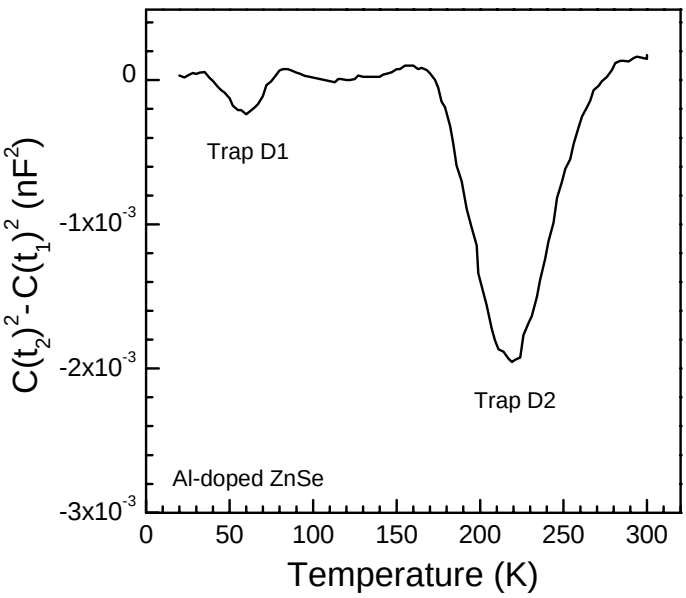

Fig. 1 DLTS spectrum of Al-doped ZnSe taken at a time constant of 1.15583sec. Reverse bais to the sample was 0.75V and filling pulse time was 5sec at 0V.

Flux Profile Modeling : Monte Carlo Simulation and Numerical Computation

Bharat Reddy Pemmireddy, Ramprasad Vijayagopal, Rama Venkat
Department of ECE, University of Nevada, Las Vegas, NV 89154-4026
venkat@ee.unlv.edu

Hwa Cheng, Rich Bresnahan
Applied Epi-Veeco
St. Paul, MN 55127

Spatial variations in flux are a result of the geometry of the Knudsen cell and the geometry of the growth chamber, i.e. the distance between the cell and substrate and relative orientation of the cell axis to the substrate normal. Two different approaches based on physical principles are employed to model the spatial flux variation on the substrate: Monte Carlo approach and numerical approach. In both approaches, direct flux from the liquid surface and the secondary flux from the walls of the Knudsen cell to the substrate are computed. Results of relative spatial flux variation obtained from the two theoretical approaches are compared between themselves and with experimental data from the literature for the case of rotated platen. The results are in good agreement. Preliminary results of flux with controlled temperature gradient on the wall of the Knudsen cell and rotated substrate will be presented and discussed. Additionally, the dependence of flux profiles on geometrical and process parameters will be presented and disccused.

Acknowledgement: R & D grant from Applied Epi-Veeco and UNLV as part of a ARI grant is gratefully acknowledged.

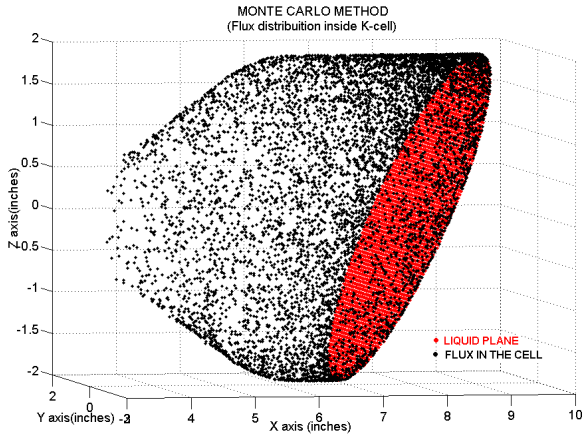
MONTE CARLO METHOD
(Flux distribuition inside K-cell)
Z axis(inches)
Y axis(inches)
X axis (inches)
LIQUID PLANE
FLUX IN THE CELL

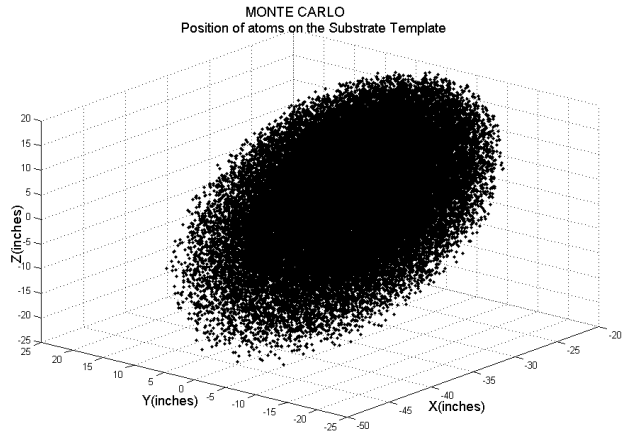
MONTE CARLO
Position of atoms on the Substrate Template
Z(inches)
Y(inches)
X(inches)

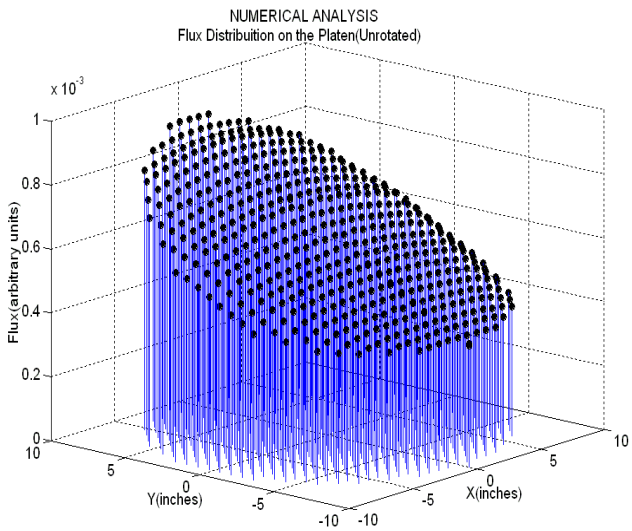
NUMERICAL ANALYSIS
Flux Distribuition on the Platen(Unrotated)
x 10^-3
Flux(arbitrary units)
Y(inches)
X(inches)

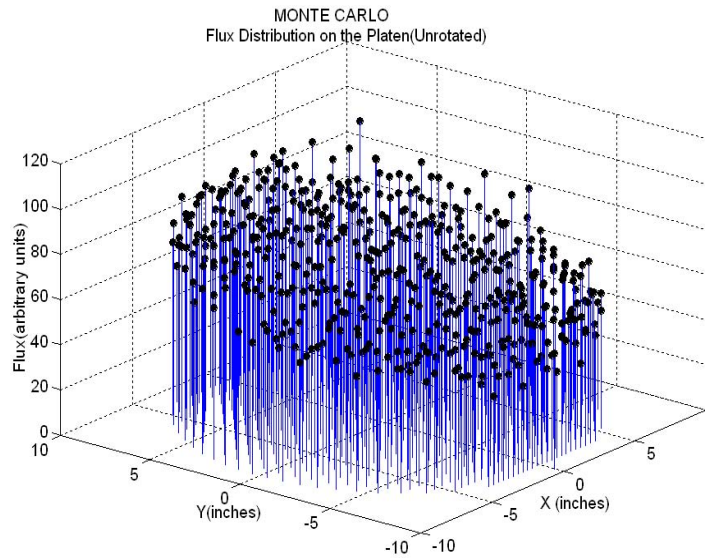
MONTE CARLO
Flux Distribution on the Platen(Unrotated)
Flux(arbitrary units)
Y(inches)
X (inches)

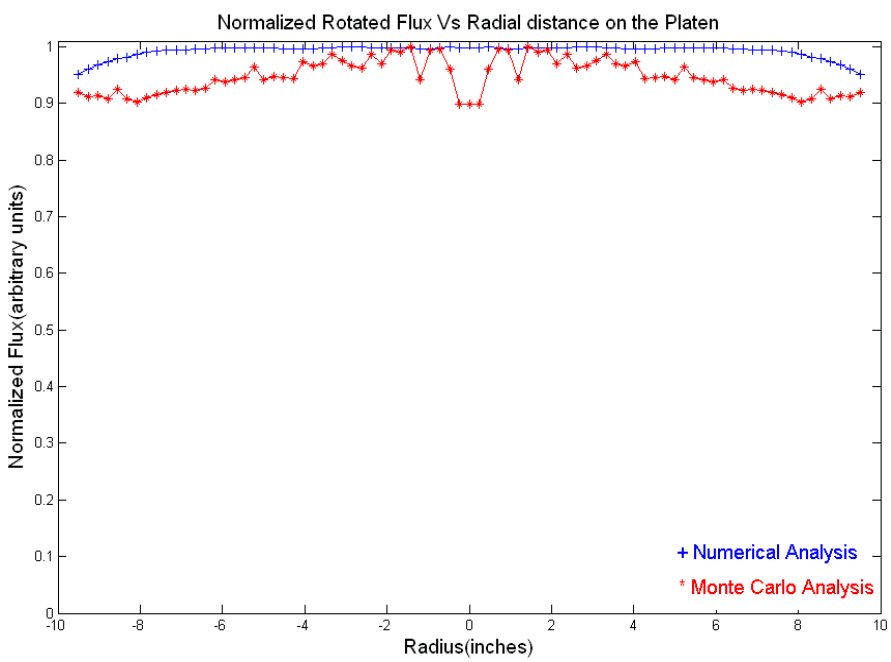
Normalized Rotated Flux Vs Radial distance on the Platen
Normalized Flux(arbitrary units)
Radius(inches)
+ Numerical Analysis
* Monte Carlo Analysis

Solid-Source Molecular Beam Epitaxy (SSMBE) growth of GaInNAs on InP substrate

Junxian Fu[1,2]*, Seth Bank[2,3], Mark Wistey[2,3], James S. Harris, Jr.[2,3]
[1] Department of Applied Physics, [2] Solid State and Photonics Laboratory, [3] Department of Electrical Engineering, Stanford University
* Corresponding Author: junxian@stanford.edu

Abstract

As a promising material for opto-electronic devices grown and fabricated on GaAs substrate[1], GaInNAs has been extensively studied in the optical communication field[2]. The small size of nitrogen atoms[3], the bandgap bowling effect of GaN_xAs_{1-x}[4], and the compressive strain in the active region layer grown on GaAs substrate significantly reduce the bandgap[5] and make possible long wavelength optoelectronic devices operating at 1.3μm and 1.55μm[6].

On the other hand, the wavelength range of 2-2.5μm is of specific interest to gas sensing, chemical detection, and especially near-infrared Fourier transform spectrometer. Latticed-matched $Ga_{0.47-3x}In_{0.53+3x}N_xAs_{1-x}$ grown on InP substrate has the potential to reach that wavelength with only a little bit of nitrogen introduced[7].

In this paper, the GaInNAs sample was grown consecutively in two SSMBE systems. In system I, a sublimation cell with GaP source was used to provide P_2 atmosphere to blowoff the oxide on the substrate at 510°C. After a InP buffer layer was grown at 450°C, the growth was interrupted and the substrate was cooled down. When the P_2 was almost pumped clean in the growth chamber, an arsenic cracker cell with needle valve was used to grow lattice-matched $In_{0.53}Ga_{0.47}As$ buffer layer. Before the sample was transferred to the other SSMBE system, arsenic-capping technique was utilized to protect the substrate from exposing to the air. In system V, a rf-nitrogen plasma source was used to grow nitride layer. After the blow-off of the arsenic capping layer at 510°C, the substrate was cooled to 300-350°C, and lattice-matched bulk layer of GaInNAs was grown.

The process was monitored by *in-situ* RHEED before and after the GaInNAs layer was grown. The samples were characterized by *ex-situ* XRD and room temperature photoluminescence. Preliminary results show that bulk layer of latticed-matched GaInNAs can be grown on InP substrate with the interest wavelength.

Reference:

1. Kondow, M; Uomi, K; Niwa, A, et.al., J. J. App. Phys. Part 1, Feb 1996; v.35, no.2B, p.1273-1275
2. Harris, JS, Semi. Sci. Tech.; Aug 2002; v.17, no.8, p.880-891
3. Shan, W; Walukiewicz, W; Ager, JW, J. App. Phys., Aug 15 1999; v.86, no.4, p.2349-2351
4. Lindsay, A; O'Reilly, EP, Sol. Sta. Comm., 1999; v.112, no.8, p.443-447
5. Chow, WW; Jones, ED; Modine, NA, App. Phys. Lett., Nov 8 1999; v.75, no.19, p.2891-2893
6. Nakahara, K; Kondow, M; Kitatani, T, et.al., IEEE Photon. Tech. Lett., Apr 1998; v.10, no.4, p.487-488
7. Gokhale, MR; Wei, J; Wang, HS; Forrest, SR, App. Phys. Lett., Mar 1 1999; v.74, no.9, p.1287-1289

Optimisation of SiGe/Si hetero-interface in GSMBE aided by RHEED intensity oscillations

X.B. Li and J. Zhang[†]

Department of Physics and Centre for Electronic Materials and Devices, Blackett Laboratory, Imperial College London, Prince Consort Road, London SW7 2BW UK.

The formation of Si/SiGe hetero-interface during epitaxial growth is critical in the many device applications ranging from microelectronics[1] to optoelectonics[2]. The segregation of Ge causes substantial problems in the formation of these hetero-interfaces by smearing the sharp composition profiles required by some of the applications. The optimisation of SiGe to Si interface has been studied extensively[3] and the control parameters available are the substrate temperature and growth rate. The focus of this contribution is the Si to SiGe interface where pre-deposition of Ge could improve the sharpness of the profile.

The amount of Ge to pre-deposited, in the case of GSMBE growth can be assessed by the RHEED intensity oscillation technique. The growth rate of a SiGe alloy is an function of the surface Ge concentration due to the kinetics controlling the growth reactions[4]. The measured growth rate immediately after Ge pre-deposition then give an indication where steady state surface Ge concentration has been reached for the intended alloy composition. The amount of Ge deposited from the GeH_4 precursor could also ben measured directly from the RHEED intensity oscillations. This optimisation procedure is carried out for substrate temperature of 520, 560 and 600°C for growth of 30% SiGe alloys. A typical RHEED intensity oscillation without Ge pre-deposition is shown in Figure.1

The amount Ge pre-deposition required for 560 and 600°C were found to be in excess of 1ML of Ge. The excessive amount of Ge required to achieve steady state suggest that there exist a mechanism for transporting Ge from the surface layer to the subsurface layer. Given the amount of Ge required increase with sustrate temperature, this mechanism is clearly thermally activated in contrast to the overall two sites exchange model of the segregation process. One of the possible mechanisms is diffusion.

Despite the large amount of Ge pre-deposited, there is no evidence of accumulation of Ge at the interface from cross-section TEM images. Si/SiGe supperlattice produced using this technique (strain balanced on SiGe virtual substrate) shows strong satellite in X-ray rocking curves (see Figure 2) indicating presence of sharp interfaces. The incorporation of Ge into the underlying Si layer should be accounted for in structure design of superlattice involving thin Si layers.

[1] D.J. Paul. Physics World, 13 (2000), p27
[2] G. Dehlinger et al. Science 290 (2000), p2277
[3] E.S. Tok et al. , J. Cryst. Growth 209 (2000), p321
[4] S.M. Mokler et al. Appl. Phys. Lett. 61 (1992) p2548

[†] Email: jing.zhang@imperial.ac.uk Tel: +44 (0)20 75947594 Fax: +44 (0)20 75813817

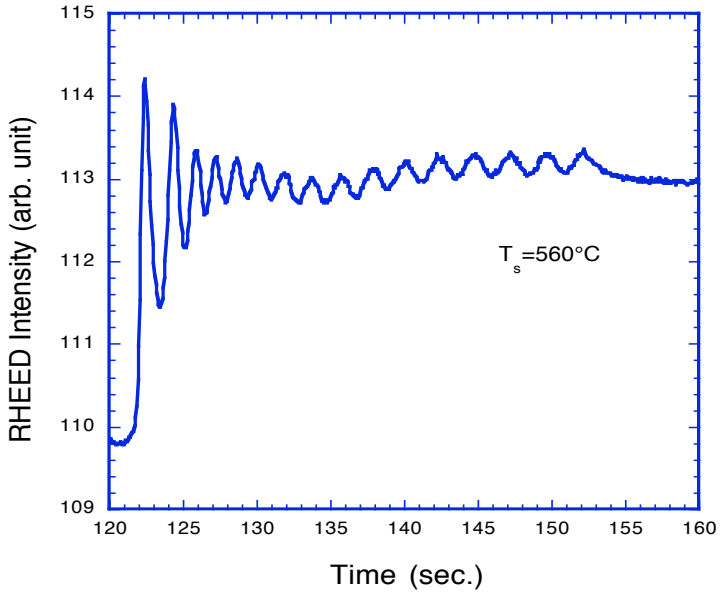

Figure 1. RHEED Intensity oscillation during growth of SiGe on Si(001) without Ge pre-deposition. The variation in period of oscillations indicates the gradual change in the surface Ge concentration.

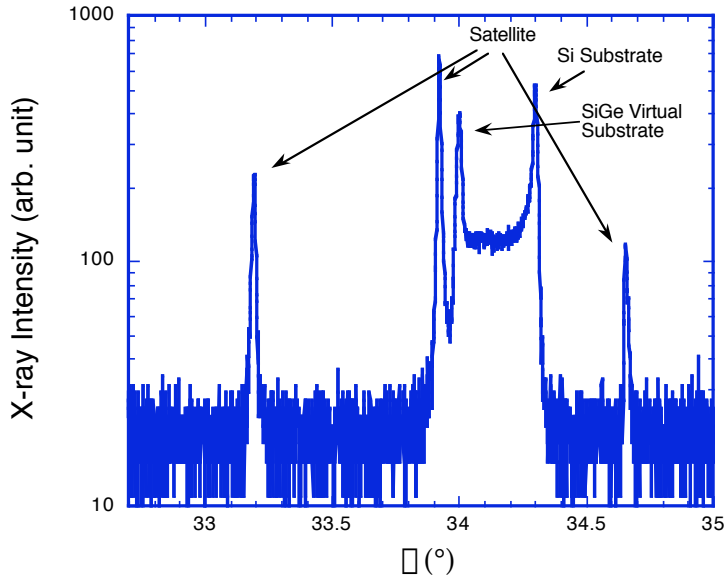

Figure 2. X-ray rocking curve of (004) reflection from a 300 periods $Si_{0.7}Ge_{0.3}$/Si superlattice structure grown on a SiGe virtual substrate. Strong satellite peaks indicate the presence of good interfaces.

Molecular beam epitaxial growth of antimony compounds on indium-free GaSb substrates

J.B. Héroux[1], C. Pei and W. I. Wang
Dept of Electrical Engineering
Columbia University
New York, NY 10027

GaSb-based heterostructures are used for a variety of applications in the 2-5 and 8-14 μm wavelength ranges. For the realization of high performance optoelectronic devices, the growth of very high quality, low defect density Sb-related compounds is critical. In this work, data are presented to show that the use of indium solder between the substrate backside and the molybdenum block during MBE growth has an effect on the crystalline quality of GaSb substrates and epilayers.

Figure 1 shows x-ray diffraction spectra of GaSb bulk layers grown on substrates placed: on a molybdenum block where the sample was held in place with indium solder (a); and on a custom-made block where the sample was held in place mechanically without indium (b). The use of an indium-free block results in a decrease by a factor of four of the full width at half maximum of the substrate peak. The improvement in material quality is explained by the fact that avoiding the use of indium solder prevents the formation on the back of the GaSb substrate of an indium-containing alloy generating strain and dislocations propagating through the substrate and epilayers.

Figure 2 shows the light-current curve and emission spectrum of an $In_{0.3}Ga_{0.7}As_{0.14}Sb_{0.86}$ single quantum well edge-emitting laser sample grown without indium on the backside of the substrate. A 4.5 mW laser output power was obtained at a wavelength of 2.49 μm with a 1 μs pulse width at room temperature. The growth of similar structures using indium solder on the substrate backside resulted in significantly degraded performance, showing the importance of this experimental factor for the epitaxial growth on a GaSb substrate.

[1]Email address: jbh14@columbia.edu

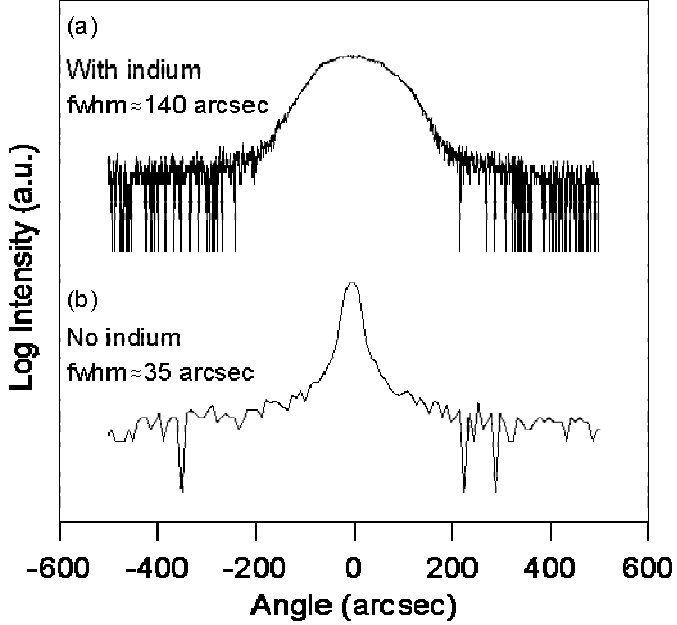

Figure 1: XRD spectra in the [400] crystal plane of GaSb bulk layers grown with (a) and without (b) indium solder on the substrate backside.

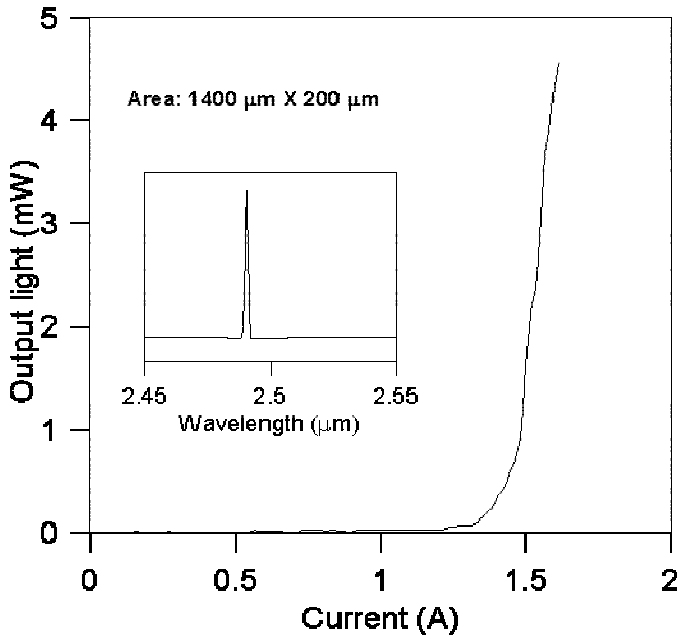

Figure 2: Light-current curve and emission spectrum of an InGaAsSb edge-emitting laser diode grown on an indium-free GaSb substrate.

Title:

"Real-time Ion Count from Nitrogen Plasma Source"

Authors:

Mark A. Wistey, Seth R. Bank, Homan B. Yuen, Lynford L. Goddard, James S. Harris

Affiliation:

Stanford University, Palo Alto, California, 94305

Contact:

Mark Wistey, 650-725-6909, wistey@snowmass.stanford.edu,
CIS, Via Ortega MC4070, Stanford CA 94305

Abstract

Dilute nitrides grown on gallium arsenide, such as GaInNAs, have dramatically extended the range of wavelengths available for uncooled, robust lasers for communications and spectroscopy. The growth of dilute nitrides by MBE generally requires the use of a plasma source in order to excite inert nitrogen molecules into more reactive species, such as nitrogen ions (N-), radicals (N2), and neutral atoms, whether excited or in the ground state. Unfortunately, ions cause significant damage to the semiconductor, particularly at the low temperatures required for dilute nitride growth.

We present a method of measuring the ion density in the plasma in real time, which allows the rapid optimization of plasma cell conditions in order to reduce ion damage. We have used this method to make several changes to our RF plasma cell, with consequent improvement in GaNAs and GaInNAsSb growth. We present photoluminescence (PL) results showing a 3-5x increase in peak PL intensity at wavelengths from 1400-1500nm (Figure 1), as well as a possible decrease in PL linewidth.

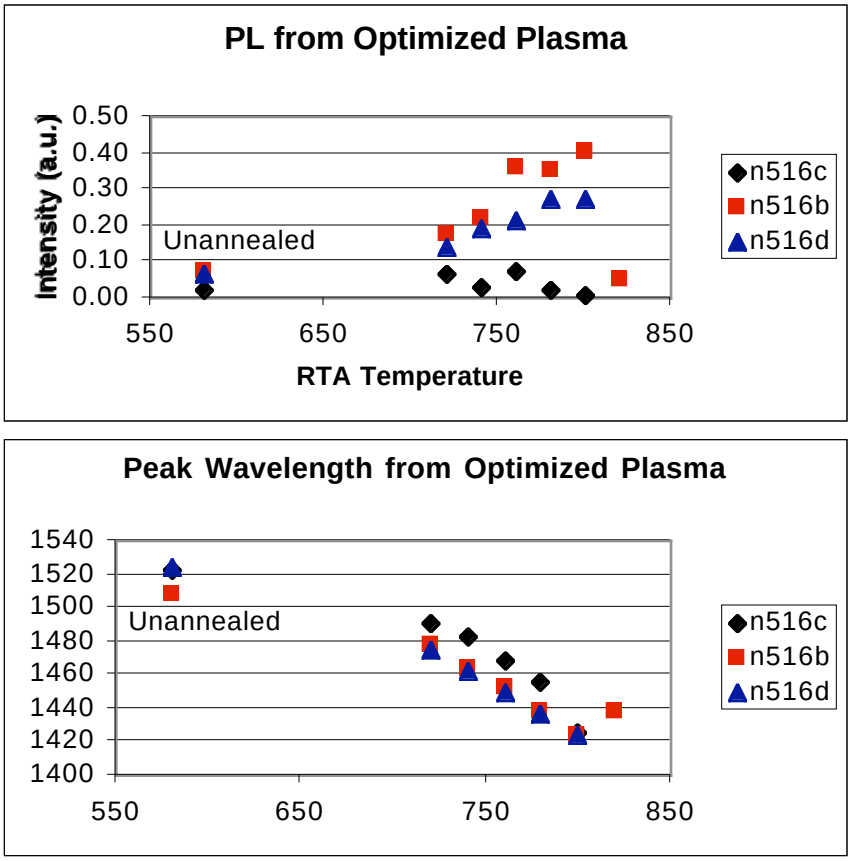

Figure 1: An optimal plasma condition greatly increases photoluminescence intensity (n516b and n516d, top), while maintaining long wavelength emission (bottom). Note that the redshift is too small to explain the improvement in PL intensity.

Regrowth of Extrinsic Contacts for High-Speed InP-based HBT Devices

V. Gambin, D. Mensa, M. Lange, A. Cavus, D. Sawdai, T. Block, A. Gutierrez-Aitken, and A.Oki
Northrop Grumman Space Technology, Redondo Beach, CA, USA
Phone: (310) 812-6251; *Fax:* (310) 813-0418; *E-mail:* vincent.gambin@ngc.com

Increased flexibility in MBE growth has recently become more important in device design, enabling more sophisticated, higher performance circuits. Techniques such as epitaxial regrowth, polycrystalline growth and growth on dielectric templates are critical elements, enhancing the overall value of state-of-the-art MBE growth technology. In current HBT designs, the parasitic capacitance of extrinsic layers ultimately limits device speed. Separating extrinsic junctions by dielectric layers while growing low-resistance polycrystalline large area contacts can dramatically improve performance by reducing capacitance and contact resistance. Furthermore, growing on templates that have been previously planarized can lead to increased circuit integration for more superscalar designs. Current processes such as self-aligned metal liftoff techniques with mesa-type structures tend to have low yields particularly at submicron dimensions. With new growth tools, these steps can be eliminated, replaced by low contact-resistance single-crystal, metamorphic, and polycrystalline layers regrown on previously processed substrates.

Among III-V materials, there are many candidates which can be used as *n* and *p* type ohmic contacts. The choice for polycrystalline contacts is more limited, restricted to the only smallest bandgap materials, such as InAs and InSb. This work primarily focuses on the development of new contact materials for InP-based electronic devices. Electrical performance, such as sheet resistance, carrier concentration, and contact resistance, is the highest priority. To ensure scalability for optical lithography, the morphology of metamorphic and polycrystalline layers was also studied. InAs doped with Si was found to have the highest performance for *n* type polycrystalline contacts. Figure 1 shows an incremental improvement of polycrystal *n* type InAs surface roughness, by optimizing growth conditions such as doping, substrate temperature and group-V overpressure. Optimal growth conditions were found to be different between both polycrystalline and metamorphic material, and *n* and *p* type material. InSb doped with Be was found to be best candidate for *p* type metamorphic and polycrystalline contacts. Figure 2 shows an SEM image of the surface of metamorphic InSb. Other techniques, such as compositionally-graded contacts, were also studied and evaluated based on morphology and electrical performance.

To separate contacts from active device layers, dielectric layers are used for electrical isolation. One refractory dielectric that was studied was SiN. Due to the difference in thermal expansion, thick SiN layers tend to fracture or delaminate during the thermal stress of MBE growth. By varying deposition conditions, several SiN films were found to survive the thermal shock during growth. The resistance to cracking from thermal stress was found to be independent of deposited film stress. Atomic force microscopy (AFM) nanoindentation was used to measure difference in thin film mechanical properties in order to predict the fracture resistance of thick SiN layers.

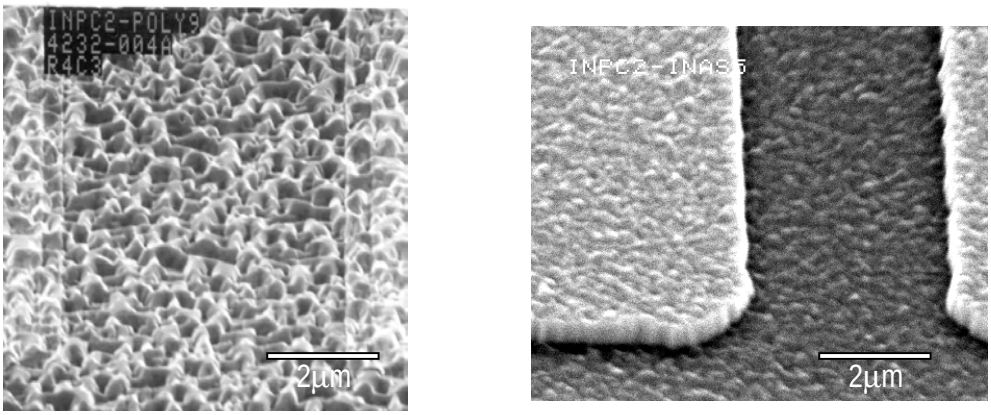

Figure 1. SEM images showing improvements which were made to *n*-type poly-InAs grown on SiN. The left sample was grown with optimized single crystal growth conditions, while the right was optimized for polycrystalline growth. Brighter contrast material is deposited metal contacts.

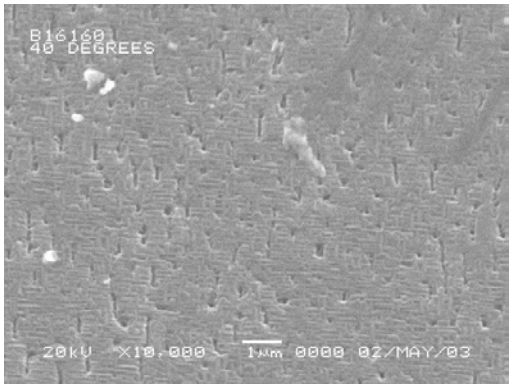

Figure 2. SEM image of surface morphology of 0.1μm *p*-type metamorphic InSb.

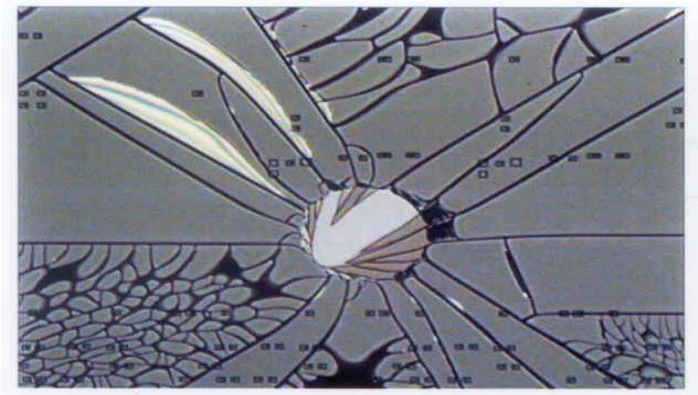

Figure 3. Optical image of a 1μm thick SiN film on InP that fractured during MBE regrowth.

Optical Properties of Very Low Temperatures Grown Compound Semiconductor by MBE

K. L. Chang, J. H. Epple, K. Y. Cheng, and K. C. Hsieh
University of Illinois at Urbana-Champaign, Micro and NanoTechnology Lab. Urbana, IL 61801

Compound semiconductors grown at very low temperatures (< 200 °C) (VLT) by molecular beam epitaxy (MBE) have been studied since 1980. Matsumoto *et. al.* have studied the electrical and optical properties of the amorphous GaAs film deposited on Si and SiO_2 extensively.[1] The refractive index and absorption coefficient of amorphous GaAs are both higher than those of single crystal GaAs, and they show a strong dependence of the film composition (Ga/As ratio). Recently, we discovered that the microstructures of VLT (~100 °C) grown compound semiconductors can be controlled between polycrystalline and amorphous by altering the group V overpressure during growth. Using this VLT-MBE growth and water vapor wet oxidation techniques, the polycrystalline (Ga,P)/amorphous (Al,As) and polycrystalline (Ga,As)/amorphous (Al,As) material systems were used to develop high reflectivity substrate-independent distributed Bragg reflectors for 0.6 and 1.55 μm vertical cavity surface emitting laser applications.[2-3] Due to the lack of crystalline structure in amorphous materials, we can apply these materials on arbitrary substrates without the generation of dislocations. For optoelectronic device applications, it is very important to understand the optical properties of these VLT-MBE grown materials.

In this study, the materials were grown by solid-source MBE at low temperatures of 100~200 °C with different group V overpressure. The atomic composition ratios of III/V were determined by Auger electron spectroscopy, and the optical transmission measurements were utilized to determine the refractive index and absorption coefficients

of the amorphous/polycrystalline compound semiconductor materials. It was found that, for an identical film thickness, polycrystalline (Ga,As) allow more light to transmit through the layer than amorphous (Ga,As) in the shorter wavelength region, as shown in Figure 1. The refractive indices are 4.04 and 3.54 for amorphous (Ga,As) (As overpressure: 1×10^{-6} torr) and polycrystalline (Ga,As) (As overpressure: 3.3×10^{-7} torr), respectively. In addition, we found that the amorphous material could recrystallize to form the polycrystalline structures under proper annealing conditions. However, it is noted that the annealed polycrystalline material may result in blocking the light transmission through the film, which might be due to the As precipitation, as shown in Figure 2.

[1] N. Matsumoto and K. Kumabe, Jap. J. Appl. Phys. Vol. 19, No. 9, 1583 (1980)

[2] G. W. Pickrell, K. L. Chang, H. C. Lin, K. C. Hsieh, and K. Y. Cheng, J. Vac. Sci. Technol. B 19(4), 1536 (2001)

[3] D. W. Wohlert, H. C. Lin, K. L. Chang, G. W. Pickrell, J. H. Epple, K. C. Hsieh, and K. Y. Cheng, Appl. Phys. Lett. Vol. 75, 1371 (1999)

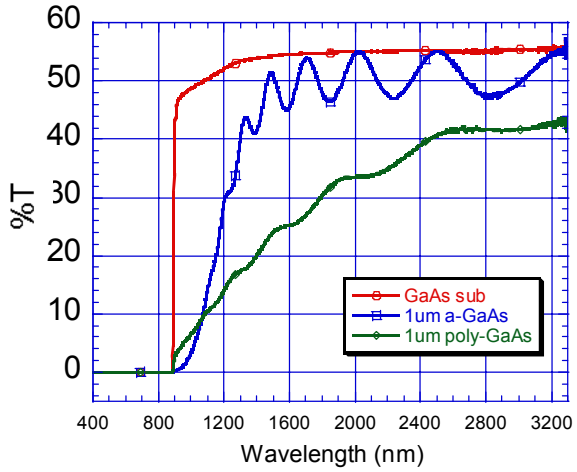

Figure 1.

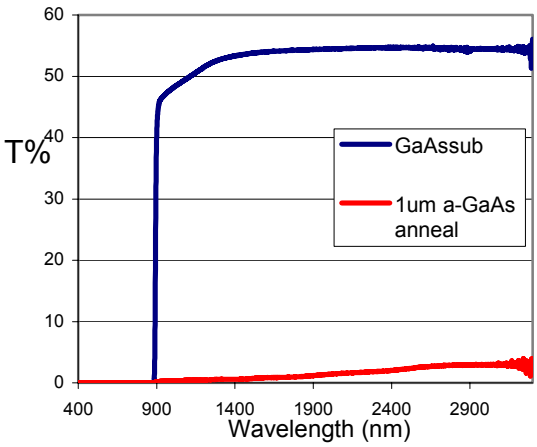

Figure 2.

NAMBE 2003 Program

Wednesday, October 1, 2003

8:00-9:40: Dilute Nitrides

Chair: James Gupta (NRC)

WA-1: Influence of the N_2 background pressure on the incorporation of Arsenic during MBE growth of GaAs
T. Dieing and B.F. Usher
La Trobe University, Australia

WA-2: The effect of hydrogen on the formation of gallium vacancies in GaInNAs
A.J. Ptak, Sarah Kurtz, R.C. Reedy, W.K. Metzger, M.H. Weber*, and K.G. Lynn*
National Renewable Energy Laboratory; *Washington State University

WA-3: Similarities between GaInNP and GaInNAs grown on GaAs (001) substrates
Y. G. Hong, A. Nishikawa, and C. W. Tu
University of California, San Diego

WA-4: Temperature dependence of optical properties of GaInNAs quantum dots grown on GaAs (001)
A. Nishikawa, Y. G. Hong, and C. W. Tu
University of California, San Diego

WA-5: 1.3 micron single lateral mode lasers based on InAs QDs and InGaAsN quantum wells
A.R.Kovsh[1,2], D.A.Livshits[1,2], N.A.Maleev[1,2], A.E.Zhukov[1], V.M.Ustinov[1],J.S.Wang[2], R.S.Hsiao[2], G.Lin[2], J.Y.Chi[2], and N.N.Ledentsov[3]
[1]Ioffe Physico-Technical Institute, Russia; [2]Industrial Technology Research Institute,Taiwan; [3]Technical University of Berlin, Germany

Influence of N_2 background pressure on the incorporation of Arsenic during MBE growth of GaAs

T. Dieing[¶] and B.F. Usher
Department of Electronic Engineering, La Trobe University, Victoria, 3086, Australia.

MBE growth of the dilute nitride III-V compound semiconductor GaAsN on GaAs(100) substrates typically uses RF or microwave plasmas as sources of nitrogen[1,2,3]. The Tectra™ nitrogen plasma source used in our MBE system uses a 2.45GHz microwave generator and an ion trap to eliminate charged species from the beam. The N_2 background pressure in the growth chamber during normal operation of the source is in the range of 1-6x10^{-5} Torr since only a small fraction of the beam emitted from the source is in the form of atomic nitrogen. While plasma sources are far from ideal, they have been used to successfully grow GaAsN of a quality suitable for the fabrication of devices such as lasers[4], photodetectors[5] and solar cells[6]. An outstanding challenge is to grow device-quality material at the higher N fractions required to create structures suitable for 1.3-1.55μm optical communications applications which to date have had weak luminescence properties[7,8].

With materials such as GaAs and AlGaAs, which are typically grown by MBE at substrate temperatures in the range 600°C to 650°C, the best material properties are generally obtained by performing the growth as close as possible to the group V stoichiometric limit, with the As_4 flux set as close as is practicable to the minimum required for a given gallium flux and substrate temperature. With GaAsN many studies have found that the optimal growth temperature is much lower, around 480°C, at which temperature the minimum Arsenic flux required is expected to be reduced due to less As_4 desorption losses. However we have found that at this temperature the minimum Arsenic flux required to maintain stoichiometric growth, although reduced, is significantly higher for GaAsN than for the growth of a GaAs layer at the same temperature. This effect could be due to the fact that GaAsN is a different material to GaAs, with a significantly different growth surface chemistry, although the nitrogen fractions we are working with are at the low level of ≅ 1% and less and so this would appear unlikely. Alternatively the effect could be due to the high N_2 background pressure in the growth chamber interfering either with the beam between source and substrate or with the growth process at the surface itself.

To investigate this effect we have firstly measured the minimum As_4 flux required to maintain stoichiometric growth of GaAs as a function of substrate temperature in the absence of significant nitrogen in the chamber. Further measurements were performed to determine the minimum As_4 pressure required in the presence of N_2 at a background level of 6x10^{-5} Torr. During these measurements the plasma was not ignited thus GaAs was grown with the only influence being the level of nitrogen in the chamber. To further investigate the role of the nitrogen another set of measurements were performed with the nitrogen shutter open, allowing a direct stream of N_2 onto the growth surface. No measurable increase in a flux gauge monitor reading, placed in the sample position, was observed when the shutter was open.

Each of the three data sets in Figure 1 show a decrease of the threshold As_4 pressure required to maintain stoichiometric growth with decreasing temperature, as expected. The As_4 pressures required in cases when a high nitrogen background was present with the nitrogen shutter closed lay systematically above the values measured without the nitrogen background. When the nitrogen shutter was opened the threshold As_4 pressures obtained lay above those obtained when the N_2 shutter had been closed. SIMS measurements indicated that no nitrogen had been incorporated into any of the grown layers. These measurements firstly indicate that a higher As_4 pressure is required for stoichiometric growth of GaAs at substrate temperatures between 400°C and 600°C in the presence of a high nitrogen background. Secondly, this effect becomes more pronounced as the substrate temperature is reduced towards 400°C. This behaviour can not be explained by interference of the nitrogen beam with the As_4 beam as it passes from source to substrate, but is explicable in terms of physisorbed nitrogen occupying surface sites which reduces the available sites for As_4. Model calculations will be presented to support these conclusions.

¶ Electronic address: t.dieing@ee.latrobe.edu.au

[1] S. G. Spruytte, C. W. Coldren, A. F. Marshall, et al., Mrs Internet Journal of Nitride Semiconductor Research **5**, W8.4 (2000)
[2] H. C. Alt, A. Y. Egorov, H. Riechert, et al., Physica B **302**, 282 (2001).
[3] S. A. Lourenco, I. F. L. Dias, L. C. Pocas, et al., Journal of Applied Physics **93**, 4475 (2003).
[4] M. Kondow, T. Kitatani, S. Nakatsuka, et al., Ieee Journal of Selected Topics in Quantum Electronics **3**, 719 (1997).
[5] G. S. Kinsey, D. W. Gotthold, A. L. Holmes, et al., Applied Physics Letters **77**, 1543 (2000).
[6] J. F. Geisz and D. J. Friedman, Semiconductor Science and Technology **17**, 769 (2002).
[7] A. R. Kovsh, J. S. Wang, L. Wei, et al., Journal of Vacuum Science & Technology B **20**, 1158 (2002).
[8] M. A. Pinault and E. Tournie, Applied Physics Letters **79**, 3404 (2001).

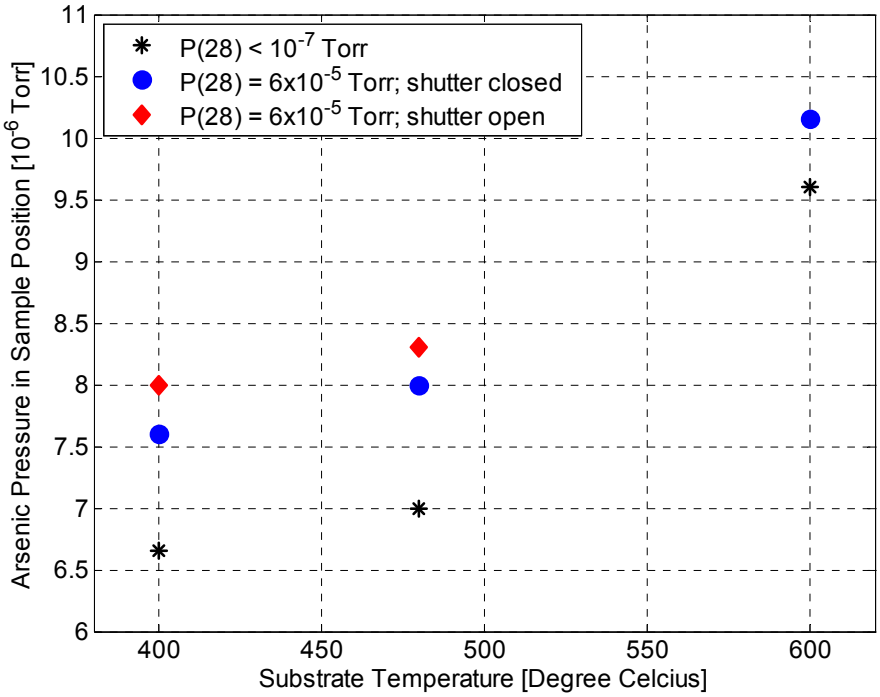

Figure1: Minimal required arsenic pressure as a function of substrate temperature for the three cases: No nitrogen (*), nitrogen partial pressure $6x10^{-5}$ Torr and shutter closed (•) and nitrogen pressure $6x10^{-5}$ Torr and shutter open (♦).

The effect of hydrogen on the formation of gallium vacancies in GaInNAs

A.J. Ptak, Sarah Kurtz, R.C. Reedy, and W.K. Metzger
National Renewable Energy Laboratory, Golden, CO 80401

M.H. Weber and K.G. Lynn
Department of Physics and Center for Materials Research, Washington State University, Pullman, WA 99164

The role of various defects in GaInNAs is only beginning to be resolved. Still, there is very little known about the chemical composition of these defects and the effects that they have on material quality. More importantly, little is known about how to reduce them. Here, we illuminate the formation of the gallium vacancy (V_{Ga}) in GaInNAs and the role that it plays in the electrical and optical properties of the material.

Recent theoretical calculations [1] indicate that gallium vacancies are much more likely to form in GaInNAs in the presence of hydrogen. In fact, the formation energy for V_{Ga} is more than 2 eV lower in GaInNAs with significant concentrations of hydrogen than in similar GaAs, increasing the expected concentration of vacancies by orders of magnitude. It was proposed, therefore, that V_{Ga} should be much more common in GaInNAs grown by metal-organic chemical vapor deposition (MOCVD) or gas-source molecular-beam epitaxy (MBE) than in solid-source MBE. We present experimental evidence that this is the case by comparing GaInNAs grown by both solid-source MBE, with and without growth under an atomic hydrogen (a-H) flux, and MOCVD.

Figure 1 compares the normalized S parameter determined from positron annihilation spectroscopy (PAS) beam measurements for three samples grown by MBE: GaAs, GaInNAs with a bandgap of approximately 1.1 eV, and GaInNAs with nominally the same bandgap grown under a flux of a-H. The S parameter is related to the concentration and type of open-volume defects in a material, preliminarily assigned here to the V_{Ga}. Only the GaInNAs sample grown under a-H shows a signal above background, indicating that the hydrogen is facilitating the formation of V_{Ga}. Figure 2 shows a similar plot of MOCVD-grown samples, including a GaAs reference, an as-grown GaInNAs sample, and a similar GaInNAs sample that has been annealed. The MBE-grown GaInNAs sample (without a-H) is included for reference. Clearly, the MOCVD-grown GaInNAs sample contains the highest concentration of V_{Ga} and annealing reduces, but does not remove, them. The difference in defects measured by positrons in the first 200 nm of the measurement is due to different passivating cap layers.

The behavior of the V_{Ga} will also be discussed, including their effect on the background hole concentration, and possible role in the reduction of the photoluminescence intensity. These results indicate that the V_{Ga} defect can be reduced or avoided by growing GaInNAs by MBE, while it may continue to pose problems for material grown by MOCVD.

[1] A. Janotti, Su-Huai Wei, S. B. Zhang, Sarah Kurtz, and C. G. Van de Walle, "Interactions between nitrogen, hydrogen, and gallium vacancies in $GaAs_{1-x}N_x$ alloys," Phys. Rev. B **67**, 161201 (2003).

Contact Author: Aaron J. Ptak
MS3212 / 1617 Cole Blvd.
Golden, CO, 80401
Phone: (303) 384-6660
Fax: (303) 384-6430
e-mail: aaron_ptak@nrel.gov

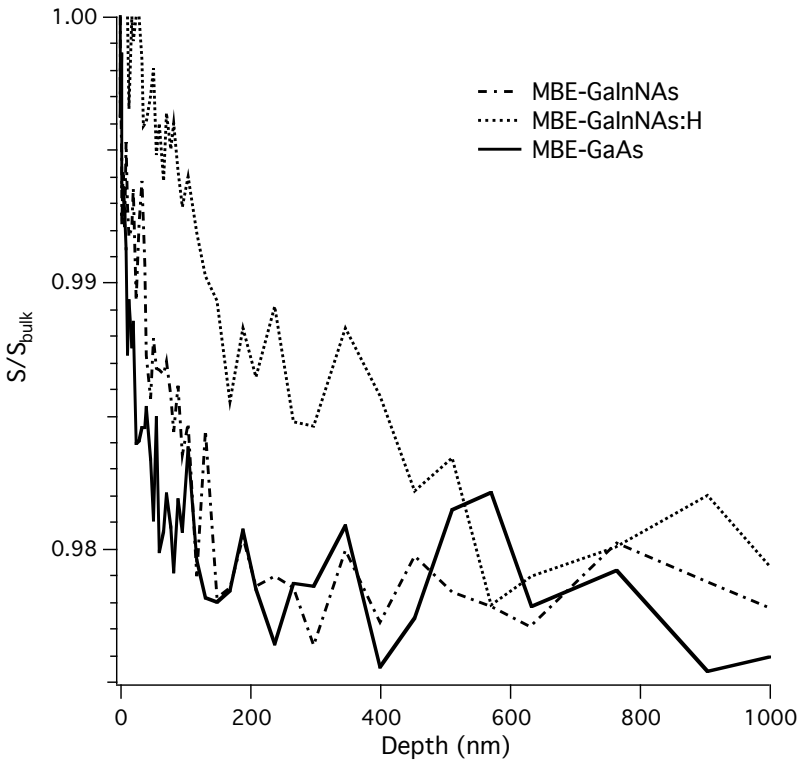

Fig. 1 A comparison of the vacancy concentrations in MBE-grown samples. Only the GaInNAs sample grown under an atomic hydrogen flux shows vacancies.

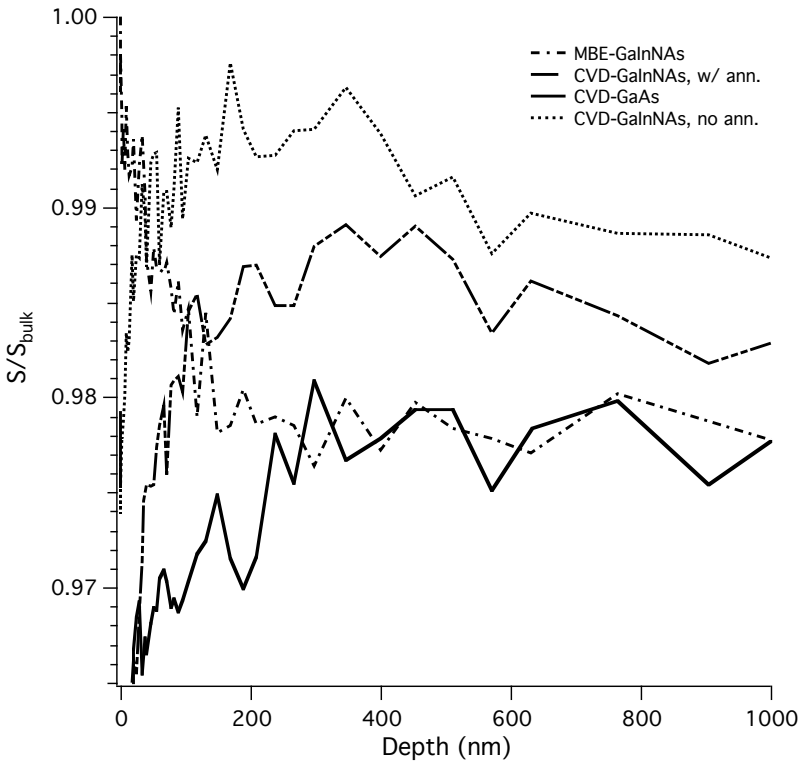

Fig. 2 A comparison of the vacancy concentrations in MOCVD-grown samples. The as-grown GaInNAs sample has the highest concentration of vacancies, with a reduction visible due to annealing.

Similarities between $Ga_{0.48}In_{0.52}N_yP_{1-y}$ and $Ga_{0.92}In_{0.08}N_yAs_{1-y}$ grown on GaAs (001) substrates

Y. G. Hong, A. Nishikawa and C. W. Tu
University of California, San Diego. La Jolla, CA 92093-0407, U.S.A.
Tel: (858) 534-3014, Fax: (858) 534-2486, E-mail: yghong@ucsd.edu

Abstract

Recently, several III –V dilute nitride alloys with their giant bandgap bowing offer an exciting possibility of increasing the flexibility in the choice of semiconductor bandgaps available. The $Ga_{1-x}In_xN_yAs_{1-y}$ alloy system has attracted much interest due to electronic and optoelectronic applications. In our previous work we find the N incorporation into $Ga_{0.48}In_{0.52}P$ reduces the bandgap, which happens mainly from lowing of the conduction band. Thus, $Ga_{0.48}In_{0.52}N_yP_{1-y}$ may be a suitable material for the emitter and collector of a heterojunction bipolar transistor (HBT), specifically, the tunnel-collector HBT. Until now there have been few reports on $Ga_{1-x}In_xN_yP_{1-y}$. The effect of N incorporation is still not fully understood. In this paper, we investigate the effect of N on the optical and electrical transport properties of $Ga_{0.48}In_{0.52}N_yP_{1-y}$ and compare it with $Ga_{0.92}In_{0.08}N_yAs_{1-y}$. The many similarities between $Ga_{0.48}In_{0.52}N_yP_{1-y}$ and $Ga_{0.92}In_{0.08}N_yAs_{1-y}$ can be explained by the intrinsic properties of N as an isoelectronic impurity.

All the $Ga_{0.48}In_{0.52}N_yP_{1-y}$ and $Ga_{0.92}In_{0.08}N_yAs_{1-y}$ samples were grown on (100) GaAs substrates by gas-source molecular beam epitaxy. Figure 1 shows low-temperature photoluminescence (PL) spectra of $Ga_{0.48}In_{0.52}N_yP_{1-y}$ and $Ga_{0.92}In_{0.08}N_yAs_{1-y.}$ The red shift of the PL peak with nitrogen incorporation indicates bandgap reduction. Low-temperature PL shows significant line shape difference between the $Ga_{0.44}In_{0.56}P$ and $Ga_{0.44}In_{0.56}N_{0.01}P_{0.99}$ sample, as shown in Fig. 1(a). The nitrogen-containing sample has an asymmetric PL line shape with a large low-energy tail, indicating the presence of localized states. Compared to $Ga_{0.92}In_{0.08}N_yAs_{1-y}$ in Fig. 1(b), similarities of the PL line shape shows that N-related localized states dominate the radiative recombination processes.

To investigate the electron transport properties of $Ga_{0.48}In_{0.52}N_yP_{1-y}$, Si-doped samples were grown with the same Si flux but different N flow rates. Hall measurements show a decreasing free electron concentration and mobility with increasing N concentration, which is similar to the $Ga_{0.92}In_{0.08}N_yAs_{1-y}$ system. In order to improve the sample quality, we rapid-thermal annealed (RTA) the samples for 10 seconds under N_2 ambient. For the $Ga_{0.48}In_{0.52}P$ sample, the free electron concentration decreases from 5.1×10^{18} to 1.1×10^{18} cm^{-3} (see Fig. 2(a)) as the RTA temperature increases to 800°C, whereas that of $Ga_{0.48}In_{0.52}N_{0.005}P_{0.995}$ decreases much faster, from 4.4×10^{18} to 8.0×10^{16} cm^{-3}. The monotonic decrease with annealing temperature of GaInNP is similar to the behavior of GaInNAs as a function of annealing temperature, as shown in Fig. 2(b). Recently, Yu *et al.* [1] proposes a model of mutual passivation between Si and N. Si is passivated by N through the formation of Si-N pairs because N is more electronegative than P (the Pauling electronegativity of N and P being 3.04 and 2.19, respectively) and, thus, has a tendency to bind the free valence electron of Si. When $Ga_{0.48}In_{0.52}N_yP_{1-y}$ is grown at a relatively low temperature (~450 °C) by MBE, Si atoms are randomly distributed in the Ga sublattice. During RTA at high temperatures, Si atoms have enough thermal energy to diffuse to be near N to form Si-N pairs. This passivation process results in a significant decrease in the electron concentration in N-containing $Ga_{0.48}In_{0.52}N_{0.005}P_{0.995}$ and $Ga_{0.92}In_{0.08}N_{0.03}As_{0.97}$.

---

[1] K.M. Yu, W. Walukiewicz, J. Wu, D.E. Mars, D.R. Chamberlin, M.A. Scarpulla, O.D. Dubon, J.F. Geisz, Nature Materials, **1**, 185 (2002)

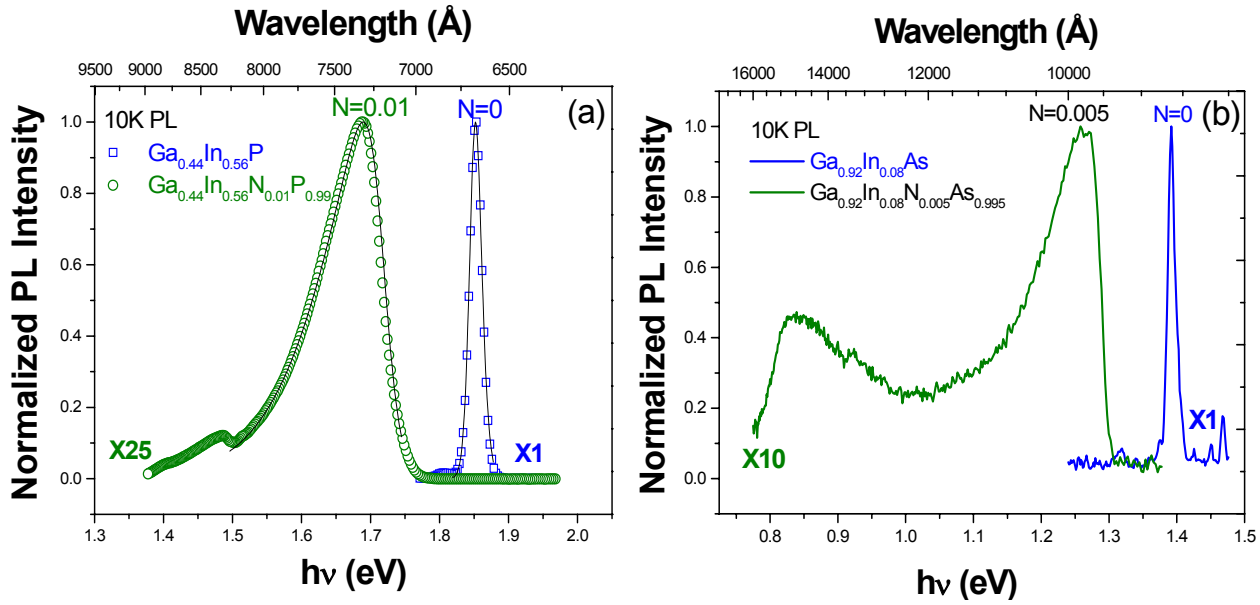

Figure 1. Nitrogen effect on 10K PL spectra of $Ga_{0.48}In_{0.52}N_yP_{1-y}$ (a), and $Ga_{0.92}In_{0.08}N_yAs_{1-y}$ (b). PL intensity is normalized.

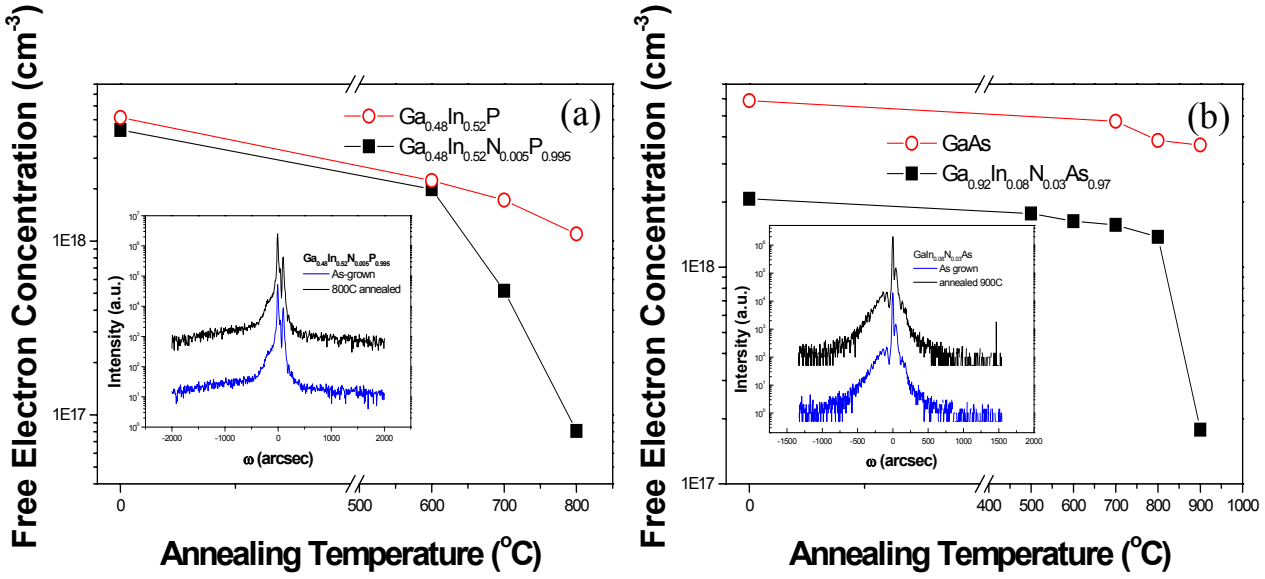

Figure 2. Free electron concentrations of Si-doped $Ga_{0.48}In_{0.52}N_yP_{1-y}$ (a), and $Ga_{0.92}In_{0.08}N_yAs_{1-y}$ (b). Results were obtained by Hall-effect measurements as function of rapid thermal annealing temperature. The inset of figure 2 (a) is X-ray result of as-grown and 800 °C annealed Si-doped $Ga_{0.48}In_{0.52}N_{0.005}P_{0.995}$, respectively. The inset of figure 2 (b) is X-ray result of as-grown and 900 °C annealed Si-doped $Ga_{0.92}In_{0.08}N_{0.03}As_{0.97}$, respectively.

Temperature Dependence of Optical Properties of $Ga_{1-x}In_xN_yAs_{1-y}$ Quantum Dots Grown on GaAs (001)

A. Nishikawa, Y. G. Hong. C. W. Tu
Dept. of Electrical and Computer Science Engineering, Univ. of California, San Diego
9500 Gilman Dr. La Jolla, California 92093-0407, USA
e-mail: anishikawa@ece.ucsd.edu

Self-assembled $Ga_{1-x}In_xN_yAs_{1-y}$ (GaInNAs) quantum dots (QDs) have attracted much attention because of the application in long-wavelength lasers and the advantages in fabricating laser structure with QDs. Reports on optical properties of GaInNAs QDs have been few so far due to the poor crystalline quality with nitrogen incorporation into GaInAs QDs. By optimizing growth condition, we have obtained $Ga_{0.3}In_{0.7}N_{0.02}As_{0.98}$ QDs with high photoluminescence (PL) intensity, comparable to that of GaInAs QDs [1]. We have observed one sharp PL peak from each GaInNAs QD sample even at room temperature (RT). In this report, we investigate the temperature dependence of the optical properties of GaInNAs QDs.

GaInNAs QD samples were grown on GaAs (001) substrates by gas-source molecular beam epitaxy (GSMBE) equipped with a rf plasma nitrogen source. Thermally cracked arsine was used as an As precursor. The nominal thickness and growth temperature of the QD layer was 4 monolayers (MLs) and 450°C, respectively. The nominal nitrogen composition was varied from 0 to 4%. Photoluminescence spectroscopy was carried out with an argon ion laser for excitation and an InGaAs photodiode for detection.

Figure 1 shows the PL spectra of GaInNAs QDs measured at 10 K and RT. One sharp peak is observed in each spectrum. With increasing nitrogen composition, the peak shifts to longer wavelength. The emission from the wetting layer or first excited state of GaInNAs QDs is not observed.

Figure 2 shows the temperature dependence of the PL peak of GaIn(N)As QDs. The curves are fitted by the Varshni equation ($E(T)=E(0)-\alpha T^2/(T+\beta)$) with reasonable values of parameters ($\alpha=4\times10^{-4}$ eV/K, $\beta=250$ K for $Ga_{0.3}In_{0.7}N_{0.02}As_{0.98}$ QDs). Since the temperature dependence of the peak shift follows the theoretical equation which assumes band-to-band transitions, we conclude the emission comes from the ground state of GaIn(N)As QDs, not from defect-related states. Therefore, the S-shaped temperature dependence that is often observed in GaInNAs/GaAs quantum wells due to localized states is not observed in the GaInNAs QDs. The full width at half maximum (FWHM) of the peak monotonically increases with increasing temperature, as shown in Fig. 3.

Figure 4 shows the integrated PL intensity as a function of inverse temperature. The activation energies derived from the slopes of the straight-line portion of the curves are 110, 63, and 53 meV for nominal nitrogen compositions of 0, 2, and 4%, respectively. With increasing nitrogen composition, the activation energy decreases. The 110 meV activation energy for GaInAs QDs corresponds to the conduction band offset minus the quantized energy level and the values of the activation energy are lower with nitrogen incorporation, and they correspond to non-radiative recombination centers in the QDs and/or at the well/barrier interfaces due to nitrogen incorporation.

[1] A. Nishikawa, Y. G. Hong, and C. W. Tu, submitted to Phys. Stat. Sol.

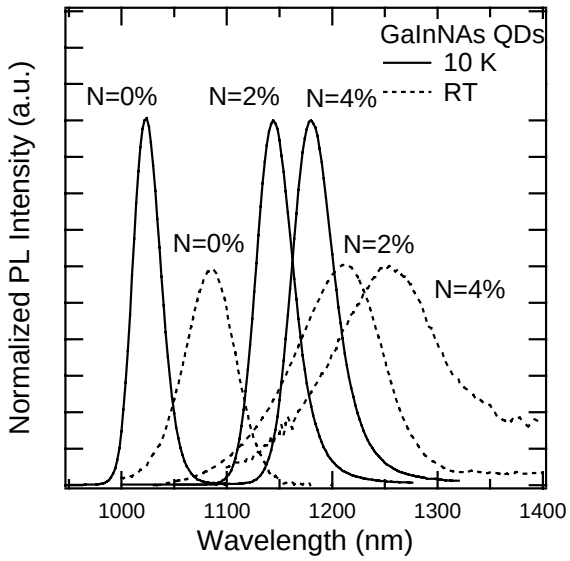

Fig. 1. PL spectra of GaInNAs QDs with different nitrogen compositions measured at 10 K and RT.

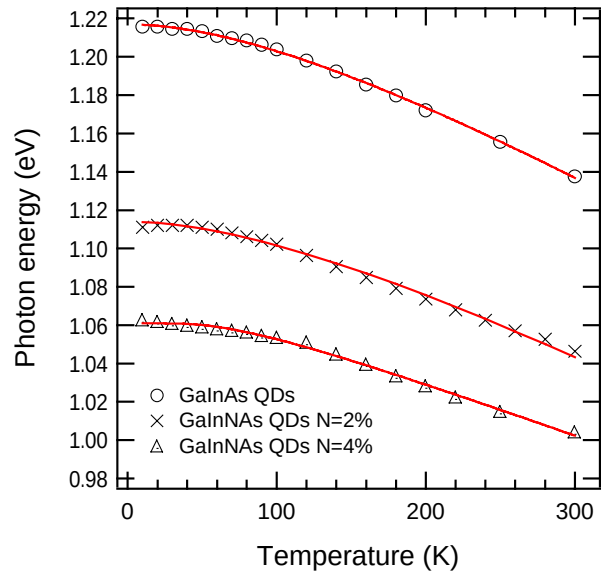

Fig. 2. Temperature dependence of the emission wavelength from GaIn(N)As QDs. The curves are fitted by the varshni equation.

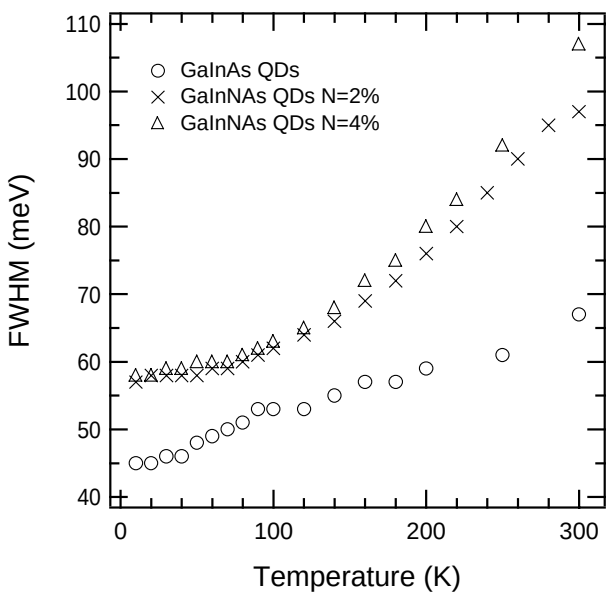

Fig. 3. Temperature dependence of the FWHM of the PL peak from GaIn(N)As QDs.

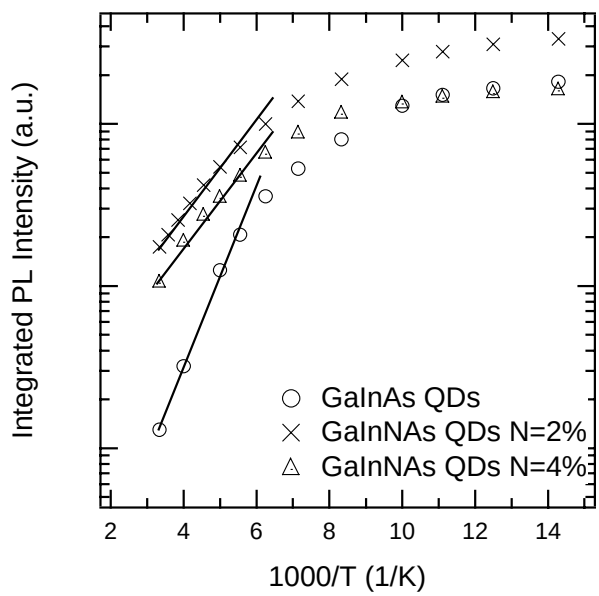

Fig. 4. Integrated PL intensity of GaIn(N)As QDs as a function of the inverse temperature. The activation energies derived from from the slopes of the straight portions of the curves are 110, 63, and 53 meV for nominal nitrogen compositions of 0, 2, and 4%, respectively.

1.3 micron single lateral mode lasers based on InAs quantum dots and InGaAsN quantum wells

A.R.Kovsh[1,2], D.A.Livshits[1,2], N.A.Maleev[1,2], A.E.Zhukov[1], V.M.Ustinov[1], J.S.Wang[2], R.S.Hsiao[2], G.Lin[2], J.Y.Chi[2], N.N.Ledentsov[3]
[1]*Ioffe Physico-Technical Institute, St. Petersburg, Russia*
[2]*Industrial Technology Research Institute, Hsinchu, Taiwan, ROC*
[3] *Technical University of Berlin, Berlin, Germany*

InAs quantum dots (QD) and InGaAsN quantum wells (QW) are promising candidates to be used as an active region of edge-emitting lasers and VCSELs emitting at 1.3 m.

In this work we present single mode Fabri-Perrot lasers fabricated based on both these approaches. Development of MBE growth, which led to significant improvement of laser characteristics (high differential efficiency, $_{dif}$>65% for both cases) will be addressed.

The active regions of QD (1.28 m) and QW (1.29 m) lasers contained several planes (2, 5 and 10) of InAs/InGaAs/GaAs QDs and single InGaAsN/GaAs QW, respectively. Ridge waveguide stripes of 3 and 5 micron width were formed by high-density-plasma dry etching. As-cleaved or coated laser bars were evaluated by standard *L-I-V* and spectrum measurement. For lasers based on InGaAsN QW both pulsed and CW driving conditions have been performed. QD lasers were measured under pulsed operation. Bonding of QD lasers is currently in the process and their CW performance will be presented at the conference.

Threshold current (I_{th}) and $_{dif}$ of QD lasers can be varied within a wide range by means of changing the number of QD planes as well as cavity length (*L*) and type of facet coatings. For example, laser diode based on 2 QD planes with L=600 m and HR/HR facets shows I_{th} as low as 1.4 mA and $_{dif}$ of 8%. To the best of our knowledge this is the lowest value of I_{th} reported for unburied laser diodes. $_{dif}$ achieves noticeable value of 19% for L=400 mm while I_{th} increases only slightly to 2 mA. In spite of extremely low threshold current the characteristic temperature (T_0) is still reasonably high and varies from 70 to 90 K. The differential quantum efficiency as high as 75% has been achieved for 1-mm long diode based on 5 QD layers with as-cleaved facet (CL/CL) (I_{th}=3.7 mA). Characteristics of such a diode are shown in Fig.1.

We found that the total output power of our ridge waveguide QD lasers is limited by current induced switching of lasing from ground state to first excited state. The physical reason of this effect is carrier accumulation on the excited state when drive current is increased.

InGaAsN/GaAs QW lasers with as-cleaved facets of 1 mm length demonstrated the following characteristics in pulsed operation: lasing wavelength was 1.285 micron at the threshold and it shifts to 1.3 micron at higher operation currents, threshold current was 20.6 mA, total slope efficiency was 0.67 W/A (69%). Characteristic temperature was found to be 110K for 10-micron wide multimode devices. Good I-V curve (series resistance as low as 4.3 and turn on voltage of 1.2 V) together with high slope efficiency ensures high output power in CW operation. Indeed, after facet coating and bonding the lasers packaged into TO46 cans demonstrated more than 200 mW CW operation limited by thermal rollover (Fig.2). Using of longer diodes (L > 1 mm) will increase the value of power. Lasers in this study were also processed into unburied deep mesa devices (etched through waveguide) of 3 micron width. Surprisingly, only insignificant worsening of laser performance (about 20%) was observed. This fact indicates that using the InGaAsN dramatically suppresses the side wall surface recombination. We believe that this effect is due to the lowered electron mobility in InGaAsN QW caused by alloy scattering.

In conclusion, we have demonstrated high-performance operation of narrow-stripe 1.3 micron lasers based on InAs/InGaAs/GaAs quantum dots and InGaAsN/GaAs quantum wells. Possible advantages and disadvantages of both approaches for high power single mode lasers will be discussed.

A.R.Kovsh, Politekniceskaya 26, 194021, St.Petersburg, Russia, ph: +78122479132, e-mail: kovsh@beam.ioffe.ru

Fig.1. RW laser based on 5 layers of QDs

L-I-V curves

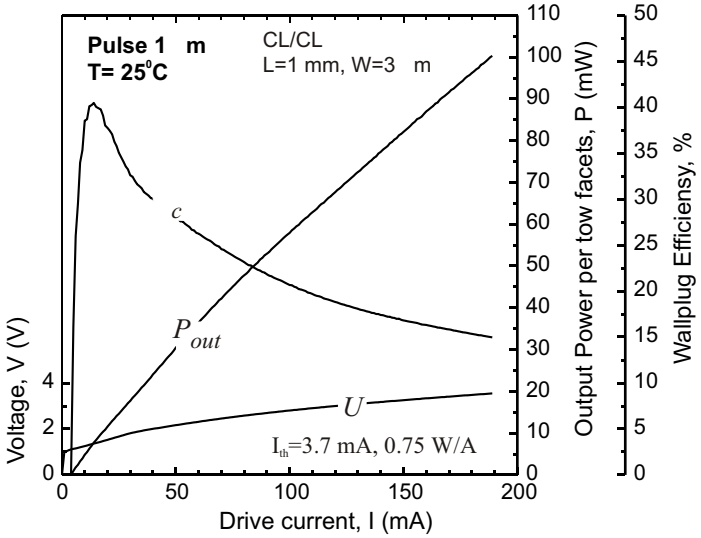

Lateral far field pattern

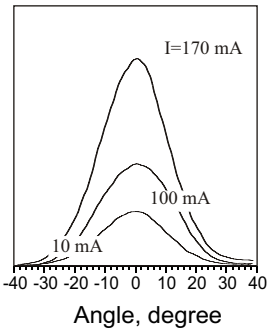

Lasing spectra

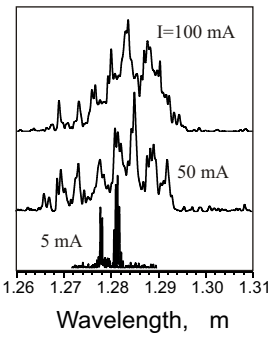

for HR/HR short diodes
(L<1 mm, W=5 m)
I_{th} =1.4-2 mA
$_{dif}$=8-19%

bonding and CW measurements are in the process

Fig.2. RW laser based on single InGaAsN/GaAs QW

L-I-V curves

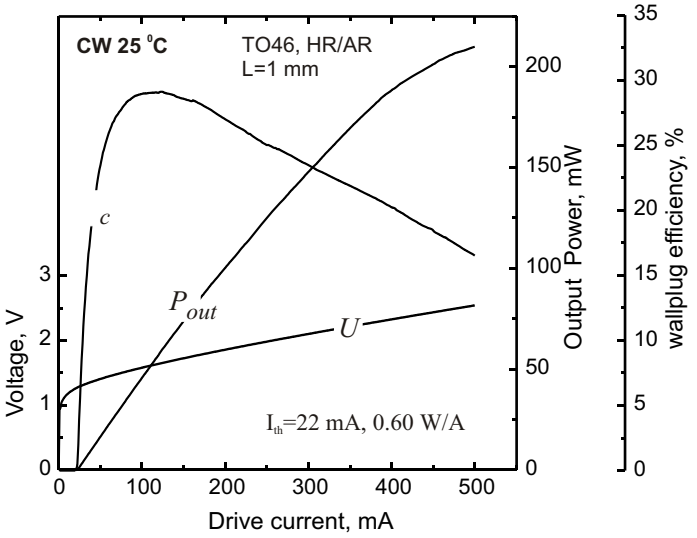

Lateral far field pattern

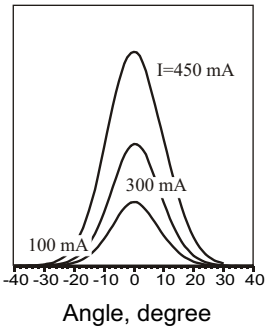

Lasing spectra

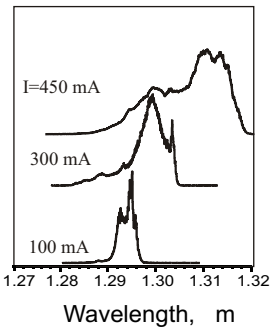

TO46

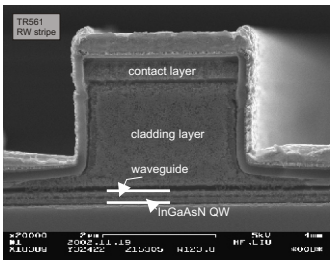

SEM image

A.R.Kovsh et al
1.3 micron single mode...

NAMBE 2003 Program

Wednesday, October 1, 2003

10:10-11:50: Devices and Device Structures I

Chair: Brian Bennett (NRL)

WB-1: High-Power Room-Temperature Continuous Operation of Molecular Beam Epitaxy grown Type-I In(Al)GaAsSb/GaSb diode lasers at 2.7 and 2.8 microns
J.G. Kim#, L. Shterengas*, R. Martinelli# G. Belenky*
#Sarnoff Corporation; *State University of New York at Stony Brook

WB-2: Correlation of Growth Conditions with Photoluminescence and Lasing Properties of Mid-IR Antimonide Type-II "W" Structures
C. L. Canedy, W. W. Bewley, C. S. Kim, M. Kim, I. Vurgaftman, and J. R. Meyer
Naval Research Laboratory

WB-3: MBE Growth of High Power 980 nm Pump Lasers Using In-situ and Ex-situ Monitoring for Production Control
W. Liu, A. Kussmaul, S. Deng, G. Yang, and S.C. Palmateer
Corning Lasertron

WB-4: MBE Growth of Quantum Cascade Lasers on GaAs (111)B Substrates for Second Harmonique Generation
X. Marcadet, V. Ortiz, J.-Y. Bengloan, M. Calligaro, Isabelle Maurin*, and Carlo Sirtori*
Thales Research & Technology, France; *Université Denis Diderot, France

WB-5: Polarization-Controlled lasing of a self-organized InGaAs quantum wire VCSEL grown on (775)B-oriented GaAs substrates by MBE
Y. Ohno[a], Y. Takasuka[b, c], M. Ogurac, K. Komori[c], S. Shimomura[a] and S. Hiyamizu[a]
[a]Osaka University, Japan; [b]Shibaura Institute of Technology, Japan; [c]National Institute of Advanced Industrial Science and Technology, Japan

High-Power Room-Temperature Continuous Operation of Molecular Beam Epitaxy grown Type-I In(Al)GaAsSb/GaSb diode lasers at λ = 2.7- and 2.8-µm

J.G. Kim#, L. Shterengas*, R. Martinelli# G. Belenky*
 # Sarnoff Corporation, 201 Washington Rd., Princeton, NJ 08543 USA
** State University of New York at Stony Brook, Stony Brook, NY 11794 USA*
e-mail: jgkim@sarnoff.com

High-power mid-infrared laser sources are required for wide range of remote gas monitoring, infrared counter-measures, LIDAR, and secure free-space communications. Room temperature (RT) continuous wave (CW) operation capability of these lasers will have significant advantages in overall system design and performance over the systems based on lasers with limited, pulsed-mode or cooling required for CW, operation. Electrically pumped GaSb-based lasers with type-I InGaAsSb quantum-well (QW) active region operating CW at RT with wavelength up to 2.7-µm were reported by our group [1]. Recently, we have improved the design of laser structures and achieved 1 W CW power at 2.5-µm [2]. Present work demonstrates that RT CW operation of type-I QW GaSb-based diode lasers can be extended up to 2.8-µm. CW output powers of 500 and 160 mW at 16 ºC were achieved from 2.7- and 2.8-µm lasers, respectively (Figure 1).

InGaAsSb/AlGaAsSb/GaSb QW structures were grown by solid source MBE. The laser active region contained two compressively strained InGaAsSb QWs. To keep the QW material composition out of the miscibility gap, the QW compressive strain is 1.2-1.6 %. To minimize optical loss, the broadened waveguide (about 830 nm total width) laser design was used. Wafers were processed into 100-µm-aperture, 2-mm-long lasers. The facets were coated (0.03/0.95), and the devices were mounted p-side down on water-cooled Cu heatsinks.

This work was supported by AFOSR, grant F496200110108.

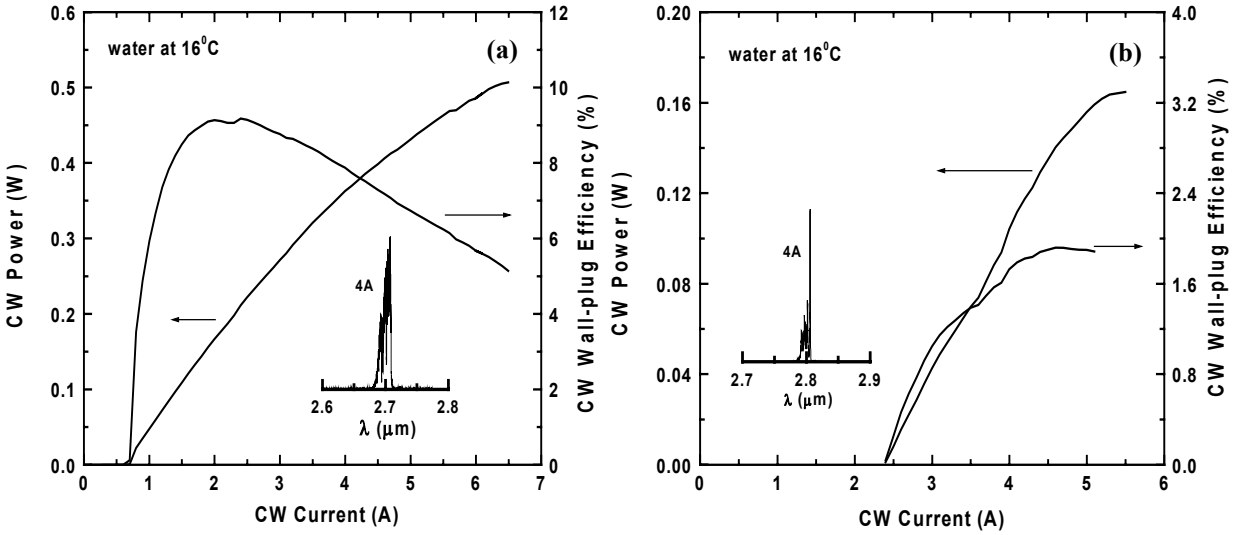

Figure 1. CW performance of 2.7-µm (a) and 2.8-µm (b) diode lasers.

1. D.Z. Garbuzov, et. al., *IEEE Photon. Tech. Lett.* **11** (1999), p. 794
2. J.G. Kim, et. al., *Appl. Phys. Lett.* **81** (2002), p. 3146

Correlation of Growth Conditions with Photoluminescence and Lasing Properties of Mid-IR Antimonide Type-II "W" Structures

C. L. Canedy, W. W. Bewley, C. S. Kim, M. Kim, I. Vurgaftman, and J. R. Meyer
Code 5613, Naval Research Laboratory, Washington, DC

"W" laser structures with four-constituent type-II active regions have displayed higher cw and pulsed operating temperatures than any other interband III-V lasers emitting at wavelengths beyond 3 μm. While the strong sensitivity of the laser performance to growth quality is quite well known, optimization of the antimonide-based systems remains an ongoing challenge, especially in complicated quantum well (QW) structures such as the "W" which incorporates three distinct material systems encompassing a wide range of optimal growth conditions. To address this issue, we have carried out a limited exploration of the correlation of critical MBE growth parameters with a variety of evaluation figures of merit based on the photoluminescence (PL) and lasing properties. A Riber 32P MBE system was used to grow "W"-test structures with identical active regions [InAs(18Å)/$Ga_{0.7}In_{0.3}Sb$(34Å)/InAs(18Å)/$AlAs_{0.106}Sb_{0.894}$(234Å), for which λ = 3.6-3.8 μm at 78 K] on GaSb substrates with lattice-matched $AlAs_{0.08}Sb_{0.92}$ digital-alloy buffer layers. Samples grown for PL measurements had 5 QWs, while laser samples had 10 QWs. In addition, the laser samples had thicker $AlAs_xSb_{1-x}$ buffer layers (2.5 μm), which served as bottom optical claddings as well as 0.5-μm-thick GaSb separate confinement layers above the active regions.

Interpretation of the results was simplified considerably by the finding that the PL intensity at 78 K correlated quite strongly with all of the other figures of merit. That is, higher PL intensity at 78 K nearly always implied higher PL intensities at 5 K and 300 K, narrower PL linewidth at 5 K (dominated by scattering and inhomogeneous broadening), narrower lasing linewidth, lower lasing threshold, and higher optical-pumping power-conversion efficiency. One surprising finding was that the optimal PL integrated intensities and linewidths were obtained for growth temperatures in the ≈ 475-500ºC range, which is considerably higher than the substrate temperatures used in most previous type-II antimonide laser growths at NRL and elsewhere. For these growths, the PL linewidth decreased from 240 nm at 78 K to 120 nm at 5 K. A comparison with the theoretical spontaneous emission spectrum at low temperatures then allows us to establish an upper bound of 5 meV for the inhomogeneous energy broadening. This may be compared with an energy difference of 30 meV that would result from a single-monolayer fluctuation of the InAs QW width. Thus whereas previous STM characterizations have clearly shown the presence of monolayer-scale steps at the QW interfaces, our results confirm that on the scale of the electron de Broglie wavelength the *average* QW width remains quite uniform, laterally as well as from QW to QW along the growth axis. The QWs were all grown with random interface bond types and preliminary results indicate that forcing InSb-like interface bonds actually degrades the lasing performance. Although the laser samples were all grown at the non-optimal lower substrate temperature, they nonetheless yielded low lasing thresholds (< 200 W/cm^2 at 78 K), long Shockley-Read lifetimes (> 20 ns at 78 K, from the threshold analysis), and low internal losses (< 5 cm^{-1} at 78 K, from a cavity-length study).

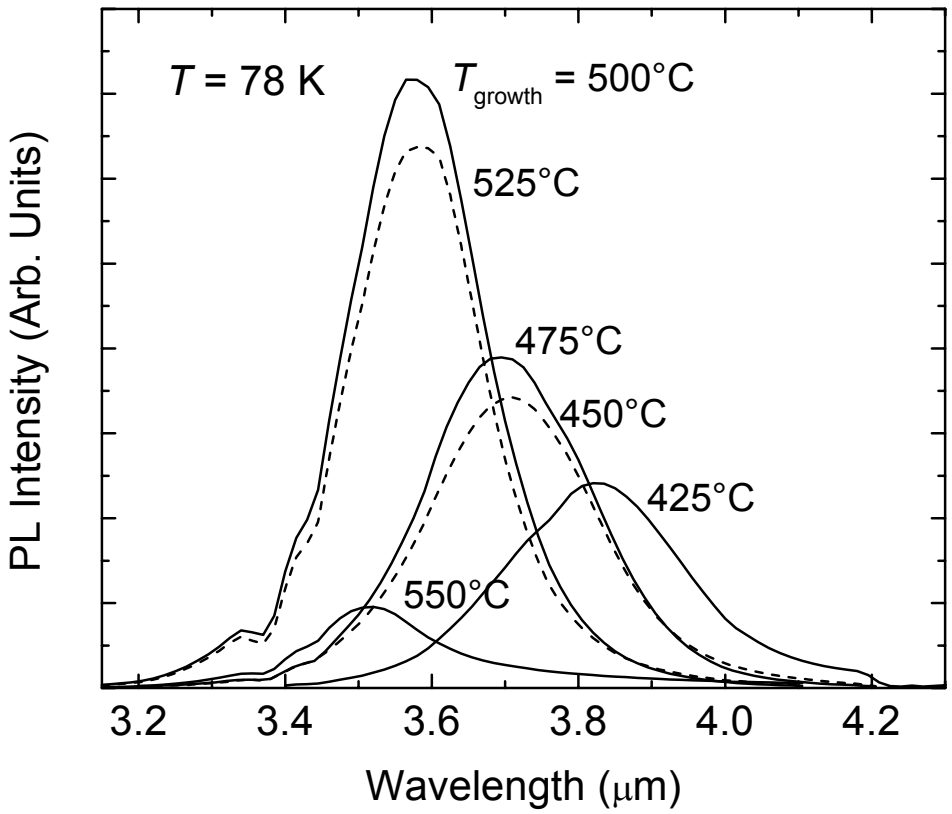

Figure 1 - PL spectra at 78 K for six "W" structures with identical 5-period active regions [InAs(18Å)/$Ga_{0.7}In_{0.3}Sb$(34Å)/InAs(18Å)/$AlAs_{0.106}Sb_{0.894}$(234Å)] and identical growth conditions, apart from the indicated substrate temperatures

Molecular Beam Epitaxial Growth of High Power 980nm Pump Lasers Using In-situ and Ex-situ Monitoring for Production Control

W. Liu, A. Kussmaul, S. Deng, G. Yang and S.C. Palmateer
Corning Lasertron, 11 Oak Park, Bedford, MA 01731

980nm-pump lasers are the key active component for amplification in telecommunication systems. Customers require high power, high stability and high reliability for the amplifier performance. We will report on the performance of molecular beam epitaxial grown high power 980nm pump lasers using in-situ and ex-situ monitoring techniques for production control. In order to meet the tight product specifications with high yields at low cost we need to control the thickness and compositions for all the epitaxial layers to less than 1%.

In-situ ellipsometry allows for real time monitoring and screening of epi-wafers to improve yields and reduce costs. Ellipsometry produces a "fingerprint" of the laser structure which is used to monitor repeatability of the growth process ie growth rate and alloy composition. Fig.1 shows a typical ellipsometry spectrum of a laser structure. Growth rate, composition and layer thickness can be checked by real-time simulation. An accuracy of 1% for the cladding layer thickness can be extracted from this monitoring along with composition and quantum well (QW) information.

We designed a growth rate-quantum well (QW)-composition indicator structure, which consists of a QW, superlattice and cladding layer, for ex-situ measurements. This structure serves two purposes: (1) it is used to verify the in-situ ellipsometry results and (2) it is used as a quick routine system calibration check. The structure was measured using high-resolution x-ray diffraction (HRXRD) and photoluminescence (PL) mapping. Fig.2 is the HRXRD data and simulation curves. The QW thickness and composition, Al composition and GaAs growth rate can be obtained from the HRXD spectra by running a fit to the curve. The data from this indicator structure verfied the growth rate and composition data obtained with ellipsometry. This unique structure gives us all the necessary information in one MBE run with an accuracy of less than 1% for thickness and composition. It dramatically improves our epi-growth efficiency, reducing costs and improving yields.

We have also developed an etching process for the full laser structure that allows us to extract more precise information for the QW position, wavelength and uniformity, and cladding layer position from HRXRD and PL. Fig. 3 shows HRXRD after etching. From the x-ray data we can extract the QW and cladding position information for the full laser structure. PL mapping performed on a post etched full laser structure ensures the lasing wavelength and uniformity are to specification. The reader is referred to reference 1 for further details on precise measurement of wavelength for pump lasers.[1]

Using well-controlled in-situ and ex-situ monitoring processes we are able to supply commercially qualified 980nm pump laser modules with powers of 500 mW for and prototype 980nm chips up to 1000mW with wavelength controlled at ±1nm. These in-situ and ex-situ monitoring techniques play an important role in the yield and performance improvement efforts to reduce costs.

References: 1."Precise Control of 980 nm Pump Lasing Wavelength," Sherry D Young, Andreas Kussmaul, Wayne Liu, S C. Palmateer, submitted to The 30th International Symposium on Compound Semiconductors, San Diego, CA, August 27, 2003.

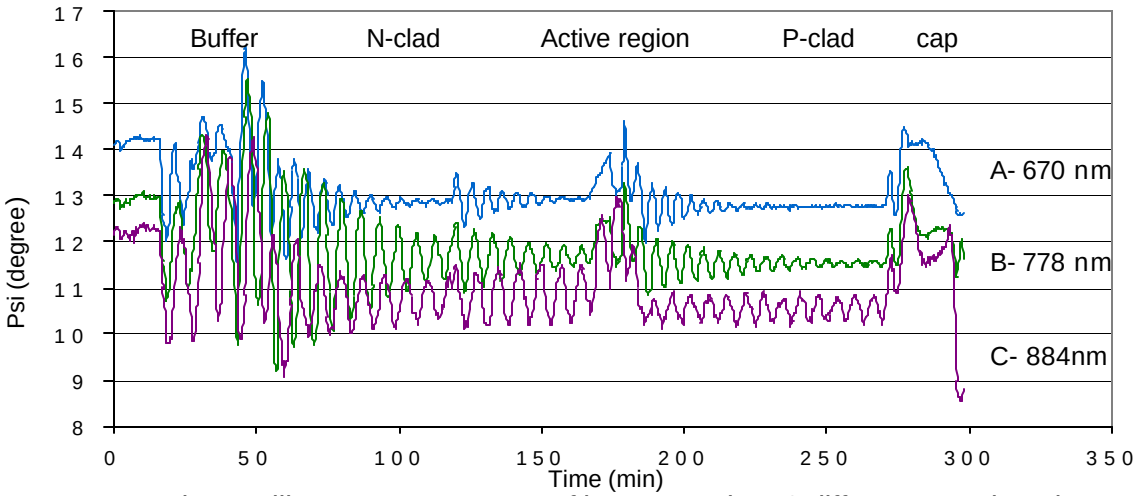

Fig. 1. Ellipsometry spectrum of laser growth at 3 different wavelengths.

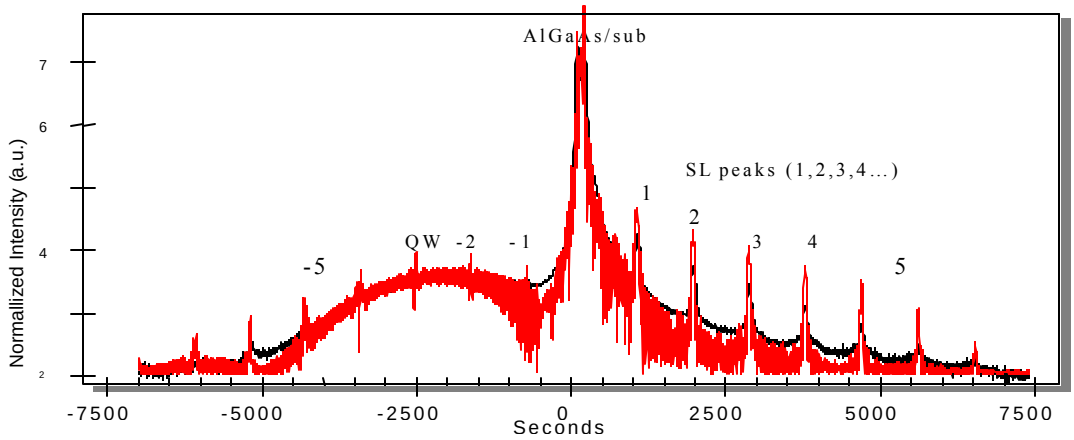

Fig.2 . HRXRD data and its simulation curve of the growth indicator structure

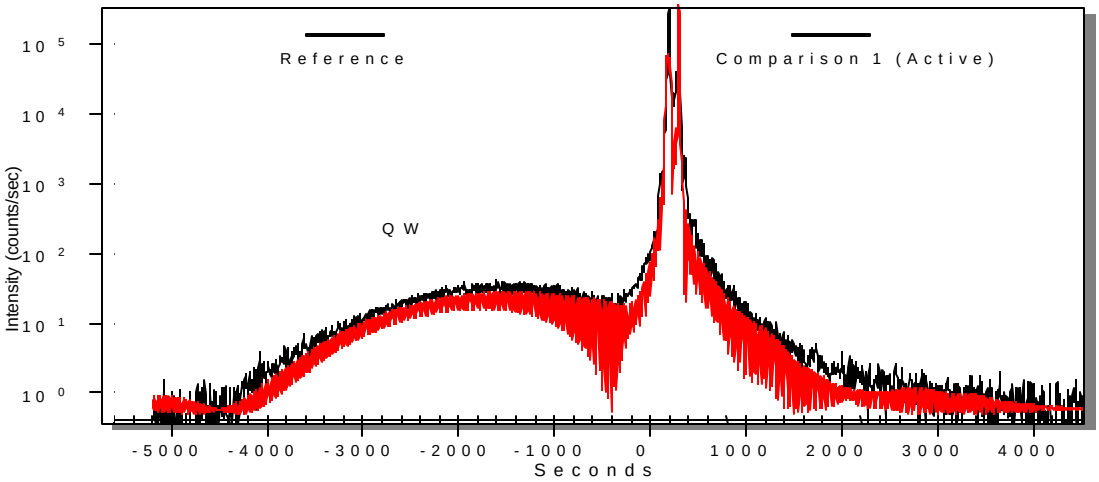

Fig. 3. HRXRD data and its simulation curve of etched full laser structure

MBE Growth of Quantum Cascade Lasers on GaAs (111)B Substrates for Second Harmonique Generation

X. Marcadet, V. Ortiz, J.-Y. Bengloan, M. Calligaro
Thales Research & Technology, Domaine de Corbeville, 91404 Orsay Cedex, France
e-mail: xavier.marcadet@thalesgroup.com, Phone: 33.1.69.33.07.18, Fax: 33.1.69.33.09.12

Isabelle Maurin, Carlo Sirtori
Matériaux et Phénomènes Quantique, Université Denis Diderot - Paris 7, Paris, France

Since the pioneering work of Cho [1], it is well known that it is difficult to obtain high quality material on GaAs (111)B substrates by MBE. Thus, most of the III-V devices have been grown and optimised on (100) oriented substrates. Some attempts have been made to take advantage of the lack of centre of symmetry of the zinc-blend structure in order to produce visible surface-emitting second-harmonic generators on GaAs (111)B substrates [2]. However, sum frequency generation within the cavity of a diode laser is a process very difficult to exploit because of the strong re-absorption of the resulting photons by the semiconductor. This is not the case for Quantum Cascade (QC) lasers where the emitted photons are well within gap and twice or three times their energy is still in the transparency region of the semiconductor. For this reason, frequency doubling in QC lasers is very attractive and can be an alternative way to access the short mid-infrared wavelength region (3–4μm), where it is known that both diode and QC lasers have poor performances. Since the QC lasers are normally TM polarised due to the intersubband selection rules, the non-linear susceptibility is zero for QC lasers grown on (100) substrates. On the contrary, the second order polarizability can be excited in QC lasers grown on (111) substrates.

In this paper, we present the preliminary work on the growth of QC laser structures on GaAs (111)B substrates. Emission of coherent light at 5.75μm wavelength has been obtained by intracavity frequency doubling by exploiting the non-linear susceptibility of bulk GaAs.

The growth conditions have been deduced from the previously described MBE growth mechanisms on vicinal GaAs (111)B surfaces [3]. Even if the growth of such a long superlattice on (111)B substrate is not yet optimised, high structural quality AlGaAs/GaAs QC lasers can be grown on (111)B GaAs as shown by the presence of high order sharp satellites in the X-rays rocking curve of fig. 1. The structure is a GaAs/$Al_{0.45}Ga_{0.55}As$ QC laser with emission wavelength at 11.5μm with an active region and waveguide similar to those described in reference [4]. In order keep low operating current the data are taken at 77K. In Fig. 2) the evidences of sum frequency generation are reported. Fig. 2a) presents the light versus current characteristic for the second harmonic generation. The maximum optical power is in the order of 1μW. The shape of the curve has a perfect quadratic dependence on the injected current. This follows from the linear behaviour of the laser light output as shown on Fig. 2b). In the insets of the figure the high resolution spectra of the pump and the generated frequency are illustrated.

References :

1) A. Y. Cho, J. Appl. Phys. **42** (1971) 2074.

2) R. J. Fisher and D. Vakhsoori, J. Vac. Sci. Technol. B 10 (2) , 986 (1991)

3) X. Marcadet, J. Olivier, J. Nagle, Appl. Surf. Sci. **123/124** (1998) 699-703

4) P. Kruck, H. Page, C. Sirtori, S.Barbieri, M. Stellmacher, and J. Nagle, Appl. Phys. Lett. **76**, 3340 (2000)

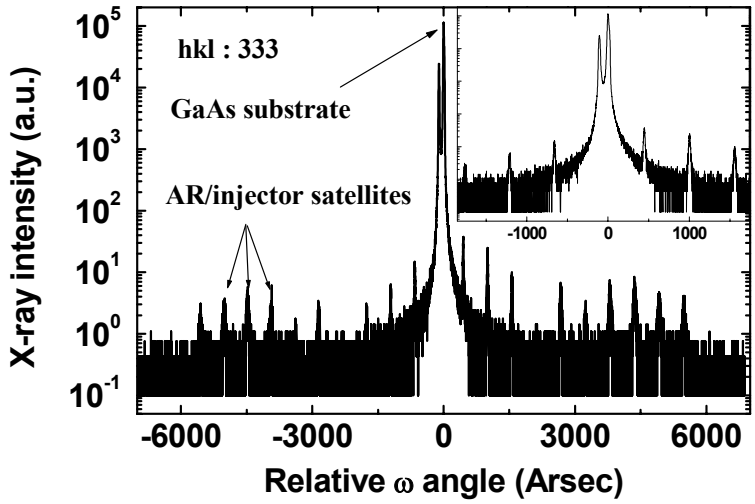

Figure 1 : High Resolution X-Ray Diffraction experimental rocking-curve in the vicinity of the symmetrical (333) GaAs reflection for a typical quantum cascade laser grown on GaAs (111)B 2° off towards (2-1-1).

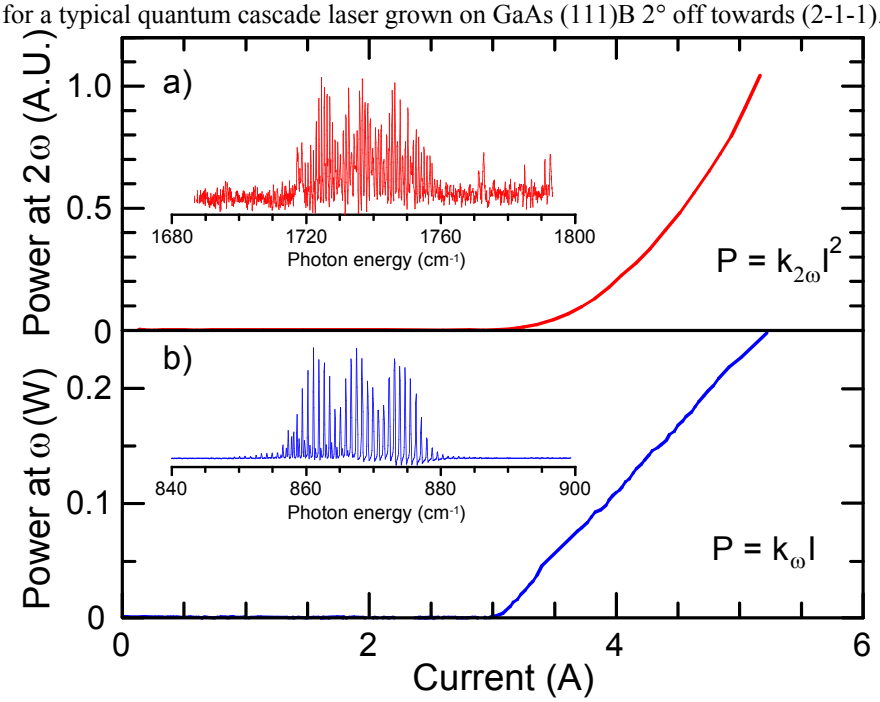

Figure 2: Light output power versus injected current for the second harmonic generation and the laser light, 2a) and 2b) respectively. In the insets: high resolution spectra at 2ω and ω.

Polarization-controlled lasing of a self-organized InGaAs quantum wire vertical cavity surface emitting lasers grown on (775)B-oriented GaAs substrates by MBE

Y. Ohno[a1], Y. Takasuka[b, c], M. Ogura[c], K. Komori[c], S. Shimomura[a] and S. Hiyamizu[a]

[a] *Graduate School of Engineering Science, Osaka University, 1-3 Machikaneyama, Toyonaka, Osaka 560-8531, Japan*

[b] *Graduate School of Engineering, Shibaura Institute of Technology, 3-9-14 Shibaura, Minato-ku, Tokyo 108-8548, Japan*

[c] *National Institute of Advanced Industrial Science and Technology, 1-1-1 Umezono, Tsukuba, Ibaragi 305-8568, Japan*

Recently, we have reported that self-organized InGaAs quantum wires (QWRs) grown on so-called (775)B-oriented [$(57\bar{7})$B plane; 8.5° off from $(11\bar{1})$B toward (011)] GaAs substrates by molecular beam epitaxy (MBE) and their laser applications. Surface of a $In_{0.1}Ga_{0.9}As$ layer grown on the (775)B GaAs substrate is regularly corrugated with a lateral period of 40 nm and a vertical amplitude of 1.5 nm as shown in Fig. 1, while that of a (775)B AlAs layer is almost flat. Because of this corrugated InGaAs/AlAs interfaces, electrons and holes are accumulated in the thick regions of a (775)B InGaAs/AlAs quantum well, which result in formation of (775)B self-organized QWRs. Semiconductor lasers with the (775)B InGaAs QWRs showed room temperature oscillation [1]. QWR lasers can take advantage of their one-dimensional characteristics if the cavity direction is perpendicular to the QWRs [2], but cleaved planes cannot be used as the Fabry-Pérot mirrors for the (775)B InGaAs QWR lasers with the cavity perpendicular to the QWRs. Hence, vertical cavity surface emitting lasers (VCSELs) are most suitable applications for the (775)B InGaAs QWR lasers because the cleaved planes are not necessary [3]. Moreover, VCSELs with a QWR active region have been expected to resolve the problem of polarization unstableness of conventional VCSELs. In this letter, we report the room temperature lasing action (wavelength of 0.83 μm) of the (775)B InGaAs QWR VCSELs and their polarization controlled lasing characteristics.

Figure 2 shows a schematic structure of the (775)B InGaAs QWR VCSEL. A bottom n-type distributed Bragg reflector (DBR) was made of 28 pairs of Si-doped $AlAs/Al_{0.15}Ga_{0.85}As$ layers, and a top p-type DBR was of 24 pairs of Be-doped $AlAs/Al_{0.15}Ga_{0.85}As$ layers. Carrier concentrations of the both DBRs was 2×10^{18} cm^{-3}. The active region consists of five $In_{0.1}Ga_{0.9}As/(GaAs)_6(AlAs)_1$ QWR layers sandwiched by Si- and Be-doped $Al_{0.15}Ga_{0.85}As$ clad layers. We optically pumped the QWR VCSEL with titanium-doped sapphire laser at room temperature (30 nsec/5 kHz). The pump light was focused on a spot size of about 20 μm-diameter of the sample surface. Figure 3 shows excited pump power dependence of emission intensity for the parallel and perpendicular to the QWRs. Clear lasing action was seen for the direction parallel to the QWRs, while no lasing could be obtained for the direction perpendicular to the QWRs. Emission spectra at pump power before lasing (A), around threshold (B) and after lasing (C) for the both directions are shown in Fig. 4. Observed lasing wavelength was around 830 nm.

References

[1] Y. Ohno et al., J. Vac. Sci. Technol. B **18** (2000) 1672.
[2] M. Asada et al., Jpn. J. Appl. Phys. **24** (1985) L95.
[3] Y. Ohno et al., Physica E **13** (2002) 892.

[1] Corresponding author. (Yasuhide OHNO)
Present address: The Institute of Scientific and Industrial Research, Osaka University, 8-1 Mihogaoka, Ibaraki, Osaka 567-0047, Japan,
E-mail: ohno@sanken.osaka-u.ac.jp, Phone: +81-6-6879-8412, Fax: +81-6-6879-8414

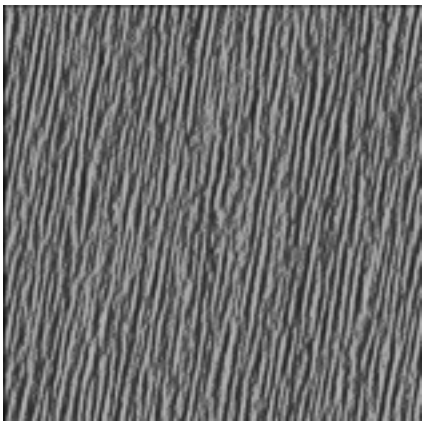

Fig. 1: AFM surface image of $In_{0.1}Ga_{0.9}As$ layer grown on (775)B GaAs substrates by MBE.

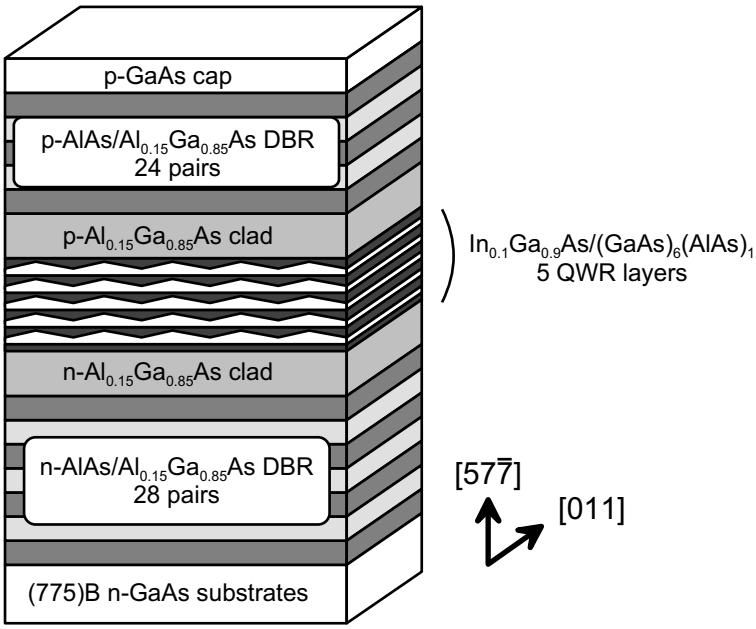

Fig. 2: Schematic illustration of a VCSEL structure with the self-organized (775)B QWRs in its active region.

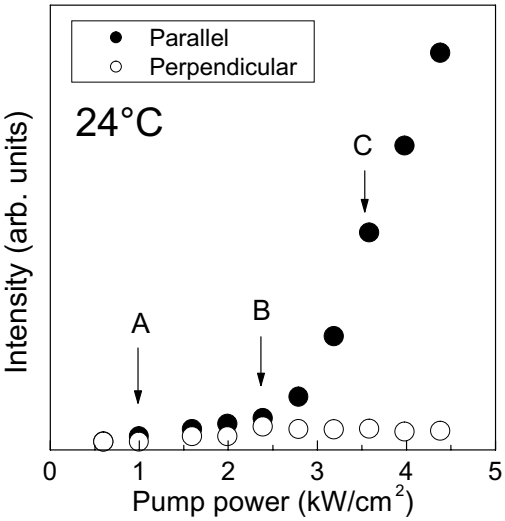

Fig. 3: Typical excited pump power versus light output intensity property of the (775)B QWR VCSEL structure. Closed (open) circles indicate intensity poralized parallel (perpendicular) to the QWRs

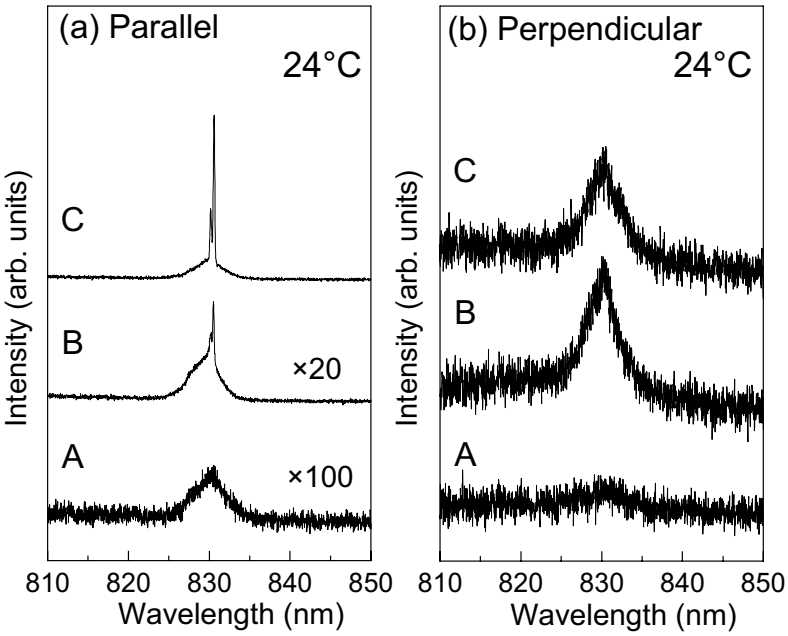

Fig. 4: Emission spectra from the (775)B QWR VCSELs for poralization parallel to the QWRs (a) and perpendicular to the QWRs (b).

NAMBE 2003 Program

Wednesday, October 1, 2003

1:30-3:10: Devices and Device Structures II

Chair: Dan Mars (Agilent)

WC-1: Comparison of As- and P-Based Metamorphic Buffers for High Performance InP HBT and HEMT Applications
D. Lubyshev, J. M. Fastenau, X.-M. Fang, Y. Wu, C. Doss, and W. K. Liu
IQE, Inc.

WC-2: Regrowth of InAlAs/InGaAs/InP DHBT Active Layers
V. Gambin, D. Mensa, M. Lange, A. Cavus, D. Sawdai, T. Block, A. Gutierrez-Aitken, and A.Oki
Northrop Grumman Space Technology

WC-3: Metamorphic 6.00 Å HBTs on InP by MBE
M. Lange, C. Monier, R. Sandhu, A. Cavus, T. Block, V. Gambin, D. Sawdai, and A. Gutierrez-Aitken
Northrop Grumman Space Technology

WC-4: Comparison AlInAs and InAsP Tunnel Barriers for Implementation in InAs-Based Bipolar Transistors
K. L. Averett[1] X. Wu[2], M. W. Koch[2], and G. W. Wicks[2]
[1]Air Force Research Laboratory; [2]University of Rochester

WC-5: MBE Growth of AlGaPSb/InP DBRs on InP
J. F. Klem[1], D. K. Serkland[1], J. Kim[2], and T.- Y. Wang[2]
[1]Sandia National Laboratories; [2]Honeywell International

End of Main Conference

Submitted for presentation at the 21st NAMBE Conference (Sept 29–Oct 2, 2003, Keystone, CO).

Comparison of As- and P-Based Metamorphic Buffers for High Performance InP HBT and HEMT Applications

D. Lubyshev, J. M. Fastenau, X.-M. Fang, Y. Wu, C. Doss and W. K. Liu*
IQE, Inc., Bethlehem, PA 18015, USA.
** Email:aliu@iqep.com, Tel: (610) 332-3220, Fax: (610) 332-7730*

Through the use of a metamorphic buffer layer, the high speed performance of InP-based devices becomes available on the more mature GaAs substrates. One challenge for cost effective volume manufacturing has been the InP substrates, which are more expensive, brittle, and only now reaching 6-inch diameters. A variety of metamorphic buffers (M-buffers) have been employed [1, 2], and a graded InGaAlAs M-buffer is currently used in production of M-HEMT circuits which have passed full reliability testing [2]. As circuit density and speeds increase, the need to dissipate heat from the device circuits will become more important. This paper compares the structural, thermal, and electrical properties of M-HBTs and M-HEMTs grown with M-buffers consisting of In(Ga)AlAs, In(Ga)AlP, and InP alloys.

The growths for this work were performed in a single-wafer Varian GEN II reactor and in a multi-wafer Thermo-VG V-100 MBE system. The metamorphic and the baseline lattice-matched (LM) structures were grown on 3-, 4- and 6-inch diameter GaAs and InP substrates, respectively. The structural properties were evaluated using optical microscope, AFM, HRXRD, room-temperature PL, and TEM. The surface morphology of the graded M-buffers show a cross-hatched pattern, while the bulk InP M-buffer has a more random surface roughness (Figure 1). We attribute this to the difference in strain relaxation mechanisms [3]. We will discuss the mechanisms in detail, as well as the effect of growth conditions on surface morphology and device characteristics. Strain-related non-uniformity on large-diameter growth will also be discussed. The thermal characteristics of the various M-buffers and M-HBTs were studied using Scanning Thermal Microscopy and Single-Substrate-Temperature techniques [4,5]. The thermal resistance of a M-HBT grown on the InP M-buffer (275°C/W) is orders of magnitude lower than the same M-HBT grown on In(Ga)AlAs M-buffers.

Hall measurements and large-area device testing were used to evaluate and compare the quality of the M-HBT and M-HEMT epiwafers. The M-HBTs have similar properties to baseline LM-HBT structures grown on InP substrates, although those grown on the InP M-buffers tend to show more degradation in gain and breakdown. Room temperature Hall measurements on the baseline LM-HEMTs showed a channel charge of 3e12 cm^{-2} with a mobility of 10,000 cm^2/Vs. M-HEMTs grown on the InAlAs M-buffer have slightly higher charge and similar mobility values. To our knowledge, no data has been published concerning M-HEMT growth using the InP M-buffer. We report experimental results on the optimization of this M-HEMT growth. The channel transport and device properties are very sensitive to the growth conditions of the InP M-buffer, and current leakage through the binary buffer is a concern. However, there is no clear correlation between surface roughness and large-area DC characteristics for either M-HEMTs or M-HBTs grown on the InP M-buffer.

[1] D. Lubyshev, et al, J. Vac. Sci. Technol **B19**, 1510 (2001).
[2] R. E. Leoni III, et al, Digest of Papers, 2002 Intl. Conf. on Compound Semiconductor Manufacturing Technology, pp. 272–275, April 2002.
[3] E. Lefebvre, et al, 15th Indium Phosphide and Related Materials Conference, Santa Barbara, CA, May 2003.
[4] Y. M. Kim, et al, IEEE Electron Device Letters **23**, 297 (2002).
[5] X.-M. Fang, et al, CS-MAX 2002 Technical Digest, pp 57 –58, November 2002.

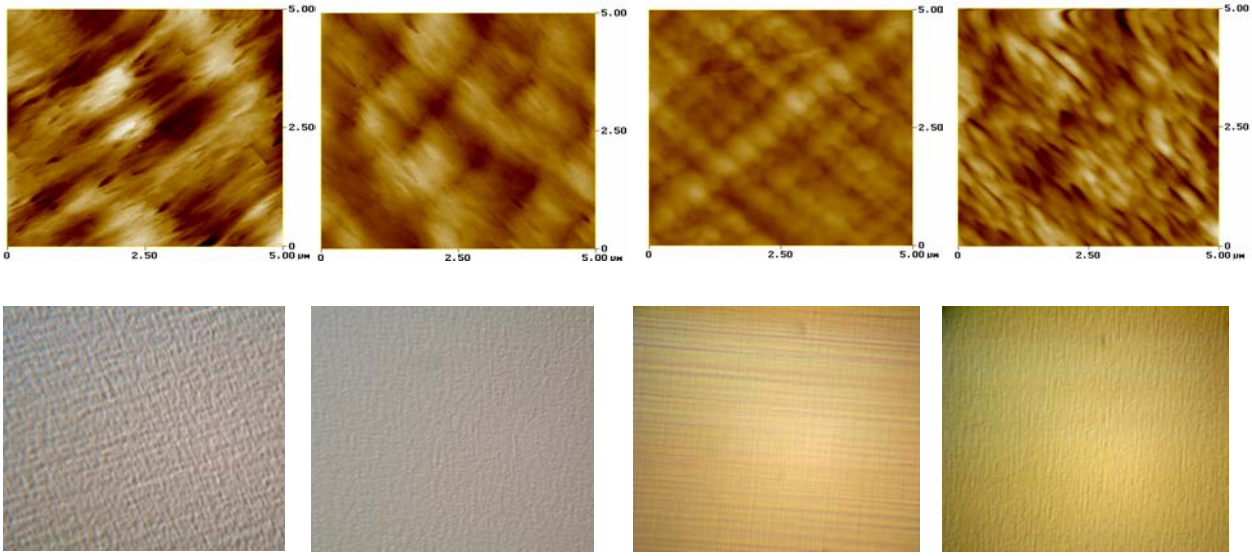

(a) (b) (c) (d)

Figure 1. AFM (top) and optical microscope (bottom) surface morphology of M-HBTs (a, b) and M-HEMTs (c, d) grown using a graded InAlAs M-buffer (a, c) and using a bulk InP M-buffer (b, d).

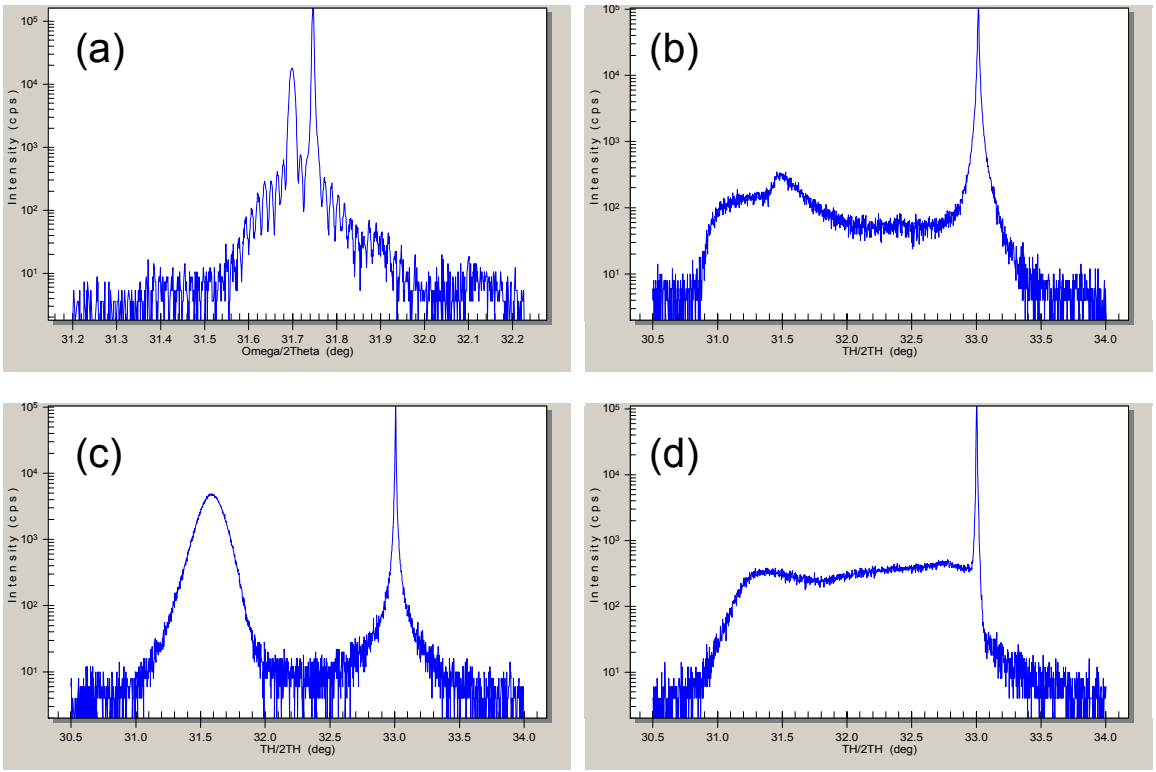

Figure 2. HRXRD scans of (a) baseline LM-HEMT and M-HEMTs with (b) InAlAs, (c) InP and (d) InGaP M-buffers.

Regrowth of InAlAs/InGaAs/InP DHBT Active Layers

V. Gambin, D. Mensa, M. Lange, A. Cavus, D. Sawdai, T. Block, A. Gutierrez-Aitken, and A.Oki
Northrop Grumman Space Technology, Redondo Beach, CA, USA
Phone: (310) 812-6129; *Fax:* (310) 813-0418; *E-mail:* vincent.gambin@ngc.com

A major factor limiting f_τ in traditional mesa-type HBT devices is the parasitic capacitance of the intrinsic junctions and extrinsic contact layers. To increase speed, the development of new fabrication technology is necessary to reduce capacitive effects inherent in current single-growth epitaxy. Furthermore, to increase circuit integration and improve yields, a new planar process is critical to overcome the shortcomings of the traditional mesa-type structures and lift-off processes. In future device designs, selective epitaxial regrowth techniques will be valuable tools to help minimize parasitic capacitances while maintaining low contact resistances. This technology has been widely developed in SiGe processing[1] and has been explored in III-V materials[2], but has yet to reach full maturity. The InP system offers distinct advantages over Si and other III-V's due to a higher peak and saturation velocity, higher electron mobility, reduced inter-valley scattering, along with flexible bandgap and band-alignment engineering capabilities.

A new process has been proposed to reduce junction capacitances and create a more planar device using multiple epitaxial regrowth steps. In this process, extrinsic junctions are replaced by dielectrics while maintaining large contact areas for device layers. In the initial epitaxial growth, the subcollector and collector are first grown. SiN is then deposited, patterned, and planarized to isolate the extrinsic base contacts from the collector. The top of collector and the entire base is then regrown, avoiding a regrowth interface directly at the collector-base heterojunction. The wafer is patterned a second time with SiN to isolate the extrinsic emitter from the base. The top of the base and emitter is regrown by MBE. In this second regrowth step, the emitter is regrown in a submicron opening to reduce the emitter-base capacitance. The overall layer structure is shown in Figure 1 with the two regrowth interfaces highlighted. While significantly higher device speeds can be expected with this approach, the challenges are significant. Two issues immediately faced are reducing contamination at the regrowth interface and growing smooth single-crystal and polycrystalline material on submicron patterned substrates.

In this talk, both planar regrowth and regrowth in lithographically defined submicron openings are explored. Material was characterized by atomic force microscopy (AFM) to measure the surface morphology of regrown layers. To optimize the regrowth interface, secondary ion mass spectrometry (SIMS) was used to measure impurities adversely affecting device performance. The crystal quality of regrown material, and the continuity between polycrystalline material grown on the dielectric and the single-crystal material was imaged by transmission electron microscopy (TEM). Figure 1 shows a cross-section TEM image of a regrown emitter in a submicron SiN opening. Due to faceting of the regrown crystal and shadowing of the deposited material by the SiN sidewalls, good continuity between polycrystalline and epitaxial material was difficult to achieve. Finally, the performance of fabricated devices was used to compare regrowth with single-growth epitaxy.

---

1. S.J. Jeng, *et al.*, IEEE EDL 22, 542 (2001).
2. D. Scott, *et al.*, 60th DRC, June 24-26 (2002).

n+ InGaAs Contact
n- InAlAs Emitter
p+ InGaAs Base
n- InP Collector
n+ InP Subcollector
SI InP Substrate

Figure 1. The HBT layer profile. The dashed lines indicate the regrown interfaces.

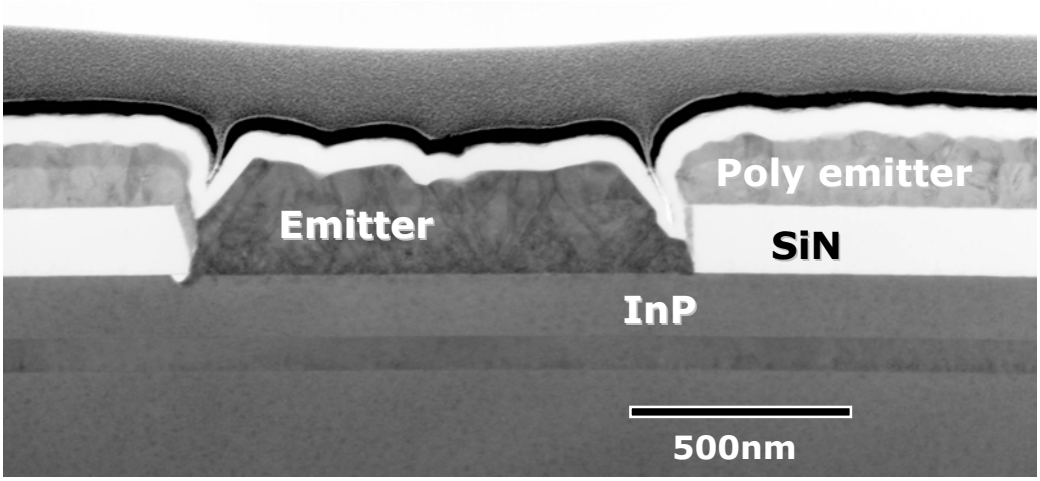

Figure 2. Cross-section TEM image of a regrown emitter in a SiN defined opening.

Metamorphic 6.00 Å HBTs on InP by MBE

M. Lange*, C. Monier, R. Sandhu, A. Cavus, T. Block, V. Gambin, D. Sawdai, and A. Gutierrez-Aitken
Northrop Grumman Space Technology, One Space Park, Redondo Beach, CA 90278, USA

Abstract:

Narrow band-gap semiconductors offer many advantages for very high frequency device and circuit operation. Heterojunction bipolar transistors (HBT) benefit from the superior transport characteristics of these materials as well as the lower power consumption enabled by the small band-gaps. This can be accomplished in InGaAs on InP HBTs by increasing the indium concentration, provided that the corresponding increase in lattice parameter is accommodated. One method for accommodating the increased lattice parameter is to use a metamorphic buffer to grade the lattice parameter from the substrate to the desired lattice constant.[1] In this work, metamorphic graded buffers were used to create 6.00 Å lattice parameter material and then grow single- and double-heterojunction bipolar transistors (SHBT and DHBT) by solid-source MBE. Graded InAlAs buffers were grown on the InP substrate, graded in composition from InP lattice-matched $In_{0.52}Al_{0.48}As$ at 5.87 Å to $In_{0.86}Al_{0.14}As$ at 6.00 Å. The In composition grade rate was 4% per 1000 Å. Once the final InAlAs composition was reached, the buffer was finished with 3000 Å or more of additional material of that composition. The graded buffer layer shown in Figure 1 exhibits the cross-hatched morphology associated with the strain relaxation process. The strain relaxation and density of threading dislocations reaching the surface were investigated and will be presented separately.

Using the above approach, $In_{0.86}Ga_{0.14}As/In_{0.86}Al_{0.14}As$ SHBT and DHBT device layers were grown, and small (1.5x10 μm^2) transistors were fabricated. All devices exhibited significantly lower operating and knee voltages compared to GaAs and lattice-matched InGaAs on InP technologies, as can be seen in Figure 2. The 6.00 Å SHBT demonstrated a $V_{BE} \sim 0.4$ V for operation at 1 mA compared to 0.7 V for lattice-matched InGaAs on InP and 1.3 V for GaAs. The 6.00 Å HBT approach additionally benefits from a favorable valence band alignment between the *p*-type $In_{0.86}Ga_{0.14}As$ base and the *n*-type $In_{0.86}Al_{0.14}As$ emitter (Figure 3), which reduces hole injection into the emitter and increases device current gain. RF measurements of this structure exhibited f_T of 105 GHz. The DHBT profile increased the breakdown voltage BV_{CE0} a factor of 3x over the SHBT to 7 V, as shown in Figure 4. This will allow further vertical scaling of the device to reduce collector transit time.

1. W.E. Hoke, P.J. Lemonias, T.D. Kennedy, A. Torabi, E.K. Tong, R.J. Bourgqu, J.-H Jang, G. Cueva, D.C. Dumka, I. Adesida, K.L. Chang, and K.C. Hsieh, J. Vac. Sci. Technol. B **19**, 1505 (2001).

*Corresponding author: mike.lange@ngc.com, phone (310) 812-5241, fax (310) 812-4378.

This work is supported by ONR Contract No. N00014-01-2-0014, DARPA ABCS program.

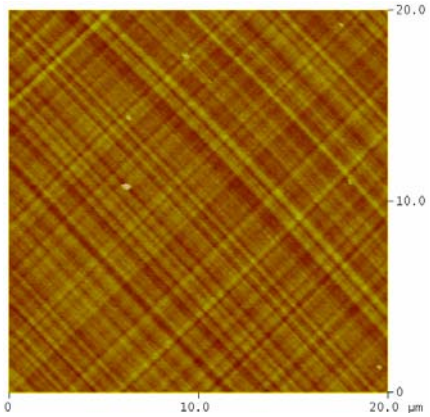

Fig. 1. Typical cross-hatch surface morphology of a 1.5 µm thick InAlAs graded buffer layer on GaAs, 5 nm RMS. The lattice parameter at the surface is 6.00 Å.

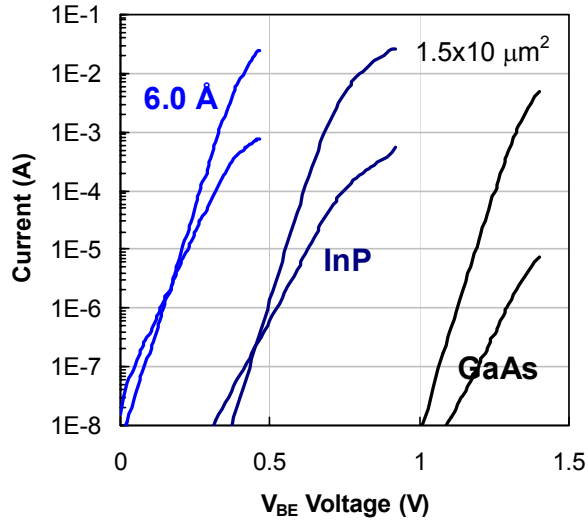

Fig. 2. Gummel plots for InP, InGaAs lattice matched on InAlAs and GaAs.

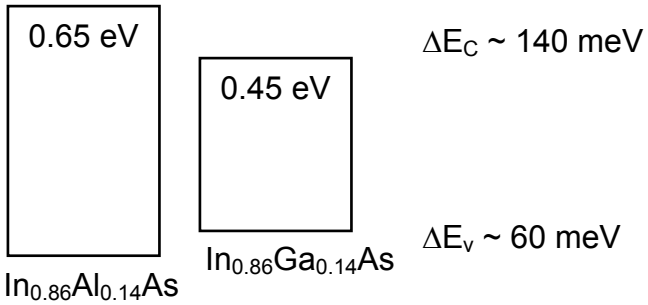

Fig. 3. Schematic of the 6.00Å InAlAs/InGaAs band alignment

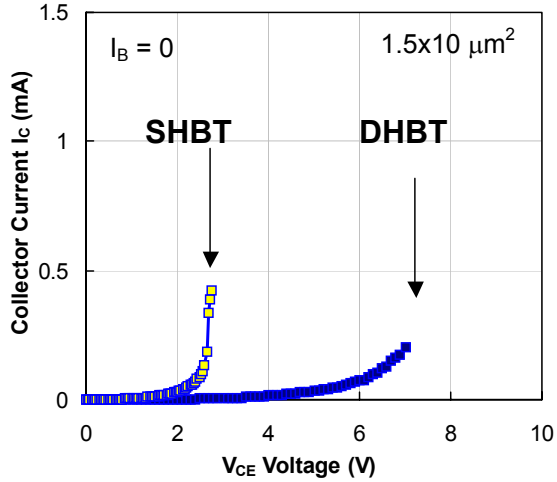

Fig. 4. Breakdown voltage comparison between SH

This work is supported by ONR Contract No. N00014-01-2-0014, DARPA ABCS program.

Comparison AlInAs and InAsP Tunnel Barriers for Implementation in InAs-Based Bipolar Transistors

K. L. Averett,[1] X. Wu,[2] M. W. Koch,[3] G. W. Wicks[3]

[1]*Air Force Research Laboratory, Materials and Manufacturing Technology Directorate, Wright-Patterson AFB, OH 45433*

[2]*Department of Physics and Astronomy, University of Rochester, Rochester NY 14627*

[3]*The Institute of Optics, University of Rochester, Rochester NY 14627*

The large electron mobility, and saturation velocity, associated with InAs has motivated an investigation of this material for future high speed bipolar transistors. Conventional heterojunction bipolar transistors designs in InAs-based materials are not possible, since no wide-bandgap material exists, which forms a stable, type-I heterojunction, of good quality, and lattice-matched to InAs. An alternative approach has been investigated: the tunneling emitter bipolar transistor (TEBT) in InAs-based materials. This design[1] employs a tunnel barrier at the emitter-base junction, which selectively passes electrons but inhibits hole transport, thereby enhancing the current gain of npn transistors.

A comparison of tunnel barriers of different materials and thicknesses has been performed to investigate the quality of the tunnel barrier, along with its usefulness in an InAs-based TEBT device. The present work shows comparisons of band offsets, calculated by strained bandgap theory[5], and interface quality, shown through high resolution x-ray diffraction (HRXRD). Barrier materials investigated include AlInAs, and $InAs_yP_{1-y}$, which were grown by solid source molecular beam epitaxy (MBE). Test structures were grown for interface studies, and the full transistor structure for examination of current gain vs. barrier thickness.

Non-optimal InAsP barriers, as well as all AlInAs barriers, were found degrade the current gain of TEBTs with respect to simple InAs bipolar junction transistors. However correctly optimized InAsP barriers enhance the current gain. This observation is consistent with the expected larger valence band offset of InAsP/InAs relative to that of AlInAs/InAs.

Interference fringes in the x-ray diffraction of test barriers suggest that interface roughness is worse in InAsP/InAs barriers than in AlInAs/InAs barriers. Future efforts to improve MBE growth to produce smoother interfaces should result in further improvements in current gain of InAsP/InAs TEBTs.

This work was supported by DARPA (J. Shah), ONR (C.E.C. Wood), NSF and AFRL/MLPS.

Email: kent.averett@wpafb.af.mil

References:

(1) J. Xu, M. Shur, "A Tunneling Emitter Bipolar Transistor", IEEE Electron Device Letters, **7**, 416-8 (1986).
F.E.Najjar, D.C.Radulescu, Y.K.Chen, G.W.Wicks, P.J.Tasker and L.F.Eastman "DC Characterization of the AlGaAs/GaAs Tunneling Emitter Bipolar Transistor", ,Appl.Phys.Lett. **50**, 1915 (1987).

(2) C.G. Van de Walle, R.M. Martin, "Theoretical Study of Band Offsets at Semiconductor Surfaces", Physical Review B, **35**, 8154-65 (1987).

MBE Growth of AlGaPSb/InP Distributed Bragg Reflectors on InP

J. F. Klem and D. K. Serkland
Sandia National Laboratories
Albuquerque, NM 87185
Tel: 505-845-8225 email: jklem@sandia.gov

J. Kim and T.- Y. Wang
Honeywell International
Minneapolis, MN 55418

Distributed Bragg reflectors (DBRs) intended for vertical cavity optoelectronic devices should ideally be composed of materials with high refractive index contrast, high thermal conductivity, and small band offsets. Although 1550 nm vertical-cavity surface-emitting lasers have been demonstrated with a variety of approaches, device characteristics have generally been limited by compromises in the choice of DBR materials. The combination of AlGaPSb and InP should possess good contrast and reasonable thermal and electrical conductivity, but the growth and properties of AlGaPSb have not been widely studied. In this work, we have investigated the MBE growth of AlGaPSb alloys lattice matched to InP substrates as well as the incorporation of AlGaPSb as the high-index layer in AlGaPSb/InP DBRs.

AlGaPSb alloys lattice matched to InP were grown by MBE using the combination of elemental Al, Ga, and Sb, with P derived from cracked phosphine. Sb was supplied by a valved cracking source. At a growth temperature of 470° C, the lattice constant of AlGaPSb was found to be critically dependent on the Sb/III ratio, while the P flux had almost no effect. Films with Al fractions of 0 to 0.04 and thicknesses of 500 nm had low defect densities and RMS surfaces roughness of less than 0.5 nm. Room-temperature photoluminescence (PL) from nearly lattice-matched GaPSb exhibited a full-width half-maximum linewidth of 72 meV, and based on measured PL spectra and an approximate bowing parameter we estimate a lattice-matched GaPSb bandgap of 0.85 eV. The addition of 4% Al was found to shift the PL peak to approximately 0.905 eV (1370 nm), yielding a material that should be suitably transparent at 1550 nm.

A 15-period $Al_{0.04}Ga_{0.96}PSb$/InP DBR was grown and characterized. The surface of the DBR was slightly corrugated, with an RMS roughness of approximately 0.7 nm. Figure 1 shows the x-ray diffraction spectrum of the DBR. The structure is well lattice-matched, and sharp, weak satellites are observable up to at least 25th order. This indicates that the AlGaPSb compositional uniformity is good and that the structure is relatively free of the highly strained layers sometimes observed at interfaces between materials which differ in both group III and group V species. Figure 2 shows the measured reflectance spectrum for the DBR as well as a spectrum calculated using a refractive index contrast Δn of 0.41. Reasonable agreement between the measured and calculated curves demonstrates the potential of this material combination for high-quality DBRs for 1550 nm devices. Additional characteristics of these materials will be reported.

Sandia is a multiprogram laboratory operated by Sandia Corporation, a Lockheed Martin Company, for the United States Department of Energy's National Nuclear Security Administration under contract DE-AC04-94AL85000.

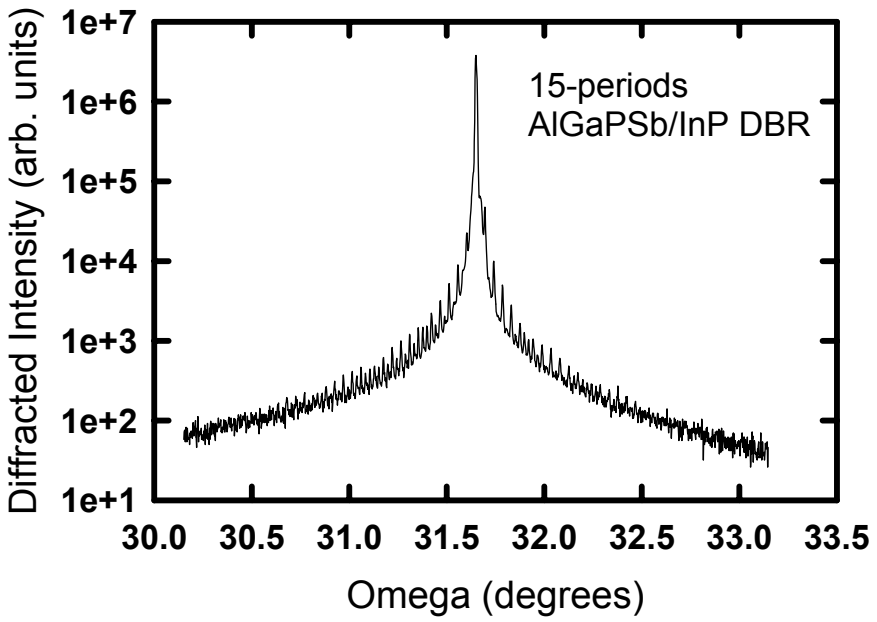

Figure 1. X-ray diffraction spectrum of 15-period AlGaPSb/InP DBR grown on InP.

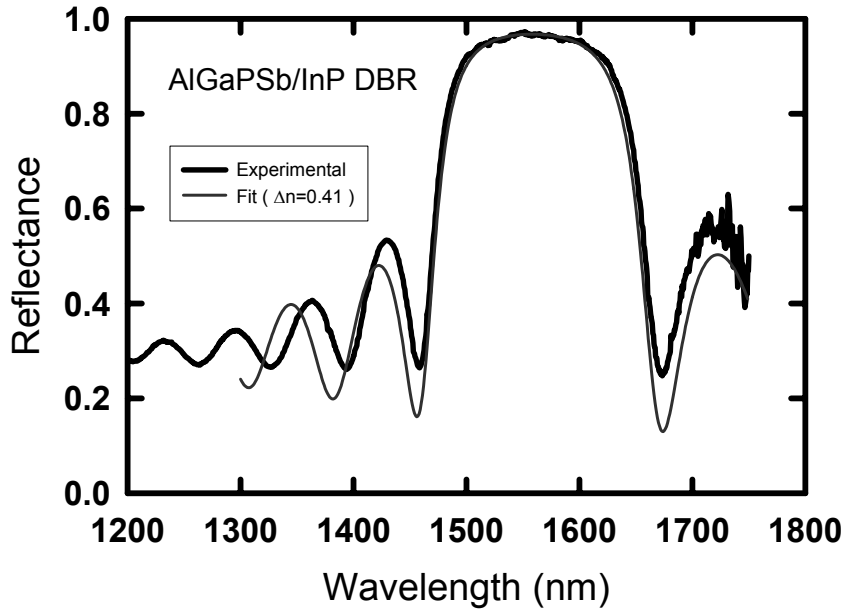

Figure 2. Reflectance spectrum of the AlGaPSb/InP DBR.

NAMBE 2003 Program

Thursday, October 2, 2003

Workshops are scheduled from 8:00-3:00, including a morning coffee break and lunch.

1. **Production of Next-Generation MBE Materials**
   Chairman: Tom Block, Northrop Grumman Space Technology (thomas.block@ngc.com)
   This workshop will explore moving next-generation MBE materials into production. The format of the workshop will be presentations by experts in the different materials, followed by group discussions. Each speaker will address the following topics in their presentation:
   - Advantages of new materials over existing production technologies
   - Applications and opportunities for new materials
   - Significant growth-mechanics related challenges remaining
   - Equipment improvements desirable for production

   The final portion of the workshop will follow up previous workshops on in-situ measurement and safety.

   List of Invited Speakers:

   Ben Heying, Northrop Grumman Space Technology
   "GaN for electronics"
   Henning Riechert, Infineon Technologies
   "Dilute nitrides"
   Brian Bennett, Naval Research Labs
   "Sb materials for electronics,"
   Aaron Ptak, National Renewable Energy Lab
   "Novel III-Vs for solar cells,"
   Amy Liu, IQE
   "Novel III-V production technology"
   Paul Pinsukanjana, Intelligent Epitaxy Technology
   "In-situ monitoring and control in MBE,"
   Kris Bertness, National Institute of Standards and Technology
   "Absolute composition calibration standards,"
   Thomas Block, Northrop Grumman Space Technology
   "Phosphorous maintenance safety,"

NAMBE 2003 Program

Thursday, October 2, 2003

Workshops are scheduled from 8:00-3:00, including a morning coffee break and lunch.

2. Long Wavelength Optoelectronics
Chairman: Yong-Hang Zhang, Arizona State University (yhzhang@asu.edu)

The Long Wavelength Optoelectronics Workshop offers a great forum for the MBE growth of optoelectronic materials and devices. More emphasis will be placed on the growth and materials related issues, new approaches for their improvement, and device concepts. It will be organized in two serial sessions, i) Near IR Session, which will cover the wavelengths up to 2 micron; ii) MWIR and Beyond, which covers from 2 micron up to THz radiation. The workshop will be casual and stimulating. We strongly encourage every attendee, from university graduate students to senior researchers, to actively participate.

List of Invited Speakers

Near IR Session

James Harris, Stanford University.
"GaInNAsSb, A New Material in the Quest for Communication Lasers"
James Gupta, NRC, Canada
"MBE Growth of Dilute Nitrides for Long Wavelength Optoelectronics"
Shane Johnson, S. Chaparro, P. Dowd, *et. al.*, Arizona State University and Lytek Corporation
"Long Wavelength GaAsSb/GaAs VCSEL on GaAs Substrate"
A.R.Kovsh, A.F.Ioffe Physico-Technical Institute and Industrial Technology Research Institute, Hsinchu, Taiwan, ROC.
"Recent Achievements in MBE Technology of Long-Wavelength (1.3 -1.5 um) Quantum Dot Lasers Based on GaAs"

MWIR and Beyond

John Reno, Sandia National Laboratory
"MBE growth of THz Quantum Cascade Lasers on GaAs,"
Cory J. Hill, Baohua Yang, and Rui Q. Yang, Jet Propulsion Laboratory, California Institute of Technology
"Growth of Antimonide-Based Interband Cascade Lasers on Gallium Arsenide Substrates,"
Z. Shi, F. Zhao, A. Majumda, H. Z. Xu, X. Lu, L. Jayasinghe, S. Khosravani, V. Kelkar, R. Singh, D. Ray, University of Oklahoma
"MBE growth of Mid-infrared IV-VI lead-salt QW VCSEL"

Contributed talks

Y. Cao, S. Yu, X. Jin, D. Ding, J. Wang, S. Johnson, and Y.-H. Zhang, Arizona State University
"Room Temperature CW Operation of 2.1 um Quantum Well Lasers Grown on GaSb"

NAMBE 2003 Program

Thursday, October 2, 2003

Workshops are scheduled from 8:00-3:00, including a morning coffee break and lunch.

3. MBE for Quantum Information

Co-chairmen: Richard Mirin, NIST (mirin@boulder.nist.gov)
Nitin Samarth, Penn State (nsamarth@psu.edu)

This workshop will focus on new materials and devices for Quantum Information. Materials such as dilute magnetic semiconductors and quantum dots will be discussed. Important topics of discussion will include what advances need to be made in MBE growth in order to advance the area of Quantum Information.

List of Invited Speakers

Prof. Jeremy Levy, University of Pittsburg
"Oxide-Semiconductor Materials for Quantum Computation"

Prof. Michael Flatté, University of Iowa
1. An Introduction to Quantum Information Technologies: A Range From "You Can Buy It Now" to "Can It Ever Be Done?"
2. Molecular Beam Epitaxy Challenges from Quantum Information Technologies

Dr. Tom Reinecke, Naval Research Laboratory
"Semiconductor Nanostructures for Quantum Information Technology"

Dr. David Pappas, National Institute of Standards and Technology
"Epitaxial materials for solid state quantum computing applications"

The workshop will consist of talks in the morning, followed by a panel discussion after lunch. The goal of this workshop is to examine critical issues that MBE needs to address in order to expedite progress in realizing solid state quantum computers.

NAMBE 2003 Program

Thursday, October 2, 2003

Workshops are scheduled from 8:00-3:00, including a morning coffee break and lunch.

2. Long Wavelength Optoelectronics
Chairman: Yong-Hang Zhang, Arizona State University (yhzhang@asu.edu)

The Long Wavelength Optoelectronics Workshop offers a great forum for the MBE growth of optoelectronic materials and devices. More emphasis will be placed on the growth and materials related issues, new approaches for their improvement, and device concepts. It will be organized in two serial sessions, i) Near IR Session, which will cover the wavelengths up to 2 micron; ii) MWIR and Beyond, which covers from 2 micron up to THz radiation. The workshop will be casual and stimulating. We strongly encourage every attendee, from university graduate students to senior researchers, to actively participate.

List of Invited Speakers

Near IR Session

James Harris, Stanford University.
"GaInNAsSb, A New Material in the Quest for Communication Lasers"
James Gupta, NRC, Canada
"MBE Growth of Dilute Nitrides for Long Wavelength Optoelectronics"
Shane Johnson, S. Chaparro, P. Dowd, *et. al.*, Arizona State University and Lytek Corporation
"Long Wavelength GaAsSb/GaAs VCSEL on GaAs Substrate"
A.R.Kovsh, A.F.Ioffe Physico-Technical Institute and Industrial Technology Research Institute, Hsinchu, Taiwan, ROC.
"Recent Achievements in MBE Technology of Long-Wavelength (1.3 -1.5 um) Quantum Dot Lasers Based on GaAs"

MWIR and Beyond

John Reno, Sandia National Laboratory
"MBE growth of THz Quantum Cascade Lasers on GaAs,"
Cory J. Hill, Baohua Yang, and Rui Q. Yang, Jet Propulsion Laboratory, California Institute of Technology
"Growth of Antimonide-Based Interband Cascade Lasers on Gallium Arsenide Substrates,"
Z. Shi, F. Zhao, A. Majumda, H. Z. Xu, X. Lu, L. Jayasinghe, S. Khosravani, V. Kelkar, R. Singh, D. Ray, University of Oklahoma
"MBE growth of Mid-infrared IV-VI lead-salt QW VCSEL"

Contributed talks

Y. Cao, S. Yu, X. Jin, D. Ding, J. Wang, S. Johnson, and Y.-H. Zhang, Arizona State University
"Room Temperature CW Operation of 2.1 um Quantum Well Lasers Grown on GaSb"

NAMBE 2003 Program

Thursday, October 2, 2003

Workshops are scheduled from 8:00-3:00, including a morning coffee break and lunch.

3. MBE for Quantum Information

Co-chairmen: Richard Mirin, NIST (mirin@boulder.nist.gov)
Nitin Samarth, Penn State (nsamarth@psu.edu)

This workshop will focus on new materials and devices for Quantum Information. Materials such as dilute magnetic semiconductors and quantum dots will be discussed. Important topics of discussion will include what advances need to be made in MBE growth in order to advance the area of Quantum Information.

List of Invited Speakers

Prof. Jeremy Levy, University of Pittsburg
"Oxide-Semiconductor Materials for Quantum Computation"

Prof. Michael Flatté, University of Iowa
1. An Introduction to Quantum Information Technologies: A Range From "You Can Buy It Now" to "Can It Ever Be Done?"
2. Molecular Beam Epitaxy Challenges from Quantum Information Technologies

Dr. Tom Reinecke, Naval Research Laboratory
"Semiconductor Nanostructures for Quantum Information Technology"

Dr. David Pappas, National Institute of Standards and Technology
"Epitaxial materials for solid state quantum computing applications"

The workshop will consist of talks in the morning, followed by a panel discussion after lunch. The goal of this workshop is to examine critical issues that MBE needs to address in order to expedite progress in realizing solid state quantum computers.

NAMBE 2003 Program

Thursday, October 2, 2003

Workshops are scheduled from 8:00-3:00, including a morning coffee break and lunch.

1. **Production of Next-Generation MBE Materials**
   Chairman: Tom Block, Northrop Grumman Space Technology (thomas.block@ngc.com)
   This workshop will explore moving next-generation MBE materials into production. The format of the workshop will be presentations by experts in the different materials, followed by group discussions. Each speaker will address the following topics in their presentation:
   - Advantages of new materials over existing production technologies
   - Applications and opportunities for new materials
   - Significant growth-mechanics related challenges remaining
   - Equipment improvements desirable for production

   The final portion of the workshop will follow up previous workshops on in-situ measurement and safety.

   List of Invited Speakers:

   Ben Heying, Northrop Grumman Space Technology
   "GaN for electronics"
   Henning Riechert, Infineon Technologies
   "Dilute nitrides"
   Brian Bennett, Naval Research Labs
   "Sb materials for electronics,"
   Aaron Ptak, National Renewable Energy Lab
   "Novel III-Vs for solar cells,"
   Amy Liu, IQE
   "Novel III-V production technology"
   Paul Pinsukanjana, Intelligent Epitaxy Technology
   "In-situ monitoring and control in MBE,"
   Kris Bertness, National Institute of Standards and Technology
   "Absolute composition calibration standards,"
   Thomas Block, Northrop Grumman Space Technology
   "Phosphorous maintenance safety,"

NAMBE 2003 Program

Thursday, October 2, 2003

Workshops are scheduled from 8:00-3:00, including a morning coffee break and lunch.

2. Long Wavelength Optoelectronics
Chairman: Yong-Hang Zhang, Arizona State University (yhzhang@asu.edu)

The Long Wavelength Optoelectronics Workshop offers a great forum for the MBE growth of optoelectronic materials and devices. More emphasis will be placed on the growth and materials related issues, new approaches for their improvement, and device concepts. It will be organized in two serial sessions, i) Near IR Session, which will cover the wavelengths up to 2 micron; ii) MWIR and Beyond, which covers from 2 micron up to THz radiation. The workshop will be casual and stimulating. We strongly encourage every attendee, from university graduate students to senior researchers, to actively participate.

List of Invited Speakers

Near IR Session

James Harris, Stanford University.
"GaInNAsSb, A New Material in the Quest for Communication Lasers"
James Gupta, NRC, Canada
"MBE Growth of Dilute Nitrides for Long Wavelength Optoelectronics"
Shane Johnson, S. Chaparro, P. Dowd, *et. al.*, Arizona State University and Lytek Corporation
"Long Wavelength GaAsSb/GaAs VCSEL on GaAs Substrate"
A.R.Kovsh, A.F.Ioffe Physico-Technical Institute and Industrial Technology Research Institute, Hsinchu, Taiwan, ROC.
"Recent Achievements in MBE Technology of Long-Wavelength (1.3 -1.5 um) Quantum Dot Lasers Based on GaAs"

MWIR and Beyond

John Reno, Sandia National Laboratory
"MBE growth of THz Quantum Cascade Lasers on GaAs,"
Cory J. Hill, Baohua Yang, and Rui Q. Yang, Jet Propulsion Laboratory, California Institute of Technology
"Growth of Antimonide-Based Interband Cascade Lasers on Gallium Arsenide Substrates,"
Z. Shi, F. Zhao, A. Majumda, H. Z. Xu, X. Lu, L. Jayasinghe, S. Khosravani, V. Kelkar, R. Singh, D. Ray, University of Oklahoma
"MBE growth of Mid-infrared IV-VI lead-salt QW VCSEL"

Contributed talks

Y. Cao, S. Yu, X. Jin, D. Ding, J. Wang, S. Johnson, and Y.-H. Zhang, Arizona State University
"Room Temperature CW Operation of 2.1 um Quantum Well Lasers Grown on GaSb"

NAMBE 2003 Program

Thursday, October 2, 2003

Workshops are scheduled from 8:00-3:00, including a morning coffee break and lunch.

3. MBE for Quantum Information

Co-chairmen: Richard Mirin, NIST (mirin@boulder.nist.gov)
Nitin Samarth, Penn State (nsamarth@psu.edu)

This workshop will focus on new materials and devices for Quantum Information. Materials such as dilute magnetic semiconductors and quantum dots will be discussed. Important topics of discussion will include what advances need to be made in MBE growth in order to advance the area of Quantum Information.

List of Invited Speakers

Prof. Jeremy Levy, University of Pittsburg
"Oxide-Semiconductor Materials for Quantum Computation"

Prof. Michael Flatté, University of Iowa
1. An Introduction to Quantum Information Technologies: A Range From "You Can Buy It Now" to "Can It Ever Be Done?"
2. Molecular Beam Epitaxy Challenges from Quantum Information Technologies

Dr. Tom Reinecke, Naval Research Laboratory
"Semiconductor Nanostructures for Quantum Information Technology"

Dr. David Pappas, National Institute of Standards and Technology
"Epitaxial materials for solid state quantum computing applications"

The workshop will consist of talks in the morning, followed by a panel discussion after lunch. The goal of this workshop is to examine critical issues that MBE needs to address in order to expedite progress in realizing solid state quantum computers.

An Introduction to Quantum Information Technologies: A Range From "You Can Buy It Now" to "Can It Ever Be Done?"

Michael E. Flatté
Department of Physics and Astronomy and Optical Science and Technology Center,
University of Iowa, Iowa City, IA 52242

The first devices based on the transport and detection of quantum information, quantum key distribution systems, are now commercially available. Much more sophisticated and powerful devices that process quantum information, such as quantum computers, likely are at least many years away from practical implementation. Quantum repeaters, intermediate in difficulty between quantum key distribution systems and quantum computers, remain to be demonstrated. This brief introduction to quantum information technologies will describe the basic terminology and elementary operations of quantum information, the commonly-considered special examples of quantum information devices and the problems they solve, and the (known) essential physical conditions for successful manipulation of quantum information. Other leading physical approaches to quantum computation, and their current achievements, will be outlined for comparison with solid state strategies.

Abstract for NAMBE 2003 Workshop
at the Keystone Resort, Keystone, CO,
Sept 28 - Oct 3

Semiconductor Nanostructures for Quantum Information Technology*

Tom Reinecke
Naval Research Laboratory
Washington, DC 20375
email: reinecke@nrl.navy.mil

Semiconductor nanostructures based on MBE are of current interest in the search for solid state implementations for quantum bits ('qu-bits') and for quantum gates between them for application in quantum information technology and related areas. Single quantum dots formed by Stranski-Krastanov growth and isolated by lithography exhibit sharp optical spectra with relatively long decoherence times. Spins doped into these structures are particularly attractive candidates as qu-bits. Closely spaced pairs of quantum dots can be formed by growth on adjacent MBE layers, and it has been demonstrated that the coupling between such dots can be coherent [1]. It has been found that the coupling between these dots can be controlled with an electric field, and two bit quantum gates have devised from spins in these 'vertically coupled quantum dot molecules' [2].

Semiconductor microcavities offer the possibility of fast distant coupling between quantum dots via the confined photon states, and they are also of interest in a variety of other applications, such as nanoemitters and nanolasers. These structures are fabricated lithographically from VCSELS (vertical cavity surface emitting laser structures) grown by MBE. These microcavity structures have been shown to exhibit fully confined discrete photon modes [3], a rich variety of coupled modes in coupled pairs of cavities [4] and full photon band gaps in chains of such cavities [5].

This work is supported by ONR and by DARPA.

[1] M. Bayer *et al*, Phys. Rev. Lett. **90**, 6404 (2003).
[2] G. Ortner *et al*, to be published.
[3] J.-P. Reithmaier *et al*, Phys. Rev. Lett. **78**, 378 (1998).
[4] M. Bayer *et al*, Phys. Rev. Lett. **83**, 5374 (1999).
[5] M. Bayer *et al*. Phys. Rev. Lett. **81**, 2582 (1998).

Oxide-Semiconductor Materials for Quantum Computation

Jeremy Levy
Department of Physics
University of Pittsburgh

I will describe the goals and activities of our center for oxide-semiconductor materials for quantum computation (COSMQC,http://cosmqc.net). The materials basis for our quantum computing architecture relies on the growth of ordered arrays of ultrasmall Ge quantum dots on Si, and an epitaxial overgrowth of a coherently strained ferroelectric material. Quantum information is stored in electron spins localized around the Ge quantum dots. Spin-polarized electrons are created in Ge quantum dots using optical orientation. Fast optical gating occurs via optical rectification in the epitaxial ferroelectric. This approach takes advantages of native excitations and interactions in the solid state: (i) electron spins, charges, and photons for initialization and readout, (ii) quantum-mechanical (Heisenberg, Zeeman, spin-orbit) and classical (magnetic, electric, optical intensity) couplings for quantum gating, and (iii) bandgap engineering for preserving long coherence times (semiconductor bandgaps, 3D quantum confinement, spin gaps). Recent results from COSMQC will be presented, as well as an overview of ongoing work and future directions.

Molecular Beam Epitaxy Challenges from Quantum Information Technologies

Michael E. Flatté
Department of Physics and Astronomy and Optical Science and Technology Center,
University of Iowa, Iowa City, IA 52242

Progress in several areas of crystal growth is required for the realization of new quantum information devices, especially quantum computers. Room temperature magnets epitaxially grown on semiconductors are highly desirable for use in spin-polarized carrier sourcing and detecting. High-quality optical properties, both in the semiconducting and magnetic materials, are also very desirable for high-speed coherent spin manipulation, and long spin coherence times are essential for the persistence of quantum information. Confinement of an electron spin in a quantum dot dramatically improves the spin coherence time, and also assists in the manipulation of the electron spin orientation. The highest temperature ferromagnetic semiconductors grown are typically grown at low growth temperatures, yielding high defect concentrations, low mean free paths, short spin coherence times, and poor optical properties. Progress in these material properties would offer significantly improved device performance, which would lead to enhanced flexibility in quantum information device design. Sharp interfaces that permit coherent transport of carriers from magnetic materials to nonmagnetic materials also would greatly simplify device design. Each of these presents new challenges for crystal growth.

Epitaxial materials for solid state quantum computing applications

David Pappas
National Institute of Standards and Technology
325 Broadway
Boulder, CO 80305
e-mail: pappas@boulder.nist.gov

With the advent of new, potentially useful algorithms for quantum computation, the race for a scalable quantum computer has emerged. A few of the critical issues that need to be addressed for a given quantum computing paradigm are (1) the identification of the quantum bit that can be readily controlled; (2) a scalable method for coupling many of them, and (3) demonstrating that complex circuits can be designed and implemented. While early demonstrations of simple, few qubit quantum operations have been achieved with ion traps and nuclear magnetic resonance in molecules, it is not clear that all of these criteria can be met. Due to the success of modern fabrication methods in scaling existing electronics, a concerted effort to develop a solid state quantum computer is emerging. At present, superconducting Josephson junction qubits are the leading candidates in this area. Other efforts, such as nuclear spins in semiconductors and spin polarized quantum dots, however, have also considered as possible candidates. In this presentation, the role of epitaxial growth of materials in these systems will be discussed, and the potential applications of molecular beam epitaxy in this area evaluated.

NAMBE 2003 Exhibitor Information

Addon Company
19 rue des entrepreneurs
Carrieres Sur Seine, France 78420
Pierre Bouhaib
Phone: (33 1 39 15 39 99) FAX: (33 1 39 15 56 36)
e-mail: mbecells@wanadoo.fr

AXT Inc.
4281 Technology Drive
Fremont, CA 94538
Lisa Tan
Phone: 510-226-435 FAX:510-683-5901
e-mail: Lisa.Tan@axt.com

Bede Scientific Inc.
141 Inverness Drive, East, H-100
Englewood, CO 80112
Mandy Robbins
Phone: 303-790-8647 FAX: 303-790-8648
e-mail: Mandy.robbins@bede.com

DCA Instruments
4 Piper Court
Blauvelt, NY 10913
Dr. Myung B. Lee
Phone: 845-398-1962 FAX: 845-398-1963
e-mail: dcausa@optonline.net

GE Advanced Ceramics
22557 West Lunn Road
Strongsville OH, 44149
Greg Strosaker
Phone: 440 878-5700 FAX:440-878-5928
e-mail: greg.strosaker@gesm.ge.com

Geo Gallium
3201 Enterprise Parkway, Suite 490
Cleveland, OH 44122
Gary Evans
Phone: 514-769-0300 FAX: 514-769-8928
e-mail: gme@videotron.ca

NAMBE 2003 Exhibitor Information

InPACT Inc
3984 Washington Blvd, #15
Fremont, CA 94538
Christine Convers
Phone: 510-573-1882 and 33 479 24 72 86 FAX: 510-573-0820 and 33 479 24 72 95
e-mail: cconvers@inpactsemicon.com

k-Space Associates Inc.
3626 W. Liberty Road
Ann Arbor, MI 48103
Kristine Krueger
Phone: (734-668-4644) FAX: 734-668-4663
e-mail: khkrueger@k-space.com

MBE-Komponenten GmbH
Gutenbergstraβe B, D-71263 Well der Stadt
Germany
Frank Huber
Phone: 49 7033 693773 FAX: 49 7033 693720
e-mail: huber@mbe-components.com

Riber Inc.
3880 Park Ave
Edison NJ 08820
Paul Dargan
Phone: 805-892-5511 FAX: 805-892-5510
e-mail: pdargan@riber-us.com

SINTEC Keramik USA, Inc.
540 Barnum Ave.
Bridgeport, CT 06608
Ana Vieira
Phone: (203) 331-0778 FAX: 203-331-0779
e-mail: ana.vieira@sintec-keramik.com

Specs Scientific Instruments Inc.
635 S. Orange Ave
Sarasota, FL 34236
Dietrich Von Diemas
Phone: (941-362-4877) FAX: 941-364-9706
e-mail: didi@specs.com

NAMBE 2003 Exhibitor Information

Sumitomo Electric SemiConductor Materials Inc.
7230 NW Evergreen Parkway
Hillsboro, OR 97124
Mike Dean
Phone: 503 693-3100, X207 FAX: 503-693-8275
e-mail: mdean@sesmi.com

SVT Associates
7620 Executive Drive
Eden Prairie, MN 55344
Stacey Schmitz
Phone: (952-934-2100) FAX: 952-934-2737
e-mail: johannes@svta.com

United Mineral & Chemical Corporation
1100 Valley Brook Avenue
Lyndhurst, NJ 07071-3608
Irwin Drangel
Phone: 201-507-3300 FAX: 201-507-1506
e-mail: idrangel@umccorp.com

Vacuum Barrier Corp
4 Barten Lane
Woburn, MA 0801-0529
EJ Hanlon
Phone: 781-933-3570 FAX: 781-932-9428
e-mail: ejh@vacuumbarrier.com

VBS International
808 East McGlincey
Campbell, CA 95008
Sharon Ritchie
Phone: 408-371-3303 FAX: 408-371-3320
e-mail: sharon@vbsflex.com

Veeco Instruments Inc.
4900 Constellation Drive
St Paul, MN 55127
Molly Doran
Phone: (651-494-5511) FAX: 651-482-0600
e-mail: mdoran@veeco.com

Wafer Technologies, Ltd
106 East Bonita Road, #53
Payson, AR 85541
Tom Taylor
Phone: 928-468-2204 FAX: 928-468-2342
e-mail: ttaylor.t2@att.net